Mechanisms of Progressive Multiple Sclerosis

A thesis submitted in fulfilment of the requirements for the degree of Doctor of Philosophy

by

Justin Yehuda Garber

Faculty of Medicine and Health

University of Sydney

2023

Statement of originality

The work presented in this thesis is, to the best of my knowledge and belief, original except as acknowledged in the text. I hereby declare that I have not submitted this material, either in full or in part, for a degree at the University of Sydney or other institution.

Justin Yehuda Garber

Acknowledgements

I wish to acknowledge and pay respect to Aboriginal people past and present as the traditional owners of the land on which I conducted this research, namely the Gadigal people of the Eora Nation, whose ancestral lands the University of Sydney is built upon.

I wish to thank all the patients with MS who have taken part in our studies. Your commitment to improving our understanding of MS in the face of hardship is inspiring.

I am deeply grateful to my mentor and supervisor for this thesis Michael Barnett. Thank you for your tremendous effort supporting my research, as well as your continuous encouragement for me as a clinician working in MS. I hope we can maintain a fulfilling academic, clinical and personal relationship into the future.

I would also like to thank the team at the Brain and Mind Centre, University of Sydney and Sydney Neuroimaging Analysis Centre for your expertise, patient tutelage and support, especially Chenyu Wang, Fernando Calamante, Marinda Taha, Oren Civier, Jinglei Lv, Josh Barton, Heidi Beadnall, Lynette Masters, Annmaree O'Connell, Kain Kyle, Deleni Walters, Ishana Dixit, Rene Yon and Miriana Mitrevski. Thank you to everyone at the Buffalo Neuroimaging Analysis Centre for your inviting and generous spirit of collaboration, especially Tom Fuchs and Michael Dwyer.

Finally I would like to thank my whole family for your unfailing love and encouragement. Reuben and Louis, I couldn't ask for more loving boys, and Jemma, this thesis simply wouldn't have been possible without your love and support.

Thesis Abstract

Multiple sclerosis (MS) is a chronic inflammatory demyelinating disease of the central nervous system with features of progressive neurodegeneration. The mechanisms of progressive neurodegenerative disease are incompletely understood but include inflammatory and non-inflammatory processes that lead to focal and diffuse axonal loss. Magnetic resonance imaging (MRI) is an indispensable technique that has been used to develop numerous biomarkers of inflammatory disease in MS. These biomarkers are used for diagnosis, monitoring disease activity and clinical trial outcomes. MRI biomarkers of the neurodegenerative components of MS have also been developed but lack the same level of sensitivity as inflammatory biomarkers, which has limited their uptake into clinical use and clinical trials.

This thesis explores techniques using diffusion-based MRI in order to characterise mechanisms underlying progressive MS. Refined methods of assessing microstructural damage and structural network disruption are described and evaluated. Several potential biomarkers are proposed to describe and predict progression in MS.

Thesis Outcome

Journal Articles

- Garber, J. Y. & Barnett, M. H. We should focus more on finding therapeutic targets for the non-inflammatory damage in MS – Yes. *Multiple Sclerosis Journal* **24**, 1272–1274 (2018).
- Barton, J. L., Garber, J. Y., Klistorner, A. & Barnett, M. H. The electrophysiological assessment of visual function in Multiple Sclerosis. *Clin Neurophysiol Pract* **4**, 90–96 (2019).
- Barnett, Y., Garber, J. Y. & Barnett, M. H. MRI biomarkers of disease progression in multiple sclerosis: old dog, new tricks? *Quant Imaging Med Surg* **10**, 527–532 (2020).
- Garber, J. Y., Beadnall, H. N. & Barnett, M. H. Multiple Sclerosis: The role of the GP in diagnosis and lifetime care. *Medicine Today* **21**, 14–25 (2020).

Conference papers and abstracts

- Garber, J. Y., Wang, C., Beadnall, H., Hardy, T. A., Matamala, J. M., Howells, J., Reddel, S. W., Kiernan, M. C., & Barnett, M. H. (2017). Structure and function of the corticospinal tract and motor cortex in multiple sclerosis. *ECTRIMS*
- Wang, C., Klistorner, A., Barton, J., Beadnall, H. N., Ly, L., Liu, S., Garber, J. Y., Reddel, S. W., & Barnett, M. H. (2018). Alteration of visual cortical microstructure is associated with pathology along the optic radiation in patient with MS: An asymmetry analysis of posterior visual pathway. *ECTRIMS*. ECTRIMS.
- Garber, J. Y., Wang, C., Beadnall, H. N., Howells, J., Matamala, J. M., Kiernan, M. C., Klistorner, A., & Barnett, M. H. (2018). Investigating the Mechanisms of Microstructural and Functional Changes in the Motor Pathway in Multiple Sclerosis. *PACTRIMS*.
- Garber, J. Y., Wang, C., Calamante, F., & Barnett, M. (2020). Implications for the registration of white matter structures in MS connectome analysis. *ACTRIMS-ECTRIMS*.

- Garber, J. Y., & Barnett, M. H. (2020). Quantifying T1 hypo-intensity in MS lesions. *ACTRIMS-ECTRIMS*.
- Krieger, S. C., Billiet, T., Maes, C., Chatterjee, A., De Barros, N., Van Hecke, W., Ribbens, A., Wang, C., Kyle, K., Ly, L., Garber, J. Y., & Barnett, M. H. (2022). AI-based characterisation of multiple sclerosis clinical symptomatology using lesion parenchymal fraction: Consistency with the topographical model of MS. *ECTRIMS*. ECTRIMS.
- Krieger, S. C., Billiet, T., Maes, C., De Barros, Van Hecke, W., Ribbens, A., Wang, C., Kyle, K., Ly, L., Garber, J. Y., & Barnett, M. H. (2023). AI-based characterization of multiple sclerosis clinical symptomatology using lesion parenchymal fraction: Empirical support for the topographical model of MS. *AAN*.

Table of Contents

Glossary of Abbreviations

5TT: 5-tissue type

9HPT: Nine-hole peg test

ACT: Anatomically constrained tractography

AD: Axial diffusivity

ADC: Apparent diffusion coefficient

AFD: Apparent fibre density

ANTs: Advanced normalisation tools

ATR: Anterior thalamic radiations

BBB: Blood-brain barrier

CC: Corpus callosum

COMMIT: Convex optimisation modelling for microstructure-informed tractography

CIS: Clinical isolated syndrome

CNS: Central nervous system

CSD: Constrained spherical deconvolution

CSF: Cerebrospinal fluid

CST: Corticospinal tract

dMRI: Diffusion magnetic resonance imaging

DMT: Disease modifying therapy

dRL: Damped Richardson-Lucy

DTI: Diffusion tensor imaging

DWI: Diffusion weighted imaging

EAE: Experimental autoimmune encephalomyelitis

EDSS: Expanded disability status scale

EEG: Electroencephalography

EPI: Echo planar imaging

FA: Fractional anisotropy

FLAIR: Fluid attenuation inversion recovery

fMRI: Functional magnetic resonance imaging

fODF: Fibre orientation distribution function

FOD: Fibre orientation distribution

FS: Functional system

GM: Grey matter

HARDI: High angular resolution diffusion imaging

HC: Healthy control

IQR: Inter-quartile range

MD: Mean diffusivity

mfVEP: Multifocal visual evoked potential

MRI: Magnetic resonance imaging

MS: Multiple sclerosis

MSFC: Multiple sclerosis functional composite

NAWM: Normal appearing white matter

NBS: Network based statistic

NfL: Neurofilament light

NODDI: neurite orientation dispersion and density imaging

OCT: Optical coherence tomography

ON: Optic neuritis

OR: Optic radiation

PASAT: Paced auditory serial addition test

PIRA: Progression independent of relapse

PML: Progressive multifocal leukoencephalopathy

PMS: Progressive multiple sclerosis

PNS: Peripheral nervous system

PPMS: Primary progressive multiples sclerosis

pwMS: Persons with multiple sclerosis

QSM: Quantitative susceptibility mapping

RD: Radial diffusivity

RF: Radio frequency

ROI: Region of interest

RRMS: Relapsing-remitting multiple sclerosis

SD: Standard deviation

SDMT: Symbol digit modalities test

SIFT: Spherical-deconvolution informed filtering of tractograms

SMN: Sensorimotor network

SPMS: Secondary progressive multiple sclerosis

SS3T-CSD: Single-shell 3-tissue constrained spherical deconvolution

SWI: Susceptibility weighted imaging

T25FW: Timed 25 foot walk

TDI: Tract density imaging

Treg: Regulatory T cell

WM: White matter

Chapter 1

Introduction

1.1 Multiple Sclerosis

1.1.1 Background

Multiple sclerosis (MS) is a chronic disease of the central nervous system (CNS) with features of autoimmunity, immune dysregulation and neurodegeneration (Lassmann et al., 2007). The first formal description was made over 150 years ago by Charcot using his “anatomoclinical” method of correlating clinical features with post-mortem pathology (Kumar et al., 2011), although reports consistent with a chronic relapsing demyelinating CNS disease stretch back to centuries earlier (Ward & Goldman, 2022). Whilst being a clearly defined entity for over a century, MS has eluded a conclusive pathophysiological description, despite substantial advances in disease understanding and therapeutics.

MS affects some 2.8 million people worldwide as of 2020, including over 30 000 Australians at a prevalence of ~1.2:1000 (Walton et al., 2020). The typical age of disease onset is between 20 and 40 years old, leading to MS being the most common cause of non-traumatic disabling neurologic condition in young adults in Australia. The prevalence of MS varies worldwide, with higher and lower risk areas differing in prevalence by over 20-fold (see Fig. 1.1). The prevalence is also increasing as a result of increased survival, improved detection and reporting, updating of MS diagnostic guidelines, but likely also a true increased incidence in some regions (Browne et al., 2014). Typical of other autoimmune diseases, females have an increased risk of the disease with a 2-4:1 sex ratio female:male, although males tend to have a more disabling disease trajectory (Ribbons et al., 2015).

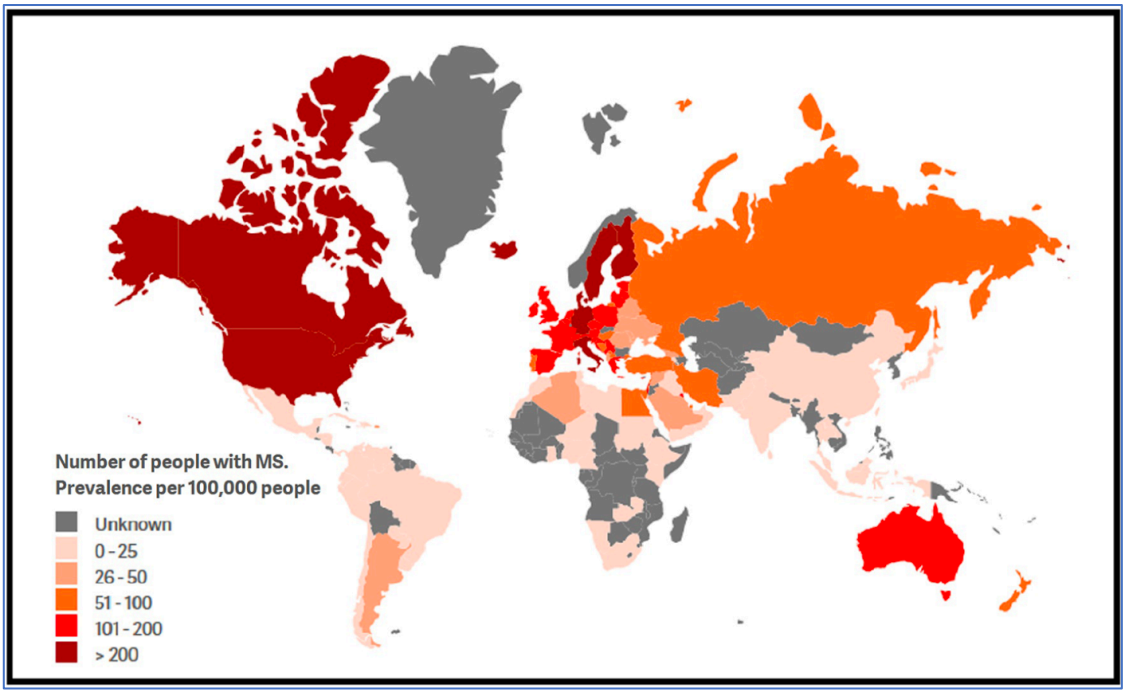

Figure 1.1 World map of MS prevalence per country. Adapted from Walton, 2020.

1.1.2 Clinical aspects and definitions of multiple sclerosis

The classification and diagnostic criteria of MS have evolved over time (McDonald et al., 2001; Polman et al., 2011; Poser et al., 1983; Thompson et al., 2017). The prevailing view is to separate the disease into several phenotypes that best characterise the mechanism of cumulative neurological disability, and aid in prognostication, clinical trial design and therapeutic choice. In ~85% of cases, MS presents with an acute syndrome of neurological dysfunction (relapse) dependent on the location of acute focal inflammation in the CNS. This phenotype is termed relapsing-remitting multiple sclerosis (RRMS) due to the typical feature that relapses improve (remit) as focal inflammation regresses, albeit not always with full neurological recovery. RRMS may be preceded by clinically isolated syndrome (CIS), essentially a first inflammatory/demyelinating relapse that does not meet diagnostic criteria for MS. Neurological deficits and disability in RRMS have traditionally been seen to be episodic, with cumulative and lasting disability occurring with accrual of relapses that lack complete recovery.

The latest diagnostic criteria (see Table 1.1) (Thompson et al., 2017) capture the clinical course of RRMS, i.e. the propensity for multifocal acute inflammation over time, by requiring proof of dissemination in space and time, through repeated clinical relapses, typical focal

inflammatory/demyelinating lesions on MRI or, in the case of time, cerebrospinal fluid (CSF)-specific oligoclonal bands. Although not absolutely required, the diagnostic criteria heavily rely on the use of MRI, and in practice MRI is essential to diagnose MS with reliable specificity. The four typical areas for lesion location in the CNS are: juxtacortical or cortical, periventricular, infratentorial and spinal cord, of which two must be present on MRI to meet radiological criteria.

	Number of lesions with objective clinical evidence	Additional data needed for a diagnosis of multiple sclerosis
≥2 clinical attacks	≥2	None
≥2 clinical attacks	1 (as well as clear-cut historical evidence of a previous attack involving a lesion in a distinct anatomical location)	None
≥2 clinical attacks	1	Dissemination in space demonstrated by an additional clinical attack implicating a different CNS site or by MRI
1 clinical attack	≥2	Dissemination in time demonstrated by an additional clinical attack or by MRI OR demonstration of CSF-specific oligoclonal bands
1 clinical attack	1	Dissemination in space demonstrated by an additional clinical attack implicating a different CNS site or by MRI AND Dissemination in time demonstrated by an additional clinical attack or by MRI OR demonstration of CSF-specific oligoclonal bands
If the 2017 McDonald Criteria are fulfilled and there is no better explanation, the diagnosis is multiple sclerosis. If multiple sclerosis is suspected by virtue of a clinically isolated syndrome but the 2017 McDonald Criteria are not completely met, the diagnosis is possible multiple sclerosis. If another diagnosis arises during the evaluation that better explains the clinical presentation, the diagnosis is not multiple sclerosis.		

Table 1.1 The 2017 McDonald Criteria for multiple sclerosis with an attack at onset, adapted from Thompson et al. 2017.

The other phenotypes of MS are termed progressive given the mode of disability accrual is slow and unrelenting (see Table 1.2). Within progressive MS (PMS), primary progressive MS (PPMS) is defined as progressive disease from onset, whilst secondary progressive MS (SPMS) is progressive disease occurring after RRMS at onset.

Primary progressive multiple sclerosis can be diagnosed in patients with: • 1 year of disability progression (retrospectively or prospectively determined) independent of clinical relapse
Plus two of the following criteria: • One or more T2-hyperintense lesions characteristic of multiple sclerosis in one or more of the following brain regions: periventricular, cortical or juxtacortical, or infratentorial • Two or more T2-hyperintense lesions in the spinal cord • Presence of CSF-specific oligoclonal bands

Table 1.2 The 2017 McDonald Criteria for primary progressive multiple sclerosis with progression at onset, adapted from Thompson et al. 2017.

The classification of SPMS is not clearly defined in the 2017 criteria beyond progressive disease that follows RRMS. In clinical practice there is much difficulty in definitively labelling people at the transition point between RRMS and SPMS, with clinical uncertainty lasting on average 3 years (Katz Sand et al., 2014). In practice, in addition to worsening disability in the absence of relapses, a certain level of disability is often required before clinicians are confident of the diagnosis (Cree et al., 2021). Research has looked at defining SPMS based on the risk of a future progressive disability trajectory. Most notably this has been studied using the large registry database MSBase, where a 3-strata progression magnitude criteria including an Expanded Disability Status Score (EDSS) ≥ 4 and pyramidal Functional System (FS) score ≥ 2, confirmed after 3 months in the absence of relapse, predicted a progressive disability trajectory and severe disability at 5 years (Lorscheider et al., 2016).

The phenotypic classification and description of MS is at a crossroads however. The tension between historical labels based on clinical onset and increasing evidence of the seamless spectrum of disease across phenotypes is only starting to be addressed in diagnostic criteria. The tension is also exacerbated by rigid clinical trial inclusion criteria, and subsequent drug authority approval conditions, which restrict clinicians within historical classifications. This has

been addressed to a degree by the International Advisory Committee on Clinical Trials of MS and The MS Phenotype Group with 2013 revisions to MS definitions, with the inclusion of a disease activity qualifier in RRMS, and a disease activity and disease progression qualifier in PMS (Lublin et al., 2014). In this context disease activity is defined as clinical evidence of relapse and/or MRI evidence of new or enlarging T2 hyperintense lesions or contrast enhancement. The 2017 McDonald criteria suggests recording the disease activity and the clinical disability progression of the previous year, although incorporating these qualifiers into disease definitions and ultimately clinical trials does not have consensus.

Several avenues of evidence have shown relapsing and progressive disease exist concurrently in MS. At the earliest stages of CIS and RRMS there is accelerated brain atrophy, a recognised marker of neurodegeneration (Calabrese et al., 2007; Radü et al., 2013). Careful clinical evaluation in RRMS has also uncovered worsening of disability independent of relapse activity variably called silent progression (Cree et al., 2019) or progression independent of relapse activity (PIRA) (Kappos et al., 2020). Remarkably these studies have found that most long-term disability worsening in RRMS is independent of relapse activity, as well as being associated with accelerated brain atrophy (Cree et al., 2019), challenging the clinical distinction between relapsing and progressive forms of the disease.

In addition to progressive disability being a feature of RRMS, similarly relapsing/inflammatory disease can be a feature of PMS. Relapses are reported at a rate up to 30% in SPMS (Paz Soldán et al., 2015) and between 5-25% in PPMS (Paz Soldán et al., 2015; Portaccio et al., 2022). The treatment of PMS with currently available disease modifying therapy (DMT) has been underwhelming (Amezcua, 2022), however sub cohort analyses of randomised control trials and registry data have revealed an effect on disability progression in PMS with concurrent clinical and radiological markers of disease activity (Kappos et al., 2018; Montalban et al., 2017; Portaccio et al., 2022). One conclusion then is that immunosuppressive DMTs in PMS are effective in reducing inflammatory/relapse activity but leave neurodegenerative mechanisms untouched leading to poor treatment response in all but the minority with significant inflammatory disease activity. This view has been paralleled in a number of drug approval jurisdictions limiting DMT use to PMS with disease activity (EMA, 2019; FDA, 2020), although not all (TGA, 2022). Other explanations have been suggested for the poor outcomes in PMS

drug trials, including trial design, trial length, inclusion criteria, and the selection of trial outcomes (Ontaneda et al., 2015).

In this thesis, RMS and PMS cohorts have been studied in comparison with an attempt to distinguish between subjects that are clearly in the inflammatory phase of MS, without evidence of progressive disability in the preceding 12 months, and those clearly in the progressive phase with no clear relapse or evidence of disease activity in the previous 2 years.

1.1.3 Clinical measures of disability

MS may affect all aspects of CNS function, but due to its multifocal nature with relative unpredictability in the regions affected the presentation is heterogenous between individuals. Visual disturbance from optic neuritis and physical disability through motor deficits are the most outwardly present symptoms contributing to disability accrual (Reich et al., 2018). However a number of symptoms of MS that contribute to reduced quality of life and disability are not as clear to outside observation and/or measurement and subsequently are under reported. These include fatigue, pain, sensory disturbance, bladder and bowel dysfunction, depression and cognitive impairment (Reich et al., 2018). Cognitive impairment is a common deficit in pwMS with up to 50% of individuals displaying deficits of information processing speed and tests of memory (R. H. B. Benedict et al., 2006). Although neuropsychological battery testing in MS can be brief, even small time additions to the clinical consult are currently impractical, and cognitive testing is often not a part of standard clinical care (Sumowski et al., 2018), although electronic and at home assessments can improve exposure (Rao et al., 2017).

This heterogenous nature of MS disability makes objective clinical assessment and comparison between individuals difficult. The clinical measures and tools used are often composite measures of a variety of scores.

The expanded disability status scale (EDSS) is the mostly widely used disability rating score in MS. Developed from the original disability status scale in 1983 it has been used in all significant clinical trials in MS (Kurtzke, 1983). The EDSS is comprised of 8 functional systems (FS) (pyramidal, cerebellar, brainstem, sensory, bowel and bladder, visual, cognitive or mood and

ambulation) that are then combined to create a final score ranging from no disability (0) to death (10) as outlined in Table 1.3. Several biases and limitations of the EDSS have been described including the over emphasis of lower limb function and mobility above a score 4.0 and the under emphasis of cognitive assessment with reliance on subjective assessment for mild levels of cognitive decline, as well as upper limb function (R. H. Benedict & Walton, 2012; Meyer-Moock et al., 2014). In addition the assessment is reliant on a component examiner with training in neurological examination and the EDSS itself, and is prone to intra-rater and inter-rater variability (Tur, Moccia, et al., 2018). These limitations have led to the active development of alternate disability measures.

0	Normal neurological exam (all grade 0 in all FS scores).
1.0	No disability, minimal signs in one FS (i.e., grade 1).
1.5	No disability, minimal signs in more than one FS* (more than 1 FS grade 1).
2.0	Minimal disability in one FS (one FS grade 2, others 0 or 1).
2.5	Minimal disability in two FS (two FS grade 2, others 0 or 1).
3.0	Moderate disability in one FS (one FS grade 3, others 0 or 1) or mild disability in three or four FS (three or four FS grade 2, others 0 or 1) though fully ambulatory.
3.5	Fully ambulatory but with moderate disability in one FS (one grade 3) and one or two FS grade 2; or two FS grade 3 (others 0 or 1) or five grade 2 (others 0 or 1).
4.0	Fully ambulatory without aid, self-sufficient, up and about some 12 hours a day despite relatively severe disability consisting of one FS grade 4 (others 0 or 1), or combination of lesser grades exceeding limits of previous steps; able to walk without aid or rest some 500 metres.
4.5	Fully ambulatory without aid, up and about much of the day, able to work a full day, may otherwise have some limitation of full activity or require minimal assistance; characterised by relatively severe disability usually consisting of one FS grade 4 (others or 1) or combinations of lesser grades exceeding limits of previous steps; able to walk without aid or rest some 300 metres.
5.0	Ambulatory without aid or rest for about 200 metres; disability severe enough to impair full daily activities (e.g., to work a full day without special provisions); (Usual FS equivalents are one grade 5 alone, others 0 or 1; or combinations of lesser grades usually exceeding specifications for step 4.0).
5.5	Ambulatory without aid for about 100 metres; disability severe enough to preclude full daily activities; (Usual FS equivalents are one grade 5 alone, others 0 or 1; or combination of lesser grades usually exceeding those for step 4.0).

6.0	Intermittent or unilateral constant assistance (cane, crutch, brace) required to walk about 100 metes with or without resting; (Usual FS equivalents are combinations with more than two FS grade 3+).
6.5	Constant bilateral assistance (canes, crutches, braces) required to walk about 20 meters without resting; (Usual FS equivalents are combinations with more than two FS grade 3+).
7.0	Unable to walk beyond approximately 5 meters even with aid, essentially restricted to wheelchair; wheels self in standard wheelchair and transfers alone; up and about in wheelchair some 12 hours a day; (Usual FS equivalents are combinations with more than one FS grade 4+; very rarely pyramidal grade 5 alone).
7.5	Unable to take more than a few steps; restricted to wheelchair; may need aid in transfer; wheels self but cannot carry on in standard wheelchair a full day; May require motorised wheelchair; (Usual FS equivalents are combinations with more than one FS grade 4+).
8.0	Essentially restricted to bed or chair or perambulated in wheelchair but may be out of bed itself much of the day; retains many self-care functions; generally has effective use of arms; (Usual FS equivalents are combinations, generally grade 4+ in several systems).
8.5	Essentially restricted to bed much of day; has some effective use of arm(s); retains some self-care functions; (Usual FS equivalents are combinations, generally 4+ in several systems).
9.0	Helpless bed patient; can communicate and eat; (Usual FS equivalents are combinations, mostly grade 4+).
9.5	Totally helpless bed patient; unable to communicate effectively or eat/swallow; (Usual FS equivalents are combinations, almost all grade 4+).
10	Death due to MS.

Table 1.3 EDSS adapted from Kurtzke, 1983.

The multiple sclerosis functional composite (MSFC) is a disability scale developed for assessment of MS in order to overcome the limitations of the EDSS. It comprises the timed 25 foot walk (T25FW), a measure of mobility speed; the nine-hole peg test (9HPT), a measure of upper limb function; and the paced auditory serial addition test-3 (PASAT-3), a measure of information processing speed (Fischer et al., 1999). Subsequently the symbol digit modalities test (SDMT) was validated as another measure of information processing speed to replace the PASAT-3, and is preferred in some instances due to the slightly better predictive validity and relative ease of administration (Drake et al., 2010). The reported benefits of the MSFC are that the constitutive components are independent, it is sensitive to change over one- and two-year intervals and is associated with current EDSS and predictive of EDSS change, but can be prone

to learner bias (Fischer et al., 1999; Kalkers et al., 2000). The MSFC has been increasingly used as a clinical endpoint in clinical trials of MS (Meyer-Moock et al., 2014).

The final MSFC score is derived from the average of the z-scores of each component with reference to a standard population, or the study population (Tiftikcioglu, 2018). The T25FW is calculated by averaging the time it takes to complete two 25 foot (7.62 metres) walks. A 20% change in the T25FW has been validated as a significant change of mobility (Motl et al., 2017). The 9HPT is calculated by averaging the time taken to place and remove nine pegs into a grid pattern of holes. It is a unilateral measure of upper limb function and can be used as a composite score across both arms or as a unilateral score for one arm (Solaro et al., 2020). The PASAT-3 is assessed by adding up the last two spoken digits of a continuous string of numbers paced every 3 seconds for 3 minutes. The SDMT is calculated as the number of symbols able to be matched to a numbered code in ninety seconds in either a verbal or written form. A change of 4 points or 10% in the SDMT has been validated as a significant change in information processing speed in MS (R. H. Benedict et al., 2017).

1.1.4 Risk factors for MS

Whilst the exact cause of MS has proven elusive, several avenues of research have discovered a multifaceted pathophysiology including immune dysregulation, genetic and environmental factors. The presence of CNS autoreactive immune cells indicates a breakdown of central and peripheral tolerance mechanisms. This failure can result from a myriad of factors, including compromised regulatory T cell (Treg) function or resistance to autoreactive cell suppression. The interplay between environmental and genetic risk factors may influence function and activation of autoreactive cells, thus promoting the onset of disease pathogenesis (Ward & Goldman, 2022).

1.1.4.1 Genetics

Genetic predisposition contributes to the risk of developing MS. Genome wide association studies have identified more than 200 loci that are associated with an increased risk of MS (Sawcer et al., 2014). Most of the loci identified in these studies encode proteins of the immune

system, such as the HLA-DRB*1501 allele which carries the largest genetic risk of MS (Patsopoulos et al., 2013; Schmidt et al., 2007). Although most people with MS do not have a family history of the disease, an individual's risk of MS increases 10 to 20 fold with an affected first degree relative (Reich et al., 2018). Even though there have been some differences found in genetic predisposition between the phenotypes of MS (Kiselev et al., 2019), relapsing and progressive forms largely share genetic risk (Cree, 2014).

1.1.4.2 Latitude, vitamin D and sunlight

A remarkable discovery of epidemiological studies into MS risk has been the so-called latitudinal effect, such that temperate latitudes incur several fold increases in risk compared to the equator (Simpson et al., 2019). This risk is acquired in an individual's formative years. The latitude effect is thought to be mediated by environmental factors, foremost sun exposure and subsequent vitamin D metabolism, but also potentially regional genetic differences (Reich et al., 2018). Lower serum vitamin D levels and a lack of oral vitamin D supplementation have been shown to be associated with increased risk of developing MS (Miclea et al., 2020), and increased risk of disease activity (Martinelli et al., 2014; Simpson et al., 2010; W. Z. Yeh et al., 2020). The mechanism of low serum vitamin D conferred risk is unclear but several modes of interplay between vitamin D and the immune system possibly underlie it (Hart et al., 2011; W. Z. Yeh et al., 2020).

1.1.4.3 Epstein-Barr Virus (EBV)

EBV is associated with increased risk of developing MS, evidenced by higher EBV antibody titres in persons with MS (pwMS), a significantly increased rate of MS after infectious mononucleosis (Belbasis et al., 2015), as well as a temporal association with EBV seroconversion (Bjornevik et al., 2022). Studies have revealed almost all pwMS have positive EBV serology, although with a high background rate of EBV serology positivity in the healthy population, MS only manifests in a tiny proportion of EBV exposure (Sollid, 2022). This has raised the prospect of EBV being a necessary but insufficient cause of MS. Other viruses have been proposed as causative but have not been proven (Waubant et al., 2019). EBV has several effects on the immune system that may underlie its increased risk of MS, as well as increased risk with other autoimmune disorders

such as SLE (Ascherio & Munger, 2015) and immune mediated malignancies (Farrell, 2019). EBV contributes to MS likely through reprogramming of latently infected B lymphocytes and chronic presentation of viral antigens inducing autoreactivity through molecular mimicry (Soldan & Lieberman, 2023).

1.1.4.4 Metabolism, lifestyle and gut microbiome

Obesity in childhood and early adolescence is a weak risk factor for both childhood and adult-onset MS (A. K. Hedström et al., 2021). Cigarette smoking is associated with an increased risk of MS disease development, but also an increased risk of a progressive and more severe phenotype (Hawkes, 2007; A. Hedström et al., 2016). Vascular risk factors outside of smoking have also been shown to contribute to worsening neurological disability especially in progressive disease (Kappus et al., 2016). Recent study into the gut microbiome has found associations with MS disease risk at onset and progression of disease (Ochoa-Repáraz et al., 2018), potentially through immune tolerance mechanisms.

1.1.5 Pathophysiology of MS

The pathophysiological model of MS has developed in sophistication and detail over the past 25 years, and it is now clear that MS involves a complex interaction between both the adaptive and innate immune systems, compartmentalised within and migrating to the CNS, causing demyelination and axonal loss in focal and diffuse regions. There exists a spectrum of processes from acute inflammation to neurodegeneration, that are variably present at different times of the disease course, and in different degrees dependent on phenotype, although features of inflammation and neurodegeneration are present to some degree in all pwMS.

1.1.5.1 Pathophysiology of acute demyelinating MS lesions

The pathological hallmark of the disease is focal demyelinating lesions in the CNS, which occur in the white matter, cortical grey matter, deep grey matter structures of the brain or spinal cord. White matter lesions typically form around a central vein or venule (Lassmann et al., 2007), whilst cortical demyelinating lesions can be associated with focal leptomeningeal inflammation

(Lassmann et al., 2012). Although the root cause for acute inflammatory lesions has not yet been confirmed as occurring within or outside the CNS, primed autoreactive T cells migrate into the CNS through the blood brain barrier (BBB), interact with microglia and B cells and cause demyelination and axonal cleavage. CD4+ T cells (Th1 and Th17) and CD8+ T cells are both present within MS lesions, although CD4+ cells are more concentrated in the perivascular cuff, whereas CD8+ cells are widely distributed in the parenchyma (Dendrou et al., 2015; Ward & Goldman, 2022). B cells role in the disease process is likely through antigen presentation and cytokine production which can be directly oligodendrocyte toxic, more so than antibody secretion (Comi et al., 2020).

Innate immune cells are also heavily involved in acute MS pathophysiology. Peripheral macrophages infiltrate active MS lesions and remove myelin, cellular and inflammatory by-products. The resident CNS phagocytes, microglia, have widespread activation throughout the CNS parenchyma, even at remote distances from focal inflammation, as well migrating to the site of MS lesions in large numbers (Guerrero & Sicotte, 2020). Their role is complex and likely multiple activation states occur mediating both inflammation and neural protective mechanisms (Zrzavy et al., 2017). The complex interplay between glia, resident and peripheral immune cells is starting to be identified and described and will open up new avenues for therapeutic targeting (Bittner & Zipp, 2021).

Acute demyelinating lesions in the white matter may remyelinate to varying degrees after acute inflammation settles, partially mediated by anti-inflammatory microglia. In the absence of remyelination, lesions can be left as wholly denuded axons, the so-called chronic inactive lesions, or develop chronic inflammation with a more innate inflammatory milieu and slow axonal loss, the so-called smouldering or slowly expanding lesions (Reich et al., 2018).

1.1.5.2 Differing inflammatory mechanisms of progressive multiple sclerosis

Several pathophysiological features are more prevalent in progressive forms MS where neurodegeneration is more marked, mediated by inflammatory and non-inflammatory mechanisms (Correale et al., 2016; Lassmann et al., 2012).

Inflammation in progressive disease is compartmentalised within the CNS, and B cells appear to play a more significant role than other peripheral adaptive immune cells as mediators of ongoing chronic inflammation (Hemmer et al., 2002; Lassmann et al., 2012). During the early stages of the disease, B cells with clonally related Variable Heavy sequences can be found on both sides of the BBB. However, as the disease progresses, B cells in the CNS eventually form a compartmentalised population that is independent of the peripheral B cell pool (Lovato et al., 2011).

Follicle-like structures in the subarachnoid leptomeninges near inflamed blood vessels are important for the retention of immune cells within the CNS in PMS. These structures contain proliferating B cells, plasma cells, helper T cells, and follicular dendritic cells and are found in close proximity to underlying grey matter lesions and parenchyma infiltrates at different stages of development (Magliozzi et al., 2010). Follicular dendritic cells produce CXCL13, which is essential for the recruitment, maturation, and antigenic selection of B cells (Magliozzi et al., 2022). Follicle structures are present in 40-70% of SPMS cases. The structures likely result from repeated bouts of intense inflammation and can maintain a high level of humoral response independent of peripheral inflammation behind an intact BBB (Fraussen et al., 2016). Meningeal inflammation in PPMS is less clustered into follicles, but more diffuse throughout (Choi et al., 2012).

Focal demyelinating lesions in PMS have different profiles with smouldering lesions and cortical lesions being more prevalent. Smouldering lesions are frequently observed, particularly with long disease duration or at the transition to clinically progressive disease (Correale, 2014; Reich et al., 2018). These lesions are characterised by chronic inflammatory activated microglia surrounding a relatively inactive lesion centre (Prineas et al., 2001; Zrzavy et al., 2017). Increasing volume of cortical grey matter lesions is associated with progressive disease phenotype and worsening disability (see Fig. 1.2). Of the cortical lesions, subpial lesions are a unique feature of MS, not observed in other neuroinflammatory or metabolic diseases (Lassmann et al., 2007, 2012). They are particularly prevalent in progressive forms of the disease and are associated with an earlier onset of progressive disease. Subpial lesions are independent of white matter lesions and lack a high inflammatory component, including a lack of blood-brain barrier breakdown, immune cell infiltration, perivascular cuffs, or complement

activation. Instead, microglial activation appears to be the primary immune cell mediator involved in subpial lesion formation (Correale, 2014).

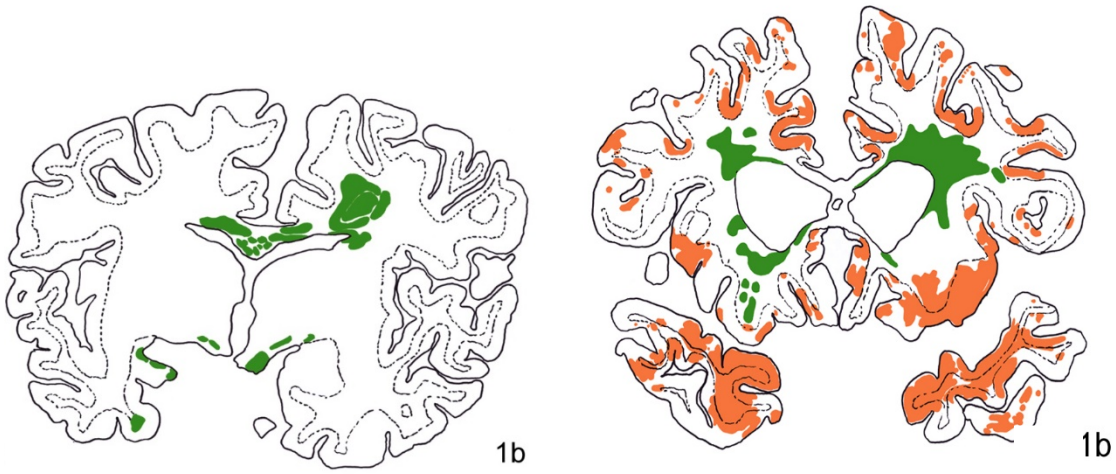

Figure 1.2 Comparison of RMS (left) and PMS (right) coronal views of the brain. Green depicting white matter lesions, and orange depicting grey matter lesions. Cortical grey matter lesions and atrophy prevalent in progressive MS. Adapted from Lassman et al. 2007.

1.1.5.3 Non-inflammatory pathogenic mechanisms of multiple sclerosis

A variety of non-inflammatory factors also contribute to CNS damage in MS, often mediating neurodegeneration. Mitochondrial dysfunction plays a central role in the pathogenesis revealed in several studies (Campbell et al., 2014). For instance, neuronal cell bodies in deep layers of the cortex have been shown to exhibit impaired functional activity of mitochondrial respiratory chain complexes, as well as alterations in motor proteins responsible for the movement of mitochondria from the cell body to axons. Furthermore in PMS, neurons in deeper cortical layers also exhibit mitochondria with mtDNA deletions, indicative of an accelerated aging phenotype (Campbell et al., 2014). The feedback cycle of mitochondrial dysfunction can be unrelenting, whereby energy deficiency leads to functional disturbance of neurons initially, followed by axonal degeneration and death and subsequent release reactive oxygen species (ROS) from impaired respiratory chain complexes leading to further mitochondrial dysfunction and mtDNA deletions (Sedel et al., 2016). Energy imbalance also leads to dysfunction of several ion channels, including Na/K ATPase, which become incapable of supporting repolarisation, and may cause the Na/Ca exchanger to reverse, increasing

intracellular Ca and causing Ca-dependent proteolytic degradation and axonal degeneration. Furthermore, demyelination leads to the anomalous distribution of Na channels, which spread across the denuded axon from nodes of Ranvier. The denuded axon then requires much higher energy to propagate depolarization, thus contributing to energy deficiency and failure (Correale et al., 2016).

Iron accumulation is also potentially an important mechanism that may exacerbate or amplify oxidative injury in MS. Iron accumulates in the aging brain and is stored in a non-toxic form in myelin, oligodendrocytes, and microglia (Hametner et al., 2013). In MS lesions, iron is liberated from these structures/cells into the extracellular space, where it can be converted into divalent ferrous forms and increase the toxicity of ROS. The liberated iron is then taken up again by microglia and macrophages and accumulates partly within these cells at the lesion margin, but is also transported into the perivascular space (Bergsland et al., 2019; Hagemeier et al., 2017; Hametner et al., 2013).

Secondary degeneration from sites of axonal damage takes the form of Wallerian (anterograde), retrograde and transsynaptic degeneration in the CNS. These mechanisms have been shown to occur in MS, and are likely the leading mediator of global neurodegeneration and atrophy (C. Wang et al., 2019). Wallerian degeneration, the degeneration of neuronal structure distal to the site of injury, is an active process which proceeds through an organised manner after axonal injury from axonal degeneration (axolemma degeneration and granular disintegration of the axonal cytoskeleton) through to myelin sheath shedding and subsequent myelin and cellular debris clearance (Vargas & Barres, 2007). The process differs in the CNS compared to the peripheral nervous system (PNS), due to a lack of BBB breakdown and maintenance of myelin structures, leading to a slower process that can take months to years to complete, and is one reason for the inhibition of axonal regeneration in the CNS (Vargas & Barres, 2007). In MS, microstructural and tract based imaging techniques have found evidence of Wallerian degeneration in vivo stemming from focal lesions (Ciccarelli et al., 2003; Fox et al., 2016; Hardy et al., 2016; Klistorner et al., 2015). Retrograde degeneration (degeneration proximal to axonal injury toward the cell body) and trans-synaptic degeneration occur in MS (Klistorner et al., 2015, 2017; Puthenparampil et al., 2017; Rocca et al., 2013), providing a mechanism for the distant effects of lesions on brain atrophy. Apoptosis underlies retrograde

and trans-synaptic degeneration as a result of absent axonal depolarisation and lack of trophic support, with demyelination preceding axonal loss seen in some disease states including MS (You et al., 2019).

1.2 Magnetic resonance imaging

1.2.1 Magnetic resonance imaging principles, theory and relaxation sequences

Magnetic resonance imaging (MRI) is an imaging tool developed through the latter half of the 20th century that has revolutionised the study of the human body and the practice of medicine, none more so than in the field of neurology and MS. MRI utilises a strong magnet to align the protons within the CNS alongside the main magnetic field. Once aligned, a radio frequency (RF) pulse is introduced, exciting the hydrogen atoms to a high-energy state. Following the RF pulse, the hydrogen atoms gradually return to their original stable status, while simultaneously releasing energy through a process known as relaxation. Two forms of relaxation exist, T1-relaxation which is the relaxation of the protons returning to their original energy state in the longitudinal direction, and T2-relaxation the transverse direction. The rate at which the hydrogen atoms relax depends on their local environment, which can be detected, creating tissue contrast. To manipulate and enhance the imaging contrast for specific tissue types, different combinations of RF pulses and gradients can be applied. By carefully adjusting these parameters, the MRI can emphasise certain physical properties unique to each tissue type ultimately enabling detailed imaging of the CNS to visualise its structure and abnormalities (Bernstein et al., 2004).

Contrast enhanced MRI is achieved by the intravenous injection of paramagnetic contrast agents, usually gadolinium-based compounds, that highlight certain structures and pathologies in the CNS including blood vessels, vascular tissues and blood brain barrier breakdown (Ibrahim et al., 2023).

The MR technique provides superior resolution and tissue contrast to the main alternate structural imaging modalities of the CNS, such as computed tomography and positron emission tomography, providing benefits for both clinical and research applications in MS (Etemadifar et al., 2021).

1.2.2 Diffusion MRI

Unencumbered water molecules randomly diffuse in 3D space according to a Gaussian distribution powered by Brownian motion. Diffusion based MRI (dMRI) exploits the restriction of water molecules to diffuse within biological tissues due to cell membranes, fibres or macromolecules that inhibit their random movement. The degree of free water restriction and directionally of the restriction give information about the microstructural features and geometric organisation of neural tissues, as well as changes in those features with physiological or pathological states. dMRI sequences are most often based on the pulsed gradient diffusion method, which consists of two strong gradient pulses separated by a set interval, the characteristics of which can be defined by the b-value and sets the degree of diffusion-weighting for the image. dMRI applications can utilise a single b-value (besides 0), so-called single shell dMRI, or multiple b-values named multi-shell dMRI. B-values usually range from 0 to 4000s/m^2. In addition, dMRI sequences are acquired from many directions providing information about the diffusion process in multiple orientations (Le Bihan & Johansen-Berg, 2012).

When there is no restriction on the orientation of diffusivity within tissue, it is described as isotropic. This holds true for free water, where there are no preferred axes or directions of diffusion. In CNS tissue the CSF and grey matter are isotropic, albeit with an overall reduction in diffusivity in grey matter compared to CSF as there is restriction imparted by the dense cellular architecture. When there is restriction to the orientation of diffusivity the tissue is said to be anisotropic, and this is properly described by the relative eigenvectors and eigenvalues and can be portrayed in the tensor (Lope-Piedrafita, 2018). In the CNS, white matter is anisotropic with the principle eigenvector (λ_1) oriented in the direction of the majority of axonal tracts that relatively inhibit the perpendicular diffusion of water due to myelin and axonal wall architecture.

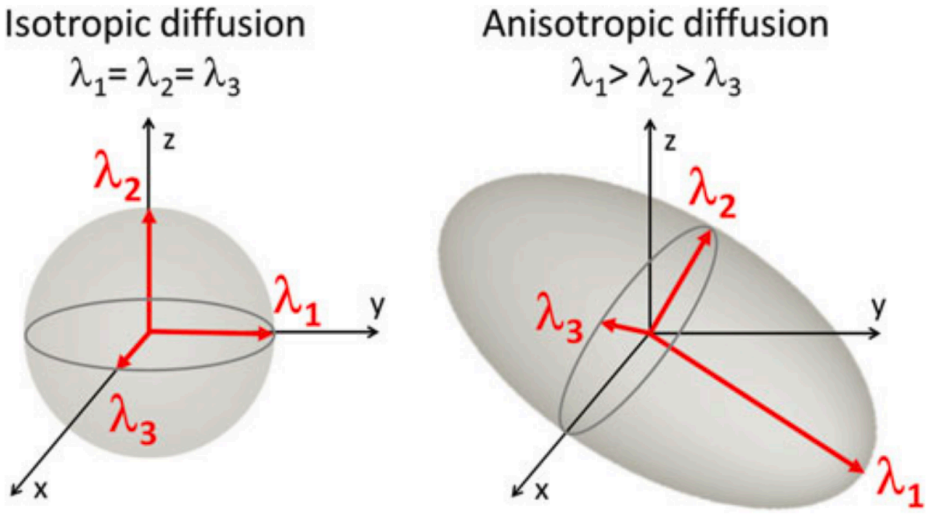

Figure. 1.3 Adapted from Lope-Piedrafita, 2018. The tensor representation of isotropic and anisotropic diffusion, with the eigenvectors and eigenvalues ($\lambda_{1\text{-}3}$) defining the tensor.

From these principle eigenvectors, several quantitative parameters can be calculated and are commonly analysed in diffusion tensor imaging (DTI) (see Fig. 1.3). The mean diffusivity (MD) or apparent diffusion coefficient (ADC) is given by

$$MD = \frac{\lambda_1 + \lambda_2 + \lambda_3}{3}$$

Fractional anisotropy (FA) measures the fraction of the diffusion signal that can be ascribed to anisotropic diffusion, given by

$$FA = \sqrt{\frac{(\lambda_1 - \lambda_2)^2 + (\lambda_1 - \lambda_3)^2 + (\lambda_2 - \lambda_3)^2}{2({\lambda_1}^2 + {\lambda_2}^2 + {\lambda_3}^2)}}$$

With isotropic diffusion the FA=0 and with increasing anisotropy the FA approaches 1.

In cases where cylindrical diffusion anisotropy symmetry is observed the axial diffusivity (AD) and radial diffusivity (RD) are often used, defined as

$$AD = \lambda_1$$

$$RD = \frac{\lambda_2 + \lambda_3}{2}$$

In the context of white matter tracts AD and RD have been suggested as putative markers to differentiate myelin loss and axonal loss. Whereas FA decreases with both myelin and axonal loss, AD reduces with axonal loss, while RD increases with myelin loss (Song et al., 2002; Yu et al., 2009), although there is evidence that RD is influenced by other mechanisms such that specificity is not high (Qin et al., 2012).

A limitation of the DTI technique is that it assumes a single dominant fibre orientation per voxel, represented by the tensor. However, save for only a few regions of the white matter such as the corpus callosum, multiple white matter fibre orientations exist within each voxel. Constrained spherical deconvolution (CSD) is a technique used to estimate the fibre orientation distribution function (fODF) in each voxel regardless of the number of underlying fibre orientations (see Fig. 1.4). The fundamental idea behind CSD is that the dMRI signal from a voxel is given by the spherical convolution of the response function of a typical biological tissue with the fODF. Therefore the desired fODF can be estimated by deconvolving the dMRI signal using an appropriate response function (Tournier et al., 2004). However, this deconvolution is an ill-posed problem due to noise and inherent limitations of the acquisition process. To overcome these challenges, CSD introduces constraints to regularise the deconvolution process such as non-negativity constraint, which assumes that the ODF should have non-negative values. The introduction of constraints in CSD greatly reduces the sensitivity to noise in the estimation process. As a result, CSD enables reliable estimation of fODF from dMRI data that is clinically feasible (Tournier et al., 2007).

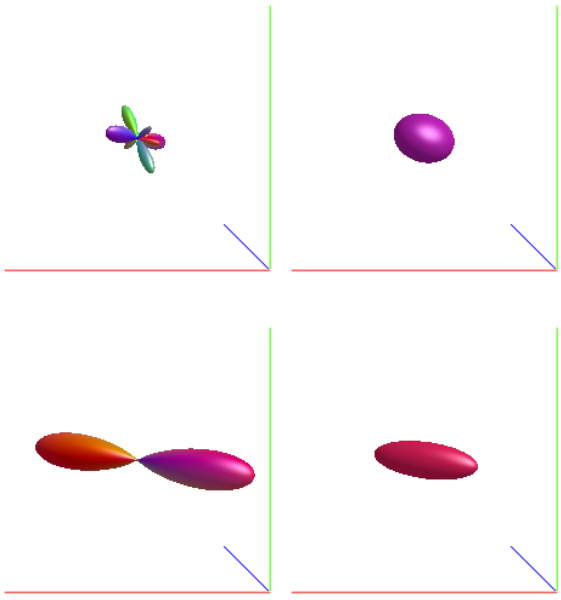

Figure. 1.4 Examples of fODF calculated using CSD and a white matter response function compared to the DTI tensor model of the same voxel. Top row is from the centrum semiovale, and Bottom row is from the corpus callosum. Left column is fODF, right column is DTI.

One application of CSD has been to derive new quantitative measures of white matter integrity, such as apparent fibre density (AFD) which is a marker of intra-axonal water volume fraction (D. Raffelt et al., 2012). The benefit of fODF derived metrics is that the AFD measurement is associated with a single fibre orientation population within the voxel, as opposed to an average of all fibre orientations inherent to DTI metrics (Jeurissen et al., 2014).

1.2.3 Tractography

Tractography is a technique used to infer the pathways of white matter tracts in the brain. It leverages the information obtained from dMRI to estimate the trajectory of fibre bundles and reconstruct the underlying anatomical connections between different brain regions (see Fig. 1.5). Tractography typically involves a number of steps (Jeurissen et al., 2019). Firstly dMRI acquisition and fibre orientation estimation provide the information about the direction of white matter fibres within each voxel. At this stage the use of CSD over DTI can extract multiple fibre orientations from a single voxel, allowing the tractography to model crossing fibres (Tournier et al., 2010). Secondly seed regions are selected to be the starting point for tracking algorithms. Seed points can be distributed randomly throughout the brain or at the grey-white matter interface for instance for whole brain tractography or specific regions for local tract reconstruction. Thirdly, starting from the seed points, tracking algorithms iteratively propagate voxel to voxel along the estimated fibre orientations to form streamlines. Several tracking algorithms exist such as probabilistic and deterministic methods, each with inherent advantages and disadvantages (Jeurissen et al., 2019). Tractography continues until specific termination criteria are met. These criteria can include reaching predefined anatomical regions, exceeding certain curvature angles and thresholds of underlying fODF amplitudes or FA values. Finally, once the streamlines have been constructed, post processing steps are helpful in filtering out spurious or improbable tracts through known anatomical or connectivity priors.

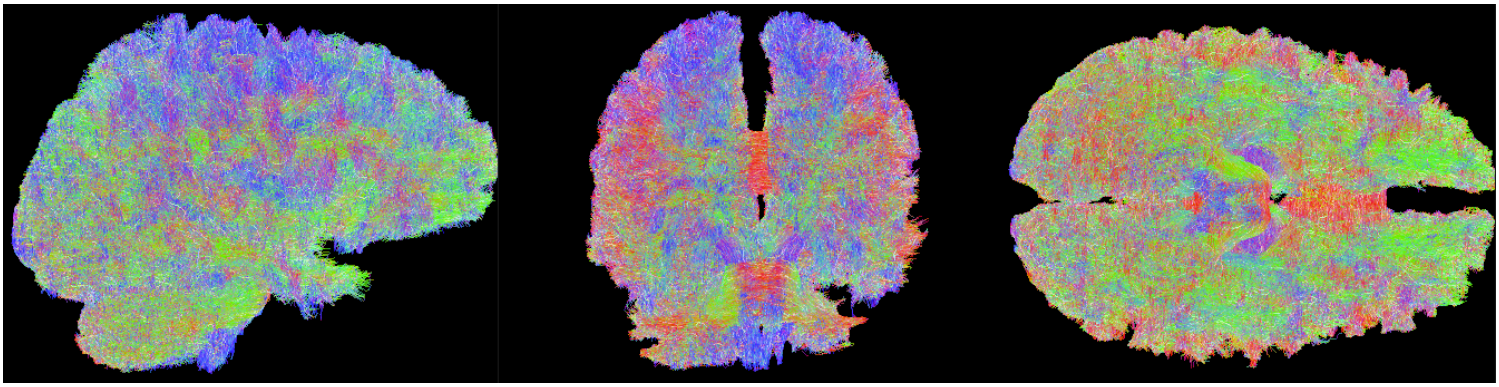

Figure. 1.5 Whole brain tractography in sagittal, coronal and axial orientation. Probabilistic tractography of 10 million streamlines, seeding from the grey-white matter interface.

Tractography has had various applications in neuroscience and MS, from reconstruction of single white matter tracts of interest (Hardy et al., 2016; Klistorner et al., 2017; Puthenparampil et al., 2017), to estimating the strength of connection between brain regions (Chen et al., 2022; Lapucci et al., 2022) finally to whole brain network based graph theory analysis (Pagani et al., 2019; Shu et al., 2018).

Tractography is still in an early stage of research (Basser, 1998; Mori et al., 1998) and clinical application in neuroscience, and has a number of limitations inherent to the technique itself (Jeurissen et al., 2019), but also its application to specific pathological brain states such as MS (Lipp et al., 2020; Zalesky, Sarwar, & Ramamohanarao, 2020). The propagation and termination criteria utilised in fibre tracking algorithms inherently rely on accurate underlying dMRI signals. However many pathological processes disturb axonal and myelin structure and interrupt the diffusion signal to such a degree that accurate white matter reconstructions can be difficult and introduce error (Filippi et al., 2001). Filtering techniques often need to take into account specific underlying pathological mechanisms, such as focal demyelinating lesions (Schiavi et al., 2020a), or surgical resection (Aerts et al., 2020). Overall, it can be said that any tractography is not universally applicable as a one-size-fits-all technique, and its reliable implementation often requires augmentation tailored to the specific pathological condition and purpose of analysis.

1.3 Organisation of structure-function topology within the brain

1.3.1 Network based structure of the brain: "The Connectome"

The structure-function topology of the brain refers to the intricate relationship between the physical organisation of the brain and its functional capabilities. The brain is a complex and highly organised collection of neurons and their connections. Understanding the structure-function topology is crucial for unravelling the mechanisms of how the brain processes information, controls behaviour and function, and generates cognition.

At a macroscopic level, the brain exhibits a hierarchical organisation. It can be divided into distinct regions, such as the cerebral cortex, hippocampus, thalamus, and cerebellum, each responsible for specific functions. Over the recent decades, the network perspective of the brain, how the distinct regions are interconnected, has had extensive study in neuroscience. The field of network neuroscience has explored the mechanisms of brain function as well as the impact that neurological disease has on brain function. A major driving force has been the application of mathematical network tools, especially measures of graph theory (Sporns, 2018).

Connectivity in the brain, or the "connectome", can be measured in two distinct ways. Structural connectivity assesses the anatomical links from region to region, most commonly through tractography, or by assessing similarity in structural features, for example with cortical thickness. Functional connectivity is assessed by looking for temporal associations in neural activity, most commonly through functional MRI (fMRI) or electroencephalography (EEG) (Chard et al., 2021). Structural and functional connectivity assess different aspects of the connectome but are interrelated, with the healthy brain showing strong correspondence between structural and functional connectivity (Schoonheim et al., 2022). In pathological brain states however functional alterations from structural damage seem to be dependent on which subnetworks of the brain are affected, with higher-order networks being potentially being more functionally susceptible to structural damage (Bartnik et al., 2022).

1.3.2 Graph theory

The main approach for describing and quantifying brain network topology is graph theory, where a "graph" represents a pairwise connectivity map of all regions of the brain. Graphs comprise of nodes representing brain regions and edges representing the connection between nodes. The healthy brain connectome reveals a combination of extensive local connectivity between neighbouring nodes, as well as shortcut connections between distant brain regions. This architecture termed "small world" is thought to allow for specialised segregated processing within local subnetworks and integrated processing between distant brain regions (Schoonheim et al., 2022). Other features of the brain's connectome have also been described including hubs which are widely connected central nodes and rich club architecture which describes a group of highly connected hubs that form an interconnected subnetwork (Fornito & Bullmore, 2015).

Graphs can be investigated at different levels of scale, with specific metrics capturing network attributes from the nodal (local) through to the whole connectome (global). Nodal measures include simple statistics such as node degree or strength, measures of how many connections individual regions have to other regions. Intermediate scales can be accessed by considering subgraphs or motifs, which are defined as subsets of network nodes whose patterns of connectivity can be classified into distinct motif categories. Global measures express network-wide attributes such as the average connections path length and related concepts such as efficiency (Sporns, 2018).

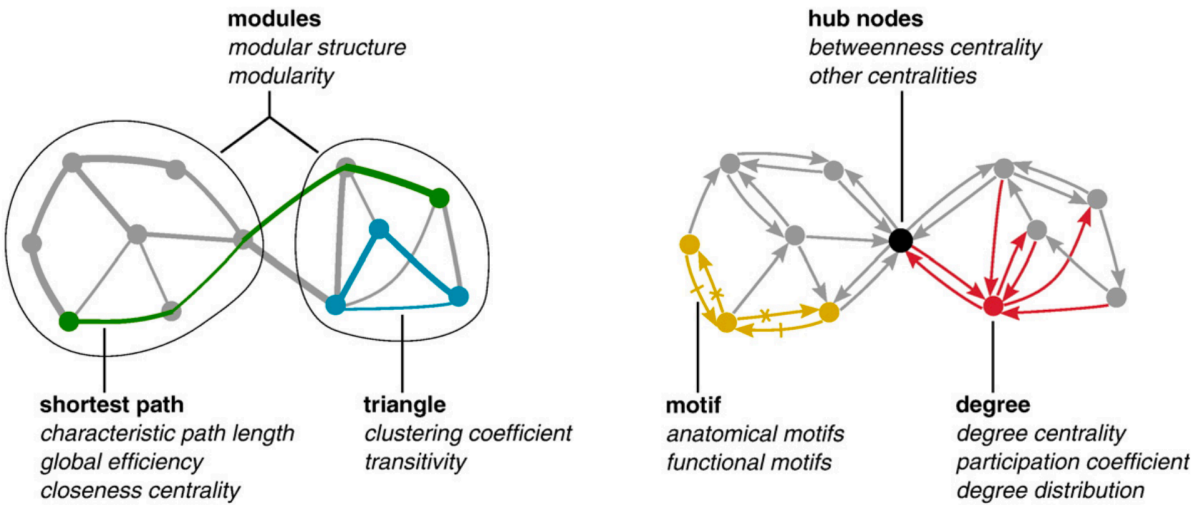

Figure. 1.6 Graph theory measures. From Rubinov & Sporns, 2010.

Figure 1.6 illustrates several common graph theory measures that can be derived from a network. In addition to simple statistics of single nodes such as degree and strength, nodes can also be characterised by their location within the wider network structure. Betweenness centrality is an important nodal feature, which measures how critical and influential a node is for information flow within the graph and is a characteristic of several brain structures including the thalamus, hippocampus, anterior cingulate cortex and insula (Schoonheim, Pinter, et al., 2021; Sporns, 2018). Damage to nodes with high centrality underlie many changes to network topology and decreased efficiency seen in disease states (Bassett & Bullmore, 2017; Power et al., 2013).

Information integration processing is measured through global efficiency and characteristic path length which describe the number of steps between nodes across the span of a network, with lower numbers of steps being defined as increased efficiency (Sporns, 2018). Most often reported as an average measure of the shortest paths in the graph (Achard & Bullmore, 2007), it can be a rather crude measure of information flow through the network, and doesn't represent multiple pathways or longer paths which may significantly contribute to integration in larger and sparser networks (Bullmore & Sporns, 2009; Estrada & Hatano, 2008).

Arguably the most unique measures in graph theory are those within the intermediate scale of network structure that describe community structure, such as modularity, clustering and transitivity. These measures are highly prevalent in brain topology, seem to be the most

biologically meaningful, and are highly specific features of network analysis with no consistent analogous measure within neuroimaging (Bullmore & Sporns, 2009; Heuvel & Sporns, 2013). The boundaries of modular partitions hold significant neurobiological importance as they serve to define nodes that are functionally related. In this way they have a crucial role in connecting communities through critical bridges and hubs and regulating information flow (Sporns, 2018). Clustering and transitivity refer to the extent to which the neighbours of a node are connected to each other, and thus form triangles or triplets (see Fig. 1.6). Community structure like this is seen as the basis of segregated specialised information processing, and a potential mediator of loss of function in states of disconnection (Schoonheim et al., 2022).

1.3.3 The "Disconnectome"

The assessment of the impact of disease on the network structure of the brain has been termed the "disconnectome" (Chard et al., 2021; Kuceyeski et al., 2018; Rise et al., 2022; Thiebaut de Schotten et al., 2015).

The application of graph theory to the brain connectome in disease states requires a high degree of interpretation. Of the several topological network features described to date it is unclear which have the greatest relevance to health and disease (Chard et al., 2021) and consideration is needed of the intent of analysis. For example, study into the pathophysiology of disease is likely to require different network analysis tools than would correlation with disability. In addition to this the selection of appropriate network models requires that the nature of the edge representation is taken into account (Sporns, 2018), for example the method of constructing the connectome of a brain with MS should contain specifics different to a case of Alzheimer's disease or indeed the healthy brain. Furthermore, particularly in disease states, paradoxical findings need to be explained rationally. For instance often reported in studies is the appearance of increased structural connectivity in comparison to healthy controls (Fleischer et al., 2017). This is difficult to coherently explain, as new axonal connections are not thought to occur in the mature CNS (Davies et al., 1997). Potentially this represents the emergence of latent network connections, but more likely is a function of bias and inaccuracy of tractography approaches in destructive pathological tissue (Chard et al., 2021).

The alteration of network topology in disease states described by graph theory is not the only method to measure the effect of pathology on white matter connections. So called disconnection syndromes describe the disconnection of paired grey matter regions that result of axonal truncating lesions, such as stroke, multiple sclerosis or trauma (Chard et al., 2021; Lapucci et al., 2022; Rise et al., 2022; Thiebaut de Schotten et al., 2015). This has been applied to specific white matter tracts with tractometry (Jandric et al., 2022; Klistorner et al., 2017; C. Wang et al., 2018; Yu et al., 2009) and whole brain tractography atlases (Kuceyeski et al., 2013, 2018).

Typical whole-brain connectomes may contain up to 120 nodes depending on the topological cortical parcellation used (Desikan et al., 2006; Fischl, 2012). Due to the resultant large number of pairwise connections in connectomes, and the potential large number of subjects included in studies, robust statistical measurements are required to control for power and family wise error rates. One such tool, the Network Based Statistic tool (NBS) combines statistical thresholding and cluster-based correction methods to control for multiple comparisons and identify robust and significant subnetworks. The NBS tool is specifically designed to identify subnetworks or modules in a network that exhibit significant differences between conditions or groups (Zalesky et al., 2010). As such it aims to answer questions such as: "Are there specific regions of the network that show different connectivity patterns between healthy individuals and patients?" or "Which nodes in the network are most strongly associated with a particular trait or behaviour?".

1.4 Magnetic resonance imaging as a biomarker in MS

1.4.1 MRI in clinical practice and therapeutic trials

MRI has become the most crucial biomarker in MS, utilised in clinical practice for diagnosis and monitoring of disease activity and safety. Guidelines for the clinical use of MRI to manage patients with MS have been developed, most recently updated with the 2021 MAGNIMS–CMSC–NAIMS consensus recommendations (Wattjes et al., 2021). These guidelines outline recommended MRI protocols at different time points of the diagnostic and monitoring process (see Table 1.4). At diagnosis this protocol facilitates the detection of MS lesion location, dissemination in space and dissemination in time, as well as MS lesion specificity. At follow-up, disease activity or active inflammation is detected through new or enlarging T2 lesions or T1-weighted gadolinium enhancement. Safety monitoring for opportunistic infections, especially progressive multifocal leukoencephalopathy (PML) in the appropriate populations, is achieved through more frequent follow-up scanning, using specific biomarkers including diffusion weighted imaging (Wattjes et al., 2021).

	Multiple sclerosis diagnosis	Monitoring disease activity	Monitoring safety of DMTs
Brain MRI sequences			
T2-weighted (axial)	Recommended (for lesion detection and morphology)	Optional	Optional
FLAIR (axial/sagittal – pref. 3D)	Recommended (for lesion detection and morphology)	Recommended	Recommended
T1-weighted (3D – high res)	Optional (for atrophy measurement)	Optional	Not required
T1-weighted (axial – post contrast)	Recommended (for disease activity)	Optional	Optional
DWI	Optional	Optional	Recommended (PML specific)
DIR or PSIR	Optional (for cortical or juxtacortical lesion detection)	Optional	Optional
SWI	Optional (for central vein sign and paramagnetic rim lesion detection)	Not required	Not required
Spinal cord MRI sequences			
At least 2 of: sagittal T2-weighted, PD or STIR	Recommended (for lesion detection and morphology)	Optional	Not required
T2-weighted (axial)	Optional (for lesion detection and morphology)	Optional	Not required
T1 weighted (sagittal – post contrast)	Recommended (for disease activity)	Optional	Not required
T1 weighted (sagittal – pre contrast)	Optional	Optional	Not required
T1 weighted (axial – post contrast)	Optional	Optional	Not required

Table 1.4 2021 MAGNIMS–CMSC–NAIMS consensus MRI protocols, adapted from Wattjes et al., 2021. DMT = disease modifying therapy, FLAIR = fluid-attenuated inversion recovery, DWI = diffusion weighted imaging, DIR = double inversion recovery, PSIR = Phase-Sensitive Inversion Recovery, SWI = susceptibility weighted imaging, PD = proton density, STIR = Short Tau Inversion Recovery, PML = progressive multifocal encephalopathy

In therapeutic clinical trials MRI biomarkers are important primary and secondary endpoints in phase 2 and phase 3 studies respectively. The most commonly used biomarkers include new T2 lesions, enlarging T2 lesions, T1 gadolinium enhancing lesions and brain atrophy measures (Pardini et al., 2019). Clinical trials in PMS have focused on MRI techniques that capture neurodegeneration i.e. whole brain atrophy (Kappos et al., 2018; Montalban et al., 2017), although more focused atrophy assessments have been suggested for this patient population such as cortical grey matter atrophy, deep grey matter atrophy and spinal cord atrophy (Ontaneda et al., 2015).

Outside of clinical and trial settings, research into the use of MRI as a biomarker for MS has advanced enormously (Gill et al., 2023). In particular, advances in understanding of the pathophysiology of progressive forms of MS have prompted the development of MRI biomarkers that represent pathological changes of neurodegeneration (Barnett et al., 2020). These include microstructural analysis of MS lesions, advanced atrophy measurement, structural tractometry, and disconnectome measurement as outlined in the sections below.

1.4.2 Lesion imaging

The pathological hallmark of MS is the inflammatory/demyelinating white matter lesion, which is typically found to be hyperintense on T2-weighted MRI. T2-weighted sequences however fail to capture much of the heterogeneity of MS lesions, such that the processes of demyelination, axonal loss, inflammatory infiltrates, oedema and gliosis may all appear hyperintense (Sahraian & Eshaghi, 2010). T1-weighted sequences have been used to differentiate some of these processes such as axonal loss, with the description of T1 black holes representing significant loss of axonal density (Bagnato, 2003; Brück et al., 1997; Lapucci et al., 2020). It follows then that T1 hypo-intense lesion volume would relate more strongly to disability than T2 lesion volume, as has been shown (Sahraian & Eshaghi, 2010; Zivadinov & Leist, 2005). Ongoing axonal loss occurs within chronic active MS lesions, which is mirrored by T1 signal reducing over time and correlates with clinical disability progression (Calvi, Tur, et al., 2022; Elliott, Belachew, et al., 2019). Axonal loss within lesions has been modelled by diffusion tensor metrics with the core of chronic MS lesions showing an increase in diffusivity, demonstrated by increased MD over time (Klistorner, Wang, et al., 2018).

Smouldering lesions or slowly expanding lesions have been identified on MRI as enlarging T2 and T1 signal change with paramagnetic rims on susceptibility weighted imaging (SWI). Pathologically these lesions show evidence of chronic inflammatory iron-laden microglia surrounding a relatively inactive lesion centre (Absinta et al., 2021; Zrzavy et al., 2017). Evidence from MR studies in MS have found these lesions to be more prevalent in PMS and associated with progressive disability (Absinta et al., 2019; Calvi, Carrasco, et al., 2022; Preziosa et al., 2021, 2022; Tozlu, Jamison, Nguyen, et al., 2021).

1.4.3 Atrophy

Brain volume loss or atrophy is considered a surrogate measure of neurodegeneration in MS and as such has prominence as a biomarker in PMS (Ontaneda et al., 2015). Several studies have found strong associations of whole brain atrophy with current and future disability in MS (De Stefano et al., 2010, 2014; Giorgio & De Stefano, 2018). In addition to whole brain atrophy, cortical grey matter and deep grey matter atrophy are associated with disability, in particular cognitive disability (Amato et al., 2007; Rojas et al., 2018; Tsagkas et al., 2020). In PMS, cervical spinal cord atrophy is more severe than is seen in RRMS and predicts decline in EDSS over 6 years better than whole brain atrophy and T2 lesion volume at baseline (Tsagkas et al., 2018). A novel biomarker named atrophied T2 lesion volume, defined as the volume of periventricular T2 lesion that is subsumed into the lateral ventricles, is more prevalent in PMS (Dwyer et al., 2018) and correlates with disability progression and conversion to SPMS (Genovese et al., 2019).

1.4.4 Structural tractography

Diffusion based tractography has been employed in the study of MS, using a variety of methods and applications. Table 1.5 lists a representative sample of studies that have employed tractography to study MS, describing the methodology used, the sample size of subjects, the main findings, whether the study was cross-sectional or longitudinal in design and if there was comparison made between MS phenotypes.

A range of methodologies have been utilised including constructions of both whole brain tractograms and individual white matter tracts. DTI and CSD diffusion modelling have both been employed with more recent studies favouring CSD based tractography methods. Both atlas based tractography, developed from healthy controls, as well as within subject tractography have been utilised. Different tractography streamline weighting algorithms have been employed including FA, COMMIT (convex optimisation modelling for microstructure-informed tractography), g-ratio, microstructural and apparent fibre density, which attempt to match the constructed tractography streamline with underlying physiological parameters.

Studies have consistently shown markers of reduced connectivity in MS, with reduced global efficiency (Bosticardo et al., 2021; Charalambous et al., 2019; Llufriu et al., 2017, 2019; Meijer et al., 2020; Pagani et al., 2019; Savini et al., 2019; Shu et al., 2011, 2016; Solana et al., 2018), reduced nodal strength (Bernabéu-Sanz et al., 2021; Charalambous et al., 2020; Has Silemek et al., 2020; Kamagata et al., 2019; Llufriu et al., 2019; Pagani et al., 2019; Schiavi et al., 2020a, 2022; Shu et al., 2016; Solana et al., 2019; Tur, Grussu, et al., 2019), reduced transitivity (Llufriu et al., 2017, 2019; Lopez-Soley et al., 2020; Pagani et al., 2019) and reduced thalamic connection (Bernabéu-Sanz et al., 2021; Bisecco et al., 2015; Bozzali et al., 2013; Charalambous et al., 2020) repeatedly reported. Community structure of modularity and clustering have had conflicting results (Boscheron et al., 2021; Bosticardo et al., 2021; Charalambous et al., 2019; Radetz et al., 2020; Tur, Grussu, et al., 2019; Welton et al., 2020), possibly explained by changes over time that are not captured in cross sectional studies (Fleischer et al., 2017).

Network studies into cognitive performance in MS, as measured most commonly by SDMT and PASAT, have implicated reduced efficiency (Savini et al., 2019; Solana et al., 2018, 2019; Welton et al., 2020), nodal strength (Solana et al., 2019), modularity (Tur, Kanber, et al., 2019; Welton et al., 2020) and small-worldness (Welton et al., 2020) as mediators of reduced processing speed; whilst local disconnection of the hippocampal networks associate with memory performance (Llufriu et al., 2019) and frontoparietal network disconnection correlate with attention and executive performance (Llufriu et al., 2017). Psychiatric symptoms of depression have been shown to be mediated by disruption of the CFPN (conscientiousness associated frontal–parietal network) (Ashton et al., 2021), right superior longitudinal fasciculus (Beaudoin et al., 2021) and hippocampal and amygdala circuits (Nigro et al., 2015).

Motor disability in MS has been shown to be mediated by global measures of reduced efficiency (Charalambous et al., 2019; Shu et al., 2011, 2016), but more robustly with disruption of the SMN (sensorimotor network) (Kamagata et al., 2019; Liu et al., 2018; Schiavi et al., 2020a) as well as transcallosal fibres (Yoon et al., 2022) and basal ganglia network (Charalambous et al., 2020).

In addition to explaining disability in MS, network neuroscience has also been employed to investigate network pathophysiological mechanisms. For instance, longer range connections (Meijer et al., 2020) as well as non-hub associated white matter tracts (Clarke et al., 2022) are associated with higher disconnection and microstructural damage in MS, suggesting a vulnerability in these brain structures to MS mediated disconnection. The accumulation of iron in deep grey matter structures is associated with microstructural damage in connected tracts, raising the possibility that increased iron concentrations and non-inflammatory neurogenerative mechanisms are in part a consequence of retrograde damage from tracts (Bergsland et al., 2017). Global dysconnectivity as measured through DTI based tractography is associated with other markers of neurodegeneration including serum NfL (neurofilament light), reinforcing its relevance in the study of MS, particularly PMS (Rise et al., 2022).

Structural connectomics has an impressive and growing evidence base in the study of MS, but despite this several limitations exist. Outside of the classification and prediction of MS phenotypes (Marzullo et al., 2019; Pagani et al., 2019; Schiavi et al., 2022), comparisons between RRMS and PMS have been underexplored. In addition, longitudinal studies of network dynamics are still rare (Boscheron et al., 2021; Fleischer et al., 2017; Rise et al., 2022). Theoretical models of progression in MS have implicated network collapse (Schoonheim et al., 2022) or loss of reserve (Krieger & Sumowski, 2018) as likely crucial steps in the disease dynamics, however the definition of these concepts have been elusive. Network neuroscience is well placed to explore these concepts though explicit study of progressive disease over longer timeframes is needed. Finally, many structural connectomic studies have neglected the specifics of MS pathophysiology when translating streamline tractography techniques developed in normal brain states to disease brain states. Further development of disease specific tractography algorithms is needed to improve the accuracy of disconnection

measurement (Lipp et al., 2020; Schiavi et al., 2020a; Zalesky, Sarwar, & Ramamohanarao, 2020).

Study	Methodology	Number of participants	Network changes reported	Cross-sectional or longitudinal	Comparison between MS phenotypes
Cognition and psychiatric symptoms					
(Tur, Grussu, et al., 2019)	CSD tractography	19 CIS 12 HC	↓ mean nodal strength in CIS Modularity neg correlated with SDMT performance	CS	N
(Bozzali et al., 2013)	ACM from DTI tractography	25 RRMS 25 HC	↓ thalamic and caudate ACM in MS Corpus callosum, cerebellum ACM correlated with PASAT performance	CS	N
(Ashton et al., 2021)	DTI tractography based atlas	32 RRMS 16 SPMS 4 CIS	Disruption of the CFPN predicted clinical depression over 5 years.	L	N
(Solana et al., 2018)	CSD tractography	91 RRMS 11 SPMS	↓ Global and local efficiency, ↑ assortativity in MS Global efficiency correlated with cognitive processing speed	CS	N
(Solana et al., 2019)	FA-weighted CSD tractography	170 RRMS 18 SPMS 45 HC	↓ Local efficiency and node strength in CI vs CP and HC	CS	N
(Kuceyeski et al., 2018)	DTI tractography based atlas	61 RRMS	Disconnections of multiple paired regions predicted impaired SDMT at 28.6 months	L	N
(Lin et al., 2008)	DTI tractography of CC	36 RRMS	CC ADC negatively correlated with PASAT	CS	N
(Savini et al., 2019)	FA-weighted CSD tractography	68 RRMS 22 HC	Global efficiency of CBL-DMN correlated with SDMT	CS	N
(Has Silemek et al., 2020)	CSD tractography	33 RRMS	↓ Nodal strength in MS vs HC	CS	N

		29 HC	Graph strength correlated with worse spatial learning, memory and SDMT		
(Fuchs et al., 2020)	DTI tractography based atlas	19 RRMS 6 PMS	Lower left precuneus/cingulate DMN disruption predicted post rehab SDMT improvement	CS	N
(Welton et al., 2020)	DTI tractography	22 RRMS 15 SPMS 23 HC	Small worldness, modularity, characteristic path length correlated with PASAT3 Small worldness, global efficiency, and characteristic path length correlated with SDMT	CS	N
(Llufriu et al., 2019)	DTI tractography	30 RRMS 21 SPMS 20 PPMS 50 HC	↓ network strength, assortativity, transitivity, global efficiency, and ↑ average path length in MS vs HC Disconnection of hippocampal network associated with worse memory performance	CS	N
(Lashkari et al., 2021)	DTI (diffusion entropy) tractography	22 MS 22 HC	↓ entropy connectivity DMN, attention, verbal memory, memory, visual-spatial memory circuits in MS vs HC	CS	N
(Llufriu et al., 2017)	FA-weighted CSD tractography	66 RRMS 6 SPMS 38 HC	↓ transitivity, global efficiency and ↑ path length in MS vs HC integrity of frontoparietal networks neg correlated with attention and executive performance	CS	N
(Beaudoin et al., 2021)	CSD tractography	24 RRMS 11 HC	↑ AFD 8 of 14 WM tracts in MS vs HC Microstructural diffusion abnormalities in right superior longitudinal fasciculus correlated with depression	CS	N
(Bisecco et al., 2015)	DTI tractography	52 RRMS 27 HC	↑ FA in thalamocortical tracts in MS vs HC WM tract DTI metrics correlated with connected thalamic DTI metrics	CS	N

			Thalamocortical tract abnormalities correlated with cognitive performance		
(Nigro et al., 2015)	DTI tractography	42 RRMS 16 HC	↑ path length in right hippocampal and amygdala circuits correlated with major depression	CS	N
(Bernabéu-Sanz et al., 2021)	DTI tractography	30 RRMS 30 HC	Thalamocortical disconnection correlated with SDMT	CS	N
(Solana et al., 2019)	FA-weighted CSD tractography	170 RRMS 18 SPMS 45 HC	↓ local efficiency and nodal strength in CP vs HC ↓ local efficiency and nodal strength of associative multimodal regions in CI vs CP	CS	N
Motor disability					
(Shu et al., 2011)	DTI tractography	39 RRMS 39 HC	↓ Global and local efficiency in MS Efficiency neg correlated with EDSS	CS	N
(Charalambous et al., 2019)	CSD tractography	58 RRMS 36 SPMS 28 PPMS 51 HC	↓ Efficiency ↓ clustering coefficient in SPMS vs RRMS vs HC ↓ Efficiency neg correlated with EDSS and pos correlated with SDMT	CS	Y
(Lapucci et al., 2022)	DTI tractography based atlas	29 RRMS 16 PMS	MS lesion DV and LV correlated with EDSS MS lesion DV predicted EDSS	CS	N
(Roca et al., 2008)	DTI tractography	12 RRMS 12 HC	↓ FA and ↑ ADC in fronto-subcortical tracts in MS vs HC PASAT correlated with FA and ADC	CS	N
(Liu et al., 2018)	DTI tractography	41 CIS 32 RRMS 35 HC	↓ inter and intra module efficiency of MS vs CIS and HC Efficiency of SMN and SMN-VN negatively correlated with EDSS	CS	Y

			Efficiency of VN, VN-SUB, DMN-FPN correlated with PASAT3		
(Charalambous et al., 2020)	CSD tractography	58 RRMS 36 SPMS 28 PPMS 51 HC	Right thalamic and putamen nodal strength neg correlated with EDSS and pos correlated with SDMT	CS	Y
(Stellmann et al., 2017)	DTI tractography	37 PPMS 21 HC	↓ rich club connectivity in PPMS vs HC and correlated with T25FW, SDMT and 9HPT	CS	N
(Shu et al., 2016)	DTI tractography	41 CIS 32 RRMS 35 HC	↓ strength, global and local efficiency and clustering in MS vs CIS vs HC Associated with PASAT3 and EDSS	CS	Y
(Schiavi et al., 2020a)	COMMIT-weighted CSD tractography	20 SPMS 22 PPMS 24 HC	↓ strength and efficiency of SMN nodes in PMS vs HC SMN modularity, density, efficiency correlated with 9HPT and T25FW	CS	N
(Kamagata et al., 2019)	g-ratio-weighted CSD tractography	14 RRMS 14 HC	↓ strength connectivity of motor, somatosensory, visual, and limbic g-ratio-weighting identified ↑ nodal strength and correlated with EDSS	CS	N
(Yoon et al., 2022)	DTI tractography based atlas	4 CIS 11 RRMS 3 SPMS	↑ IVF in TC fibres in MS vs HC ↑ IVF in TC fibres in motor disability	CS	N
(Bauer et al., 2020)	ACM from CSD tractography	46 RRMS 25 HC	↑ ACM in CST of MS vs HC ↑ ACM in left vs right correlated with motor fatigue	CS	N
Topographical organisation/MS phenotypic classification					
(Meijer et al., 2020)	CSD tractography	84 RRMS	↓ Global efficiency in MS	CS	N

		32 SPMS 17 PPMS	Long-range connection more affected by MS lesions than short range Long-range connections associated with cognition and efficiency		
(Bosticardo et al., 2021)	Microstructure weighted CSD tractography	46 RRMS 20 PMS 64 HC	↓ Global efficiency, ↑ modularity ↓ clustering in MS	CS	N
(Shu et al., 2018)	DTI tractography	41 CIS 32 RRMS 35 HC	↓ Rich club ↓ feeder and ↓ local connections in MS vs CIS and HC	CS	Y
(Pagani et al., 2019)	DTI tractography based atlas	113 RRMS 69 SPMS 45 Benign MS 50 HC	↓ Nodal strength ↓ global efficiency, ↓ transitivity in RRMS vs SPMS vs Benign MS vs HC	CS	Y
(Karavasilis et al., 2019)	DTI tractography	16 CIS 15 RRMS	↓ connectivity entorhinal and hippocampus	CS	N
(Schiavi et al., 2022)	COMMIT-weighted CSD tractography	13 RRMS 20 SPMS 22 PPMS	Accuracy for classifying MS phenotype by whole-brain network, local efficiency and node strength using machine learning of 64.5-91.1%	CS	Y
(Marzullo et al., 2019)	CSD tractography	12 CIS 30 RRMS 28 SPMS 20 PPMS 24 HC	CNN classified MS phenotypes with high accuracy Graph weighting aided the classification Local node measures were not useful in classification	CS	Y

Insights into pathophysiology					
(Rise et al., 2022)	DTI tractography based atlas	254 RRMS 25 SPMS 28 PPMS 5 CIS	GD correlated with serum NfL and age	L	N
(Clarke et al., 2022)	DTI tractography based atlas	4 CIS 11 RRMS 3 SPMS	Hub (–) WM tracts had ↑ lesion volume, ↓ ODI, NDI and ↑ IVF compared to Hub (+) WM tracts	CS	N
(Radetz et al., 2020)	DTI tractography	61 early RRMS 22 CIS	Modularity was predicted by deep grey matter volume	L	N
(Lopez-Soley et al., 2020)	CSD tractography	166 RRMS 15 SPMS	↓ cognitive reserve was associated with ↓ nodal strength, transitivity, and global efficiency	CS	N
(Fleischer et al., 2017)	DTI tractography	138 RRMS (6 cohorts based on disease duration) 32 HC	↑ modularity, local connectivity, clustering of cerebellum, cingulum and temporo-parietal regions in 1st year; with ↓ in 2nd & 3rd years	L	N
(Boscheron et al., 2021)	CSD tractography	32 early RRMS/CIS 10 HC	↑ hippocampal strength, clustering coefficient and ↓ shortest path length over 5 years in MS	L	N
(Jandric et al., 2022)	DTI tractography	102 RRMS 27 HC	Single- covariance pattern of microstructural damage appeared in all WM tracts	CS	N
(Bergsland et al., 2017)	DTI tractography based atlas	32 RRMS 25 SPMS	↑ iron concentration in deep GM is associated with DTI metrics in connected WM tracts	CS	N

		9 PPMS			

Table 1.5 Representative list of tractography studies in MS. CSD = constrained spherical deconvolution, ACM = anatomical connectivity maps, GD = global dysconnectivity, CFPN = Conscientiousness associated frontal–parietal network, MN = motor network, DV = disconnection volume, LV = lesion volume, WM = white matter, ODI = orientation dispersion index, NDI = neurite density index, IVF = isotropic volume fraction, CC = corpus callosum, ADC = apparent diffusion coefficient, PASAT3 = Paced Auditory Serial Addition Test (3-sec), FA = fractional anisotropy, CBL = cerebellum, SMN = sensorimotor network, VN = visual network, SUB = subcortical network, DMN = default mode network, FPN = Frontoparietal network, CP = cognitively preserved, CI = cognitively impaired, T25FW = timed 25-foot walk, SDMT = symbol-digit modality test, 9HPT = nine hole peg test, COMMIT = convex optimization modelling for microstructure-informed tractography (Daducci et al., 2015), CNN = convoluted neural network, IVF = isotropic volume fraction, TC = transcallosal, NfL = neurofilament light

1.5 Thesis motivation and aim

The importance of developing non-invasive biomarkers in MS, particularly in the progressive forms, is of paramount significance considering the increased understanding of neurodegeneration in MS pathophysiology and potential advancements in reparative treatments for MS. Diffusion magnetic resonance imaging (dMRI) is a proven method which has been utilised as an in-vivo indicator of microstructural damage in MS, exhibiting a resolution suitable for quantitative analysis of the underlying pathophysiological mechanisms intrinsic to neurodegeneration and disease progression, encompassing phenomena such as demyelination, axonal loss, Wallerian degeneration, retrograde degeneration, and transsynaptic degeneration. Furthermore, although the study of MS as a network disorder of the brain is still in a nascent stage, it has been proven that abnormalities in connectivity play a crucial role in disease progression and clinical manifestation. The study of connectomics in MS holds immense potential in enabling deeper understanding of the underlying disease mechanisms, resolving the clinico-radiological paradox and providing biomarkers of clinical progression.

The primary objectives of this thesis are to investigate dMRI-based models of neurodegeneration, ranging from tractometry, which focuses on the analysis of specific nerve fibre bundles, to whole brain tractography in the context of MS. Special attention will be given to the utilisation of dMRI techniques to generate biomarkers specific to progressive forms of MS. Furthermore, substantial efforts will be dedicated to refining tractography methods to accurately capture the distinctive features of MS pathophysiology.

1.6 Organisation of thesis

This thesis is organised into five chapters: one introductory and methods chapter (Chapter 1), three results chapters (Chapters 2, 3 and 4) and a summary chapter (Chapter 5). The results chapters each contain discrete studies written in a manuscript style, with multiple studies within a chapter together contributing to the focus of that chapter.

The introductory chapter, Chapter 1, provides important background information on the aetiology, pathogenesis and diagnosis of MS, with a specific focus on the unique characteristics of progressive forms of the disease. It discusses the use of MRI as a biomarker in current MS clinical practice, clinical trials and research. An introduction to network neuroscience and the techniques employed in diffusion MRI to analyse structural networks in the CNS is presented. Finally, an overview of the current body of evidence indicating structural network dysfunction in MS is presented, with a summary of deficiencies to be addressed in this thesis.

Chapter 2, the first results chapter, focuses on a study of the corticospinal tract through tractometry. The primary objective is to identify specific indicators of both Wallerian and retrograde degeneration within fibres connected to MS lesions. By employing an enhanced tractometry analysis method, the accuracy of comparator tracts is significantly improved. This refinement allows for a more robust examination that effectively distinguishes between microstructural damage directly caused by MS lesions and damage resulting from a more diffuse process. The extent of anterograde and retrograde damage is assessed in relation to intrinsic lesion damage markers, while also being investigated as a potential predictor of clinical disability in comparison cohort of RMS and PMS.

Chapter 3 investigates atlas-based disconnectome analyses in MS. The chapter comprises three studies, with the first two studies focusing on refining a novel disconnectome analysis methodology specific to MS. The culmination of these refinements is then implemented in the final longitudinal cohort study.

The initial study within Chapter 3 examines the impact of different registration techniques on the accurate registration of focal MS pathology onto health control atlas tractograms. A

cutting-edge multimodal registration method is compared against the currently prevalent registration methods to enhance accuracy and relevance in the context of MS.

The second study within this chapter introduces an innovative concept of weighting tractogram streamlines based on cumulative damage caused by MS pathology along the length of each streamline, aligning with the important principles of MS pathophysiology.

Lastly, the chapter concludes with a longitudinal cohort study that applies the refined atlas-based disconnectome method. This study investigates specific subnetworks and employs graph theory measures to assess their association with physical and cognitive disability in individuals with MS. Furthermore, the study explores the utility of network measures in predicting progression of disability in MS.

Overall, Chapter 3 presents an in-depth exploration of atlas-based disconnectome analyses in MS, encompassing refinement of methodologies, novel weighting concepts, and their practical application in understanding disability and predicting progression within the MS population.

Chapter 4, the final results chapter, focuses on the exploration of diffusion-based disconnectome modelling. It commences by conducting a comprehensive review of the advantages and disadvantages associated with diffusion-based tractography in the context of MS.

The first study within this chapter seeks to refine a pipeline of tractography based on CSD to represent the contribution of lesions to disconnection more accurately. Subsequently, the refined pipeline is implemented in a longitudinal cohort study, which explores clustering and community network structure in relation to progressive disability in MS.

In Chapter 5, the main findings of the thesis are summarised, providing a comprehensive overview of the research conducted. Additionally, potential future directions stemming from these findings are explored, highlighting areas of further investigation and potential avenues for advancements in the field.

Chapter 2

Axonal degeneration modelling in multiple sclerosis

Abstract

The mechanism of neurodegeneration and thus progression in MS remains unclear, with existing literature suggesting that neurodegeneration arises from both focal lesions and diffuse processes. Establishing a reliable biomarker to assess the neurodegenerative process would provide valuable insights into individual patients' progression and serve as meaningful endpoints for clinical trials. In this context, the use of diffusion MRI to evaluate microstructural changes in MS has garnered significant attention.

This chapter focuses on the modelling of neurodegeneration using diffusion MRI within fibre tracts connected to MS lesions, with a particular emphasis on exploring potential differences between relapsing-remitting MS and progressive MS.

2.1 Background

MS is a neurological disease with both inflammatory and degenerative components. Axonal loss within acute lesions and diffuse neurodegeneration are the main pathological correlates for, and principal drivers of, irreversible disability (Friese et al., 2014).

Although paraclinical biomarkers show detectable evidence of neurodegeneration at the earliest phases of relapsing forms of the disease (Barkhof et al., 2009; Chard et al., 2002; Petzold et al., 2010), patients with progressive forms of MS exhibit features of accelerated and more severe axonal loss, shown using surrogates such as optical coherence tomography (OCT) and magnetic resonance imaging (MRI) measurements of brain atrophy (Aymerich et al., 2017; Petzold et al., 2010; Sepulcre et al., 2006; Tovar-Moll et al., 2015). Mechanisms of axonal degeneration in MS are likely to be multiple including Wallerian (anterograde) degeneration, the apoptotic processes of retrograde and transsynaptic degeneration that stem from axonal transection within connected lesions, as well as demyelination within lesions with resultant reduction in trophic support of oligodendrocytes to connected axons (Fünfschilling et al., 2012; Haider et al., 2016; Lee et al., 2012). In addition to this, there is evidence of diffuse demyelination, microglial activation and axonal loss in normal appearing white matter (NAWM) in MS, quite separate from MRI T2 hyperintense lesions (Correale, 2014; Filippi & Rocca, 2005; Tovar-Moll et al., 2015). The relationship between focal or diffuse inflammation and neurodegenerative mechanisms is incompletely understood and there are conflicting opinions as to which process is the primary driver of axonal loss in progressive forms of MS (Friese et al., 2014).

2.2 Modelling axonal degeneration originating from lesions in the corticospinal tract in multiple sclerosis

2.2.1 Introduction

The corticospinal tract (CST) is the main neuronal pathway for higher order motor functioning directed from the cerebral motor cortex, and its involvement in MS has been studied as a predictive marker of motor disability (Hardy et al., 2016; Hubbard et al., 2016; Sechi et al., 2019; Spampinato et al., 2017; Tovar-Moll et al., 2015). The CST efferent fibres are well-defined, coherent, and longer than other defined WM bundles, making them an ideal target to study the mechanisms of lesion-related Wallerian and retrograde neurodegeneration. A robust association between MS-related damage to the CST and physical disability (Hubbard et al., 2016; Sechi et al., 2019; Spampinato et al., 2017; Tovar-Moll et al., 2015) also facilitates accurate measurement of the relative contribution of each of these mechanisms.

Diffusion MRI has the potential to model microstructural changes in the brains of patients with MS. Radial diffusivity (RD), a putative marker of myelination; and axial diffusivity (AD), a marker of axonal integrity, are the most common tensor-based metrics used (Sbardella et al., 2013). Several studies have proposed the measurement of white matter fibre tract diffusivity in relation to connected MS lesions (Bergsland et al., 2017; Hardy et al., 2016; Klistorner et al., 2015; Tovar-Moll et al., 2015; C. Wang et al., 2018; You et al., 2019). For the studies that have isolated fibre tracts that traverse lesions (lesional fibres), the comparator has been fibres that don't traverse lesions (non-lesional fibres) or entire tracts in healthy controls (Klistorner et al., 2015; Tovar-Moll et al., 2015). In the context of distinguishing between focal lesion-mediated degeneration and diffuse degeneration however, these studies might have limited value, as different tract locations are being compared. In addition, these papers have not distinguished or studied differences in relapsing (RMS) and progressive (PMS) forms of MS.

In the present study, we used novel dMRI analysis techniques to establish evidence for axonal degeneration in specific fibres connected to MS lesions with an accurate comparison based on a healthy control atlas; and to measure differences in the degree of axonal degeneration that

may exist between RMS and PMS. We hypothesised that more severe and extensive changes would be present in patients with PMS.

2.2.2 Methods

94 patients with MS (70 RMS, 24 PMS) and 41 healthy controls (HCs) were recruited after obtaining informed, written consent. The study was approved by the University of Sydney Human Research Ethics Committee (HREC number 2018/554) and was conducted according to the tenets of the Declaration of Helsinki.

Each patient with MS underwent clinical assessment with an expanded disability status scale (EDSS), including individual functional system scores (FSS).(Kurtzke, 1983) These measures were used to evaluate the degree of physical disability.

Each subject underwent MRI brain scanning on a 3T GE MR750 (General Electric, Milwaukee, WI, USA), using a multi-channel head and neck coil. The following sequences were acquired: 3D Fluid-Attenuated Inversion-Recovery (FLAIR); (TE/TI/TR=120/2100/8500 ms; 1.2mm isotropic acquisition matrix; FA=90^{o}; ETL=24); 3D high resolution T1-WI (T1) using fast spoiled gradient echo (FSPGR) with magnetization-prepared inversion recovery (IR) pulse (TE/TI/TR=3.2/900/8.2 ms, 1 mm isotropic acquisition matrix, FA=10^{o}) and axial Diffusion weighted imaging (DWI) (TE/TR=82/8325 ms) with a uniform gradient loading (b=1000s/mm 2) in 64 directions with each direction containing 68 slices in 2mm thickness to cover the entire brain (with additional two b0 imaging prior to with gradient loading acquisition), 256mm FOV and 128x128 matrix with 100% phase FOV.

DWI sequences were pre-processed with denoising, Gibb's ringing removal, and B1 field inhomogeneity correction utilising MRtrix3 standard pre-processing pipeline (Tournier et al., 2019). Susceptibility distortions were corrected utilising reversed polarity phase encoding ("blip up" and "blip down") EPI sequences and combined with eddy correction with FSL tools implemented within the MRtrix3 software platform (Andersson et al., 2003; S. M. Smith et al., 2004; Tournier et al., 2019). T1 and FLAIR sequences were co-registered to diffusion space using linear registration with FLIRT (Jenkinson et al., 2002) from FSL and checked for quality assurance.

T2 weighted MS lesions were segmented on the co-registered FLAIR using semi-automated edge detection contouring/thresholding as previously described (Zivadinov et al., 2012). Gadolinium-enhancing lesions within the CST were excluded, so as to limit the analysis to non-acute chronic lesions.

A measure of the degree of T2 lesion damage was calculated using the T1 image hypo-intensity as this has been shown to be a robust marker of axonal loss within MS lesions (Elliott, Belachew, et al., 2019; Filippi et al., 2012; van Waesberghe et al., 1999; van Walderveen et al., 1998). To achieve this the T1 sequences were corrected for B1 field inhomogeneity using the N3 correction and processed with a normalisation tool implemented by the Freesurfer program (Dale et al., 1999; Sled et al., 1998) as described previously ('MSVirtual 2020 – Poster Abstracts', 2020). This technique linearly normalises the T1 images by mapping the average NAWM to a value of 110 and average CSF to a value ~35.

In order to create a control dataset appropriate for analysis of focal regions of interest for each patient, Z-score maps were created for each DWI tensor metric of AD, RD, mean diffusivity (MD) and fractional anisotropy (FA) within the patient space. Firstly, the FA map from all HCs were individually registered to the patient FA map using ANTs (B. Avants et al., 2008; B. B. Avants et al., n.d.; Klein et al., 2009). The AD, RD and MD tensor metric maps were then transformed using this warp, utilising nearest neighbour interpolation. Subsequently, the 41 HC tensor metric maps were combined to create voxel-wise average and standard deviation maps for all HC data (S. M. Smith et al., 2004) in each patient space. A z-score map could then be created for each patient by subtracting the patient derived tensor metric map from the HC average divided by the standard deviation map, using FSL tools (S. M. Smith et al., 2004).

The program TractSeg (Wasserthal et al., 2018) was used to segment the CST fibre bundles within all patients. Final CST streamlines were checked and cleaned for extraneous streamlines by an experienced analyst. T2 lesions overlying the CST segmentation were identified using FSL tools (S. M. Smith et al., 2004) and given a unique identifier. CST streamlines were further segmented into streamlines that traversed a T2 lesion, herein called lesional fibres, and streamlines that did not traverse any lesions, herein called non-lesional fibres, using the tckedit tool of MRtrix3 (Tournier et al., 2019). In patients with multiple lesions within the CST, lesional

fibres were carefully examined and excluded if they traversed more than one lesion over their length, thereby reducing potential confounding effects generated by separate focal lesions when assessing lesion-related diffusion changes in NAWM. The lesional and non-lesional fibre tracts for each patient were utilised for tract profilometry (Jeurissen et al., 2019) by the Automated Fiber Quantification (AFQ) tool (Yeatman et al., 2012). This tool was used as it computes metrics as a function of arc length along tract-specific exemplar tracks, which minimise and downweigh values at the edge of streamline fibre bundles, and therefore weights the values of a streamline bundle from the centre out. Four locations along the length of the CST were defined in relation to each T2 lesion identified from co-registered FLAIR imaging. To standardise these regions of the CST between subjects of different brain size, each tract was divided into 100 evenly spaced "nodes" along its length, with the four regions being defined as (A) a region comprising 10 adjacent nodes, separated from the superior edge of the lesion by 5 nodes, named "close retrograde", (B) the site of the lesion, (C) a region comprising 10 adjacent nodes, separated from the inferior edge of the lesion by 5 nodes, named "close Wallerian" and (D) a site comprising 10 adjacent nodes, separated from the inferior edge of the lesion by 40 adjacent nodes, named "distant Wallerian" (See Figure 2.1). AD, RD, MD and FA values from underlying z-score maps were calculated at these four regions along the length of the CST lesional fibres. To account for potential diffuse differences in tensor metrics between subjects (unrelated to focal damage connected to lesions), the non-lesional fibre z-score value was subtracted from the lesional fibre z-score value at the same location along the CST. This ensured that diffuse changes associated with factors such as age or more advanced disease did not influence the measurement of focal damage from individual lesions.

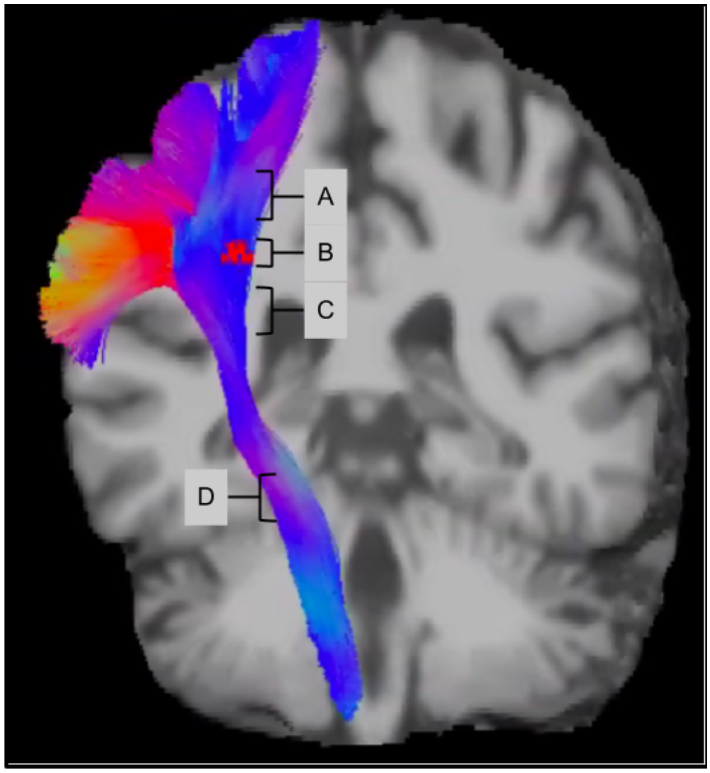

Figure 2.1 TractSeg CST reconstruction with streamline colours representing directionality. T2 lesion shown in red within the CST. The four regions of interest along the CST are shown (A) close retrograde, (B) lesion, (C) close Wallerian (anterograde) (D) distant Wallerian (anterograde).

The resultant z-score diffusion metrics along the CST were assessed by way of comparison to the standard value of 0 by either one-sample Student's t-test or Wilcoxon signed rank test dependent on normality testing. Furthermore, multiple linear regression models were created to explore the relationship between diffusion metrics, lesion characteristics and clinical and demographic data. GraphPad Prism 9.0.0, GraphPad Software LLC and SPSS version 27 (IBM SPSS Statistics 27, IBM©, Armonk, NY, USA) were used for analyses.

2.2.3 Results

A total of 80/94 patients (61 RMS, 19 PMS) had lesions within the CST that were appropriate for inclusion in the study. Demographic characteristics are shown below in Table 2.1.

	RMS	PMS	Controls
Number	61	19	41
Age years			
mean	41.1	51.4	36.4
Std. dev	9.2	9.4	10.6
Gender female n (%)	41 (67%)	10 (53%)	27 (66%)
Disease duration years			
median	5	6	NA
IQR	2 - 12	2 – 20	NA
Disease course	61 RRMS	8 SPMS/11 PPMS	NA
EDSS			
median	2	5	NA
IQR	1 – 3.5	4 - 6	NA
Pyramidal FSS			
median	1	3	NA
IQR	0 - 2	2.25 - 3	NA

Table 2.1 Demographic characteristics

For all patients the diffusion characteristics of lesional and non-lesional fibres along the CST were calculated. All datasets failed to pass Shapiro-Wilk normality testing. Thus, a non-parametric test for non-gaussian data (Wilcoxon signed rank test) was used to compare to the hypothetical median of HCs; and the Mann-Whitney test used for comparison of RMS and PMS cohorts.

Diffusion metrics are shown in Figure 2.2. Significant differences at a population level for all metrics were found at the lesion region compared to HCs. In the close Wallerian region, MD and RD were increased compared with HCs, with no significant difference between RMS and PMS cohorts. AD in this region was reduced in PMS compared with RMS and HCs. At the distant Wallerian location, RD was increased in all patients compared with HCs, with no significant differences between PMS and RMS cohorts. FA at the distant Wallerian location was reduced

in PMS patients compared to HCs, with no significant difference between RMS and PMS. There were no significant differences in AD or MD at this location between MS patients and HCs, or between RMS and PMS patients. At the close retrograde region, AD was reduced relative to HCs in both RMS and PMS with no difference between them. FA at this location was decreased in PMS compared to HCs, but not compared to RMS. RD was decreased in PMS patients only, whilst MD was increased in RMS patients only compared with HCs. See Figure 2.2 for dot plot distributions and significance.

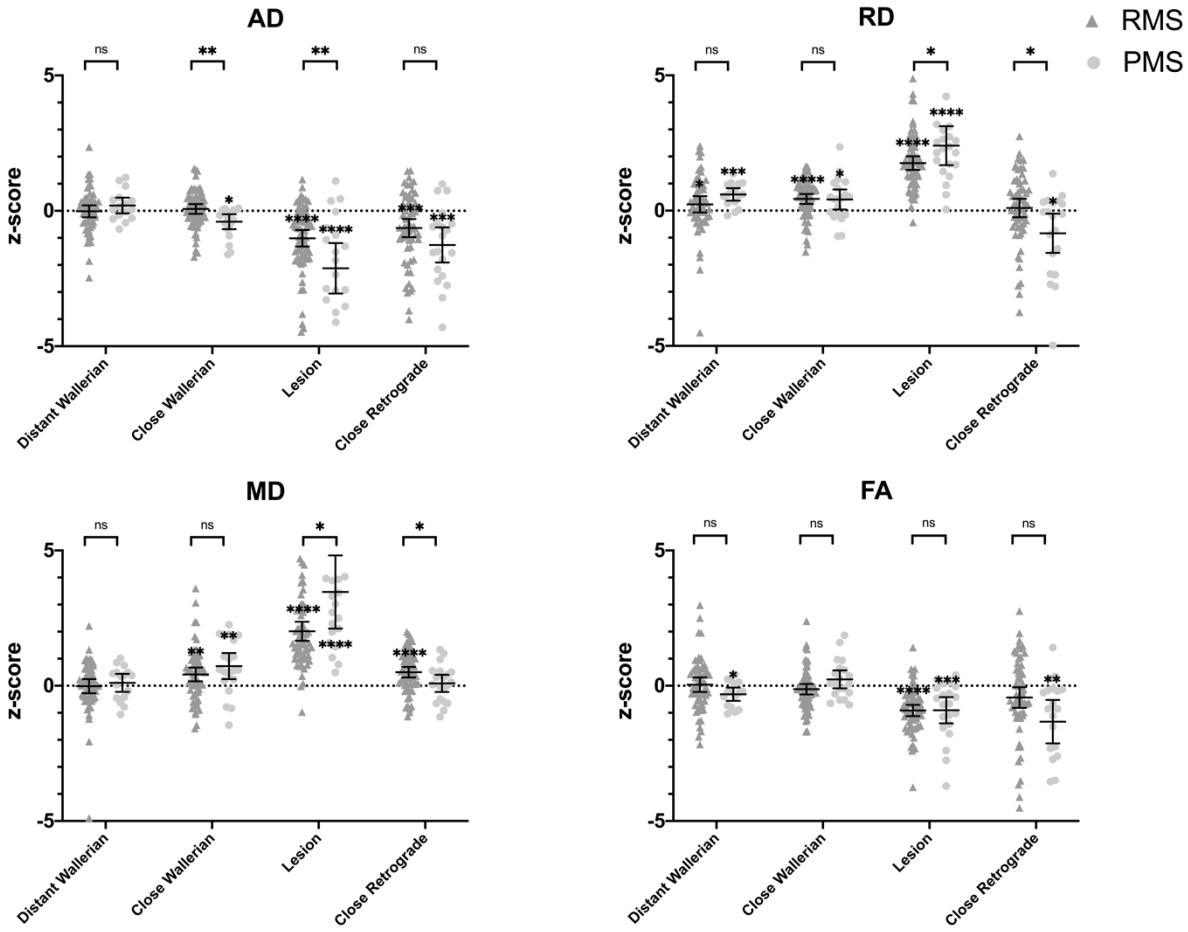

Figure 2.2 Dot plots showing z-scores for each tensor metric (AD, RD, FA, MD) for RMS and PMS cohorts at each location along the CST. Bar graphs representing median and 95% confidence intervals are shown. Significant differences are shown for each cohort at each location and comparing RMS and PMS at each location; * $p < 0.05$, ** $p < 0.01$, *** $p < 0.001$ & **** $p < 0.0001$.

A multiple linear regression was carried out to investigate whether the diffusion metrics seen in the close Wallerian region of each lesion of PMS and RMS patients could be predicted using the factors of lesion T1 lesion hypointensity, T2 lesion length, Gender, Disease duration, Age, EDSS and the pyramidal FSS score of the EDSS. The results of the regression of PMS patients

indicated that the model explained 42.2% of the variance and was a significant predictor of AD in the close Wallerian region F(6, 48) = 5.83, p=0.0001. The factors contributing significantly to this regression were T1 lesion hypointensity (β=0.398 p=0.001), disease duration (β=-0.174, p=0.02), pyramidal FSS (β=-0.305, p=0.02) and an interaction factor of gender and disease duration (β=0.506, p=0.02). The T2 lesion length (β=0.121, p=0.336) and the lower order gender factor (β=-0.045, p=0.79) did not contribute significantly. Including EDSS in place of the pyramidal FSS score produced an inferior regression model and was not significantly contributory. The inclusion of age in the regression model did not improve the explanatory power; and had high parameter covariance with disease duration. Normality of residuals was confirmed with Shapiro-Wilk testing (p=0.50). See regression equation below and Fig. 2.3.

$$AD_{\,close\ wallerian\ PMS\ patients} \sim -4.925 + 0.04.T1\ lesion_{\,hypointensity} + -0.02.Disease\ Duration_{\,years} + -0.07.Gender + -0.5.PyrFSS + 0.862.T2\ lesion_{\,length} + 0.04.Gender * Disease\ Duration_{\,years}$$

For RMS patients the regression did not significantly explain the variation in AD in the close Wallerian region, p=0.8939.

No regression model was sufficient to explain other diffusion metrics at any site.

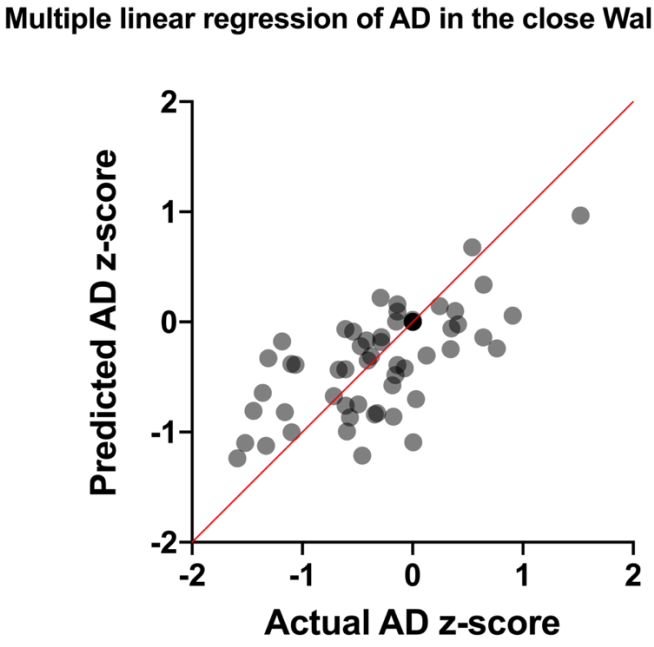

Figure 2.3 Multiple linear regression model dot plot of actual vs predicted AD close Wallerian value. The line of identity is shown in red.

An interaction plot (see Figure 2.4) was created to explore the interaction effect of gender and disease duration seen in the regression. This showed significantly different slopes between males and females with regard to disease duration and predicted AD close Wallerian metric ($p<0.001$), with the disease duration of males having a more significant effect on predicted outcome.

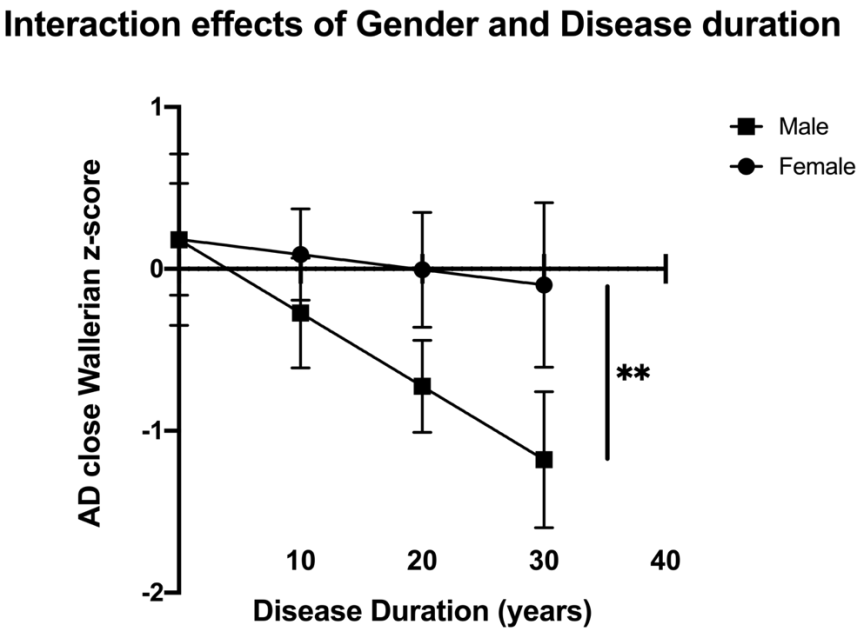

Figure 2.4 Interaction plot of the interaction factor of gender and disease duration on predicted AD close Wallerian value. ** $p < 0.01$

A multiple linear regression was also carried out to investigate whether any diffusion metric in the close Wallerian region could add to prediction of EDSS using the factors of T1 lesion hypointensity, Gender, Disease duration and Disease course (RMS vs PMS). To achieve this, the diffusion metrics and T1 lesion hypointensity were weighted by the percentage of streamlines intersected by the lesion; and then summated within each patient to create patient-wise measures to contribute to the regression model of EDSS. The results of this regression indicated that the model explained 49.28% of the variance and was a significant predictor of EDSS $F(5, 77) = 14.96$, $p<0.0001$. The factors that contributed significantly to this regression were disease course of PMS ($\beta=0.525$, $p<0.0001$), disease duration ($\beta=0.234$, $p=0.007$) and weighted average AD close Wallerian region ($\beta=-0.195$, $p=0.040$). Weighted average T1 lesion hypointensity ($\beta=-0.163$, $p=0.08$) and gender ($\beta=0.117$, $p=0.15$) did not significantly contribute.

Normality of residuals was confirmed with Shapiro-Wilk testing (p=0.50). See regression equation and Fig. 2.5 below.

$$EDSS \sim 1.263 + 2.23.\,Disease\ Course_{PMS} + 0.06.\,Disease\ Duration_{years} + -0.02.\,T1_{hypointensity} + -1.52.\,AD_{close\ wallerian} + 0.43.\,Gender$$

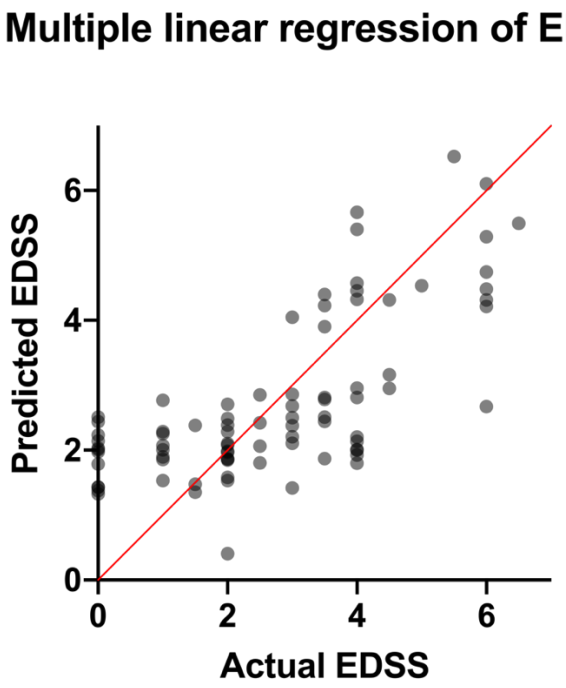

Figure 2.5 Multiple linear regression model dot plot of actual vs predicted EDSS.

A similar regression model was created to predict pyramidal FSS score with the same input metrics. This explained 29.8% of the variance of pyramidal FSS and also had disease course of PMS as a significant contributor, but no diffusivity metrics significantly contributed. (equation not shown).

2.2.4 Discussion

In summary, we found changes of diffusion MRI within lesional fibres in NAWM tracts, providing evidence of neurodegeneration both proximal and distal to MS lesions. Within the context of majority efferent fibres of the CST, this provides radiological evidence for both Wallerian and retrograde degeneration. Specifically, increased RD of lesional fibres was maintained at both sites distal to MS lesions, the close and distant Wallerian regions, without differences between RMS and PMS seen. Reduced AD in the close Wallerian region was restricted to the PMS cohort and, as such, is a candidate biomarker of progressive disease. The validity of this biomarker is also supported by its association with lesion T1 hypointensity, an indicator of the severity of axonal loss within lesions; and with disability as measured by the EDSS score. In the region proximal to MS lesions, the retrograde region, AD was reduced in both RMS and PMS cohorts without difference between them, while there was reduced RD in the PMS cohort as compared to HCs and the RMS cohort. Detailed discussion of these results is given below with a background of the use diffusion-based microstructural techniques in MS.

2.2.4.1 Wallerian and retrograde degenerative mechanisms

Wallerian and retrograde degeneration are active processes that occur within the central nervous system (CNS) after axonal injury. Most studies into the mechanisms and timing of Wallerian and retrograde degeneration have been undertaken in animal models of acute injury. These models show that Wallerian degeneration is characterised by rapid axonal degradation occurring between 1 and 7 days after injury in both the CNS and peripheral nervous system (PNS) albeit with slower progress in the CNS. Myelin breakdown, microglial/macrophage activation, clearance of tissue debris and gliosis occur at a significantly slower rate within the CNS, with retention of some neural architecture up to months or years after injury (Buss & Schwab, 2003; George & Griffin, 1994; Vargas & Barres, 2007). Retrograde degenerative mechanisms, either in the proximal portion of the axon or in the trans-synaptic connected neurons, are less well understood but are likely to include apoptosis due to loss of terminal synapses and reduction in target derived trophic factors (Peterson et al., 2001). In addition, there is evidence that demyelination as opposed to axonal degeneration may be the earliest event in transsynaptic degeneration (You et al., 2019) Proximal portions of the axon are stable

for longer than distal portions via these mechanisms of Wallerian and retrograde degeneration (Conforti et al., 2007).

2.2.4.2 Diffusion MRI correlation with neurodegeneration

Several correlation studies have attempted to analyse the alterations in MR diffusion metrics that accompany pathological changes in the brain (Budde et al., 2009; Qin et al., 2012; Song et al., 2002; Yu et al., 2009). In the majority, the pathological substrate has been acutely destructive lesions such as stroke or surgery, limiting applicability to the modelling of MS pathology. Interpretation of the results of these studies has also been incongruent; for example, some studies have attributed increased RD to demyelination which facilitates the perpendicular diffusion of water (Song et al., 2002; Yu et al., 2009). However other studies suggest that RD is not only determined by myelin content but also by axonal degeneration, microglial activation, inflammation and myelin and axonal debris (Qin et al., 2012). One suggested mechanism for increased RD in axonal degeneration is the increase in water transfer between intra- and extra-cellular locations due to loss of the axon cell wall architecture (Qin et al., 2012). AD is likely to be a more specific measure of axonal degeneration, with robust measurement across a number of studies including experimental autoimmune encephalomyelitis (EAE) mouse models of MS (Budde et al., 2009; Qin et al., 2012; Yu et al., 2009). FA and MD are potentially less specific metrics; and are perhaps redundant as they are functions of the primary eigenvectors modelled in RD and AD (see Section 1.2.2) (Klistorner et al., 2015). Unfortunately, as well as lacking specificity for myelin and axonal integrity, these metrics also suffer reduced sensitivity in regions of the brain that have crossing fibres (Farquharson et al., 2013) and region-specific variation that renders whole brain measures imprecise. Still, AD and RD are common tensor-based metrics used in the study of MS (Sbardella et al., 2013).

2.2.4.3 Methodology rationale

In this study, Wallerian and retrograde degeneration were identified using a refined technique that separates lesional and non-lesional fibres and compares their difference with equivalent focal regions in HCs. Two normalisation steps were utilised to account for global changes in

diffusivity between subjects and regional differences in diffusivity within subjects, respectively. Firstly, measuring the difference between lesional and non-lesional fibres accounts for changes in diffusion measures between patients that are not related to focal lesions (Klistorner et al., 2015). Secondly, the use of HC references allows for normalisation of diffusion measures between different locations in the brain that vary significantly, overcoming the imprecision of whole brain or whole tract measures (Ashton et al., 2021). Our use of the CST in this study allows for a clear distinction between anterograde and retrograde directions, as most fibres within the CST are unidirectional efferent upper motor neuron axons projecting from the cortex to the spinal cord.

2.2.4.4 Wallerian degeneration markers

In this study, increased RD, decreased FA and increased MD in the close Wallerian region confirm diffusivity changes in lesional fibres in otherwise NAWM. These changes were seen across both RMS and PMS cohorts and did not differ significantly between them. In addition, a reduction in AD in the close Wallerian region was restricted to the PMS cohort. The distant Wallerian region showed a similar increase in RD in both RMS and PMS; and a reduction of FA in PMS that did not significantly differ to RMS. These changes in RD may represent a distal marker of demyelination/axonal degeneration within lesional fibres and provides evidence of Wallerian degeneration in continuum with the close Wallerian region. However, we did not find distal changes in other diffusion metrics such as AD. Isolated increases in RD at the close and distant Wallerian regions has several potential explanations. First, there is evidence that (non-inflammatory) demyelination may precede axonal degeneration, moving distally along fibre tracts at a gradual pace, with trans-synaptic degeneration (You et al., 2019). Second, although most models of neurodegeneration have described changes within days to weeks of acute injury (such as stroke or surgery), and are potentially relevant to the acute MS lesion, this timing is less relevant to established chronic MS lesions, in which gradual axonal attrition may continue for many years (Elliott, Belachew, et al., 2019; Klistorner, Wang, et al., 2018). Wallerian degeneration within the CNS itself can progress over years as opposed to the weeks seen in the peripheral nervous system (PNS) (Vargas & Barres, 2007). The prolonged period that occurs between axonal degeneration and cellular and myelin debris clearance in the CNS (Vargas & Barres, 2007) may increase water diffusion between intra- and extra-cellular locations due to

loss of the axon cell wall architecture (Qin et al., 2012), while preserving parallel water diffusion due to persistent myelin structure orientation, thus increasing RD but preserving AD. A prolonged latency of neurodegeneration in MS, and heterogeneity of the age of individual lesions, may therefore have rendered the neurodegenerative process in our cohort incomplete, obscuring any effect on AD change in the Wallerian region. However, the lack of distant change of AD even in patients with a longer disease duration, a surrogate of lesion age, does not support this hypothesis. A further explanation of the changes seen at the distant Wallerian region is related to the methodology used in this study. The implementation of TractSeg in this study used probabilistic tractography to generate streamlines for the fibre bundles of the CST. Probabilistic tractography tends to generate a splaying of streamlines the further it travels within a bundle, losing some of the topographical information the further away from the region of interest (ROI) the tract is studied. Measurements closer to the ROI (in this case the lesion) are likely to be more accurate in their distinction between lesional and non lesional fibres (See Figure 2.6). Finally, this data suggests that RD is a more sensitive (albeit less specific (Qin et al., 2012) marker of axonal degeneration and demyelination, which is able to overcome the inaccuracies introduced by probabilistic tractography in the distant Wallerian region. This is in line with previous evidence that RD is a more sensitive marker of axonal degeneration in the CNS (Qin et al., 2012). This hypothesis is supported by the greater values for RD z-scores compared to AD z-scores within lesion and close Wallerian regions, suggesting higher sensitivity (RD lesion z-score median 1.765 vs. AD lesion z-score median-1.285).

2.2.4.5 AD reduction in the close Wallerian region as a biomarker of progression

This study also revealed a marker of axonal degeneration (reduction in AD in the close Wallerian region) that appears to be restricted to the PMS cohort, providing a plausible explanation of accumulating lesion-related disability in patients with PMS. Furthermore, the observed AD reduction in the close Wallerian region in patients with PMS was correlated with a marker of lesion destructiveness, namely T1 hypointensity. Three further factors also significantly contributed to the regression model of close Wallerian AD reduction, including disease duration, pyramidal FSS score and an interaction factor of gender and disease duration. In particular, longer disease duration was significantly correlated with worsening axonal degeneration as inferred by reduced AD, corroborating previous reports of accelerated brain

atrophy and disability accumulation in patients with PMS (Ge et al., 2000). In PMS, prolonged exposure to an altered microenvironment may render denuded axons more vulnerable to neurodegeneration, while a synergistic impact of aging and MS pathology may further accelerate the process.

Conversely, absolute age, above and beyond disease duration, did not significantly contribute to the model. This suggests that the length of time with MS, perhaps being a surrogate of lesion age, has more influence on neurodegeneration than does biological age. Interestingly, the correlation with disease duration was gender-specific, as shown by the regression model's interaction term and interaction plot. Compared to female subjects, male subjects showed worsening AD reduction in the close Wallerian region with increasing disease duration. This finding corroborates previous reports of accelerated progressive tissue loss in MS lesions (Klistorner, Wang, et al., 2018) and more rapid accumulation of disability (Confavreux, 2003) in male patients with PMS. Predictably for a marker of axonal degeneration, the pyramidal FSS score correlated with AD in the close Wallerian region, as axonal degeneration is suggested to be the main pathological correlate of irreversible disability.

AD in the close Wallerian region, measured as a weighted patient-wise metric across all MS patients, also contributed significantly to the regression model of EDSS, as might be expected for a marker of axonal degeneration; while the weighted patient-wise metric of lesion T1 hypointensity did not ($p=0.08$). The non-orthogonality of these two metrics likely contributed to the lack of significance of both variables as predictors within the same regression, however this data suggests that AD in the close Wallerian region of lesional fibres is potentially a more sensitive marker of clinically relevant neurodegeneration; and provides more explanatory power for eloquent disability measures than does lesion T1 hypointensity, an established MRI marker of tissue damage (Elliott, Belachew, et al., 2019; Filippi et al., 2012; van Waesberghe et al., 1999; van Walderveen et al., 1998).

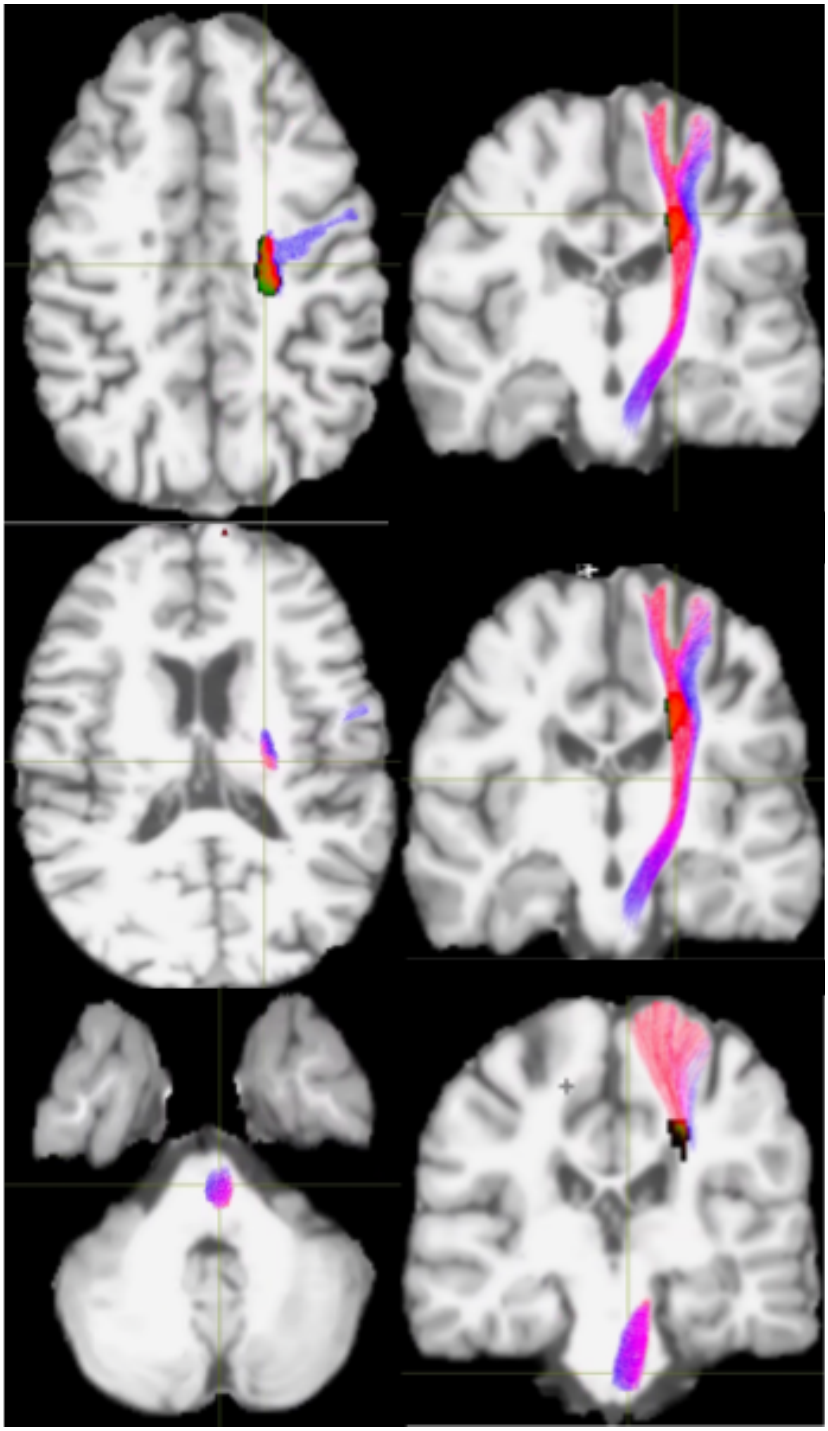

Figure 2.6 Lesional (red) and non-lesional (blue) fibres of the CST shown at three levels in axial and coronal orientations. At the site of the lesion (green) clear demarcation between lesional and non-lesional fibres is seen. At the close Wallerian region this demarcation is maintained. At the distal Wallerian region, the demarcation of lesional and non-lesional fibres is largely missing, due to the splaying of streamlines.

2.2.4.6 Retrograde degeneration markers

The results at the close retrograde degeneration region showed a reduction in AD suggesting evidence of axonal degeneration in the retrograde direction proximal to the lesion, and a decrease in FA and increase in MD suggesting more nonspecific microstructural damage. However, an increase in RD was not seen, which would be expected if the AD changes were reflecting preceding demyelination prior to axonal loss. This pattern of diffusivity change might be representative of specific mechanisms of retrograde neurodegeneration. For instance, fragmentation of the axon/myelin bundle along the length of the axon would restrict water diffusion in the longitudinal direction causing reduced AD, while maintaining the boundaries that restrict perpendicular water diffusion and restrict RD. Fragmentation has been described in both Wallerian and retrograde neurodegeneration (Öztürk et al., 2013), however it is an acute and transient phenomenon that is unlikely to be captured in the context of connections to chronic MS lesions. Evidence that MS related trans-synaptic neurodegeneration is preceded by demyelination (You et al., 2019) would have predicted a greater change in RD as opposed to AD in this region. Furthermore, evidence that proximal portions of axons are likely to be preserved longer than distal portions (Conforti et al., 2007) would predict a greater deviation of AD z-scores at the Wallerian in comparison to retrograde regions, but the opposite was seen. (AD close Wallerian median z-score -0.13 vs AD close retrograde median z-score -1.23). In addition, differences between RMS and PMS cohorts showed a relatively reduced MD and RD in the PMS cohort, suggesting reduced demyelination and microstructural damage in patients with PMS.

Given these incongruities, it does not seem plausible that the pattern of diffusivity changes seen in this study at the close retrograde region reflect a specific mechanism of retrograde degeneration. A more likely explanation is related to the complexity of CST anatomy and methodology of the study. Proximal to lesions the CST is more likely to fan out to the motor cortex, thereby spreading the tractography over a broad region, incorporating the crossing fibres of the centrum semiovale. This broad fanning out reduces the coherence of the CST bundle and is prone to inaccurate voxel wise diffusion measurements of the lesional and non-lesional fibres. Evidence for this can be seen with the increased interquartile range of values seen at the close retrograde region for all diffusion metrics (e.g. AD close Wallerian IQR = 0.889

vs AD close retrograde IQR = 2.35) (see Figure 2.2). From this point of view, it is possible that greater degrees of retrograde degeneration could have been detected if measurements were conducted using techniques like fixel analysis and apparent fibre density measures of CSD, which effectively differentiate fibre bundle orientations within voxels containing crossing fibers (D. Raffelt et al., 2012; D. A. Raffelt et al., 2017), which would be a natural extension of this research.

2.2.5 Conclusion

This study provides evidence for Wallerian degeneration in otherwise NAWM connected to T2 lesions using MR diffusivity markers. RD increase in anterograde regions of connected lesional fibres was the most sensitive metric, while a potential biomarker of progressive disease, AD in the close Wallerian region of lesional fibres was correlated with lesion severity and disability in patients with MS.

2.3 Chapter Summary

Multiple mechanisms contribute to axonal degeneration in MS, including Wallerian degeneration, retrograde and transsynaptic degeneration, demyelination within lesions, and diffuse demyelination in normal appearing white matter. The relationship between inflammation and neurodegenerative mechanisms in MS is not fully understood, and there are differing opinions on the primary driver of axonal loss in progressive forms of the disease. A biomarker of these focal neurodegenerative mechanisms would be invaluable in disease monitoring for clinical trials and patient management.

In this chapter, a novel method of tractometry was developed to measure the impact of MS lesions on white matter tracts and identify markers of neurodegeneration associated with focal lesions. The study introduced the concept of using control data from a specialised healthy control atlas, allowing for more accurate controlling of focal microstructural diffusion metrics that have high variability throughout the brain and are not easily compared to averaged values across the whole brain or whole tract. The findings revealed several interesting results, including a persistent increase in RD distal to lesions indicating Wallerian degeneration in lesional fibres. Additionally, a specific biomarker of Wallerian degeneration was identified in progressive MS patients, characterised by a reduction in AD, which correlated with disability and lesion severity. Notably, men showed a clinically relevant worsening of this biomarker as the disease duration increased.

In conclusion, this chapter makes a significant contribution to the research field by developing a new method of tractometry for studying MS lesions and identifying markers of neurodegeneration. The findings highlight the importance of further validating the changes in AD distal to lesions as a specific biomarker for PMS. Additionally, the exploration of radial diffusivity in white matter tracts emerges as a highly sensitive marker of axonal degeneration. The investigation of these biomarkers in the context of upcoming remyelinating and anti-degenerative therapies holds great promise and warrants further exploration.

Chapter 3

Atlas-based disconnectome modelling in multiple sclerosis

Abstract

The connectome, a network of interconnected nodes in the brain, plays a crucial role in brain function and can be disrupted by disease processes. MS, characterised by focal white matter inflammatory lesions that damage axonal connections, is well-suited for studying connectome disruption. Tractography with diffusion MRI is commonly used to measure the structural disconnection of white matter tracts in disease, however accurately tracking streamlines through MS lesions poses challenges. Atlas-based approaches have been employed to overcome this issue by superimposing pathological maps onto preconstructed network structures. These approaches offer advantages such as cost-effectiveness, utilisation of legacy scans, and manipulation of pathology-disconnection interaction. However, accurate registration of pathological maps onto the structural network atlas remains a limitation.

This chapter refines the atlas-based network analysis by comparing registration techniques. It also introduces a novel concept to incorporate incomplete MS lesion damage and cumulative damage along streamlines, providing a more comprehensive representation of MS pathophysiology. The chapter concludes by presenting the results of a longitudinal study that explores atlas-based disconnectome analysis as a biomarker for physical disability and disease progression in MS.

3.1 Background

One of the fundamental units of brain computation is a network of interconnected nodes, commonly referred to as the connectome (Fornito & Bullmore, 2015). Understanding this structure in neuroscience helps explains fundamental functions of the brain as well as how disease processes disrupt that function (Fornito et al., 2015). MS, like other neurological diseases, can be modelled in terms of how it effects the connectome, or disrupts the connectome (termed the "disconnectome") (Lapucci et al., 2022; Pagani et al., 2019). Given that a major pathological process in MS is the development of focal white matter inflammatory lesions that damage axonal connections (Lassmann et al., 2007), MS is a good candidate to be modelled in terms of disconnection.

Modelling brain structure as a network is an evolving methodology, with a variety of techniques and modalities being utilised (Abdelnour et al., 2022). These techniques can be broadly grouped as either structural or functional. Structural techniques utilise methods that measure either the physical connections within the brain or measure physical structures of brain regions. These methods have most often employed MRI, in which diffusion sequences uniquely facilitate the construction of white matter tracts through tractography. However, the accurate reconstruction or tracking of streamlines through focal brain lesions is problematic and hinders the implementation of tractography in MS (Pagani et al., 2019). This will be explored further in Chapter 4 of this thesis; briefly, streamline tractography relies on stepwise construction from voxel to voxel, based on diffusion data within the voxel and predetermined criteria such as amplitude and angle restrictions to limit spurious tracking (Lipp et al., 2020). Axonal loss and tissue destruction within MS lesions alters the MR diffusion signal (Klistorner et al., 2016; Klistorner, Wang, et al., 2018; Y. Wang et al., 2015) and thereby reduces the accuracy of constructed streamlines that track through them (Inglese & Bester, 2010; Lipp et al., 2020). Atlas based approaches 'side-step' the problem of accurately tracking streamlines through focal MS lesions and have been employed in a number of clinical research studies (Fuchs, Dwyer, et al., 2018; Kuceyeski et al., 2013; Ravano et al., 2021; Tozlu, Jamison, Nguyen, et al., 2021).

Atlas based tractography involves the superimposition of pathological maps onto preconstructed network structures derived from healthy control data (Kuceyeski et al., 2013).

In this way, all structural network information is derived in the absence of potentially distorting pathology. There are also several additional advantages of using an atlas-based approach. Firstly, these methods do not require sophisticated diffusion or other MRI sequences that can be costly, prone to artefacts (Kanakaraj et al., 2023; Lahti et al., 2021) and outside the scope of routine clinical scanning. As such, these methods have the ability to unlock the clinical and research potential of legacy scans from past decades (Kuceyeski et al., 2013). Secondly, healthy control diffusion based tractography can be derived from high-grade research acquisitions (Van Essen et al., 2013) that are of greater spatial and angular resolution than those usually captured in clinical or even research settings. This facilitates more accurate modelling of smaller structures and bundles included in disconnectome analysis. Thirdly, the interaction between pathology and disconnection of streamlines can be easily manipulated, allowing for a variety of pathological data to be input into the model as well as be refined to capture specific desirable aspects of the disease pathophysiology.

The method does have limitations owing to the need for registration of pathological maps onto the structural network atlas. As opposed to constructing diffusion-based streamlines within the patient's "native space", which allows for unique size and spatial differences between patients, atlas-based approaches rely on accurate registration of the images of controls and subjects. The relative size of MS pathology, such as T2 weighted lesions, compared to structural network models comprising white matter bundles and tractography streamlines, may exacerbate the inaccuracy conferred by registration i.e. small inaccuracies in the registration have the potential to place pathology in adjacent or separate white matter tracts, introducing significant errors into the analysis. MRI image registration is made more difficult in MS due to different brain volumes and atrophy rates compared with healthy controls (De Stefano et al., 2010, 2015; Zivadinov et al., 2016) even early in the course of the disease (Chard et al., 2002).

In this chapter, the model of atlas-based network analysis is refined by comparing registration techniques and demonstrating the superiority of a multimodal MRI registration method. A novel method to incorporate incomplete MS lesion damage and cumulative damage along streamlines, in order to better represent underlying MS pathophysiology, is then introduced. Finally the results of a longitudinal study exploring atlas-based disconnectome analysis as a biomarker of physical disability and progression in MS is reported.

3.2 Refining the registration method with atlas-based tractograms

3.2.1 Introduction

Recognition that pathological alteration of brain networks underpins cognitive and, to a lesser extent physical, disability in MS has heightened interest in analysis of the connectome (and its disruption) in patients with the condition (Charalambous et al., 2019, 2020; Fuchs, Dwyer, et al., 2018; Rimkus et al., 2018; Tur, Kanber, et al., 2019). However, the construction of structural connectomes requires quality diffusion MR data that is often lacking in clinical MRI acquisitions. To overcome this limitation, and to exploit the rich wealth of historical data, methods have been developed that utilise connectomes derived from healthy controls (HC) (Fuchs, Carolus, et al., 2018; Kuceyeski et al., 2013, 2018) to estimate connectome disruption in patients with MS. These methods require the accurate registration of region of interests (ROI) from patients with MS onto regional or whole brain streamline tractograms derived from HCs. ROIs may take the form of structural regions or white matter bundles but are most commonly white matter lesions; registration methods therefore need to be accurate for white matter tissue. For example, T1 based image registration of isolated white matter MS lesions may inaccurately map to HC-derived connectomes due to the lack of information within the relatively homogenous T1 signal of white matter. Comparisons of different registration methods have been undertaken but most commonly compare cortical and subcortical grey matter regions (Klein et al., 2009).

The use of MR sequences with higher contrast within white matter tissue, such as diffusion MRI, can be utilised to create fractional anisotropy (FA) or mean diffusivity (MD) maps that hold information of average fibre directions of each white matter voxel. Diffusion MR therefore has the potential to improve white matter registration. In addition, more advanced diffusion techniques, such constrained spherical deconvolution (CSD) (Tournier et al., 2007), generate fibre orientation distributions (FODs) that hold information of *all fibre directions* for each voxel. Indeed, a model of FOD registration, using an extension of Advanced Normalization Tools (ANTs) (B. Avants et al., 2007) known as symmetric diffeomorphic normalisation, outperformed FA based registration for white matter structures (D. Raffelt et al., 2011). Furthermore, as the white matter of the brain is a large and heterogenous region, it is likely that registration methods based on different contrast inputs (e.g. T1, FA and FODs) will perform better or worse

in different areas of the white matter. For example, T1 sequences are likely to perform well in the juxta cortical region of the white matter, because of excellent cortical contrast and resolution, but poorly in deep white matter regions due to the homogenous T1 signal. By contrast, FA and FOD maps might be expected to perform better in deep white matter regions where additional information of white matter bundle direction would help with contrast, as opposed to juxtacortical regions where white matter fibres are more chaotic and branched. Multimodal techniques utilising MR sequences with varying white and grey matter contrasts has been shown previously to perform well in all areas of the white matter region (Lv et al., 2022), and has the potential improve atlas based registrations in the study MS connectomes. AI-based registration techniques utilising deep learning algorithms are an active area of research (Teuwen et al., 2022; Xiao et al., 2021), and in some instances have proven to be more accurate and faster than classical methods, although widespread application is currently limited by unique pre-processing steps and relevant pathological datasets (Chen et al., 2021).

Here, we compare the accuracy of a FOD-based, T1-based, FA-based and multimodal registration in the analysis of white matter pathology in MS.

3.2.2 Methods

10 patients with MS and 10 age-matched healthy controls underwent 3T MRI scanning including high resolution 1mm 3D T1, axial diffusion weighted imaging (DWI) 1 x 1 x 2mm b=1000 s/mm^2, 64 gradient directions with additional b0 blip-up and blip-down reference data to estimate AP-PA distortion, FLAIR 3mm thickness 2D sequences. Diffusion imaging was preprocessed using MRtrix3 for denoising, Gibb's ringing artefact removal and bias field correction. FSLs eddy-current induced, motion and susceptibility-induced distortion correction was then performed, and the result interpolated to 1mm^3 resolution. FOD maps were created using MRtrix3 by first estimating group response functions (Dhollander et al., 2018) and then using a CSD algorithm designed for single shell data using MRtrix3Tissue (https://3Tissue.github.io), a fork of MRtrix3 (Tournier et al., 2019). Tensor and FA maps were created using MRtrix3. Inpainted T1 images were linearly registered to the preprocessed DWI b0 maps with FSLs FLIRT (Jenkinson et al., 2002).

Registrations were performed through a template intermediary. The use of a template intermediary reduces the number of registrations needed in comparison to direct registrations between all patients and controls by orders of magnitude, and thus the processing time for large datasets. We have adopted a novel brain template which is generated with multimodal brain MRI, including T1, T2w and Diffusion MRI (Lv et al., 2022). Specifically, we employed high-quality neuroimage data of 50 randomly selected subjects from the Human Connectome Project to generate the standard template space. The FA and MD maps were calculated from the diffusion MRI (dMRI) and subsequent FOD maps created using CSD (Tournier et al., 2007). Importantly, with this method (Lv et al., 2022), the template of FOD maps and the tractogram can also be generated in the same space.

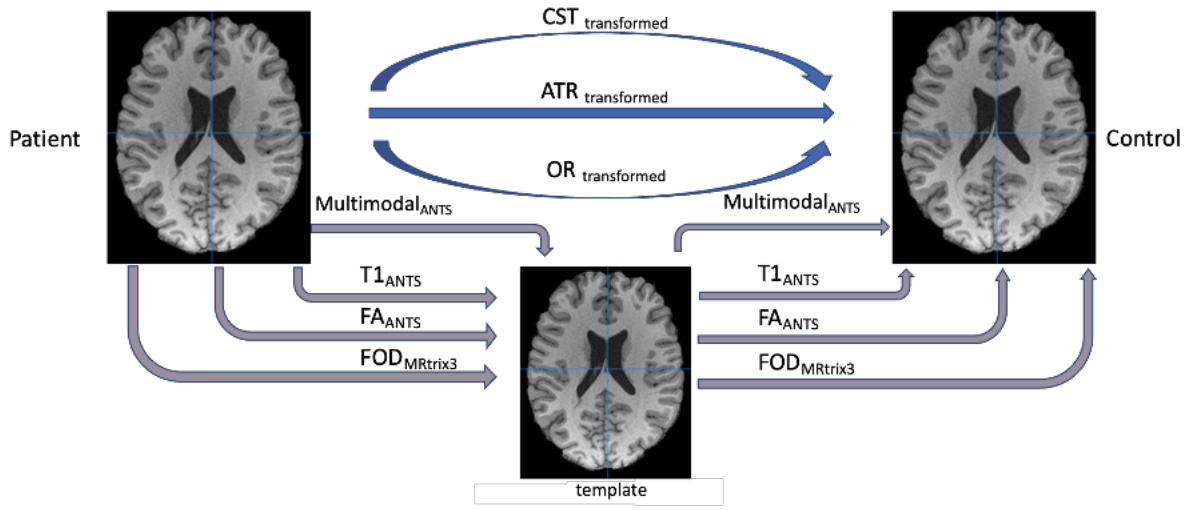

Figure. 3.1 Registrations for each method were undertaken through a template intermediary (grey arrows). Subsequent transformations of the white matter bundles were transformed from patients to controls (blue arrows).

For the T1, FA and FOD registrations, *unimodal* maps were used from the brain template. Registration was performed for each individual, including the controls and patients, to the template with non-linear registration performed with ANTs (B. Avants et al., 2007) using T1 and FA images with the input as

ANTS 3-m CC[../<fixed image>,<moving image>,1,2]-i 50x30x10-o warp-t SyN[0.25]-r Gauss[3,0]

Registration was performed using FOD maps with the MRtrix3 command

mrregister-nl_warp_full warp.mif <moving image> <fixed image>

In addition to the three unimodal registration methods, to take full advantage of the multimodal brain template, we utilised the *multimodal* registration method to register each individual to the template (B. Avants et al., 2007). However, because T2 sequences were not collected in this study, we used the T1, FA and MD to generate the nonlinear warping. As demonstrated in Lv et al. (Lv et al., 2022), the multimodal registration method exploits the complementary information from multiple modalities and takes both the grey matter geometry and the axonal distribution in the white matter into consideration when optimising spatial

alignment, therefore, the derived template preserves superior anatomical details for grey matter, white matter and subcortical nuclei (Lv et al., 2022).

antsRegistrationSyN.sh-d 3-n 50-f <fixed T1 image>-f <fixed MD image>-f <fixed FA image>-m <moving T1 image> -m <moving MD image>-m <moving FA image>-o warp

The experiment assessed each registration method in transforming three white matter tracts from patients to controls. Tracts analysed were the corticospinal tracts (CST), anterior thalamic radiations (ATR) and optic radiations (OR), to assess the registration accuracy across different areas of the brain (see Fig. 3.1). These tracts were first segmented in each patient and control using TractSeg (Wasserthal et al., 2018), a segmentation tool that utilises diffusion sequences to make fast and accurate white matter tract bundle segmentations. Each tract was generated within TractSeg using probabilistic tracking from two end region of interests (ROIs), creating 10000 streamlines per tract. Binary bundle segmentations of each tract were created. Each patient's tract segmentations were then transformed to each control using each registration method.

The resultant transformed segmentation from each registration method was compared to the control segmentation by calculating its Dice coefficient measured by:

$$\frac{2 \times |Control \cap Patient|}{|Control| + |Patient|}$$

Normality testing informed the use of either a gaussian or non-gaussian group comparison test and multiple comparison test to assess the significance of difference between each registration method.

3.2.3 Results

	Original	Transformed	Overlap
T1 Coronal	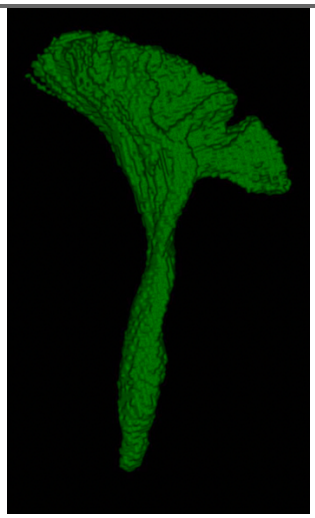	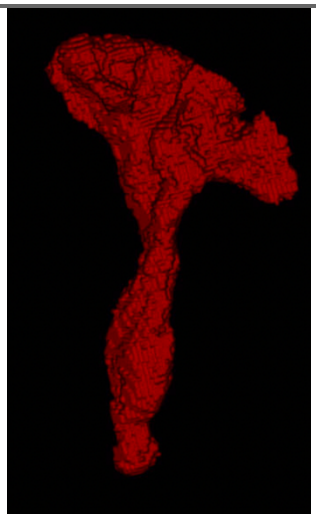	
T1 Axial	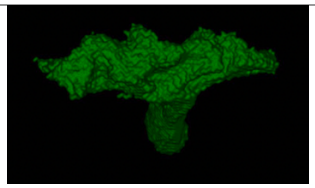	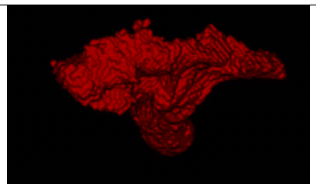	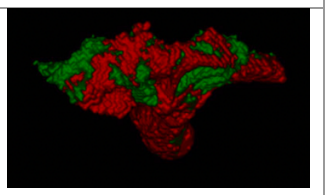
FOD Coronal	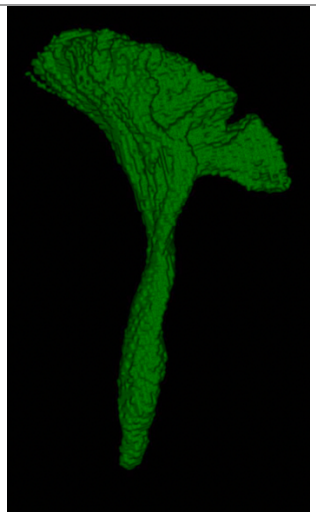	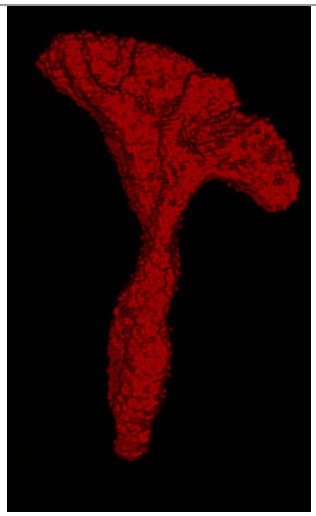	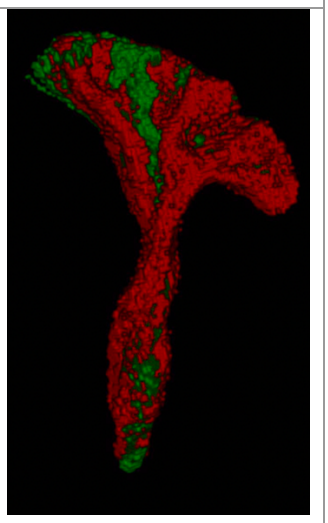
FOD Axial	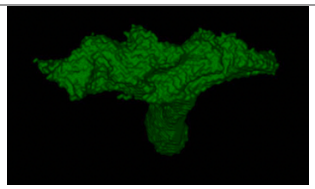	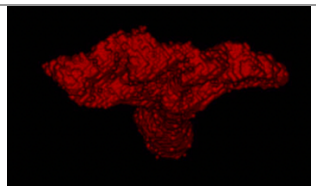	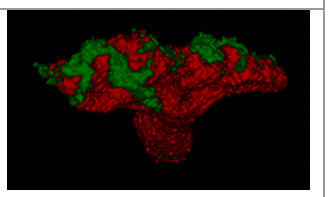

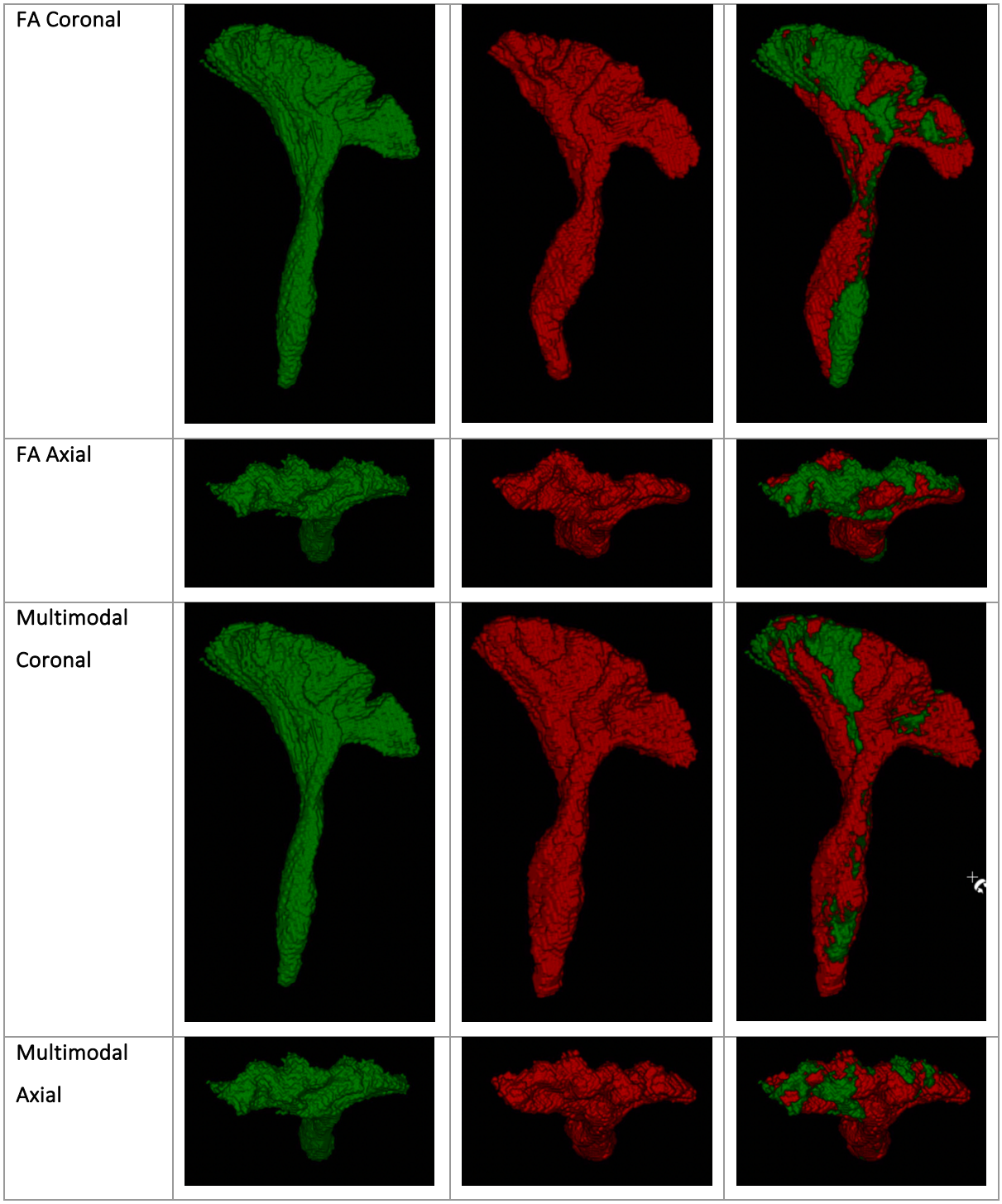

Figure 3.2 Representative example of the performance of each registration method transforming the CST.

The results of the combined tract segmentations are given first, followed by the individual tract data.

Two out of four groups were non-gaussian and therefore the non-parametric paired Freidman test and post hoc Dunn's multiple comparison test were used.

For a combination of all tract data, the Freidman test was conducted to determine the difference in the DICE coefficients depending on which registration method was used resulting in a significant difference between groups $\chi 2 = 139.1$, $p < 0.001$.

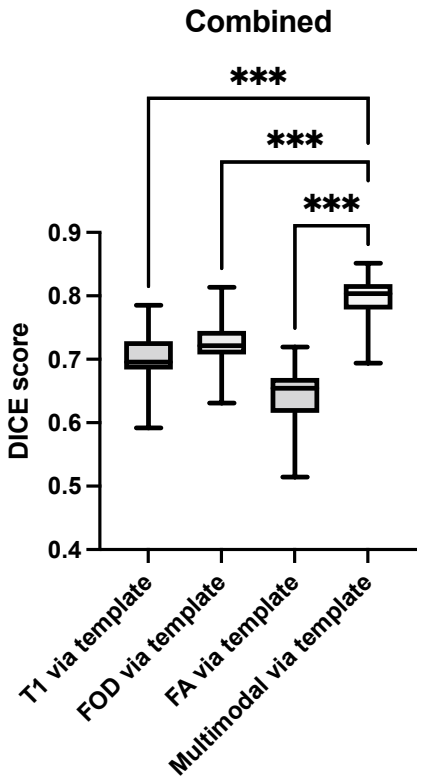

Figure 3.3 Box plot with median and range. ns – not significant, * < 0.05, ** < 0.01, *** < 0.001

Post hoc analysis with the Dunn's multiple comparison test calculated a median (IQR) DICE coefficient for the multimodal template 0.8034 (0.7787-0.8187), FOD template 0.7214 (0.7079-0.7448), T1 template 0.6957 (0.6841-0.7286) and FA template 0.6545 (0.6155-0.6706). There were significant differences between the multimodal registration and all other registration methods (vs FOD $Z = 4.099$, $p < 0.001$; vs T1 $Z = 6.783$, $p < 0.001$; vs FA $Z = 11.48$, $p < 0.001$).

For the CST, the Freidman test resulted in a significant difference between groups $\chi 2 = 45.07$, $p < 0.001$.

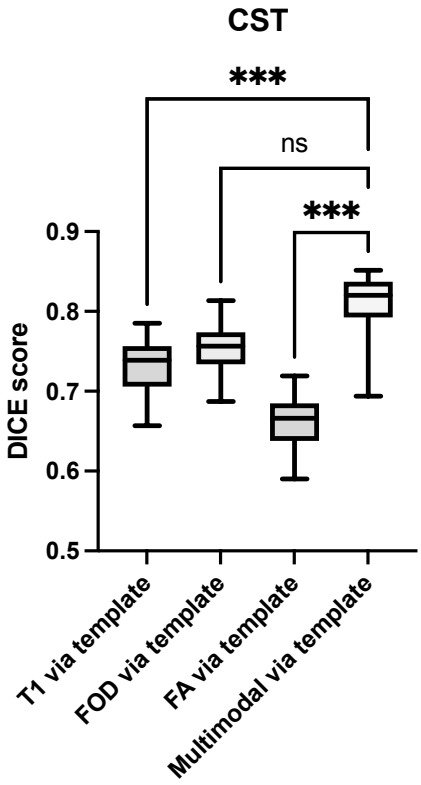

Figure 3.4 Box plot with median and range. ns – not significant, * < 0.05, ** < 0.01, *** < 0.001

Post hoc analysis with the Dunn's multiple comparison test calculated a median (IQR) DICE coefficient for the multimodal template 0.8201 (0.7925-0.8370), FOD template 0.7566 (0.7338-0.7737), T1 template 0.7388 (0.7057-0.7566) and FA template 0.6662 (0.6379-0.6850). There was no significant difference between the multimodal registration and FOD registration method; however, a significant difference between multimodal registration and T1 and FA based registration methods was observed (vs FOD $Z = 2.066$, $p = 0.12$; vs T1 $Z = 3.873$, $p < 0.001$; vs FA $Z = 6.455$, $p < 0.001$). (Figure 2)

For the ATR, the Freidman test resulted in a significant difference between groups $\chi 2 = 49.20$, $p < 0.001$.

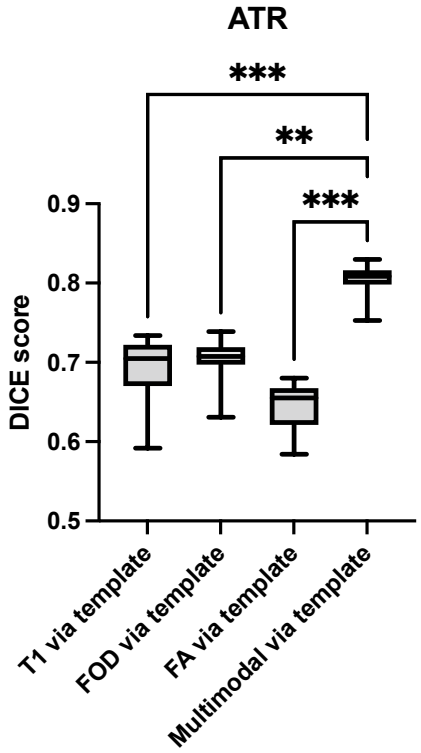

Figure 3.5 Box plot with median and range. ns – not significant, * < 0.05, ** < 0.01, *** < 0.001

Post hoc analysis with the Dunn's multiple comparison test calculated a median (IQR) DICE coefficient for the multimodal template 0.8085 (0.7981-0.8162), FOD template 0.7076 (0.6971-0.7190), T1 template 0.7048 (0.6702-0.7221) and FA template 0.6553 (0.6213-0.6676). There were significant differences between the multimodal registration and all other registration methods, (vs FOD $Z = 3.098$, $p = 0.006$; vs T1 $Z = 3.873$, $p < 0.001$; vs FA $Z = 6.971$, $p < 0.001$). (Figure 3.5)

For the OR, the Freidman test resulted in a significant difference between groups $\chi 2 = 50.60$, $p < 0.001$.

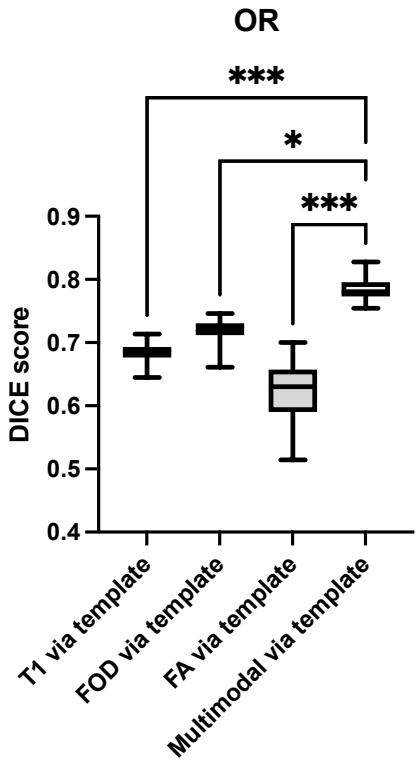

Figure 3.6 Box plot with median and range. ns – not significant, * < 0.05, ** < 0.01, *** < 0.001

Post hoc analysis with the Dunn's multiple comparison test calculated a median (IQR) DICE coefficient for the multimodal template 0.7806 (0.7733-0.7958), FOD template 0.7195 (0.7117-0.7306), T1 template 0.6867 (0.6763-0.6933) and FA template 0.6302 (0.5901-0.6571). There were significant differences between the multimodal registration and all other registration methods, (vs FOD $Z = 2.582$, $p = 0.03$; vs T1 $Z = 4.518$, $p < 0.001$; vs FA $Z = 6.842$, $p < 0.001$). (Figure 3.6)

To investigate whether the registration of cortical and juxtacortical structures contributed more to reducing the DICE coefficient, and if sequences with high grey matter contrast performed better as per the hypothesis, the same white matter tracts were transformed but with the cortical projections of the tract cropped. (Figure 3.7)

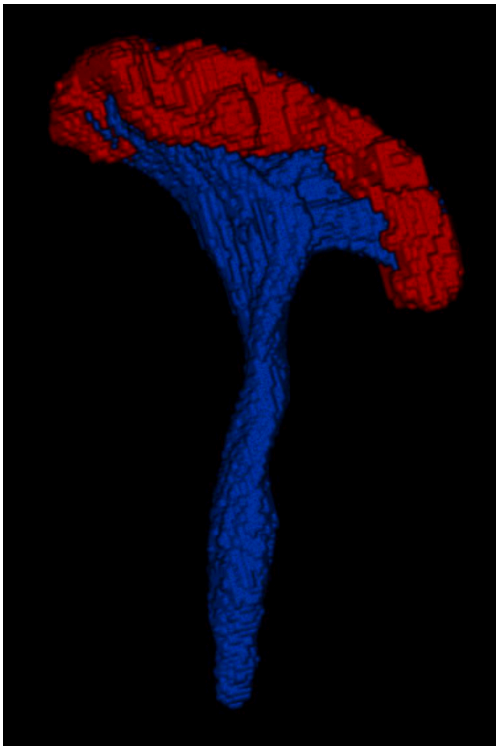

Figure 3.7. Example CST with cropped cortex

For the combination of all tracts, Dunn's multiple comparison test was used to compare the performance of each method on white matter tracts with and without the cortex cropped. Although all methods exhibited improved DICE coefficients with the cropped cortex tracts, significant differences were only observed for FOD and FA methods (FOD- $Z = 2.671$, $p = 0.03$; FA – $Z = 2.5$, $p=0.05$).

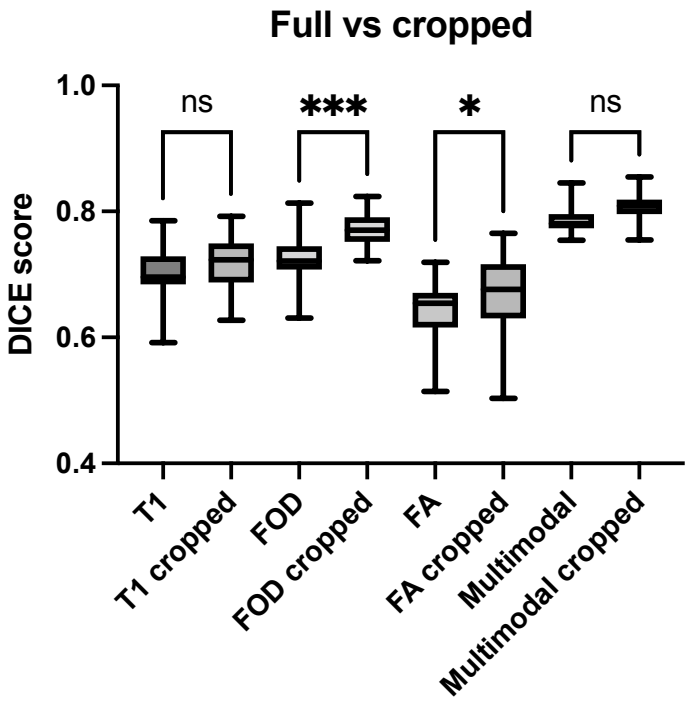

Figure 3.8. Box plot with median and range. ns – not significant, * < 0.05, ** < 0.01, *** < 0.001

3.2.4 Discussion

This is a practical study that highlights the non-trivial matter of choosing the best registration method for specific imaging tasks and applications. Consistent registration across all brain regions is especially important when studying disease states such as MS, where there is a broad distribution of pathology throughout the cerebrum.

This study specifically compares the relative benefit of using a registration method that combines multiple different MR sequences, incorporating contrast for white matter as well as cortical structures, over purely white matter microstructure informed methods (ie. FOD, FA) or grey matter macrostructure informed method (ie. T1).

In all three brain tracts tested, as well as with the combination of all three, there was a consistent hierarchy of the performance of registration methods. The multimodal method utilising T1, FA and MD maps had a median DICE coefficient of all three tracts combined of 80.43% with a tight interquartile range of 77.87%- 81.87%. This performed statistically better than the FOD method by over 8%, the T1 method by ~10% and FA method by ~15%. The consistency of the approach was seen across the three tracts studied, the CST, ATR and OR tracts, despite these tracts having varied locations and different orientations in the brain.

To investigate the limitations of the different registration methods for white matter vs grey matter, a sub-analysis was performed with the cortical and juxtacortical segment of the CST cropped. The hypothesis is that the inclusion of cortical and juxtacortical regions of the three tracts in the original analysis would likely favour grey matter informed methods such as T1 and multimodal registrations over the mainly white matter informed registrations of FOD and FA. In this sub-analysis, the DICE score for FOD and FA based registrations were improved when the cortical segmentation and juxtacortical segment of the CST was cropped (relative to uncropped, full CST images), , suggesting limitations of registration using these sequences were attributable to their relative lack of grey matter contrast, which helps to delineate complex grey matter cortical anatomy. Of note, the performance of registration methods that utilised T1 weighted sequences, namely T1 and multimodal registrations, did not improve with the cropped CST. The findings are similar to those described previously, comparing multimodal and FOD registration

methods, by Lv et al (Lv et al., 2022). However, it must be noted that juxtacortical MS lesions are commonplace, and their accurate representation in the measurement of connectome disruption is both important and desirable. Juxtacortical lesions have been shown to correlate with more severe disease progression and disability than deep white matter lesion burden (Martínez-Heras et al., 2020). Methods that focus on accurate registration of deep white matter regions without focusing on juxtacortical regions are likely to miscalculate the severity of connectome damage in MS specifically.

Comparison of image registration methods in neuroimaging have been undertaken previously, mostly comparing different algorithms for T1 based registration (Klein et al., 2009), as opposed to exploring different contrast sequences. Although numerous diffusion tensor imaging (DTI) and high angular resolution diffusion imaging (HARDI) templates have been developed (Peng et al., 2009; Varentsova et al., 2014), diffusion MRI notably lacks a robust template for FODs and tractography (Lv et al., 2022). These previous comparisons have consistently shown that utilisation of the cross-correlation metric is more robust than squared differences metrics for image registration, across T1 and FOD based methods (Babak et al., 2005; Brown, 1992; Klein et al., 2009; D. Raffelt et al., 2011). Raffelt et al. (D. Raffelt et al., 2011) explored FOD-based symmetric diffeomorphic registration and found, similar to the results presented here, that a FOD based technique significantly outperformed an FA based technique with identical code base registration method. However, in Raffelt's (D. Raffelt et al., 2011) study, a novel FOD based method was developed utilising cross-correlation image registration whereas the FOD registration technique publicly available in the MrTrix package, and utilised in this study, is based on the sum of squared differences metric. It is possible, if not probable, that using a cross-correlation approach will produce a better result here as well, however it would not be expected to improve the cortical grey matter registration that disadvantages FOD based methods in comparison to the T1 informed methods.

Finally, the incongruity of using a registration method that utilises diffusion data for analysis that has been developed for situations when diffusion data is not necessarily available has not escaped the author. One of the benefits of template based structural connectome analysis is the ability to input basic white matter lesion masks that are available from historical datasets and routine clinical MRI studies. Notably, the diffusion sequences used in the multimodal

technique in this study, namely MD and FA, are routinely available in clinical scans from common DTI sequences, and do not require HARDI data that would be required to construct accurate structural connectomes within subjects themselves. Secondly, the improvement of the multimodal method over the T1 method illustrated in this study is not trivial and will improve the robustness and accuracy of resultant analyses.

3.2.5 Conclusion

For MS lesion registration, a multimodal registration method utilising T1, FA and MD sequences is superior to unimodal registration methods, with particular utility for modelling juxtacortical lesions, which are prevalent in MS.

3.3 Refining the model to incorporate cumulative damage of multiple MS lesions along white matter tracts

3.3.1 Introduction

Multiple sclerosis (MS) can be modelled as a disconnection syndrome, whereby the regular network of connections within the brain are damaged or cut off completely by MS disease pathology (Lapucci et al., 2022). Several methods to model disconnection in the brain have been developed and can involve structural or functional techniques. For structural techniques to accurately model the disease process however, unique aspects of the pathophysiology need to be built into the model. This contrasts with functional techniques such as fMRI or EEG, as these techniques necessarily have the physiology (and therefore pathophysiology) of brain function inherent as they measure the ultimate outcome or function of the entire system.

The structural method of atlas based tractography has been extensively developed for numerous neuropathological disease models, including MS. The application of atlas based tractography techniques has evolved (Sperber et al., 2022), with early use restricted to the provision of binary pathological maps that were registered to the atlas tractogram. Subsequently these methods were refined by the incorporation of graded measures of pathology such as fractional anisotropy (FA) (Kuceyeski et al., 2013). The method involves the weighting or exclusion of healthy control atlas tractography streamlines based on the intersecting pathological map; and calculation of the resulting network changes (Kuceyeski et al., 2011). Applications of atlas based tractography to specific disease states have also varied, for example studies of the disconnectome after stroke have largely used binary lesion maps of acute stroke area or chronic gliosis (Salvalaggio et al., 2020; Yourganov et al., 2016), whereas studies of Alzheimer's Disease have utilised cortical atrophy measures integrated into the atlas based tractograms to monitor spatial progression through connected cortices (Powell et al., 2021).

In MS, various pathological map inputs have been utilised with atlas based tractography. These include T2 binary lesion maps (Tozlu, Jamison, Gu, et al., 2021), T1 binary lesion maps (Fuchs, Carolus, et al., 2018), quantitative susceptibility mapping (QSM) (Tozlu, Jamison, Nguyen, et al.,

2021) and FA graded white matter maps (Ashton et al., 2021). Besides the graded FA white matter map, which has been used as a general marker of white matter tissue integrity (Ashton et al., 2021), the lesion based methods have utilised a binary score based on the input of choice, whether it be T1, T2 or QSM (ie. QSM rim positive/negative lesions). However, the modelling of lesions in this binary system is not necessarily representative of the specific pathophysiology in MS, as inferred from histopathological (Lassmann et al., 2007, 2012) or MRI (van Walderveen et al., 1998) studies. In MRI studies, T1 weighted hypo-intensity within MS lesions correlates with pathological markers of irreversible damage, including axonal degeneration (van Walderveen et al., 1998). Indeed studies have found that T1 "black holes" have a higher correlation with clinical disability than do T2 weighted lesions (Lapucci et al., 2020); and that measurable T1 signal drop out occurs within slowly enlarging lesions or chronic active lesions, as opposed to inactive lesions, suggestive of ongoing axonal degeneration (Elliott, Wolinsky, et al., 2019). The gradual attrition of axons within lesions is a hallmark feature of progressive forms of MS (Lassmann et al., 2012) and mediates disability. Measuring the relative T1 hypointensity of lesion maps and weighting the damage to the underlying atlas streamlines accordingly seeks to better represent core MS pathology than do binary lesion maps (Elliott, Belachew, et al., 2019).

However, utilising graded lesion maps in this way begs a further question. If a lesion is not wholly destructive (ie. not a binary lesion) then how do multiple lesions along the course of a streamline effect its weighting in the final connectome? Intuitively, a white matter bundle that has within it multiple MS lesions should be effected, or disconnected, more than a bundle with a comparable single lesion (Fig. 3.9). Previous methods have weighted streamlines based on the lowest value along its course regardless of the number of lesions, akin to a weakest link analogy (Kuceyeski et al., 2013). However, many neuropathic disease mechanisms have included a description of cumulative damage, especially in the peripheral nervous system (Upton & McComas, 1973; Zimmerman et al., 2022), but also in motor disability models of MS (Kerbrat et al., 2020), being given the colloquial term double-crush or double-hit phenomenon.

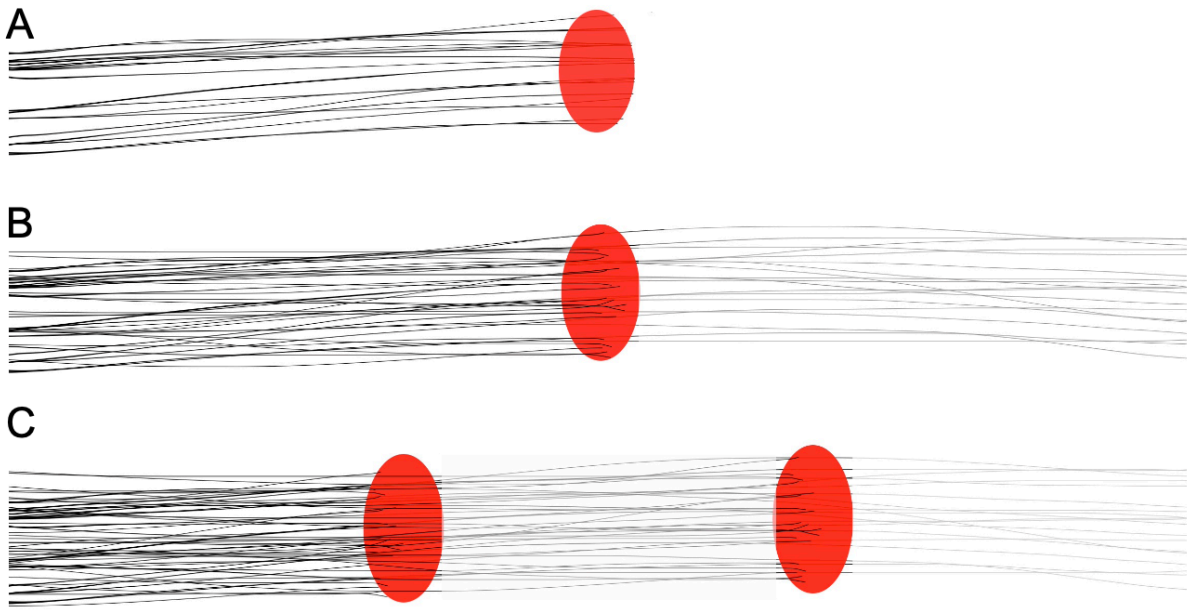

Figure 3.9. Graphical representation of the theory of cumulative damage. Each set of lines represents a white matter bundle, and the red ovals represent an MS lesion.

A shows complete axonal damage or a binary MS lesion; **B** shows incomplete axonal damage; **C** shows cumulative incomplete axonal damage with progressively more axonal loss and reduced fibre density after each lesion.

Given the resolution of an individual streamline in tractography is much lower than the represented biological system i.e. the axon, streamlines necessarily represent thousands of axonal projections. Therefore, to model cumulative damage in an atlas based tractogram, proportionally weighting the streamlines is the equivalent of reducing axonal number and fibre density, as seen above. Utilising this fact allows a model to be built that measures cumulative and incomplete damage along a white matter tract by summating the graded lesions along a streamline course and weighting the streamline accordingly.

In this study, a structural atlas based tractography model has been developed to incorporate cumulative and incomplete damage from discrete MS lesions and tested against a neurophysiological model of axonal function, i.e. multifocal visual evoked potentials (mfVEPs) in patients with MS.

3.3.2 Methods

A template tractogram was created by employing high-quality neuroimage data of 50 randomly selected subjects from the Human Connectome Project (HCP) (Van Essen et al., 2013) to generate a standard template space as previously outlined (Lv et al., 2022). FOD maps were created using CSD (Tournier et al., 2007) and subsequent whole brain probabilistic tractography was performed with MRtrix (Tournier et al., 2019) to create 20 million streamlines with included weighting calculated with "spherical-deconvolution informed filtering of tractograms" (SIFT2) (R. E. Smith et al., 2015a).

33 pwMS underwent MR brain imaging including $1mm^3$ 3D T1 using fast spoiled gradient echo (FSPGR) pre and post gadolinium administration, and 0.6 x $0.468mm^3$ FLAIR sequences. FLAIR images were resampled and linearly registered to the T1 using FLIRT (Jenkinson et al., 2002). MS lesions were segmented from the FLAIR images using JIM software. T1 intensity measurement was normalised within and between subjects via a method previously presented ('MSVirtual 2020 – Poster Abstracts', 2020 - P0622). Firstly, N3 bias correction on the T1 sequence was achieved with the Freesurfer wrapper command mri_nu_correct.mni (Sled et al., 1998). Normalisation of the T1 sequences was undertaken with the Freesurfer command mri_normalize (Dale et al., 1999) which imposes a hard ceiling effect on the white matter peak found, creating a homogenous T1 intensity at normal appearing white matter (NAWM) and floor at CSF intensity. To create an MS lesion map with graded damage based on lesional T1 intensity, the segmented T2/FLAIR lesions were graded for damage based on the average normalised T1 signal intensity within the lesion using FSL (S. M. Smith et al., 2004) from 0 to 1, representing NAWM to CSF signal intensity respectively (Image 1). This method uses T1 gradient echo sequences as opposed to spin echo sequences to grade T1 lesions. This is in line with T1 gradient echo use elsewhere (Elliott, Belachew, et al., 2019; Vaneckova et al., 2022) as well as studies showing clinical relevancy of gradient echo T1 hypointense lesion in MS (Kocsis et al., 2021), albeit with some debate (Lapucci et al., 2020). The graded damage lesion map was transformed onto the HCP template by warping inpainted T1 sequences using ANTs with nearest neighbour interpolation (B. Avants et al., 2008).

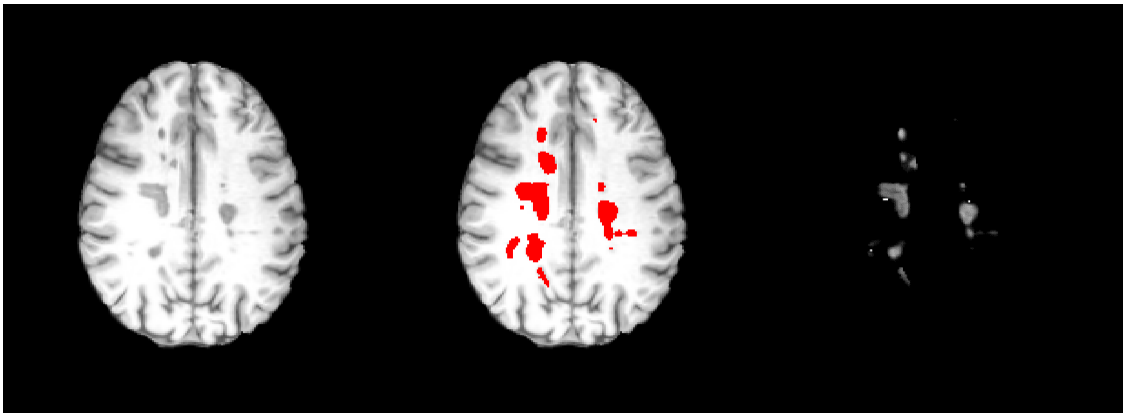

Figure 3.10. The process of creating the T1 lesional map. From left to right, the normalised T1 brain sequence is created with homogenous NAWM, and graded T1 intensity. The registered T2/FLAIR binary segmented lesions are overlayed onto the normalised T1. The T2/FLAIR lesion map graded with T1 intensity is created by extracting the underlying T1 intensities.

To model cumulative damage along each streamline, the sum of damage to voxels along each streamline was calculated and transformed with a logistic function. This was achieved by summating each voxel of the graded damage lesion map that the streamline traversed. This method allows for the calculation of both the severity of damage within a lesion (from the T1 hypointensity measure) and the length of the lesion (from the number of voxels incorporated within the lesion) to be included in the damaged weighting of the streamline. Several values of constant k, the steepness of the logistic function, were evaluated.

$$f(x) = \frac{L}{1 + e^{-k(x - x_0)}} - 1$$

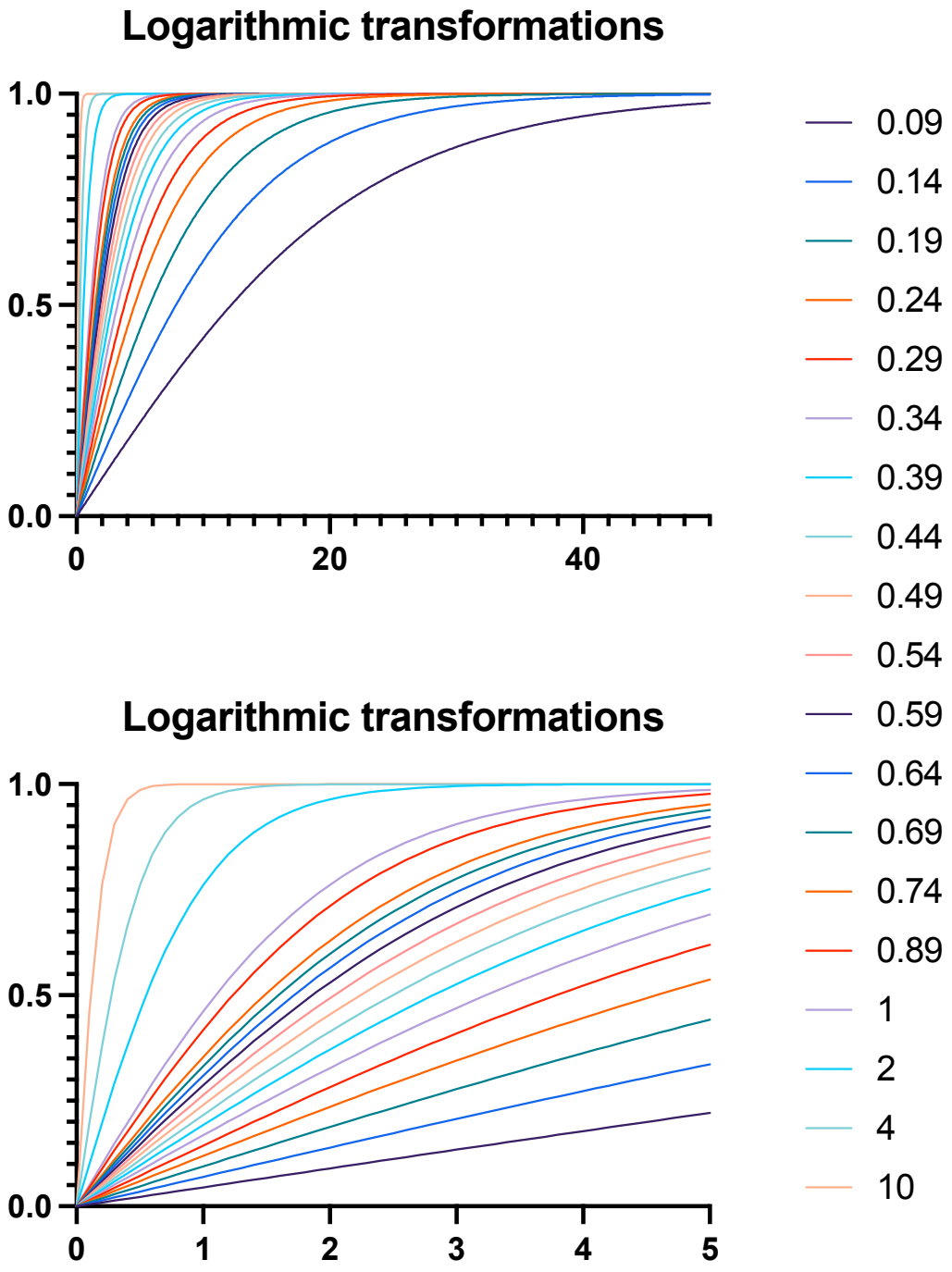

Figure 3.11. The logistic function models cumulative damage along the streamline with progressively less contribution to the damaged weighting with each subsequent damaged voxel. The *supremum L* of 2, and the *sigma mid point* x_0 of 0, allows for the function to range from 0 to 1 and include only the concave portion of the logistic sigma curve. Several values of the steepness constant *k* are graphed with coloured lines. The same graph is shown twice with different x-axis range.

The healthy control template SIFT2 weighting of each streamline was adjusted by multiplying by the additive inverse of the damaged streamline weighting. For example, a healthy control streamline SIFT2 weighting of 100, that has a damaged weighting of 0.6 after logistic transformation, would have a final streamline weighting of 40. See table 3.1 for further examples.

	Healthy control template SIFT2 weighting	Damaged weighting of 0 (i.e. no damage)	Damage weighting of 0.6 (i.e. partial damage)	Damage weighting of 1 (i.e. maximum damage)	Binary model complete damage (i.e. equivalent to 1)
Working shown	100	100 x (1 - 0)	100 x (1 - 0.6)	100 x (1 – 1)	100 x (1 – 1)
Final streamline weighting	100	100	40	0	0

Table 3.1.

The strength of the connection of each optic radiation (OR) was calculated by summating the final streamline weighting of every streamline connecting the thalamus and lateral occipital cortex defined by the Desikan-Killiany atlas (Desikan et al., 2006).

The subjects underwent mfVEP testing. Binocular average left and right hemifield latency and amplitude values, corresponding to right and left ORs respectively, were used as electrophysiological parameters of comparison.

Each value of constant k representing the steepness of the logistic curve calculating the strength of connection of the ORs was correlated with the hemifield amplitude and latency of the mfVEP on the contralateral side with Pearson's correlation testing. This was compared to models of complete lesion damage and single highest damage value along the streamline by calculation of R^2.

3.3.3 Results

33 pwMS were analysed. No patients had a clinical history of optic neuritis (ON). No patients had contrast enhancing lesions on MRI. k values between 0.09 and 10 were trialled as outlined in Figure 3.11. The value of k with the highest R^2 value corresponding to the amplitude and latency of both left and right ORs were: Left OR amplitude k=10 (R^2=0.5110); left OR latency k=1 (R^2=0.5168); right OR amplitude k=10 (R^2=0.4859); right OR latency k=2 (R^2=0.4919). A k value of 4 performed second best in three of the ORs and 4th in left OR latency and was taken as the best performing value across all four correlations (Fig. 3.12).

The k value of 4 outperformed the models of complete (binary) lesion damage and single maximum damage value in all four situations: Left OR amplitude k=4 (R^2=0.5079), binary (R^2=0.4834), max (R^2=0.4286); left OR latency k=4 (R^2=0.4867), binary (R^2=0.3728), max (R^2=0.3947); right OR amplitude k=4 (R^2=0.4744) binary (R^2=0.3922), max (R^2=0.2985); right OR latency k=4 (R^2=0.4807), binary (R^2=0.3012), max (R^2=0.4358) (Fig. 3.13).

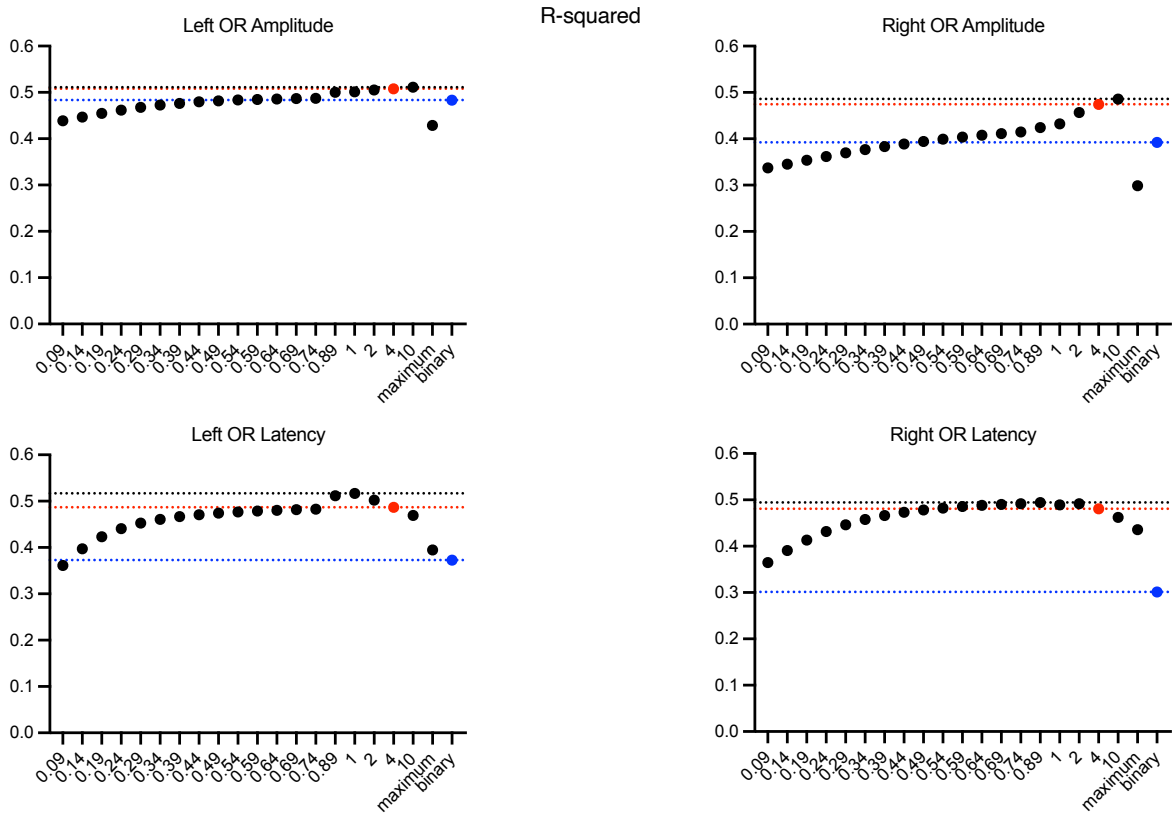

Figure 3.12. The R^2 correlation results between mfVEP metric and cumulative damage for each value of k, including the single highest damage value (maximum) and binary lesions (blue). The best preforming k value overall of 4 is highlighted in red.

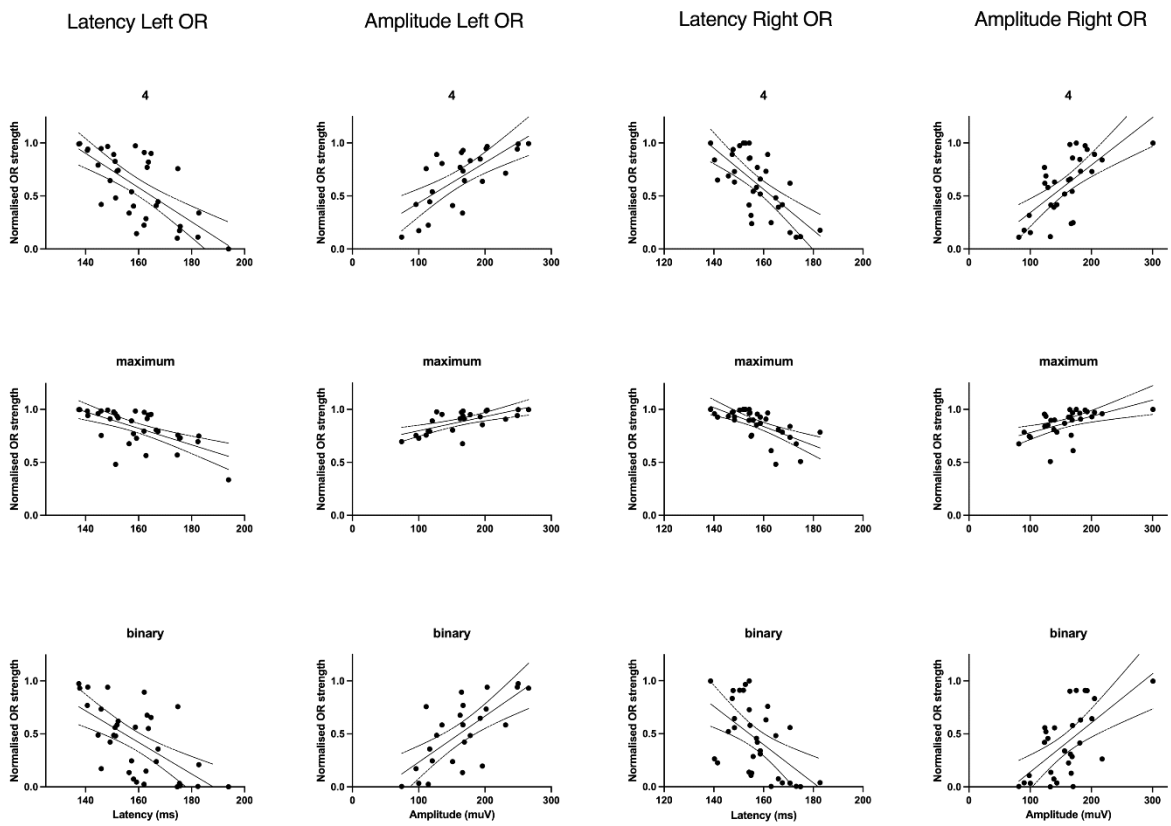

Figure 3.13. Graphs of correlation of the best performing logistic transformation k value (4), the maximum lesion damage model and the binary lesion model for the latency and amplitude of both right and left ORs. The y axis is strength of the connection of the OR measured via each method, and the x axis is either amplitude or latency of the mfVEP.

3.3.4 Discussion

This is a novel method to measure cumulative and incomplete damage along streamlines in a structural network template-based study. This allows the incorporation of known pathophysiological mechanisms of MS to be modelled more accurately in studies of the structural disconnectome. This method utilised a logistic transformation to convert the cumulative damage and found a k value of 4 was the best performing gradient of the logistic curve in this model. In addition this method compared favourably to previous models that have not measured cumulative damage, but weighted streamlines based on either binary lesion maps, where each streamline that traverses a lesion is extracted from the final connectome, or a single maximum damage weighting, where a streamline is weighted based on the single worst damage along its path.

This method utilises the SIFT2 weightings of healthy control template tractograms, which has a number of advantages. Firstly the SIFT2 method of weighting streamlines seeks to address a limitation of diffusion-based streamline mapping; i.e. the density of constructed streamlines from probabilistic tractography is not representative of the underlying white matter fibre bundle density (R. E. Smith et al., 2015a). The SIFT2 algorithm weights each streamline based on the underlying cross-sectional area informed by spherical deconvolution, to give a realistic value to a streamline and its contribution to structural connectivity in the brain. Although there has been some debate about the use of SIFT2 weighting in pathological situations (Zalesky, Sarwar, & Ramamohanarao, 2020), the application in this work is to derive the SIFT2 weighting from healthy controls, and only then adapt the SIFT2 weights based on overlayed pathology, which circumvents these concerns. The use of SIFT2 weighting provides a more realistic initial tractogram template onto which pathology can be superimposed (R. E. Smith et al., 2013). Secondly, directly manipulating the SIFT2 weights based on superimposed pathology allows for seamless integration of this method into standard structural connectome pipelines (Tournier et al., 2019) for the measurement of weighted connectomes (such as graph theory) and does not require the development of new connectivity measures.

This method had improved performance for correlations with both latency and amplitude of the mfVEPs. This is perhaps somewhat counterintuitive as T1 hypointensity, used in this method

as the graded measure of damage, is purported to be a measure of axonal density (Elliott, Wolinsky, et al., 2019) and therefore should correlate with amplitude of mfVEP, itself a marker of axonal number (Jones & Brusa, 2003), but not necessarily with latency, a marker of myelination in the optic pathway (Klistorner & Graham, 2021). However, the lack of specificity of mfVEP and T1 signal intensity to axonal loss or demyelination potentially explains the results found. The original studies investigating the association between MRI T1 hypointensity and histopathology showed clear contributions of both axonal density and myelination, with T1 signal positively correlating with both axonal and myelin density (Bitsch et al., 2001; Brück et al., 1997). T1 hypointensity was even proposed as a potential surrogate of remyelination for future remyelinating therapies (Bitsch et al., 2001). It is also noted that water content in the form of oedema, inflammation and cerebral location influence T1 signal (Bagnato, 2003; Brück et al., 1997). The present study partially controlled for these factors, given that no subjects had a history of optic neuritis (such that the location of lesions affecting visual function were restricted to the optic radiations); and no subjects had active inflammation, evidenced by the absence of gadolinium enhancing lesions. However, subclinical ON, as well as chronic inflammation without gadolinium enhancement, may have influenced the results.

The specificity of mfVEP latency for demyelination and amplitude for axonal loss is reported to be quite robust. Many studies have correlated VEP latency to demyelination, notably clinical in vivo MRI studies (van der Walt et al., 2015) and in animal studies with histopathological demyelination (Heidari et al., 2019). However, the potential influence of axonal loss on latency measures has not been excluded. The limitations of MRI specificity for the two pathological processes precludes accurate discrimination with in-vivo imaging. Animal models investigating histopathological correlations with VEP have either used a restricted model of MS with pure chemical induced demyelination (Heidari et al., 2019), or the experimental autoimmune encephalomyelitis (EAE) model but with non-quantitative assessment of axonal number (Diem et al., 2008). The specificity of VEP amplitude for axonal loss is also confounded by several factors. Acute conduction block due to acute demyelination in ON severely reduces VEP amplitude prior to compensatory axonal mechanisms, such as re-distribution of sodium channels along the axolemma, that support action potential propagation (Klistorner & Graham, 2021). In addition, the RENEW study investigating the pro-remyelinating drug opicinumab in acute ON, found a distinct protective effect of the medication on mfVEP amplitude in the

opposite eye, a finding which might in part be explained by the inhibition of subclinical axonal demyelination (Klistorner, Chai, et al., 2018).

As electrophysiological and MRI techniques lack specificity for separate pathological processes such as axonal loss and demyelination, the precise mechanisms that underpin the correlations between mfVEP parameters and OR lesion load observed in this study are uncertain. However, given that correlations exist across both latency and amplitude measures, which improved further with a model that incorporated cumulative damage, the results are deemed to be a valid contribution to the field. Future research should incorporate more specific biomarkers of axon and myelin density into such a model.

The particular parameters used in the present methodology, such as the k value and T1 signal intensity values, while appropriate for this application, may require adaptation to other MRI biomarkers. However, the overarching concept of incorporating cumulative damage along streamlines to ensure accurate connectome construction is likely to benefit the study of a range of diseases or pathological states in which white matter tracts are not wholly truncated.

3.3.5 Conclusion

Modelling cumulative damage along tractography streamlines better explains the electrophysiological function of the underlying white matter tract compared to single measurements of complete or worst damage and should be included in connectome models.

3.4 A longitudinal study of atlas-based disconnectome modelling as a biomarker for progressive multiple sclerosis

3.4.1 Introduction

Research into MRI-based structural network analysis in MS has been growing. The atlas-based approach has received ongoing development, primarily due to its numerous advantages (Kuceyeski et al., 2013), including the ability to utilise routine clinical scans for network analysis. By modelling MS as a pathology of network disconnection, this approach has yielded unique insights into the pathophysiology of the disease and provided explanations for associated disability.

For example, exploration of global connectivity metrics by atlas based network analysis in MS has found significant reduction of mean strength and global efficiency in pwMS compared to healthy controls, with further reduction seen in SPMS compared to RRMS (Pagani et al., 2019). Similarly an atlas-based approach correctly classified pwMS by disability level, even outperforming advanced diffusion and functional MRI analysis (Tozlu, Jamison, Gu, et al., 2021). Elsewhere, atlas-based approaches have been used to identify local pairwise connections in the brain that predict future information processing speed (Kuceyeski et al., 2018) as well as the psychological trait of conscientiousness in MS (Fuchs, Dwyer, et al., 2018). Similarly, local pairwise disconnection has been studied in reference to motor disability where the correlation of cerebellar disconnection and EDSS level was identified (Pagani et al., 2019). The utility of this approach has also extended to improving the understanding of the interaction of functional and structural network damage in neuroscience. Using MS as a model it was found that the function of higher order processing networks are more affected by structural damage (Bartnik et al., 2022). Overall, this approach has provided valuable insights into the pathophysiology of MS and neuroscience and also has the potential to improve prognostic classification of the disease.

Although atlas-based network analyses in MS have yielded impressive results, there are aspects of the model and pipeline that could be enhanced with respect to accuracy and specificity for disease mechanisms. For example, the registration of a subject's brain pathology maps with an

atlas-based network tractogram has the potential to introduce significant error if pathology is inaccurately projected onto the atlas. Most studies to date have utilised T1 weighted based non-linear registration (Bartnik et al., 2022; Fuchs, Dwyer, et al., 2018; Kuceyeski et al., 2013, 2018; Tozlu, Jamison, Gu, et al., 2021; Tozlu, Jamison, Nguyen, et al., 2021) despite the fact that T1 weighted images have little distinct contrast of white matter tracts (D. Raffelt et al., 2011).

The ability to tailor the input for specific pathologies is a unique aspect of atlas-based approaches and a significant advantage over other forms of structural network analysis. Although the ability to use non binary pathology maps has been a feature of atlas-based network analyses since 2013 (Kuceyeski et al., 2013), this has rarely been exploited. Ashton et al. implemented a graded FA map input by creating subject FA z-score maps compared to healthy control data (Ashton et al., 2021). FA has been studied as a marker of microstructural damage in MS, and although it is not highly specific for axonal degeneration or tract integrity, it's use is a unique attempt to include a more appropriate marker of disease mechanisms.

Finally, although some studies have explored differences between RMS and PMS with atlas-based network analysis (Pagani et al., 2019), this has not been done in a comprehensive manner.

This study utilises a refined model of atlas-based disconnection by incorporating a superior registration method, combined with a measure of cumulative damage along streamlines. With this, whole brain and subnetwork correlates of physical disability are explored, including differences between RMS and PMS. The study further investigates predictions of disability progression in a cohort of RMS and PMS subjects over 24 months with clinical and atlas-based network measurement.

3.4.2 Methods

75 pwMS with no evidence of inflammatory disease activity were recruited from a single MS centre. This cohort included 24 subjects with progressive multiple sclerosis (PMS) comprising primary progression and secondary progression with more than 24 months since last evidence of disease activity. A further 51 subjects had relapsing multiple sclerosis stable on disease modifying therapy. All subjects underwent clinical and radiological assessments over 24 months.

Clinical assessment included relapse activity, expanded disability status scale (EDSS), symbol digit modalities test (SDMT), nine-hole peg test (9HPT) and timed 25 foot walk test (T25FW). The multiple sclerosis functional composite (MSFC) was calculated using the 9HPT, SDMT and T25FW as described previously (Drake et al., 2010; Fischer et al., 1999). This involves calculating z-scores from the subject population as well as using a combined 9HPT score from both the left and right arm scores.

Radiological assessment included including $1mm^3$ 3D T1 using fast spoiled gradient echo (FSPGR) pre and post gadolinium administration, 0.6 x $0.468mm^3$ FLAIR sequences, axial diffusion weighted imaging (DWI) 1 x 1 x 2mm b=1000 s/mm^2, 64 gradient directions with additional b0 blip-up and blip-down reference data to estimate AP-PA distortion.

T1 sequences were pre-processed in the manner outlined in section 3.3.2. Briefly, T1 intensity measurement was normalised within and between subjects via N3 bias correction using the Freesurfer wrapper command mri_nu_correct.mni (Sled et al., 1998) followed by the Freesurfer command mri_normalize (Dale et al., 1999) which imposes a hard ceiling effect on the white matter peak found, creating a homogenous T1 intensity at normal appearing white matter (NAWM) and floor at CSF intensity. T2 white matter lesions were segmented via an automated in house algorithm utilising a dual path U-net convolutional neural network (Cabezas et al., 2021; Ma et al., 2022) and checked for accuracy by an expert neurologist. To create an MS lesion map with graded damage based on lesional T1 intensity, the segmented T2/FLAIR lesion voxels were graded for damage based on the normalised T1 signal intensity lesion using FSL (S. M. Smith et al., 2004) from 0 to 1, representing NAWM to CSF signal intensity respectively.

Diffusion imaging was pre-processed using MRtrix3 for denoising, Gibb's ringing artefact removal and bias field correction. FSL's eddy-current induced, motion and susceptibility-induced distortion correction was then performed, and the result interpolated to $1mm^3$ resolution. FOD maps were created using MRtrix3 by first estimating group response functions (Dhollander et al., 2018) and then using a CSD algorithm designed for single shell data using MRtrix3Tissue (https://3Tissue.github.io), a fork of MRtrix3 (Tournier et al., 2019). Tensor and FA maps were created using MRtrix3. Inpainted T1 images were linearly registered to the pre-processed DWI b0 maps with FSLs FLIRT (Jenkinson et al., 2002).

A healthy control tractogram was utilised as per section 3.2.2. This novel brain template was generated with multimodal brain MRI, including T1, T2w and Diffusion MRI (Lv et al., 2022) derived from high-quality neuroimage data of 50 randomly selected subjects from the Human Connectome Project to generate the standard template space. The fractional anisotropy (FA) and mean diffusivity (MD) were calculated from tensor-based processing within MRtrix3. A FOD map was created using CSD (Tournier et al., 2007) and subsequent whole brain probabilistic tractography was performed with MRtrix (Tournier et al., 2019) to create 20 million streamlines with included weighting calculated with "spherical-deconvolution informed filtering of tractograms" (SIFT2) (R. E. Smith et al., 2015).

Subject MR images were registered to the template using the multimodal registration process described in section 3.2.2 utilising T1, MD, FA image contrasts. Each was checked for accuracy by an expert neurologist. T2 lesion and T1 maps were then transformed onto the healthy control tractogram utilising these calculated transformation matrices.

The healthy control tractogram streamlines weightings were adjusted based on each subject's registered T1 hypointensity map as outlined in section 3.3.2. To model cumulative damage along the streamline, the sum of damage to each voxel based on the T1 hypointensity graded maps was summated using a customised variation of tcksample within MRtrix3 (Tournier et al., 2019). This sum was transformed with a logistic function outlined in section 3.3.3 with a k constant of 4, based on the results of optimising this approach. The original SIFT2 weighting of

each streamline was adjusted by multiplying by the complement of the damage, for detail see section 3.3.2.

The final complete whole brain connectome matrices were then calculated with tck2connectome (R. E. Smith et al., 2015b) using the "damage adjusted" SIFT2 weightings for each subject. The Desikan Killiany (Desikan et al., 2006) atlas was implemented in Freesurfer (Dale et al., 1999) with 84 cortical and subcortical regions, but included an additional region of the lower brainstem to capture spinal cord projections, resulting in an 85 x 85 connectivity matrix.

The connectomes of the subjects were analysed using Network Based Statistics (NBS) (Zalesky et al., 2010) to find differences in structural network disruptions and their correlation with disability metrics (9HPT, T25FW, SDMT, MSFC, EDSS) and differences between PMS and RMS patients. NBS is a method to balance family wise error and power while considering network structure. It calculates a test statistic to determine the strength of the correlation between the strength of connection grey matter region pairs and the clinical metric. P-values are assigned to clusters of these connected networks by comparing their size with the null distribution of maximal component size, obtained from 5000 permutations. NBS identifies significant sets of edges (networks), not individual edges, and results are considered significant if they reach an alpha level of 0.05. (Fuchs, Dwyer, et al., 2018; Zalesky et al., 2010) The analysis was conducted to identify patterns of structural network disruption associated with worse scores in 9HPT, T25FW, SDMT, EDSS, and MSFC. Component size was determined based on the sum of edge scores with a test-statistic threshold chosen in a semi random manner for each test as outlined in the original NBS publication (Zalesky et al., 2010).

In addition to NBS, graph theory metrics were used to analyse the structural connectome of the whole brain as well as an a priori network of interest, the sensorimotor network. The grey matter and white matter tracts included in the "sensorimotor network" have varied between publications but have broadly included primary and supplementary motor and sensory cortices, basal ganglia, thalami and cerebella (Archer et al., 2018; Pardini et al., 2015), which have been utilised here.

The standard graph theory metrics explored were global efficiency, mean local efficiency, mean strength, characteristic path length, mean modularity and mean clustering coefficient of both whole brain and the sensorimotor network calculated using the Brain Connectivity Toolbox implementation within MATLAB https://sites.google.com/site/bctnet/home (Rubinov & Sporns, 2010) . Partial correlations were calculated between these network metrics and physical disability controlling for age, disease duration, EDSS and disease course, T2 lesion volume and whole brain normalised volume using Jamovi version 2.3.21 (https://www.jamovi.org/).

Finally the network metrics were included in a logistic regression model of progression of MSFC to explore the utility of network metrics in predicting disability progression, using GraphPad Prism version 9.5.0 (https://www.graphpad.com/).

3.4.3 Results

3.4.3.1 Network Based Statistics (NBS) Cross sectional

3.4.3.1.1 Results of left upper limb 9HPT

NBS showed that left upper limb 9HPT was characterised by a single significantly disconnected subnetwork of 12 nodes and 17 edges (p = 0.015), predominantly involving ipsilateral cerebellar and basal ganglia connections.

Edge	Test statistic
Left-Cerebellum-Cortex to Left-Thalamus-Proper.	5.38
Left-Cerebellum-Cortex to Left-Pallidum.	7.16
Left-Cerebellum-Cortex to Left-Amygdala.	5.79
Left-Cerebellum-Cortex to Right-Caudate.	5.52
Left-Cerebellum-Cortex to Right-Pallidum.	5.36
Left-Cerebellum-Cortex to Right-Amygdala.	5.29
ctx-lh-parahippocampal to Right-Cerebellum-Cortex.	6.04
Left-Cerebellum-Cortex to Right-Cerebellum-Cortex.	5.58
Left-Thalamus-Proper to Right-Cerebellum-Cortex.	6.28
Left-Caudate to Right-Cerebellum-Cortex.	5.46
Left-Pallidum to Right-Cerebellum-Cortex.	8.40
Left-Hippocampus to Right-Cerebellum-Cortex.	5.34
Left-Amygdala to Right-Cerebellum-Cortex.	5.64
Left-Cerebellum-Cortex to Brain-Stem.	5.22
Left-Pallidum to Brain-Stem.	8.86
Left-Amygdala to Brain-Stem.	7.36
Right-Cerebellum-Cortex to Brain-Stem.	7.82

Table 3.2.

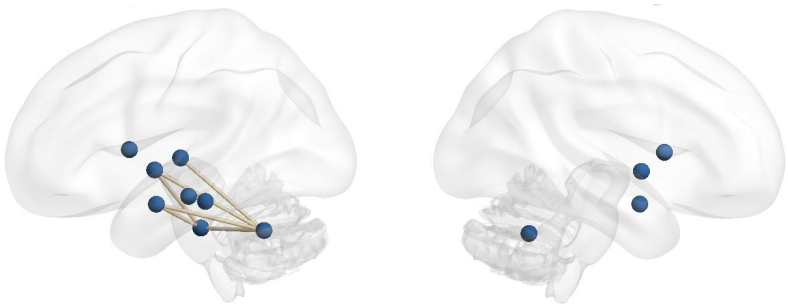

Figure 3.14.

3.4.3.1.2 Results of right upper limb 9HPT

NBS showed that right upper limb 9HPT was characterised by a single significantly disconnected subnetwork of 18 nodes and 17 edges (p = 0.049), predominantly involving ipsilateral cerebellar, basal ganglia and contralateral sensorimotor cortex connections.

Edge	Test statistic
ctx-lh-medialorbitofrontal to Right-Cerebellum-Cortex.	3.70
Right-Amygdala to Right-Cerebellum-Cortex.	3.76
ctx-rh-lateralorbitofrontal to Right-Cerebellum-Cortex.	4.00
ctx-lh-medialorbitofrontal to ctx-lh-insula.	3.95
ctx-lh-medialorbitofrontal to Left-Pallidum.	3.72
ctx-lh-temporalpole to Left-Pallidum.	4.12
Left-Thalamus-Proper to Left-Pallidum.	3.83
ctx-lh-postcentral to Left-Amygdala.	3.94
ctx-lh-precentral to Left-Amygdala.	3.73
Left-Caudate to Left-Amygdala.	3.82
Left-Pallidum to Left-Amygdala.	3.70
Left-Accumbens-area to Right-Amygdala.	3.70
Left-Hippocampus to ctx-rh-lateralorbitofrontal.	3.70
Right-Thalamus-Proper to ctx-rh-lateralorbitofrontal.	3.95
Right-Pallidum to ctx-rh-lateralorbitofrontal.	4.19
Right-Putamen to ctx-rh-parsorbitalis.	3.74
Right-Amygdala to ctx-rh-parsorbitalis.	4.41

Table 3.3

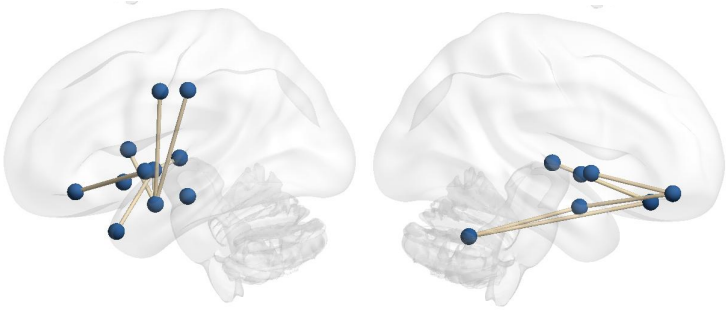

Figure 3.15.

3.4.3.1.3 Results of T25FW

NBS showed that T25FW was characterised by a single significantly disconnected subnetwork of 21 nodes and 17 edges ($p < 0.001$), predominantly involving bilateral inferior frontal cortices, basal ganglia and cerebella.

Edge	Test statistic
ctx-lh-medialorbitofrontal to Left-Cerebellum-Cortex	5.88
ctx-lh-medialorbitofrontal to Left-Thalamus-Proper	5.64
ctx-lh-medialorbitofrontal to Left-Pallidum	6.02
ctx-lh-medialorbitofrontal to Left-Amygdala	5.85
Left-Thalamus-Proper to Left-Amygdala	5.72
Left-Caudate to Left-Amygdala	5.87
Left-Pallidum to Left-Amygdala	5.97
Left-Amygdala to Left-Accumbens-area	6.02
Left-Accumbens-area to Right-Amygdala	6.03
Right-Putamen to Right-Amygdala	5.64
Right-Pallidum to Right-Amygdala	5.91
Left-Cerebellum-Cortex to ctx-rh-lateralorbitofrontal	5.79
Left-Hippocampus to ctx-rh-lateralorbitofrontal	5.94
Right-Thalamus-Proper to ctx-rh-lateralorbitofrontal	5.81
Right-Pallidum to ctx-rh-lateralorbitofrontal	6.95
Right-Hippocampus to ctx-rh-lateralorbitofrontal	5.70
Right-Amygdala to ctx-rh-parsorbitalis	5.71

Table 3.4

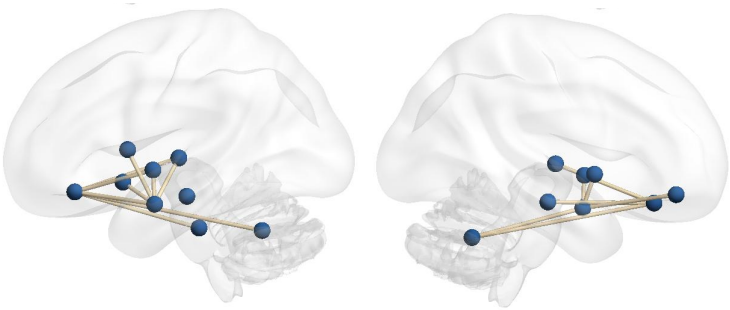

Figure 3.16.

3.4.3.1.4 Results of EDSS

NBS showed that EDSS was characterised by a single significantly disconnected subnetwork of 17 nodes and 24 edges ($p < 0.001$), predominantly involving bilateral inferior frontal cortices, basal ganglia and cerebella, with projections into the left superior frontal and sensorimotor cortices.

Edge	Test statistic
ctx-lh-medialorbitofrontal to ctx-lh-precentral	6.55
ctx-lh-medialorbitofrontal to Left-Cerebellum-Cortex	6.67
ctx-lh-medialorbitofrontal to Left-Thalamus-Proper	6.61
ctx-lh-medialorbitofrontal to Left-Pallidum	6.92
ctx-lh-medialorbitofrontal to Left-Hippocampus	6.71
Left-Pallidum to Left-Hippocampus	6.60
ctx-lh-caudalmiddlefrontal to Left-Amygdala	7.05
ctx-lh-medialorbitofrontal to Left-Amygdala	6.91
ctx-lh-superiorfrontal to Left-Amygdala	6.89
Left-Thalamus-Proper to Left-Amygdala	6.78
Left-Caudate to Left-Amygdala	7.09
Left-Pallidum to Left-Amygdala	7.07
Left-Amygdala to Left-Accumbens-area	6.95
ctx-lh-medialorbitofrontal to Right-Hippocampus	6.78
Left-Accumbens-area to Right-Amygdala	6.90
Right-Pallidum to Right-Amygdala	7.03
Left-Cerebellum-Cortex to ctx-rh-lateralorbitofrontal	7.03
Left-Pallidum to ctx-rh-lateralorbitofrontal	6.57
Left-Hippocampus to ctx-rh-lateralorbitofrontal	6.87
Right-Thalamus-Proper to ctx-rh-lateralorbitofrontal	6.74
Right-Pallidum to ctx-rh-lateralorbitofrontal	6.94
Right-Hippocampus to ctx-rh-lateralorbitofrontal	7.33
Right-Amygdala to Right-Cerebellum-Cortex	7.09
ctx-rh-lateralorbitofrontal to Right-Cerebellum-Cortex	7.17

Table 3.5

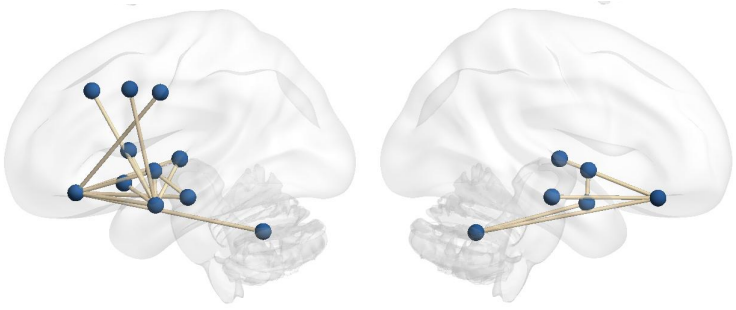

Figure 3.17.

3.4.3.1.5 Results of SDMT

NBS showed that SDMT was characterised by an extremely wide-ranging disconnected subnetwork of 64 nodes and 132 edges (p = 0.014), comprising all areas of the cerebrum and cerebellum. Table not shown.

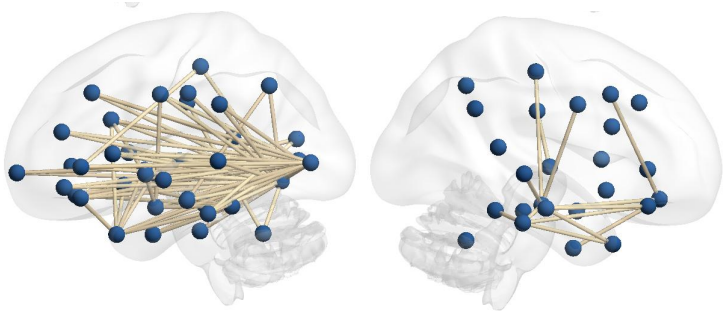

Figure 3.18.

3.4.3.1.6 Results of MSFC

NBS showed that MSFC was characterised by a single significantly disconnected subnetwork of 20 nodes and 25 edges ($p < 0.001$), predominantly involving bilateral cerebella, inferior frontal and inferomedial temporal cortices and basal ganglia, with projections into the left precentral cortex.

Edge	Test statistic
ctx-lh-medialorbitofrontal to ctx-lh-insula	6.06
ctx-lh-medialorbitofrontal to Left-Cerebellum-Cortex	6.20
ctx-lh-medialorbitofrontal to Left-Thalamus-Proper	6.13
ctx-lh-medialorbitofrontal to Left-Pallidum	6.20
ctx-lh-temporalpole to Left-Pallidum	6.31
Left-Pallidum to Left-Hippocampus	6.02
ctx-lh-caudalmiddlefrontal to Left-Amygdala	6.13
ctx-lh-medialorbitofrontal to Left-Amygdala	6.25
ctx-lh-precentral to Left-Amygdala	6.10
Left-Thalamus-Proper to Left-Amygdala	6.18
Left-Caudate to Left-Amygdala	6.35
Left-Pallidum to Left-Amygdala	6.22
Left-Amygdala to Left-Accumbens-area	6.27
Left-Accumbens-area to Right-Amygdala	6.17
Right-Pallidum to Right-Amygdala	6.20
Left-Cerebellum-Cortex to ctx-rh-lateralorbitofrontal	6.27
Left-Hippocampus to ctx-rh-lateralorbitofrontal	6.30
Right-Thalamus-Proper to ctx-rh-lateralorbitofrontal	6.55
Right-Pallidum to ctx-rh-lateralorbitofrontal	6.91
Right-Hippocampus to ctx-rh-lateralorbitofrontal	6.33
Right-Amygdala to ctx-rh-parsorbitalis	6.45
ctx-lh-medialorbitofrontal to Right-Cerebellum-Cortex	6.22
Right-Amygdala to Right-Cerebellum-Cortex	6.29
ctx-rh-lateralorbitofrontal to Right-Cerebellum-Cortex	6.50
ctx-lh-medialorbitofrontal to Brain-Stem	6.24

Table 3.6

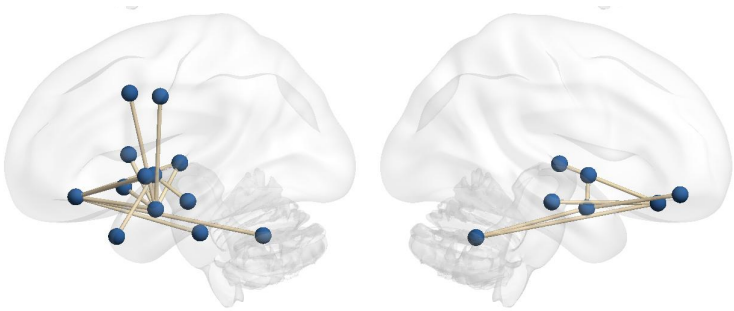

Figure 3.19.

3.4.3.1.7 Results of Relapsing MS vs Progressive MS

NBS showed a difference between the connectomes of RMS and PMS subjects, whilst controlling for age and EDSS, which was characterised by a disconnected subnetwork of 28 nodes and 52 edges ($p < 0.001$), involving bilateral cerebella, inferior frontal and inferomedial temporal cortices and basal ganglia, with projections into the left superior frontal cortices.

Edge	Test statistic
ctx-lh-medialorbitofrontal to ctx-lh-postcentral	16.31
ctx-lh-medialorbitofrontal to ctx-lh-precentral	19.14
ctx-lh-medialorbitofrontal to Left-Cerebellum-Cortex	64.11
ctx-lh-medialorbitofrontal to Left-Thalamus-Proper	39.20
ctx-lh-medialorbitofrontal to Left-Pallidum	48.74
ctx-lh-medialorbitofrontal to Left-Hippocampus	52.24
Left-Pallidum to Left-Hippocampus	30.73
ctx-lh-caudalmiddlefrontal to Left-Amygdala	16.90
ctx-lh-medialorbitofrontal to Left-Amygdala	47.83
ctx-lh-precentral to Left-Amygdala	11.94
ctx-lh-superiorfrontal to Left-Amygdala	12.79
ctx-lh-insula to Left-Amygdala	12.99
Left-Cerebellum-Cortex to Left-Amygdala	15.88
Left-Thalamus-Proper to Left-Amygdala	57.00
Left-Caudate to Left-Amygdala	50.32
Left-Putamen to Left-Amygdala	19.59
Left-Pallidum to Left-Amygdala	43.81
Left-Amygdala to Left-Accumbens-area	77.08
Left-Amygdala to Right-Caudate	15.98
Left-Amygdala to Right-Pallidum	16.34
ctx-lh-medialorbitofrontal to Right-Hippocampus	15.67
Right-Pallidum to Right-Hippocampus	14.94
Left-Cerebellum-Cortex to Right-Amygdala	16.23
Left-Pallidum to Right-Amygdala	10.98
Left-Accumbens-area to Right-Amygdala	45.32
Right-Thalamus-Proper to Right-Amygdala	13.09

Edge	Test statistic
Right-Caudate to Right-Amygdala	11.14
Right-Putamen to Right-Amygdala	23.29
Right-Pallidum to Right-Amygdala	55.37
ctx-lh-medialorbitofrontal to ctx-rh-entorhinal	12.18
Left-Cerebellum-Cortex to ctx-rh-lateralorbitofrontal	44.00
Left-Pallidum to ctx-rh-lateralorbitofrontal	16.64
Left-Hippocampus to ctx-rh-lateralorbitofrontal	59.27
Right-Thalamus-Proper to ctx-rh-lateralorbitofrontal	24.35
Right-Pallidum to ctx-rh-lateralorbitofrontal	21.79
Right-Hippocampus to ctx-rh-lateralorbitofrontal	29.35
Right-Amygdala to ctx-rh-lateralorbitofrontal	13.83
Right-Accumbens-area to ctx-rh-lateralorbitofrontal	13.08
Left-Hippocampus to ctx-rh-medialorbitofrontal	22.08
Left-Amygdala to ctx-rh-medialorbitofrontal	11.15
Right-Amygdala to ctx-rh-medialorbitofrontal	10.21
ctx-rh-entorhinal to ctx-rh-medialorbitofrontal	10.17
Left-Amygdala to ctx-rh-parstriangularis	15.92
ctx-lh-medialorbitofrontal to ctx-rh-postcentral	11.94
Left-Amygdala to ctx-rh-postcentral	11.85
ctx-lh-medialorbitofrontal to Right-Cerebellum-Cortex	33.06
Left-Amygdala to Right-Cerebellum-Cortex	21.33
Right-Amygdala to Right-Cerebellum-Cortex	29.70
ctx-rh-lateralorbitofrontal to Right-Cerebellum-Cortex	45.61
ctx-lh-medialorbitofrontal to Brain-Stem	28.56
Left-Amygdala to Brain-Stem	11.37
Right-Amygdala to Brain-Stem	18.70

Table 3.7

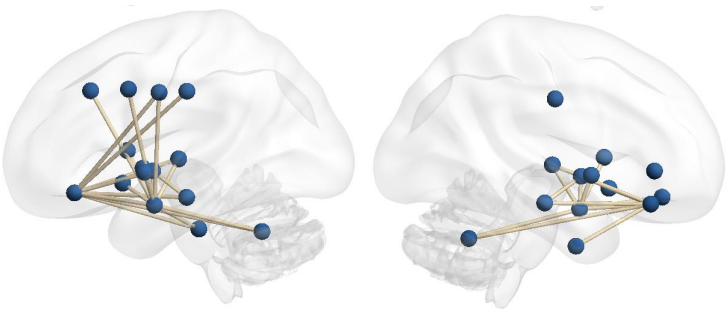

Figure 3.20.

3.4.3.2 NBS Prediction

NBS analysis was used to identify any subnetwork that could predict progression of disability over 24 months. This was analysed for each clinical disability metric as a continuous measure (via the regression function of NBS) as well as for a binary outcome at 24 months (progressors vs non-progressors based on a change in z-score). Neither approach identified any subnetwork that could predict clinical progression.

3.4.3.3 Graph theory metrics- cross sectional

Partial Pearson's correlation two tail tests of the baseline data were also calculated between sensorimotor network (SMN) graph theory metrics and the appropriate contralateral 9HPT scores. Correlations were corrected for age, disease duration, EDSS, disease course (RMS or PMS), T2 lesion volume and normalised whole-brain volume. This found that global efficiency, mean local efficiency, mean nodal strength and mean clustering coefficient, but not mean modularity were correlated with 9HPT cross sectionally (Table 3.8). These results were sustained after multiple comparisons correction with Holm-Bonferroni testing.

Left SMN Graph Theory Metric	Pearson's r with right sided 9HPT	p-value
Characteristic path length	-0.328 *	0.015
Mean Clustering coefficient	-0.379 **	0.006
Global efficiency	-0.356 **	0.009
Mean Local efficiency	-0.382**	0.005
Mean Modularity	0.031	0.32
Mean nodal Strength	-0.328*	0.015

Table 3.8. Right 9HPT partial correlations with left SMN graph theory metrics. * p-value < 0.05, ** p-value < 0.01. Corrected for age, disease duration, EDSS, disease course, T2 lesion volume and normalised whole-brain volume.

Interrogating the graphs of these correlations revealed a correlation largely driven by the PMS group. See representative graph of Left SMN mean Local efficiency in Figure 3.21.

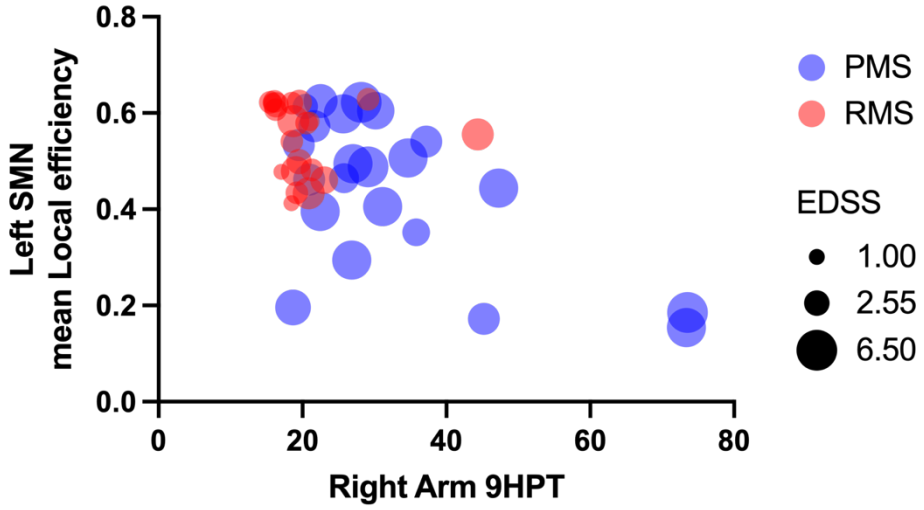

Figure 3.21.

Exploring this further revealed that only PMS subjects had correlation with 9HPT as shown in Table 3.9.

Left SMN Graph Theory Metric	RMS Pearson's r with right sided 9HPT	p-value	PMS Pearson's r with right sided 9HPT	p-value
Characteristic path length	-0.014	0.474	-0.454 *	0.034
Mean Clustering coefficient	-0.024	0.457	-0.481 *	0.025
Global efficiency	-0.011	0.481	-0.460 *	0.032
Mean Local efficiency	-0.023	0.458	-0.482 *	0.025
Mean Modularity	0.249	0.68	0.013	0.56
Mean nodal Strength	-0.014	0.474	-0.454 *	0.034

Table 3.9 Comparing Right 9HPT partial correlations of RMS and PMS subjects. * p-value < 0.05. Corrected for age, disease duration, EDSS, disease course, T2 lesion volume and normalised whole-brain volume.

The results of the right SMN were very similar to the left SMN as represented by the Figure 3.22 of right SMN mean Local efficiency and left 9HPT.

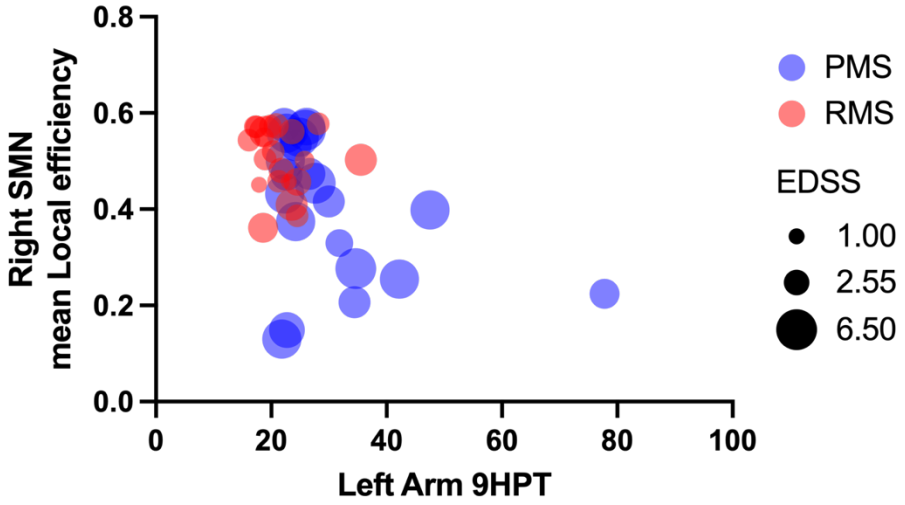

Figure 3.22.

Partial Pearson's correlation two tail tests of the baseline data were calculated between whole brain connectivity graph theory metrics and the MSFC. Correlations were corrected for age, disease duration, EDSS, disease course (RMS or PMS), T2 lesion volume and normalised whole-brain volume. This found that global efficiency, mean local efficiency, mean nodal strength and characteristic path length, but not mean modularity or mean clustering coefficient were correlated with MSFC cross sectionally (Table 3.10). These results were sustained after multiple comparisons correction with Holm-Bonferroni testing.

Whole Brain Graph Theory Metric	Pearson's r with MSFC	p-value
Characteristic path length	0.262 *	0.043
Mean Clustering coefficient	0.251	0.054
Global efficiency	0.270 *	0.038
Mean Local efficiency	0.255 *	0.047
Mean Modularity	0.214	0.182
Mean nodal Strength	0.262 *	0.043

Table 3.10. MSFC partial correlations with graph theory metrics. * indicate a significant Pearson's correlation with p-value < 0.05. Corrected for age, disease duration, EDSS, disease course, T2 lesion volume and normalised whole-brain volume.

Post hoc analysis of the partial correlations shows these correlations were driven largely by bilateral 9HPT as opposed to SDMT or T25FW.

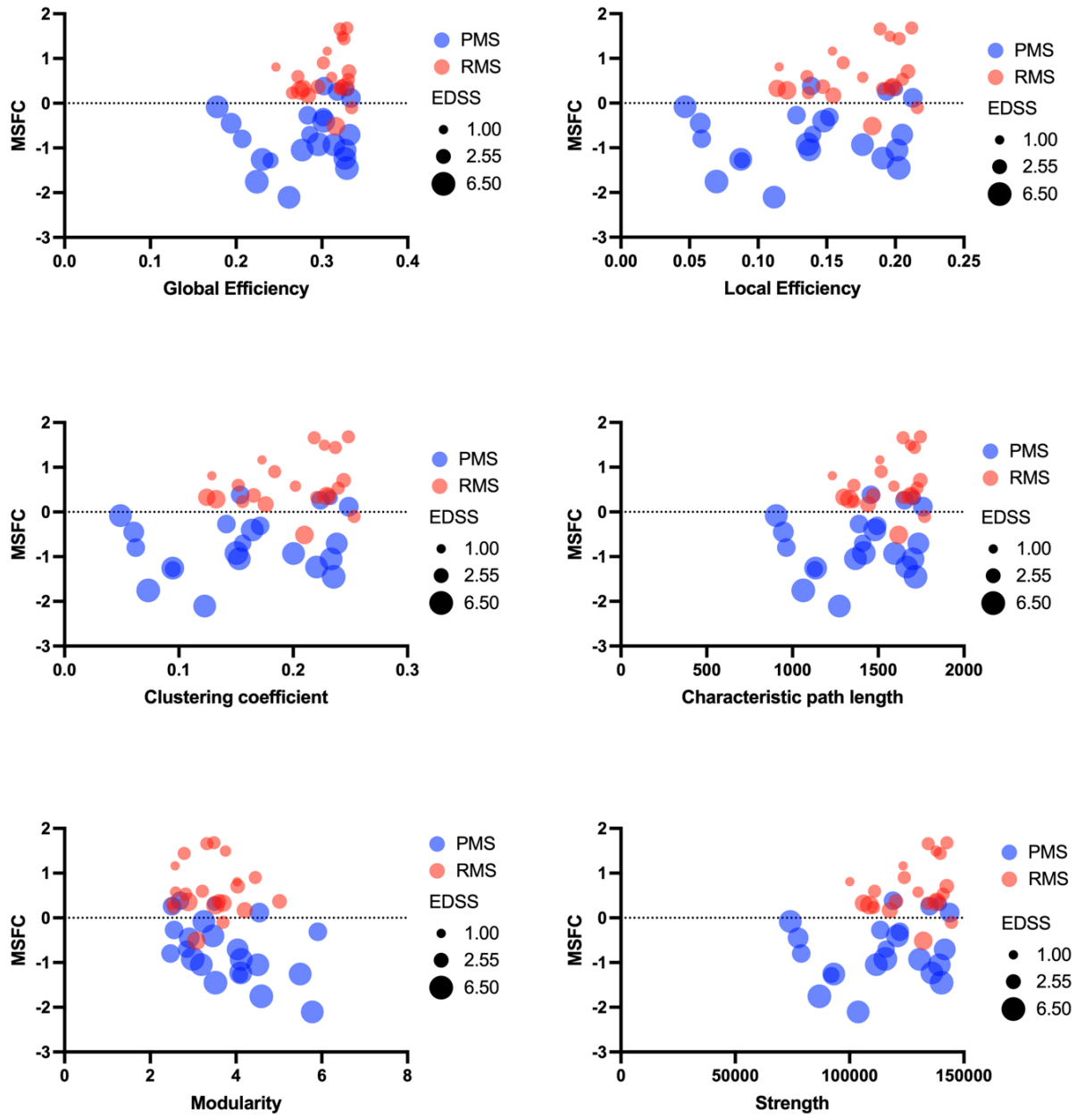

Figure 3.23.

3.4.3.4 Graph theory metrics- prediction

Logistic regression was used to analyse the relationship between baseline whole brain graph theory metrics and the probability of declining in MSFC over 24 months. These regressions were compared to a multiple logistic regression including disease course (RMS vs PMS), disease duration, baseline EDSS, T2 lesion volume, normalised whole brain volume. In this cohort, age and disease duration had a linear relationship and thus both could not be included.

Only baseline modularity contributed to predicting outcomes on MSFC. No other whole brain graph theory metric contributed to predicting outcomes on MSFC.

It was found that the odds of declining by 0.5 MSFC over 24 months increased by 16.2% (95% CI [0.07, 0.27]) for every 1-point reduction in mean whole brain modularity at baseline.

The overall model had a sensitivity of 93.3% and specificity of 62.9% at a cutoff of 0.26 (see Figure 3.24). The log-likelihood ratio versus the intercept-only model was 12.29 (p value = 0.0005) showing significance.

This model outperformed the model of factors including disease course (RMS vs PMS), disease duration, baseline EDSS, T2 lesion volume, and normalised whole brain volume with an Akaike information criterion (AICc) difference of-8.755.

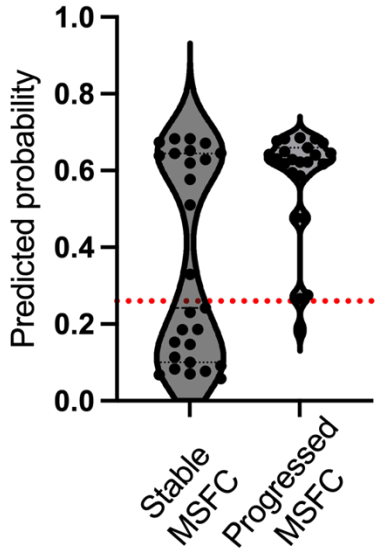

Figure 3.24. Combined RMS and PMS subjects

Further analysis of only the subjects with progressive MS found model of modularity predicting decline in MSFC at 24 months. In PMS subjects the odds of declining by 0.5 MSFC over 24 months increased by 94% (95% CI [0.44, 0.97]) for every 1-point reduction in mean whole brain modularity at baseline.

This overall model had a sensitivity of 100% and specificity of 57.14% at a cutoff of 0.5 (see Figure 3.25). The log-likelihood ratio versus the intercept-only model was 6.729 (p value = 0.0095) showing significance.

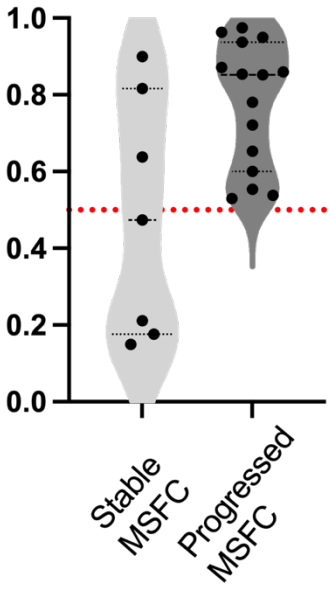

Figure 3.25. PMS subjects

3.4.4 Discussion

3.4.4.1 Local subnetworks mediate disability in MS

This study found significant measures of disconnection that correlate with cross sectional and longitudinal disability in MS. The NBS analysis, a method to find subnetworks with reduced connection that correlate with a clinical outcome, found several plausible correlations that are consistent with known neuroanatomical functions. For instance, 9HPT, which measures lateralised upper limb function including motor and sensory function with a manual dexterity task (Feys et al., 2017), was correlated with a subnetwork of ipsilateral cerebellar and basal ganglia connections, regions associated with fine motor skills and coordination that have previously shown to be major mediators of disability in MS (Tozlu, Jamison, Nguyen, et al., 2021).

The T25FW analysis found a plausible subnetwork also containing bilateral cerebella and basal ganglia nuclei, however with an expanded connection to the prefrontal regions of the medial and lateral orbitofrontal cortices. Of interest, the prefrontal cortex, while best known to mediate reward- and punishment-related behaviour (and thus motivational behaviour) (Rolls, 2004), also has numerous connections to motor centres including the basal ganglia and supplementary motor cortices (Goldman-Rakic, 1987; Schulz et al., 2019). Similarly the subnetwork associated with increasing EDSS severity also included prefrontal cortices, in addition to projections superiorly into the dominant left hemisphere sensorimotor cortices. A dominant hemisphere or lateralisation bias has not been previously reported to occur in the EDSS assessment, as has been with other disability scales like the NIHSS (Fink et al., 2002), as it is mainly determined by mobility, limb function and vision, and not dominant cortical dysfunctions of language, apraxia and other cognitive measures (Abulaban, 2020). The subnetwork connection with dominant hemisphere cortical nodes identified in this study might be a non-causal association with the EDSS, or might imply a dominant hemisphere bias as yet undescribed in the EDSS, related to motor planning and other higher order sensorimotor functions.

To my knowledge, this work is the first to implicate disconnection of the prefrontal – basal ganglia connections in physical disability associated with MS, and proposes an alternative mechanism of mobility dysfunction in MS. T25FW and EDSS worsening, largely driven by lower limb mobility, may not only be mediated by lower limb weakness, balance and sensory deficits, but possibly by the lack of integration and loss of learned coordination that prefrontal cortex dysfunction implies, from its disparate connections to the basal ganglia, thalami, somatosensory, visual and premotor cortical regions (Rolls, 2004). This could be consistent with other studies that have found independent contributions of cognitive and executive function to motor outcomes, beyond that which would be explained by T2 lesion volume (Mistri et al., 2022).

MSFC was associated with a significant subnetwork that was predictable based on the NBS results of its constitutive parts, namely the 9HPT and T25FW, i.e. a subnetwork that mimicked that seen in both analyses. The network identified by NBS to correlate with SDMT was widespread even with a high threshold, containing 64 out of a possible 85 nodes, and incorporating all cortical regions. SDMT is a measure of cognitive processing speed that influences a variety of downstream cognitive functions including memory, language and decision making (R. H. Benedict et al., 2017). It has been shown to be commonly abnormal in pwMS and a surrogate marker of cognitive dysfunction, with adoption by some, including here, into the MSFC replacing the Paced Auditory Serial Addition Test (PASAT) (Drake et al., 2010). Several imaging studies have sought to clarify the mechanism of slowed information processing speed in MS and have found associations with globally lower structural connectivity (Pagani et al., 2019) and lower connectivity of the default mode network (Has Silemek et al., 2020) as well as cortical and deep grey matter atrophy (Marzi et al., 2023; Sandroff et al., 2022). The overall capacity of MRI to predict longitudinal SDMT outcomes was rated as medium in a meta-regression analysis of all relevant studies (Pike et al., 2022), without finding any distinct biomarker that overly influences the pooled effect size. This is entirely consistent with the hypothesis that information processing speed and thus SDMT is a cortically widespread driven cognitive function with significant mediators being highly connected regions such as the thalamus. The present findings corroborate this hypothesis and, although this large network would not be a useful biomarker due to its extent, support the utility of this method to accurately model disconnection in MS.

Another interesting result seen here was the differences in disconnection between RMS and PMS subjects. The NBS method identified a differentiated subnetwork of similar nodes to that seen with the disability metrics of 9HPT, T25FW and EDSS, however with greater connection with the distal brainstem and, by extension, the spinal cord. Previous studies have highlighted regional differences between RMS and PMS at the spinal cord (Cawley et al., 2017; Tsagkas et al., 2018, 2019), anterior horn cells (Tsagkas et al., 2022), cerebellum (Parmar et al., 2022; Schoonheim, Douw, et al., 2021) and thalamus (Schoonheim, Pinter, et al., 2021). In this study, the subnetwork nodes were disconnected despite controlling for age and EDSS in an ANCOVA design implemented in NBS, which suggests that posterior fossa, basal ganglia and brainstem structures are disconnected independent of their effect on disability in patients with PMS, thereby implicating this subnetwork as a potential harbinger of future disability in PMS. However, this is inconsistent with the results of the NBS prediction analysis, which failed to find any significant subnetwork change that correlated with disability progression in a continuous regression model; and also did not predict future disability progression from baseline disconnection metrics in subjects with RMS or PMS.

It is unclear why NBS in this study did not predict future disability accrual given the correlations with cross sectional disability and difference between RMS and PMS subjects. Several possibilities might underlie this. Firstly, the sub networks involved in mediating disability may be resistant to change after disconnection occurs. That is, after the initial disconnection event further progression in disability may be mediated by factors not associated with that particular subnetwork disconnection, but perhaps by further downstream deterioration through transsynaptic degeneration or cumulative damage in more widespread support networks. Secondly, this method models change in the connectome between time points when new lesions occur, lesions increase in size or when the T1 hypointensity of lesions changes. If none of these events occur there should be no change in the connectome measured. In relapsing MS treated with modern disease modifying therapies, new lesion accrual and expanding lesions are infrequent. The change in T1 hypointensity of lesions over time has been shown in previous studies to be measurable and significant (Elliott, Belachew, et al., 2019), but perhaps the change is not sensitive enough to track with disability over the time frame of a 24 month study.

3.4.4.2 Modelling cumulative damage identifies additional disconnection

The method of modelling cumulative damage along streamlines used in the study was able to identify an extension of the subnetwork associated with EDSS. As shown in Figure 3.26. the cumulative damage method discovered a subnetwork inclusive of dominant hemisphere frontal cortical nodes, whereas the model of binary lesion damage did not.

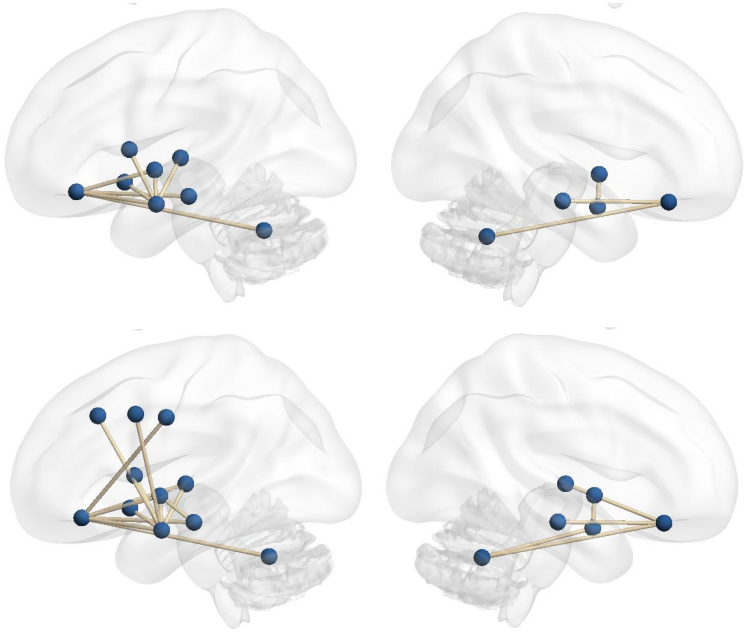

Figure 3.26. Binary lesion model above (left and right), cumulative damage lesion model below (left and right).

This is an interesting and seemingly counterintuitive finding as the binary lesion model might be thought to include more overtly damaged connections and thus more expansive subnetworks. However, the NBS model correlates the severity of disconnection with the severity of clinical outcome ie. EDSS; as such, a graded measure of damage is better suited to finding significant disconnections, which in this case generated a more expansive disconnected subnetwork of nodes (Zalesky et al., 2010).

3.4.4.3 Sensorimotor network disruption mediates upper limb physical disability in progressive MS

The sensorimotor network was analysed with standard graph metrics and found to have significant correlations to upper limb physical disability. The sensorimotor network has been implicated in a number of studies as a mediator of clinical disability in MS with network metrics derived from cortical atrophy (Cao et al., 2021), structural (Pardini et al., 2015; Shu et al., 2011), functional (Fling et al., 2019) and multimodal (Zhong et al., 2016) connectivity methods. The success of employing network analysis on the sensorimotor network in MS is a clear example of the advantages of modelling brain networks over and above focal anatomical regions or individual tracts (Lapucci et al., 2022). In this study, further utility of the sensorimotor network was explored by analysing the correlations with lateralised upper limb function in the form of 9HPT. Previous studies have mainly found the sensorimotor network to be associated with bilateral physical disability such as mobility or the EDSS, however given the network can be separated into left and right parts, there is an opportunity to further evaluate the specificity of this network with lateralised motor deficits. As mentioned earlier, the nodes chosen for this network were the contralateral primary and supplementary motor and sensory cortices, contralateral thalamus, contralateral basal ganglia and ipsilateral cerebellum. Partial correlations controlling for age, disease duration, EDSS, disease course (RMS or PMS), T2 lesion volume and normalised whole-brain volume found that global efficiency, mean local efficiency, mean nodal strength and mean clustering coefficient negatively correlated with 9HPT, meaning that reductions in these metrics correlated with a higher 9HPT time (or worse upper limb function). Importantly these correlations were independent of T2 lesion volume and EDSS. Furthermore, the plots of each correlation clearly showed a split between the RMS and PMS subjects (as shown in Figures 3.21, 3.22) and this was further demonstrated with significant partial Pearson's correlations only for the PMS subjects with strong Pearson r values of ~-0.45 (as shown in Table 3.9).

The dichotomy between RMS and PMS is intriguing. Although the RMS cohort had relatively preserved upper limb function, these results might suggest that sensorimotor network disconnection is a *necessary condition* for upper limb disability in MS, but not a *sufficient* one. As postulated earlier in the discussion with respect to NBS-identified sub networks, damage to other support networks or structures might be required for the development of upper limb dysfunction subsequent to disruption of the sensorimotor network; and it stands to reason that these support networks are more likely to be damaged in PMS due to the widespread

neurodegeneration and atrophy present in this disease phenotype (Lassmann et al., 2012). In other disease processes, such as stroke, functional connections of “extra motor” networks including cingulo-opercular and default mode networks have been found to predict motor recovery and response to physical therapy following damage to the sensorimotor network (Mattos et al., 2023), whereas others have found specific connections within the sensorimotor network that are more important in predicting long term disability after stroke such as the primary sensorimotor cortex – putamen connection (Bonkhoff et al., 2021).

This concept that disability in MS is driven by two components, a substrate and support component, has been previously proposed as the so called “topographical model of MS and recapitulation theory” (Krieger et al., 2016). Briefly, this theory explicates the observed clinical-radiological paradox in MS by stating that focal lesions and relapses will only manifest if their severity is above a certain threshold, but that the threshold can change over time, thereby unmasking previously recovered deficits or even previously clinically silent lesions. The concept of a progressive reduction in this threshold is identified as loss of functional neurological reserve. Initially in this model the site of neurological deficit is defined by the location of focal lesions (the topographic concept), and the reserve by whole brain atrophy (‘ECTRIMS 2022 – EP0997’, 2022; Krieger et al., 2016). However, the model is also open to other constructs of topography and reserve and it remains to be discovered what metric, whether it be structural or functional, may best determine these components (Krieger & Sumowski, 2018). The results of the present study could be consistent with the topographical framework, in which sensorimotor network disconnection replaces focal lesions as the topographic substrate, and an as yet undiscovered metric that is preferentially affected in PMS, represents neurological reserve within the system. It is interesting to note that the correlations of sensorimotor network disconnection and 9HPT here were independent of whole brain volume, suggesting that atrophy as a global measure of functional reserve is not adequate in this instance.

3.4.4.4 Whole brain graph metrics of disconnection correlate with global disability

The whole brain connectome made up of 85 x 85 nodes was analysed with graph metrics and found to have significant correlations with the MSFC at baseline. As can be appreciated from the graphs in Figure 3.23, the correlations of global efficiency, mean local efficiency, mean nodal

strength, characteristic path length and mean clustering coefficient with MSFC were similar, with all but mean clustering coefficient surviving multiple comparisons testing for significance. However, when these graph metrics were used in a logistic regression model to predict decline in MSFC at 24 months only baseline mean modularity contributed to the model's predictive power. Mean modularity outperformed a model of disease course (RMS vs PMS), disease duration, baseline EDSS, T2 lesion volume and normalised whole brain volume, predicting progression in MSFC in the full cohort of RMS and PMS with a sensitivity of 93.3% and specificity of 62.9%. Furthermore, in PMS subjects, the sensitivity was 100% and specificity of 57.14%, with a calculated odds of declining by at least 0.5 MSFC over 24 months increased by 94% (95% CI [0.44, 0.97]) for every 1-point reduction in mean whole brain modularity at baseline.

One weakness of this study is the relatively small number of subjects who did not worsen on the MSFC within the PMS group (see Figure 3.25). Given the low numbers of non-progressors in this group, definitive conclusions about the utility of baseline mean modularity in PMS cannot be made. However when combining the two cohorts of RMS and PMS, overall baseline mean modularity performed well in predicting 24 months MSFC progression.

Modularity as a metric describes the extent to which individual subnetworks (otherwise termed modules) are segregated from the rest of the network structure (Newman & Girvan, 2004). High modularity describes the state in which subnetworks have a high amount of intra-network connection but relatively less connection to other subnetworks. Modularity of the brain connectome has been implicated in enabling complex cognitive processes and neuroplasticity (Baniqued et al., 2018) as well as reducing with age, potentially explaining reduction in cognitive faculties with age (Chan et al., 2014; Onoda & Yamaguchi, 2013). Outside of the field of MS, modularity has been positively correlated with cognitive level in Alzheimer's (de Haan et al., 2012) and with responsiveness to cognitive training in disease processes such as traumatic brain injury (Arnemann et al., 2015), but also in healthy individuals (Gallen et al., 2016), giving support for its use as a general biomarker across multiple situations and interventions (Baniqued et al., 2018).

However, in the field of MS, the story has been mixed. Liu et al. found that inter-module efficiency (a metric closely related to more classical modularity) was reduced in pwMS

compared to healthy controls and furthermore associated with physical and cognitive disability (Liu et al., 2018). In contrast, others have found modularity to be inversely correlated with cognitive function using PASAT-3 and the SDMT (Gamboa et al., 2014; Welton et al., 2020), especially in CIS and early RRMS (Tur, Grussu, et al., 2019). In addition, long range connections have been found to be more disrupted than short range connections in MS, a feature that would tend to increase modularity as inter module connections are more likely to be long range than intra module connections, which are necessarily short range. Furthermore, these long range disconnections were correlated with lower cognitive performance (Meijer et al., 2020).

The reason for the distinction between MS and other brain disease states in relation to modularity is not clear. However, Fleischer et al. observed that modularity in MS followed an inverse U-shape that was evident over the first 5 years after diagnosis (Fleischer et al., 2017). Understood in this way, the initial increase in modularity observed might be related to early compensatory mechanisms, which tend to fail even over a relatively short time. Indeed, most of the studies identifying modularity as a potential biomarker in MS were undertaken in the early stages of the disease, potentially in the initial upslope of modularity change, and may have missed the dynamic changes observed by Fleischer et. al, and the eventual reduction in the metric. Given this, the results found here that modularity predicts 24 month decline in MSFC, more so in the cohort of PMS, could still be in keeping with previous studies into early MS, but more comfortably consistent with known mechanisms in neuroscience (Chan et al., 2014; Onoda & Yamaguchi, 2013) and other neurological disease states (Arnemann et al., 2015; de Haan et al., 2012).

3.4.5 Conclusion

This study provides evidence that disconnection of sub-networks involving posterior fossa structures and deep grey matter mediate disability in MS and are a distinguishing marker between RMS and PMS. This was further confirmed with the correlation of sensorimotor network disconnection to focal lateralised upper limb disability in PMS. Whole brain network disruption of modularity architecture can predict progressive disability in MS and should be explored further as a biomarker of progression in expanded datasets over longer timeframes.

3.5 Chapter Summary

This chapter explored the use of atlas-based network analysis in MS. The aim of this analysis was to refine the existing atlas-based approach by incorporating disease specific mechanisms into the analysis.

The chapter provided evidence that a multimodal registration technique, incorporating T1, FA, and MD tissue contrast sequences, improves registration compared to unimodal registration techniques. This refinement is particularly relevant to MS pathology, considering the heterogeneous location of MS lesions, including cortical/juxtacortical regions and deep white matter regions.

A novel concept of modelling cumulative damage along streamlines was introduced. This approach demonstrated a better correlation with a functional measurement of mfVEP along the optic tracts in MS patients. It outperformed classical binary or wholly truncated lesion models, as well as so-called weakest link models.

Finally, the refined atlas-based tractography approach was studied in a longitudinal cohort of MS patients over a period of 24 months, including RRMS and PMS. The analysis revealed the presence of subnetworks in the basal ganglia and posterior fossa, which were found to mediate much of the disability in MS and contribute to PMS progression. Additionally, reduced modularity was identified as a predictor of future disability in MS, highlighting its potential as a biomarker that warrants further investigation with larger datasets.

This chapter significantly advances atlas-based network analysis in MS research, emphasising its ability to incorporate disease-specific mechanisms. It introduces two refined components for atlas-based network measurement in MS: accurate registration and modelling of cumulative damage. The findings shed light on the role of specific subnetworks in MS pathology and provide insights into potential biomarkers for disability prediction and monitoring.

Chapter 4

Diffusion-based disconnectome modelling in multiple sclerosis

Abstract

Diffusion-based structural network analysis is widely utilised, however its effectiveness is compromised in MS and other pathological conditions where white matter axons are truncated. Alterations in the underlying diffusion signal due to focal pathology can lead to inaccuracies in streamline propagation that rely on coherent diffusion signals to recreate white matter bundles.

This chapter explores both the advantages and disadvantages of employing diffusion tractography in MS. A refined method of tractography is described, which aims to improve the accuracy of tract density within destructive MS lesions. Lastly, a longitudinal study is reported, utilising this refined method to investigate network community structure in MS and assess its potential for predicting disease progression.

4.1 Background

The use of diffusion-weighted magnetic resonance imaging (dMRI) constitutes a non-invasive modality that enables the assessment of white matter integrity in the context of MS. By characterising the white matter microstructure, researchers have gained valuable insights into the pathophysiology of MS (Boonstra et al., 2022; Kato et al., 2022; Solana et al., 2018; Storelli et al., 2022). This technique has the ability to identify early changes in white matter integrity that are not detectable by other imaging modalities (You et al., 2019), such as conventional MRI.

Disconnectome modelling represents a further application of dMRI, in which disrupted connections within the white matter network of the brain are characterised with structural tractography based on the dMRI signal (C.-H. Yeh et al., 2021). This approach has proven useful in identifying specific networks and regions of the brain that are most affected by MS (Ashton et al., 2021; Cao et al., 2021; Schoonheim, Douw, et al., 2021; Schoonheim, Pinter, et al., 2021; Tur, Eshaghi, et al., 2018), and in elucidating complex mechanisms underlying neurodegeneration (Chen et al., 2022; Hardy et al., 2016; Rocca et al., 2013).

The accuracy of tractography has been interrogated in a wide range of brain pathologies over the past 10 years. The particular impact of each pathology on accurate streamline construction must be assessed; and in the case of MS significant challenges remain. These issues include the distorting effect of MS lesion diffusion isotropy on streamline propagation (Lipp et al., 2020); the effect of atrophy on streamline construction; and the appropriate weighting of streamlines given focal MS lesion damage (Sarwar et al., 2019; Schiavi et al., 2020b; R. E. Smith et al., 2015a; R. E. Smith, Calamante, & Connelly, 2020b; R. E. Smith, Calamante, Gajamange, et al., 2020; Zalesky, Sarwar, & Ramamohanarao, 2020).

Graph theory provides a framework for analysing networks, including the brain's white matter network (Fornito et al., 2015). A key advantage of using graph theory is the ability to identify complex patterns of connectivity, such as clustering and community structure (Newman & Girvan, 2004; Sporns, 2018). These patterns are not readily apparent through other network metrics, such as degree or strength, which primarily reflect nodes in isolation, nor in other

imaging methods of analysis such as routine structural anatomical imaging. Some studies have described changes to clustering and community structure in MS and associations with disability (Charalambous et al., 2019; Fleischer et al., 2017; Schiavi et al., 2020b; Tur, Eshaghi, et al., 2018), however few have analysed these over significant periods of time (Fleischer et al., 2017; Tur, Eshaghi, et al., 2018), and fewer still have attempted to correct for problems that are inherent to tractography construction in MS (Schiavi et al., 2020b).

In this chapter, we review the relative advantages and disadvantages of diffusion based tractography in MS, before refining a pipeline of CSD based tractography to better represent MS lesion contribution to the disconnectome in MS. Finally, we apply this refined pipeline to a longitudinal cohort of pwMS to explore the contribution of clustering and community structure to progressive disability in MS.

4.1.1 Advantages of diffusion-based approach

Of the many methods described for measuring the human connectome and the pathological disconnectome in MS, diffusion-based structural tractography has many benefits. Direct measurement of the diffusion signal within the subject's space, that is without the need for registration to healthy control templates, has advantages over atlas-based methods. Firstly, it allows for retention of high-resolution spatial information, especially in areas of high anatomical variability. This is problematic for registration algorithms in heterogenous cohorts such as MS that exhibit significant variance in individual pathology and atrophy characteristics, both regionally and globally (Ge et al., 2000; Kezele et al., 2008). Atlas-based approaches are convenient but oblivious to individual variability in tract size and shape (Lipp et al., 2020), whereas direct measurement of white matter pathways, achievable in diffusion based tractography, captures subject-level differences. Secondly, working in subject space avoids the introduction of interpolation artifacts inherent to the registration of complex multidirectional diffusion signals within each voxel (Geng et al., 2011; Le Bihan et al., 2006; D. Raffelt et al., 2011), and retains high resolution spatial information improving the accuracy of including smaller structures in the brain. Several smaller regions that benefit from the increased accuracy of diffusion-based tractography have been implicated in MS disease pathology, especially progressive disease pathology, such as the thalamus (Kipp et al., 2015; Wagenknecht et al.,

2016; Zivadinov et al., 2013), other deep grey matter nuclei (Lassmann et al., 2012; Rovaris et al., 2005) and brainstem (Andelova et al., 2022).

In addition to spatial advantages, diffusion based tractography allows for the capture of pathology that is sensitive to the diffusion signal of MRI. Many studies have found widespread diffusion changes in NAWM, indicating reduced tissue organisation or damage (Cercignani & Gandini Wheeler-Kingshott, 2018; Kato et al., 2022; Toschi et al., 2019); and within lesions, indicative of progressive tissue destruction due to axonal loss (Bergsland et al., 2021; Klistorner, Wang, et al., 2018; Shi et al., 2023).

4.1.2 Disadvantages of diffusion-based approach

Despite the advantages of structural diffusion-based tractography, measurement of the disconnectome in MS using this approach presents a number of unique challenges. Tractography involves the generation of artificial streamlines within the brain white matter that follow the underlying direction of diffusivity through the method of fibre-tracking. However, MS white matter lesions typically change the diffusivity profile of the underlying white matter due to demyelination, axonal degeneration, oedema and gliosis, generally increasing isotropy (Filippi et al., 2001). This makes it a challenge to accurately propagate streamlines through MS lesions and different methods perform differently in this regard (Lipp et al., 2020). At each step of fibre tracking, a diffusion-based measure (e.g. FOD amplitude, or FA) and angle are used as criteria for the continuation of fibres to the next voxel or step, or for fibre termination or removal from the connectome. Tractography methods use different thresholds based on the underlying diffusion algorithm to achieve this. For instance, early studies with tensor imaging used FA as the amplitude criterion for streamline truncation, however this was recognised as inaccurate (Ciccarelli et al., 2008) due to the significant effect of MS lesions on FA signal. More recent implementations of tractography that utilise CSD (Tournier et al., 2019) have substantive benefits over tensor-based approaches for modelling multiple fibre directions within a single voxel, a key element in overcoming tensor based tractography limitations of crossing fibres. CSD has revealed that up to 90% of brain white matter voxels contain crossing fibres (Jeurissen et al., 2013), emphasising the superiority of the technique over DTI for tractography applications (Jeurissen et al., 2019). The amplitude criterion for fibre tracking used in CSD is

based on the fibre orientation distribution (FOD) amplitude for a given direction arc. The choice of threshold for the FOD amplitude is arbitrary, as there is no clear in-vivo relationship with axonal damage; and its accurate application is reliant on dMRI quality, acquisition type (single vs multi-shell) and angular resolution. The choice of FOD amplitude threshold in MS walks the 'tight rope' between too high a value, which may result in inaccurate termination of streamlines due to damaged diffusion signal from MS lesions; and too low a value, which increases the number of spurious streamlines or false positives (Lipp et al., 2020). Within the MRtrix3 application, a default FOD amplitude threshold of 0.1 is used, informed by the number of false positive orientations reconstructed on a multifiber simulation as shown by Jeurissen et. al. below:

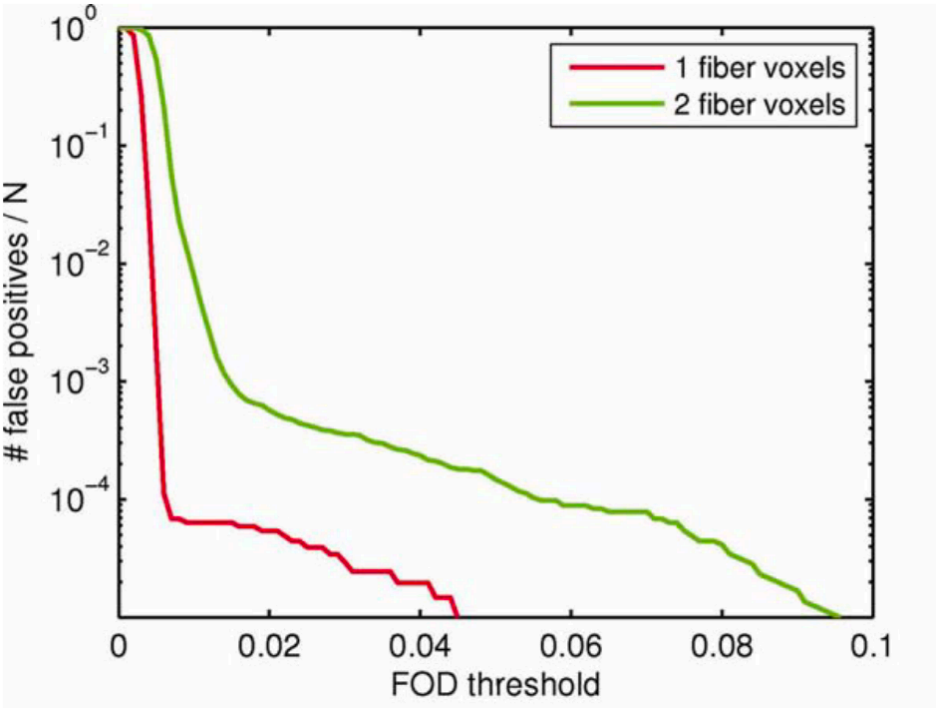

Figure. 4.1. Extracted and adapted from Jeurissen et. al., shows the default threshold of 0.1, which minimises the number of spurious or false positive orientations generated for multifiber or crossing fibre voxels (Jeurissen et al., 2013).

In a comparison study between DTI, CSD and damped Richardson-Lucy (dRL) deconvolution based tractography in MS, Lipp et al. found that in a simulated dataset of single and crossing fibres, CSD with a FOD amplitude threshold of 0.1 generated false positive peaks in up to 25% of voxels, which was only corrected by raising the threshold to 0.3. In addition, after

tractography with an FOD amplitude termination criterion of 0.1 and angular termination criterion of 45°, more streamlines were terminated within lesions due to the angular criterion than the amplitude criterion. This suggests that in lesional tissue CSD streamlines were more likely to follow spurious peaks and be terminated due to excessive curvature than be terminated due to low FOD amplitude (Lipp et al., 2020). Despite this, T1 hypointense lesions did show lower FOD amplitudes than T1 iso-intense (but T2 hyperintense) MS lesions, suggesting some degree of representation of FOD amplitude for axonal degeneration. It is probable that these results are contingent on the single tissue CSD and dMRI acquisition protocol used, and may not be generalisable to multi-shell acquisitions or multi-tissue resolved CSD as the isotopic compartments would be modelled differently.

Amplitude and angular streamline criteria are not the only implemented methods for reducing spurious fibre tracking. Boundary constraints have been used to further reduce spurious streamline generation, such as the implementation of anatomically constrained tractography (ACT) (R. E. Smith et al., 2012) for CSD tractography in the MRtrix3 application. Accurate fibre tracking is aided in this regard by high resolution T1-weighted tissue-type segmentation, which can include pathological tissue with bespoke criteria limited to MS lesional tissue. For instance, in one application optic tract reconstruction was improved by the use of automated ACT without the need for further manual segmentation, because ACT prevented the occurrence of the most implausible tracks (Horbruegger et al., 2019). The utility of ACT is also further signified by the permissiveness of a lower FOD amplitude threshold when ACT is engaged in streamline tracking within the MRtrix3 application (R. E. Smith et al., 2012; Tournier et al., 2010).

In addition to boundary constraints, tractogram filtering is a method of either removing or weighting the final streamline construction based on underlying plausible white matter tracts informed by the *explainability of the diffusion signal* (Jörgens et al., 2021). In MRtrix3, SIFT analyses the contribution of each streamline to the underlying FOD signal and determines whether that streamline is deemed redundant/noisy or not (Jörgens et al., 2021). In the original SIFT application (R. E. Smith et al., 2013), streamlines are excluded based on these criteria, but in the second generation SIFT2 application (R. E. Smith et al., 2015a) streamlines are weighted based on these criteria. Disagreements have emerged about the performance of the SIFT2 algorithm in pathological states, especially truncating pathology such as MS (Sarwar et al.,

2019; R. E. Smith, Calamante, & Connelly, 2020a, 2020b; R. E. Smith, Calamante, Gajamange, et al., 2020; Zalesky, Sarwar, & Kotagiri, 2020; Zalesky, Sarwar, & Ramamohanarao, 2020). One key element is that the SIFT2 algorithm weights a streamline based on an *average* of the underlying cross sectional fibre density along its entire path, thus truncating focal pathology is essentially averaged out of influencing the final weighting. Smith et. al. proposed a modification of SIFT2 to modulate the streamline weighting based on the lowest fibre density value along its course, which seemed to better reflect estimated fibre density on diffusion imaging (R. E. Smith, Calamante, Gajamange, et al., 2020). Although this is a promising development, it has yet to be shown whether modulating the streamline weighting based on the lowest fibre density does not affect network construction in healthy tissue outside of truncating pathology and has not been released in the MRtrix3 package.

The disadvantages of the diffusion-based approach to network analysis in MS outlined here has mainly been framed around the inaccurate reconstruction of a full tractogram and whole brain connectome in the presence of interfering destructive pathology. Few studies have explored the relative diffusion profiles of MS lesions using advanced diffusion techniques (Martínez-Heras et al., 2020; Rahmanzadeh et al., 2022; Shi et al., 2023) and even fewer the effect of lesions on disconnectome modelling in MS (Lipp et al., 2020; Sarwar et al., 2019; R. E. Smith, Calamante, Gajamange, et al., 2020). However, if the goal of the study is to model the *dis*connectome that is caused by MS lesions, a representative tractogram that accounts for streamline loss from MS lesions would provide an ideal framework for analysing disconnection. The next section outlines such an approach.

4.2 Refining the modelling of lesional damage in tractography

4.2.1 Introduction

MS lesions seen on MRI contribute significantly to MS disability progression, despite the so-called clinico-radiological mismatch (Barkhof, 2002; D. K. B. Li et al., 2006). The term, which highlights the weak correlation between MS T2 lesion volume and clinical disability, has been often invoked but also increasingly recanted. Further study into specific biomarker characteristics of MS lesions beyond T2 hyperintense signal have yielded improved correlations with disability, including T1 hypointensity, slowly expanding lesions (Elliott, Belachew, et al., 2019; Elliott, Wolinsky, et al., 2019), paramagnetic rim lesions (Tozlu, Jamison, Nguyen, et al., 2021), focal diffusion tensor signals such as MD (Klistorner, Wang, et al., 2018) and multi-compartment spherical mean technique values such as intra-neurite volume fraction (Martínez-Heras et al., 2020). In addition to microstructural biomarkers, modelling of MS lesion distribution beyond a raw whole brain volume analysis significantly improves the explanatory power of MS lesions on disability, with evidence for motor pathway and spinal cord involvement (Keegan et al., 2018; Sechi et al., 2020), specific subnetwork (Y. Li et al., 2022; Llufriu et al., 2017) and whole brain network (Charalambous et al., 2019; Pagani et al., 2019; Tur, Eshaghi, et al., 2018) disconnection. Microstructural heterogeneity and variance in lesion distribution therefore account for much of the clinic-radiological paradox.

While MS lesions hinder the propagation of streamlines (section 4.2.2) and therefore potentially impact the accuracy of tractography, this apparent shortcoming may be exploited to provide more granular explication of the disconnectome. The challenge is how to propagate the correct number of streamlines through lesions to accurately reflect underlying axonal loss and accurately represent the disconnection that is occurring.

The MRtrix3 diffusion MRI analysis package uses an advanced diffusion model (CSD), which is able to model multiple fibre orientations within a single voxel and accurately model crossing fibre bundles (Tournier et al., 2019). The whole brain tractogram pipeline developed within MRtrix3 computes FODs for each voxel and then generates voxel to voxel streamlines. The MRtrix3 probabilistic tractography algorithm uses a FOD amplitude and angular threshold as

well as anatomically constrained tractography (ACT) to accurately limit streamline propagation. For the default second order integration probabilistic tractography method (iFOD2) utilised in MRtrix3 (Tournier et al., 2010), the default FOD amplitude threshold is 0.1, reduced to 0.05 when combined with ACT, and the angular threshold is 45°. Lipp et al. found that, with these parameters, the average peak FOD amplitude along the direction of streamline tangents was not different between voxels of lesions and those of normal appearing white matter (Lipp et al., 2020), however this is likely to be an insensitive measure due to averaging. In addition, the high rate of spurious or false positive streamlines (albeit without ACT) stemming from MS lesions at this amplitude and angular threshold make these parameters unsuitable. While one could increase the FOD amplitude threshold to better capture lesion related diffusion changes, the impact of this change on white matter tract construction in non-pathological NAWM, and connectome graph theory metrics of interest, is not well defined. The guidance on threshold choice given by Jeurissen et. al. suggested a lower threshold level at which false positive orientations were reduced, but as shown in the extracted Figure 4.2, no upper threshold level is obvious as there is no stability across threshold values that maintains equal distribution of white matter voxels that contain 1, 2 or 3 fibre orientations (Jeurissen et al., 2013). However up to a threshold of 0.15 the number of voxels without resolved fibre orientations is negligible, and there still exists a high number of multi-fibre orientation voxels, making this value a reasonable upper bound to investigate.

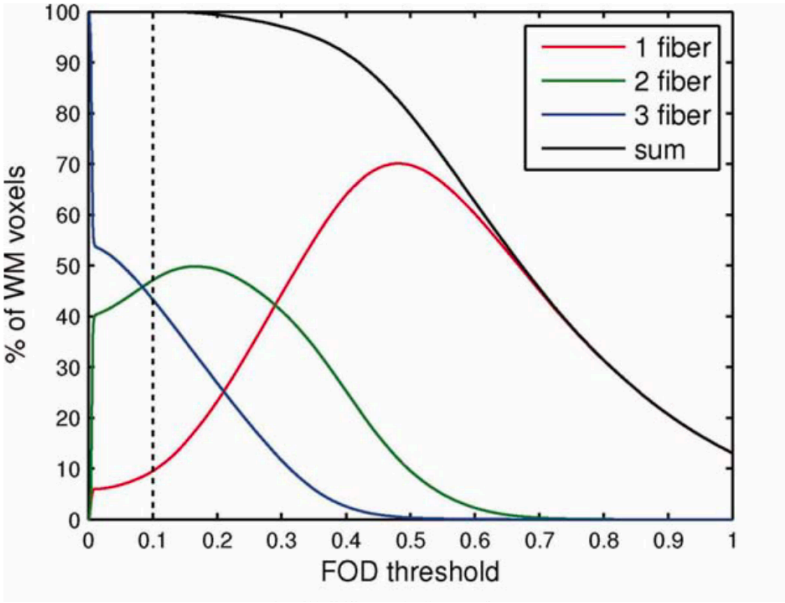

Figure. 4.2. Extracted and adapted from Jeurissen et. al., shows the effect of FOD amplitude threshold change on the percentage of WM voxels modelling 1, 2 or 3 fibre orientations (Jeurissen et al., 2013).

This study explores an FOD amplitude threshold that would simultaneously maintain good network construction through stability of graph theory metrics, whilst better modelling the destructiveness of MS lesions by reducing lesional streamline density.

4.2.2 Methods

10 healthy controls subjects and 10 pwMS stable on disease modifying therapy underwent MR scanning at a single timepoint. MR scans were acquired on a 3T GE MR750 (General Electric, Milwaukee, WI, USA), using a multi-channel head and neck coil. The following sequences were acquired: 3D Fluid-Attenuated Inversion-Recovery (FLAIR); (TE/TI/TR=120/2100/8500 ms; 1.2mm isotropic acquisition matrix; flip-angle=90^{o}; ETL=24); 3D high resolution T1-WI (T1) using fast spoiled gradient echo (FSPGR) with magnetization-prepared inversion recovery (IR) pulse (TE/TI/TR=3.2/900/8.2 ms; 1mm isotropic acquisition matrix; flip-angle=10^{o}) before and after (pwMS) gadolinium contrast; axial Diffusion weighted imaging (DWI) (TE/TR=82/8325 ms) with diffusion b-value = b=1000s/mm^2 in 64 directions with each direction containing 68 slices in 2mm thickness to cover the entire brain (with additional two b0 imaging at the start of the DWI acquisition), 256mm FOV and 128x128 matrix with 100% phase FOV; and additional b0 blip-up and blip-down reference data, acquired to correct for DWI image distortion.

DWI data were pre-processed with denoising, Gibb's ringing removal, and B1 field inhomogeneity correction utilising MRtrix3 standard pre-processing pipeline (Tournier et al., 2019). Susceptibility distortions were corrected utilising reversed polarity phase encoding ("blip up" and "blip down") EPI sequences and combined with eddy correction with FSL tools implemented within the MRtrix3 software platform (Andersson et al., 2003; S. M. Smith et al., 2004; Tournier et al., 2019). The result was interpolated to 1mm^3 resolution. Single-Shell 3-Tissue CSD (SS3T-CSD) was performed to obtain WM-like FODs as well as GM-like and CSF-like compartments in all voxels using MRtrix3Tissue (https://3Tissue.github.io), a fork of MRtrix3. Multi-tissue informed log-domain intensity normalisation was then undertaken to normalise tissue components corrected for the effects of intensity inhomogeneities between subjects (Dhollander et al., 2021; D. Raffelt et al., 2017; Tournier et al., 2019).

T1 and FLAIR sequences were co-registered to diffusion space using linear registration with FLIRT (Jenkinson et al., 2002) from FSL; and checked for quality assurance. In subjects with MS, T2 white matter lesions were segmented via an automated in house algorithm utilising a dual path U-net convolutional neural network (Cabezas et al., 2021; Ma et al., 2022) and checked for accuracy. A 5-tissue-type (5TT) image was created (R. E. Smith et al., 2012) by first running

Freesurfer recon-all on the registered T1 sequences to segment cortical grey matter, sub-cortical grey matter, CSF and white matter tissue (Fischl, 2012). The Hybrid Surface and Volume Segmentation (tckgen hsvs) algorithm was used to create the 5TT image utilising Freesurfer and FIRST FSL functions (Ardekani & Bachman, 2009; Fischl, 2012; Patenaude et al., 2011; R. Smith et al., 2020; R. E. Smith et al., 2012). The 5TT mask used by ACT provides boundaries that dictate criteria for streamline propagation or termination within five different tissue types. In order to best represent the pathophysiology of MS lesions, segmented T2 MS lesions were classified as "white matter" within the 5TT image in order to allow termination *and rejection* of streamlines should they fail the FOD amplitude and angular criteria within lesions (R. E. Smith et al., 2012).

Whole-brain tractography was undertaken for each healthy control subject using the iFOD2 probabilistic tractography algorithm to produce 10 million streamlines with the following parameters: default step size, default angle threshold of 45°, dynamic seeding utilising the SIFT model (R. E. Smith et al., 2015a) and ACT (R. E. Smith et al., 2012). The FOD amplitude threshold was tested at 5 different values between the default value of 0.05 and the upper limit of 0.15, as informed by the discussion in section 4.2.3.1. FOD amplitude thresholds of 0.05, 0.08, 0.10, 0.13 and 0.15 were chosen, yielding 5 different tractograms for each subject. SIFT2 analysis was undertaken on each tractogram to weight each streamline to match the underlying fixel-wise fibre densities (R. E. Smith et al., 2015a), and subsequent SIFT2 weightings, and the final value of SIFT proportionality coefficient mu, were used to create tract density imaging (Calamante et al., 2010, 2012). The final whole brain connectome matrices for each FOD amplitude threshold were then calculated with tck2connectome (R. E. Smith et al., 2015b) using the SIFT2 weightings for each subject. The Desikan Killiany (Desikan et al., 2006) atlas was implemented in Freesurfer (Fischl, 2012) with 84 cortical and subcortical regions, but including an extra region of the lower brainstem to capture spinal cord projections, resulting in an 85 x 85 connectivity matrix.

The connectomes were analysed using the Brain Connectivity Toolbox implementation within MATLAB https://sites.google.com/site/bctnet/home (Rubinov & Sporns, 2010) by calculating graph theory metrics of interest, including community structure and clustering such as

transitivity, clustering coefficient and efficiency/diffusion properties such global and local efficiency (Sporns, 2018).

A measure of the degree of lesion damage was calculated using the T1 image hypo-intensity as this has been shown to be a robust marker of axonal loss within MS lesions (Elliott, Belachew, et al., 2019; Filippi et al., 2012; van Waesberghe et al., 1999; van Walderveen et al., 1998). To achieve this, the T1 intensity measurement was normalised within and between subjects via N3 bias correction using the Freesurfer wrapper command mri_nu_correct.mni (Sled et al., 1998) followed by the Freesurfer command mri_normalize (Dale et al., 1999), which imposes a hard ceiling effect on the white matter peak found, creating a homogenous T1 intensity at normal appearing white matter (NAWM) and floor at CSF intensity, as previously described in section 3.3.2.

Firstly, in order to assess the effect of FOD amplitude criterion increase on normal network construction in healthy controls, the graph metrics for each FOD amplitude were compared for difference via a one-way ANOVA or non-parametric Friedman test according to normality testing, with post hoc Dunnett's or Dunn's multiple comparison's testing to the default FOD amplitude of 0.05.

Secondly, in order to assess the effect of FOD amplitude criterion on MS lesion streamline propagation, mean individual lesion tract density and mean T1 intensity values were calculated using FSL (S. M. Smith et al., 2004) from co-registered T2 lesion masks. Pearson's or Spearman's correlations were processed for T2 hyperintense lesions in all MS subjects depending on normality testing. Gadolinium-enhancing lesions were excluded so as to limit the analysis to chronic lesions. Lesions with a volume of less than 10mm3 were excluded in order to reduce the impact of partial voluming. All analysis done was performed using GraphPad Prism 9 for MacOS, GraphPad Software, San Diego, California USA, www.graphpad.com.

4.2.3 Results

The graph metrics of global efficiency, transitivity, left and right thalamic local efficiency and clustering coefficient were calculated for each healthy control subject, across each FOD amplitude threshold test of 0.05, 0.08, 0.10, 0.13 and 0.15. All datasets passed normality testing using D'Agostino & Pearson and Shapiro-Wilk methods. Subsequent paired one-way ANOVA was performed to compare the effect of changing FOD amplitude threshold on each graph metric. One-way ANOVA revealed that there was a statistically significant difference in global efficiency, left thalamic clustering coefficient and local efficiency and right thalamic clustering coefficient between at least two FOD amplitude groups, but not transitivity and right thalamic local efficiency as outlined in Table 4.1.

	Global efficiency	Transitivity	Left thal. clustering coefficient	Right thal. clustering coefficient	Left thal. local efficiency	Right thal. local efficiency
One-way ANOVA F (dfn, dfd)	F (1.077, 9.696) = 133.7	F (1.645, 14.81) = 3.413	F (1.939, 17.45) = 61.13	F (1.508, 13.57) = 19.76	F (2.443, 21.99) = 41.04	F (1.166, 10.50) = 0.7467
P value	p<0.001	p=0.07	p<0.001	p<0.001	p<0.001	p=0.43
Dunnett's multiple comparisons test (0.05 vs 0.15) Mean difference	0.05132	N/A	0.03590	0.03585	0.01538	N/A
P value	p<0.001	N/A	p<0.001	p=0.009	p<0.001	N/A

Table 4.1.

Dunnett's multiple comparisons test found that the mean value of global efficiency, left thalamic clustering coefficient and local efficiency and right thalamic clustering coefficient was significantly different between FOD amplitude 0.05 and FOD amplitude 0.15, but there were no significant differences between the other FOD amplitude thresholds tested.

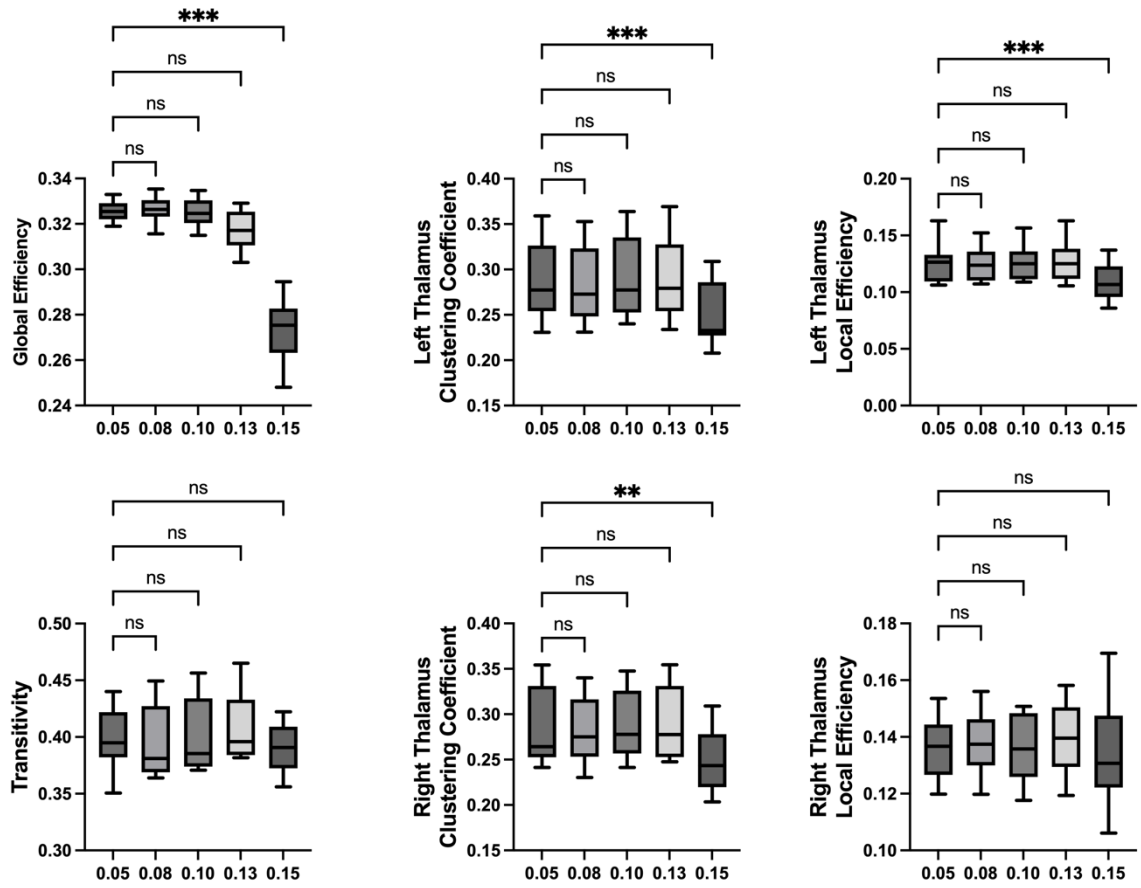

Figure 4.3.

112 MS T2 lesions from 10 pwMS had mean tract density calculated for each FOD amplitude threshold, excluding 0.15 as this was not a desirable threshold due to poor performance in maintaining network graph metrics. All datasets passed normality testing using D'Agostino & Pearson and Shapiro-Wilk methods. Mean lesional T1 hypointensity and tract density were correlated using Pearson's correlation, for each FOD amplitude threshold, with results shown in Table 4.2.

	T1 vs. 0.05	T1 vs. 0.08	T1 vs. 0.10	T1 vs. 0.13
R	0.2600	0.5519	0.6172	0.6213
95% confidence interval	0.07821 to 0.4250	0.4081 to 0.6689	0.4874 to 0.7202	0.4925 to 0.7235
R^2	0.06760	0.3046	0.3809	0.3860
P value	0.006	<0.001	<0.001	<0.001

Table 4.2.

The scatterplots of each correlation are shown below in Figure 4.4. with regression lines fitted.

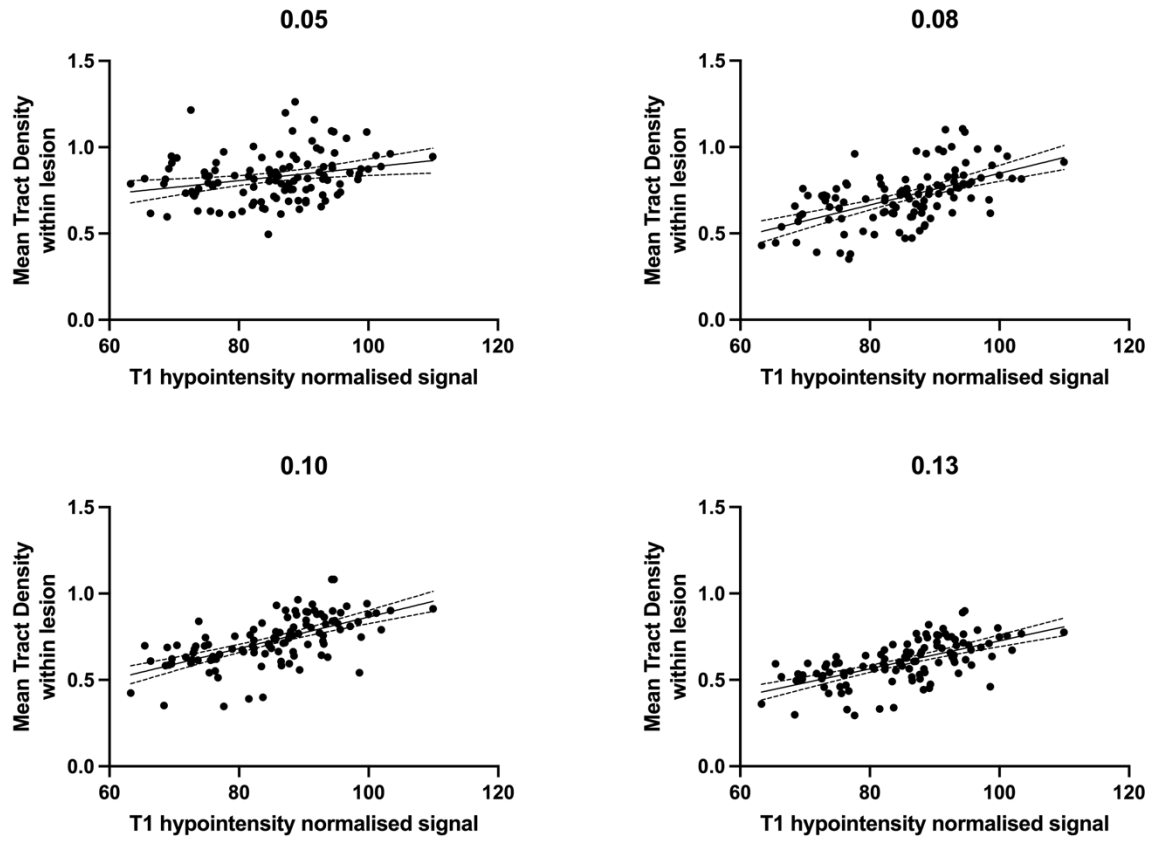

Figure 4.4.

4.2.4 Discussion

In this study, we analysed the effect of varying FOD amplitude thresholds on graph metrics of interest and resultant intralesional streamline generation. The paired one-way ANOVA found that the distributions of these graph metrics in healthy controls were significantly different when using a FOD threshold of 0.15 compared to the default values of 0.05 with ACT. Our findings suggest that there exists a practical threshold for increasing FOD thresholding. Beyond this threshold of 0.13, we observed a sharp decline in the network structure. However, we also observed that the graph metrics measured remained stable when the FOD amplitude was below this threshold value. This was evident for global metrics of efficiency as well as local metrics of community structure around the central node of the thalamus, suggesting this threshold is relevant to both whole-brain and regional network construction.

Increasing the FOD amplitude threshold improved the correlation of intra-lesional tract density with T1 hypointensity at each level. Notably the default level of 0.05 had a poor correlation of intra-lesional tract density with T1 hypointensity and likely does not stop many streamlines through MS lesions, similar to what has been shown elsewhere (R. E. Smith, Calamante, Gajamange, et al., 2020). Increasing values increased the strength of the correlation but there was a ceiling effect evident with minimal difference between 0.10 and 0.13.

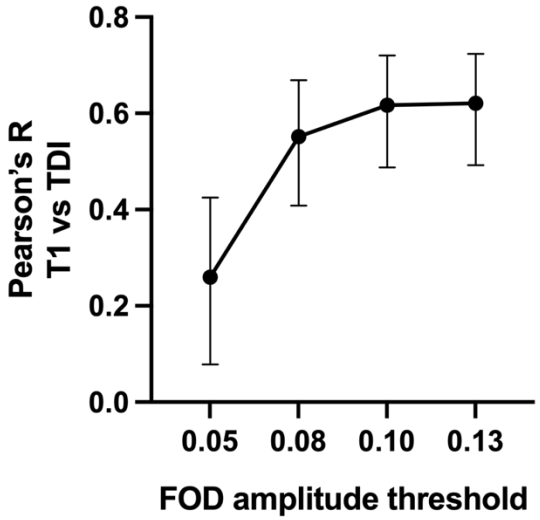

Figure 4.5. Pearson's R correlation strength of increasing FOD amplitude thresholds showing an evident ceiling effect.

Analysis of an example subject, shown in Figures 4.6. – 4.8., reveals a notable drop out of T1 signal and FOD amplitude in the lateral aspect of the T2 lesion in the left frontal lobe. The streamline construction with FOD amplitude thresholds of 0.05 and 0.13 are respectively shown side by side, illustrating a clear reduction in streamline construction at the 0.13 threshold. This is also seen in the TDI mapping (see arrow), which better corresponds to the T1 hypointensity seen.

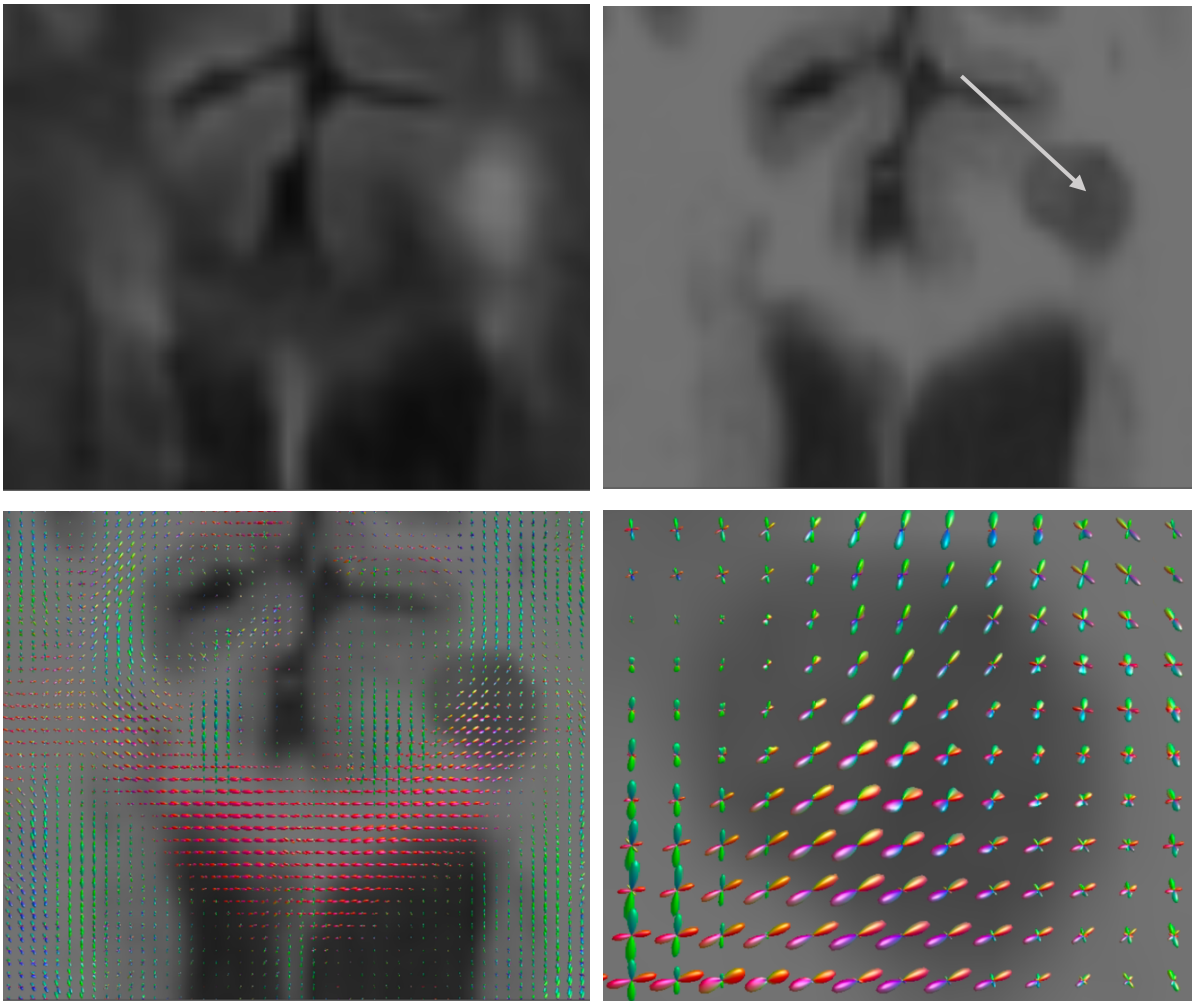

Figure 4.6. MS lesion in the left frontal lobe adjacent to the genu of the corpus callosum; Top left FLAIR T2 hyperintensity; Top right T1 hypointensity; Bottom left T1 overlaid with FODs; Bottom right close-up of lesion T1 with overlaid FODs. Arrow shows the lower T1 signal in the lateral aspect of the lesion.

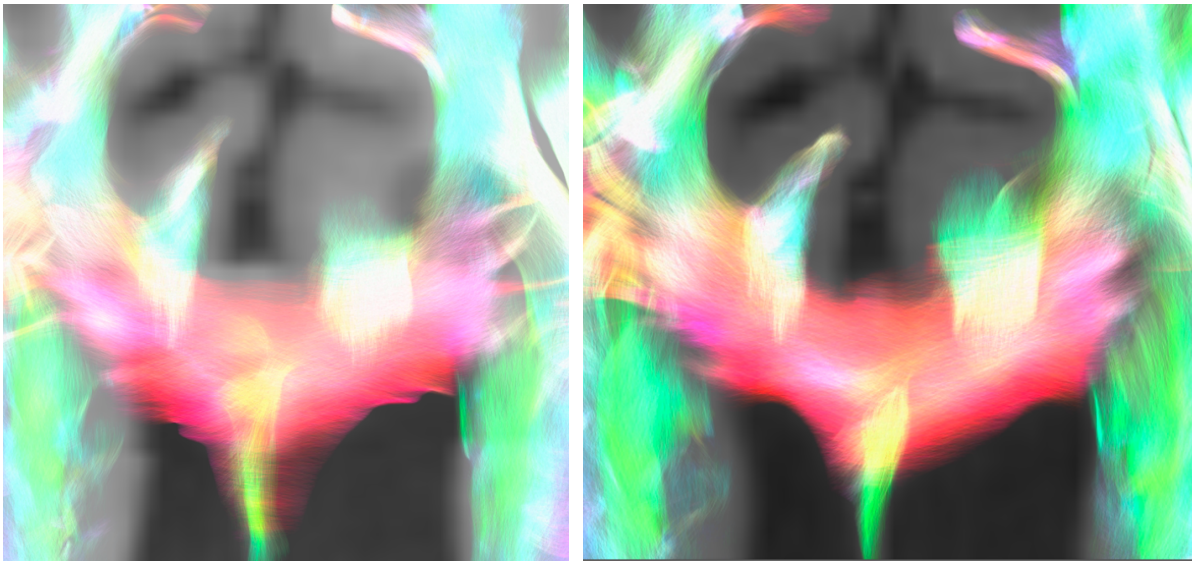

Figure 4.7. Streamline tractogram at FOD amplitude threshold 0.05 (left) and 0.13 (right).

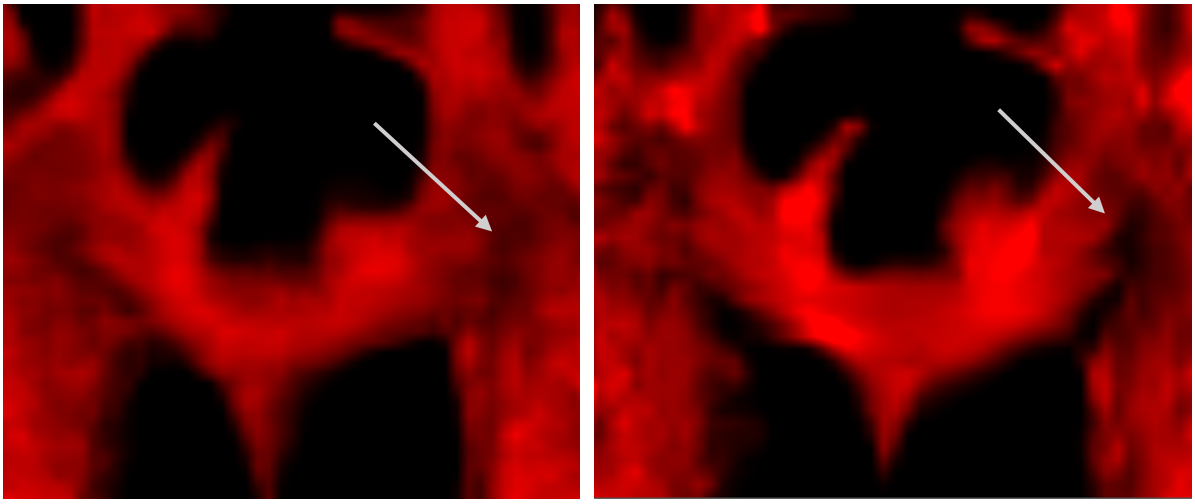

Figure 4.8. TDI at FOD amplitude thresholds of 0.05 (left) and 0.13 (right). The arrows show the difference in tract density at the lateral portion of the lesion.

The poor performance of the MRtrix3 default 0.05 FOD amplitude threshold has implications for several studies that have used this in their tractography pipeline. For instance, Charalambous et al. used this default FOD amplitude threshold in studies (Charalambous et al., 2019, 2020) investigating network structure in MS and its correlation with disability. However the use of the default FOD amplitude threshold and SIFT2 likely undervalued the disconnection as a result of MS white matter lesions, notwithstanding the significant findings of the studies.

A clear limitation of this study, and a matter yet to be resolved in the literature, is the use of the SIFT2 algorithm in its original published form, for modelling truncating pathology. The use in this study was unavoidable given the inherent requirement for filtering algorithms on tractograms. The potential inaccuracies develop from the fact that streamlines passing through pathological tissue will be overweighted, as their so called “weakest link” is averaged across the streamline length. The reduction in streamline number that would be expected given the more stringent FOD amplitude threshold criterion used, will be somewhat countered by the SIFT2 algorithm that will increase the weighting of the resultant fewer streamlines (Zalesky, Sarwar, & Kotagiri, 2020). Despite this we did see a clear difference in tract density and better correlation with T1 hypo-intensity in MS lesions with the higher FOD amplitude threshold suggesting that this approach was still an improvement on default settings when applied to MS disconnectome modelling. Further study into the utility of modulated SIFT2 algorithm, including incorporating the approach from section 3.3, in this dataset would be of interest.

Finally, it is unlikely that the FOD threshold value chosen with this method will be generalisable across all MR datasets with different diffusion weighted sequences, such as higher b-values. Our dataset here utilised a single shell acquisition protocol with relatively low b-value, albeit with a HARDI (high angular resolution diffusion imaging) procedure of 64 directions and utilised the SS3T CSD method to estimate FODs. A more robust multi-shell acquisition and CSD method might improve the current trade-off between global network reconstruction and focal lesional streamline dropout.

4.2.5 Conclusion

Increasing the FOD amplitude threshold criteria for streamline tracking can improve the accuracy of underlying streamline modelling in pathological MS white matter without impairing global network construction.

4.3 A longitudinal study of diffusion-based disconnectome modelling as a biomarker for progressive multiple sclerosis

4.3.1 Introduction

Clustering and community structure refer to the degree to which nodes tend to form clusters or subgroups within a network and the topology with which these are formed. Network metrics that describe community structure include the clustering coefficient, local efficiency, transitivity and modularity. Clustering, and the closely related transitivity, describe the amount of connection between nodes that have a common neighbour. This phenomenon is frequently observed in many real-world networks, including the brain's connectome. Seminal studies have shown that structural and functional cerebral networks are organised into a highly efficient small world structure (Bullmore & Sporns, 2009; Rubinov & Sporns, 2010). Local neighbourhood clustering, as measured by the clustering coefficient and transitivity, is a key feature of small world topography in the brain (Heuvel & Sporns, 2013), which minimises the number of long range connections and improves the efficiency of information propagation (Achard & Bullmore, 2007; Sporns & Kötter, 2004). Clustering has been shown to mediate a variety of systems that require functional specialisation (Passingham et al., 2002) and integration (Friston, 2002), key features of central structures such as the thalamus.

The clustering coefficient is defined as the fraction of possible connections among its neighbours that are actually present in the network. In graph theory notation, the clustering coefficient is defined as follows:

$$C_v = \frac{(2 \times n_e(v))}{\left(k_v\,(k_v - 1)\right)} = \frac{\text{number of actual connections between the neighbours of node v}}{\text{total number of possible connections between the neighbours of node v}}$$

where C_v represents the clustering coefficient of node v, $n_e(v)$ is the number of edges connecting the neighbours of node v and k_v is the number of neighbours of node v, or the degree of node v. (Dubitzky et al., 2013)

The clustering coefficient can have values between 0 and 1, taking the value of 1 if all of a nodes neighbours are connected to each other, and 0 if none of a nodes neighbours are connected to each other, as shown.

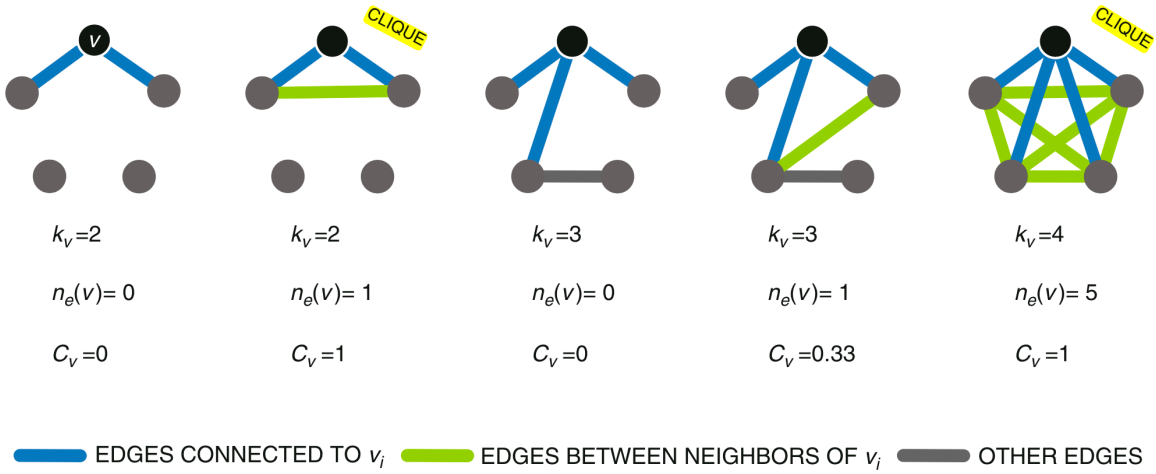

Figure 4.9 Representations of different clustering coefficients (C_v) for node v shown. Adapted from (Dubitzky et al., 2013)

To achieve a global measure of clustering, the mean clustering coefficient is usually normalised individually for each node and may therefore be disproportionately influenced by nodes with a low degree. Transitivity, on the other hand, is a similar clustering metric but is normalised collectively and therefore does not suffer from this bias (Rubinov & Sporns, 2010). Transitivity is defined as the fraction of the number nodes making up triangles to the total number of triplets in the whole brain.

The identification of clustering and community structure in the cerebral network provides novel insights into the underlying neuropathology of MS. For example, previous studies have reported reduced clustering and disrupted community structure in patients with MS compared to healthy controls, indicating a breakdown in the normal patterns of connectivity in the brain, as well as lower degrees of global clustering in progressive MS in comparison to relapsing MS, suggesting a potential contribution to disability (Charalambous et al., 2019). Additionally, the degree of clustering and community structure has been shown to be associated with clinical measures of disease severity, such as EDSS and cognitive performance (Cho et al., 2022; Lopez-Soley et al., 2020).

The thalamus has been implicated as mediator and biomarker of disability in MS. Selective atrophy of the thalamus has been found in the earliest stages of MS (Levy et al., 2022) with persistence throughout disease (Azevedo et al., 2018). The utility of thalamic atrophy as a biomarker for disability progression has been confirmed, with correlations found with information processing speed (Naghavi et al., 2023), cognition (Engl et al., 2020) and walking speed (Nourbakhsh et al., 2016; Tsagkas et al., 2021). Several differing mechanisms of thalamic atrophy have also been explored, including intrathalamic demyelinating lesions (Kipp et al., 2015), wallerian/retrograde degeneration in connected thalamic white matter tracts (Weeda et al., 2020), ependymal/CSF boundary gradient degeneration (Magliozzi et al., 2022) and iron accumulation (Burgetova et al., 2022; Pontillo et al., 2021). The central importance of the thalamus as a hub within the wider connectome has been highlighted (Schoonheim et al., 2022) with several lines of enquiry finding associations between thalamic connectivity and disability, including anatomical connectivity mapping (Bozzali et al., 2013) and thalamic functional connectivity with the wider sensorimotor network (Schoonheim, Pinter, et al., 2021). Thalamic atrophy has a been explored as a secondary endpoint in pharmaceutical trials given it's clear importance in MS pathophysiology (Arnold, Sprenger, et al., 2022).

In this study we used a refined model of diffusion-based network construction to further explore community structure and thalamic connectivity, in particular the potential differences between relapsing and progressive MS, as well as their usefulness for describing and predicting progressive disability in MS.

4.3.2 Methods

A total of 75 participants were recruited from a single MS centre, including 54 pwMS and 21 healthy controls. Among the pwMS group, there were 24 subjects with primary or secondary progression who had not experienced disease activity for at least 24 months, while the remaining 30 individuals had relapsing multiple sclerosis stable on disease modifying therapy. All participants underwent clinical and radiological assessments for a period of 24 months.

The clinical evaluation incorporated relapse activity, the expanded disability status scale (EDSS), the symbol digit modalities test (SDMT), the nine-hole peg test (9HPT), and the timed 25-foot walk test (T25FW). To determine the multiple sclerosis functional composite (MSFC), the 9HPT, SDMT, and T25FW were employed, as previously described (Drake et al., 2010; Fischer et al., 1999) by calculating z-scores based on the subject population, as well as combining the scores of the 9HPT from both the left and right arms.

MR scans were acquired on a 3T GE MR750 (General Electric, Milwaukee, WI, USA), using a multi-channel head and neck coil. The following sequences were acquired: 3D Fluid-Attenuated Inversion-Recovery (FLAIR); (TE/TI/TR=120/2100/8500 ms; 1.2mm isotropic acquisition matrix; flip-angle=90^{o}; ETL=24); 3D high resolution T1-WI (T1) using fast spoiled gradient echo (FSPGR) with magnetization-prepared inversion recovery (IR) pulse (TE/TI/TR=3.2/900/8.2 ms; 1mm isotropic acquisition matrix; flip-angle=10^{o}) with pwMS also undergoing post gadolinium sequences; axial Diffusion weighted imaging (DWI) (TE/TR=82/8325 ms) with diffusion b-value = b=1000s/mm^{2} in 64 directions with each direction containing 68 slices in 2mm thickness to cover the entire brain (with additional two b0 imaging at the start of the DWI acquisition), 256mm FOV and 128x128 matrix with 100% phase FOV; and additional b0 blip-up and blip-down reference data, acquired to correct for DWI image distortion.

DWI sequences were pre-processed with denoising, Gibb's ringing removal, and B1 field inhomogeneity correction utilising MRtrix3 standard pre-processing pipeline (Tournier et al., 2019). Susceptibility distortions were corrected utilising reversed polarity phase encoding ("blip up" and "blip down") EPI sequences and combined with eddy correction with FSL tools implemented within the MRtrix3 software platform (Andersson et al., 2003; S. M. Smith et al.,

2004; Tournier et al., 2019). The result was interpolated to $1mm^3$ resolution. Single-Shell 3-Tissue CSD (SS3T-CSD) was performed to obtain WM-like FODs as well as GM-like and CSF-like compartments in all voxels using MRtrix3Tissue (https://3Tissue.github.io), a fork of MRtrix3. Multi-tissue informed log-domain intensity normalisation was then undertaken to normalised tissue components corrected for the effects of intensity inhomogeneities between subjects (Dhollander et al., 2021; D. Raffelt et al., 2017; Tournier et al., 2019).

The T1 and FLAIR sequences were registered to the diffusion space through linear registration using FLIRT from FSL (Jenkinson et al., 2002), and were subsequently verified for quality. In subjects with MS, automated segmentation of T2 white matter lesions was performed using a dual path U-net convolutional neural network (Cabezas et al., 2021; Ma et al., 2022), and the results checked for quality assurance. A 5TT image was generated by first utilizing Freesurfer recon-all on the registered T1 sequences to segment cortical grey matter, sub-cortical grey matter, cerebrospinal fluid, and white matter tissue (Fischl, 2012). The Hybrid Surface and Volume Segmentation (tckgen hsvs) algorithm was then utilized with Freesurfer and FIRST FSL functions to create the 5TT image (Ardekani & Bachman, 2009; Fischl, 2012; Patenaude et al., 2011; R. Smith et al., 2020; R. E. Smith et al., 2012). This 5TT image provided tissue type boundaries that dictate criteria for streamline propagation or termination within five distinct tissue types. To best represent the pathophysiology of MS lesions, segmented T2 MS lesions were classified as "white matter" within the 5TT image, thereby enabling the rejection of streamlines that failed to meet the FOD amplitude and angle criteria within lesions (R. E. Smith et al., 2012).

Whole-brain tractography was undertaken for each subject using the iFOD2 probabilistic tractography algorithm to produce 10 million streamlines with the following parameters: default step size, default angle threshold of 45°, dynamic seeding utilising the SIFT model (R. E. Smith et al., 2015a) and ACT (R. E. Smith et al., 2012). The FOD amplitude threshold of 0.13 was used as informed by the experimentation in section 4.2. The implementation of this amplitude threshold enhances the precision of streamline modelling in diseased MS white matter while having no detrimental effect on global network construction.

The final whole brain connectome matrices were then calculated with tck2connectome (R. E. Smith et al., 2015b) using the SIFT2 weightings for each subject. The Desikan Killiany (Desikan et al., 2006) atlas was implemented in Freesurfer (Fischl, 2012) with 84 cortical and subcortical regions, but including an extra region of the lower brainstem to capture spinal cord projections, resulting in an 85 x 85 connectivity matrix.

The connectomes were analysed using the Brain Connectivity Toolbox implementation within MATLAB https://sites.google.com/site/bctnet/home (Rubinov & Sporns, 2010), by calculating the graph theory metrics global assortativity, transitivity and mean modularity as well as local thalamic clustering coefficient, efficiency and strength. In addition, the inferiofrontal-thalamic edge strength, found to be associated with walking disability in section 3.4.4.1, was again calculated.

At the baseline timepoint, inter-group differences in community structure graph metrics were analysed using a one-way ANOVA or non-parametric Kruskal-Wallis, depending on normality testing. Post-hoc Tukey or Dunn's multiple comparison testing was performed between each group. Additionally, partial Pearson's correlations were conducted between community structure graph metrics and clinical metrics (EDSS, 9HPT, T25FW, SDMT, and MSFC) at baseline, while controlling for disease course, disease duration, age, whole brain T2 lesion volume, and whole brain volume.

To investigate the comparative change in community network structure over time, intra-group metrics were analysed over 24 months with student’s t-test, and inter-group difference analysed with one way ANOVA and post hoc Dunnett’s T3 multiple comparisons testing.

To investigate the contributions of network disconnection to progressive disability, changes in graph metrics were correlated with changes in clinical measurements over a 24-month period via partial Pearson's correlations, while controlling for disease course, disease duration, age, whole brain T2 lesion volume, and whole brain volume.

Finally, a logistic regression model was developed to examine the predictive value of network metrics in disability progression. The model included network metrics as covariates and MSFC

progression as the outcome variable. Statistics were performed using GraphPad Prism version 9.5.0 (https://www.graphpad.com/) and Jamovi version 2.3.21 (https://www.jamovi.org/).

4.3.3 Results

Datasets of assortativity, transitivity, inferior-frontal to thalamic strength and thalamic clustering coefficient passed D'Agostino & Pearson test and Shapiro-Wilks normality testing, whereas mean modularity and thalamic strength did not. One-way ANOVA with post hoc Tukey multiple comparison testing as well as Kruskal-Wallis with post hoc Dunn's was performed for the appropriate datasets.

4.3.3.1 Cross-sectional

Baseline global community structure network metrics were analysed between the groups HC, RMS- PMS. ANOVA testing compared the means of HC, RMS and PMS groups on **assortativity**, $F(2, 72) = 2.793$, $p=0.0679$, without significant difference found. ANOVA testing comparing means of HC, RMS and PMS groups on **transitivity**, $F(2, 72) = 12.15$, $p<0.001$, with post-hoc Tukey's HSD test revealing that the mean difference between HC- PMS was significant ($p<0.001$) as was the mean difference between RMS- PMS ($p<0.001$), but not between HC- RMS ($p=0.57$). Kruskal-Wallis test comparing HC, RMS and PMS groups on **mean modularity**, $H=8.395$ $df=2$, $p=0.02$, with post-hoc Dunn's test revealing that the mean rank difference between HC- PMS was significant ($p=0.01$), but not between RMS- PMS ($p=0.21$) nor HC- RMS ($p=0.61$).

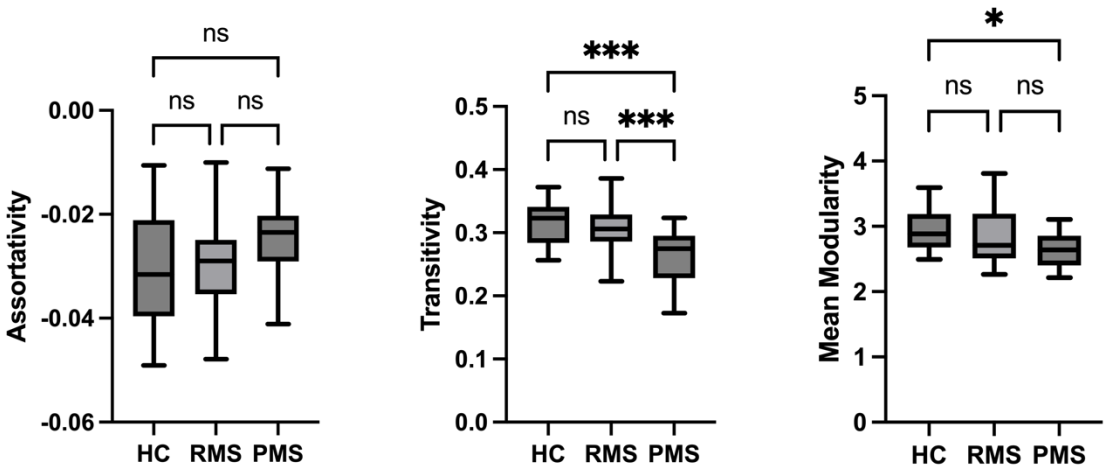

Figure 4.10.

With regard to baseline thalamic connectivity and clustering, Kruskal-Wallis test comparing HC, RMS and PMS groups on **left thalamic strength**, H=10.39 df=2, p=0.006, with post-hoc Dunn's test revealing that the mean rank difference between RMS- PMS was significant (p=0.006), but not between HC- PMS (p=0.05) nor HC- RMS (p=0.99). **Right thalamic strength** comparison showed significant mean rank differences between the groups on Kruskal Wallis testing, H=9.755 df=2, p=0.008, with post-hoc Dunn's test revealing that the mean rank difference between RMS- PMS was significant (p=0.009), but not between HC- PMS (p=0.07) nor HC- RMS (p=0.99). ANOVA testing comparing means of HC, RMS and PMS groups on **left inferiofrontal-thalamic strength**, F(2, 72) = 7.284, p=0.001, with post-hoc Tukey's HSD test revealing that the mean difference between HC - PMS was significant (p=0.03) as was the mean difference between RMS- PMS (p=0.001), but not between HC- RMS (p=0.64). ANOVA testing comparing means of HC, RMS and PMS groups on **right inferiofrontal-thalamic strength**, F(2, 72) = 12.77, p<0.001, with post-hoc Tukey's HSD test revealing that the mean difference between HC- PMS was significant (p=0.02) as was the mean difference between RMS- PMS (p<0.001), but not between HC- RMS (p=0.62). ANOVA testing compared means of HC, RMS and PMS groups on **left thalamic clustering coefficient**, F(2, 72) = 1.448, p=0.24, with post-hoc Tukey's HSD test revealing that there was no significant mean difference between HC- PMS (p=0.23), RMS- PMS (p=0.47), nor HC- RMS (p=0.81). ANOVA testing compared means of HC, RMS and PMS groups on **right thalamic clustering coefficient**, F(2, 72) = 0.6982, p=0.50, with post-hoc Tukey's HSD test revealing that there was no significant mean difference between HC- PMS (p=0.95), RMS - PMS (p=0.49), nor HC- RMS (p=0.72).

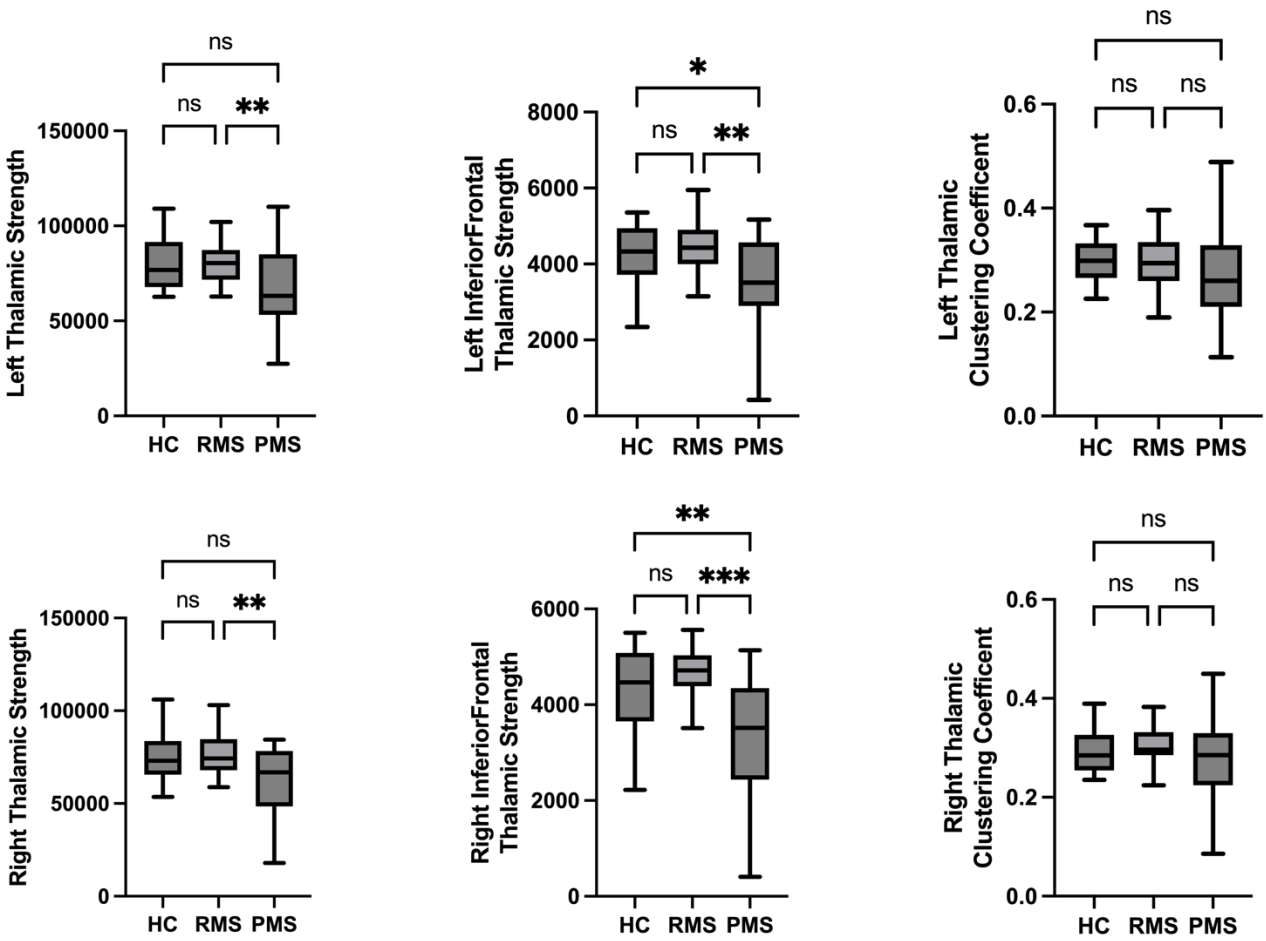

Figure 4.11.

Partial Pearson correlations were calculated between baseline graph metrics and clinical metrics, controlling for disease course, disease duration, age, whole brain T2 lesion volume, and whole brain volume. This found **transitivity** to be correlated with **1/9HPT** (r=0.296, p=0.02), **SDMT (z-score)** (r=0.316, p=0.015) and **MSFC (z-score)** (r=0.271, p=0.033) (see Figure. 4.12). **Left** and **right thalamic local efficiency** correlated with **SDMT (z-score)** (left r=0.395, p=0.003; right r=0.320, p=0.014) and **MSFC (z-score)** (left r=0.235, p=0.047*; right r=0.366, p=0.006). The combined **average thalamic local efficiency** across sides also correlated positively with **SDMT (z-score)** (r=0.385, p=0.008). All significant correlations were maintained through Bonferroni corrections for multiple comparisons, except left thalamic local efficiency with MSFC (marked with *).

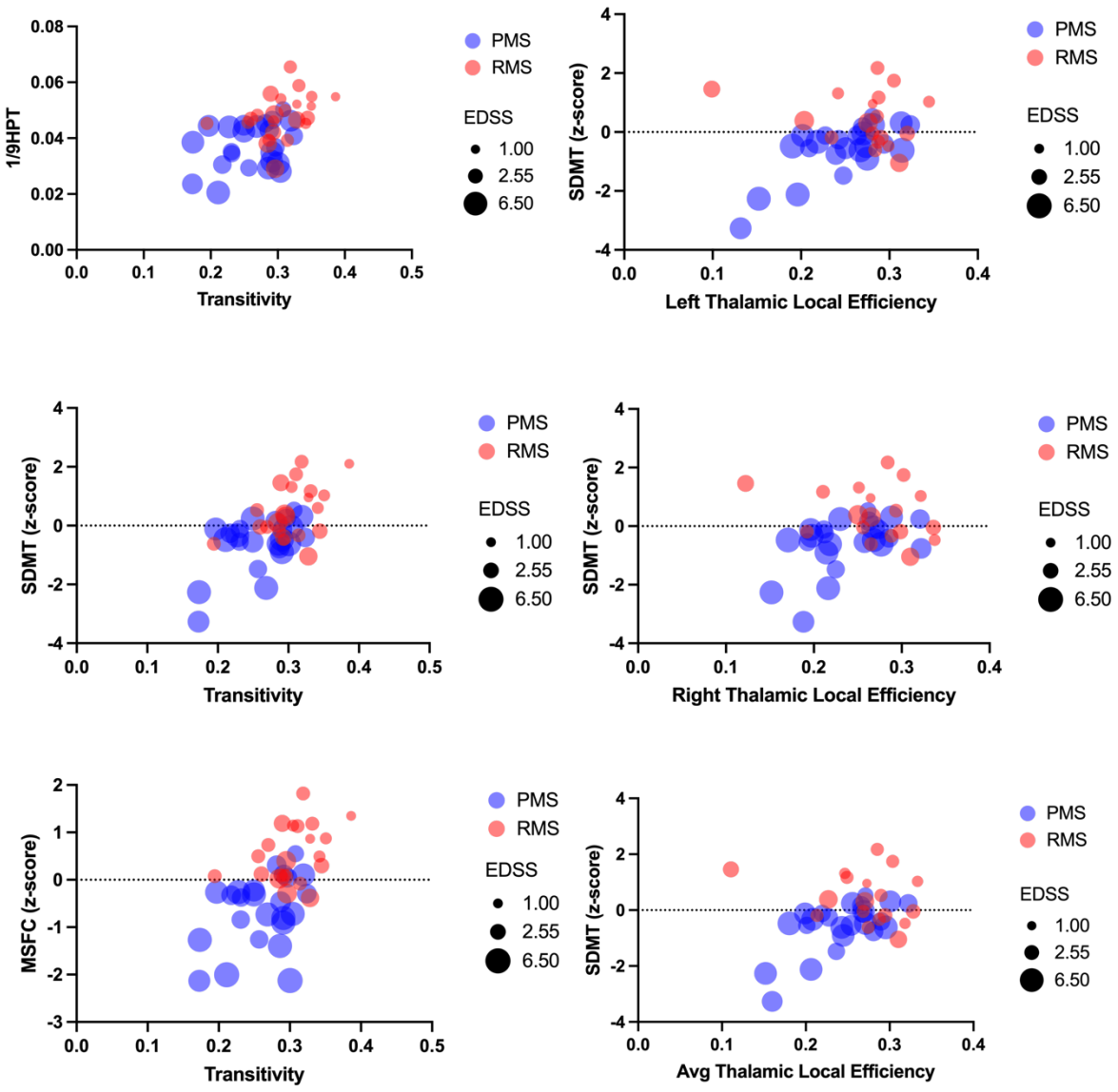

Fig. 4.12.

4.3.3.2 Longitudinal

Change in **transitivity** over 24 months was compared between the groups (see Fig. 4.13.). A one-way ANOVA F(2,48.01) = 18.07, p<0.001, with post hoc Dunnett's T3 multiple comparisons test found a significant difference in mean change over 24 months between HC- RMS (p=0.32), HC- PMS (p<0.001) and RMS- PMS (p=0.001). One sample t-test revealed significant change in transitivity over the 24 months for the RMS cohort (*M* =-0.01488, *SD* = 0.02138; t(25)=3.549, p=0.002) and the PMS cohort (*M* =-0.04605, *SD* = 0.02917; t(21)=7.403, p<0.001) but not the

HC cohort which had no significant change in transitivity over 24 months (*M* =-0.002058, *SD* = 0.01019; t(20)=0.9257, p=0.37), as shown in Fig. 4.13.

Assortativity and **mean modularity** showed no significant change over 24 months in any cohort.

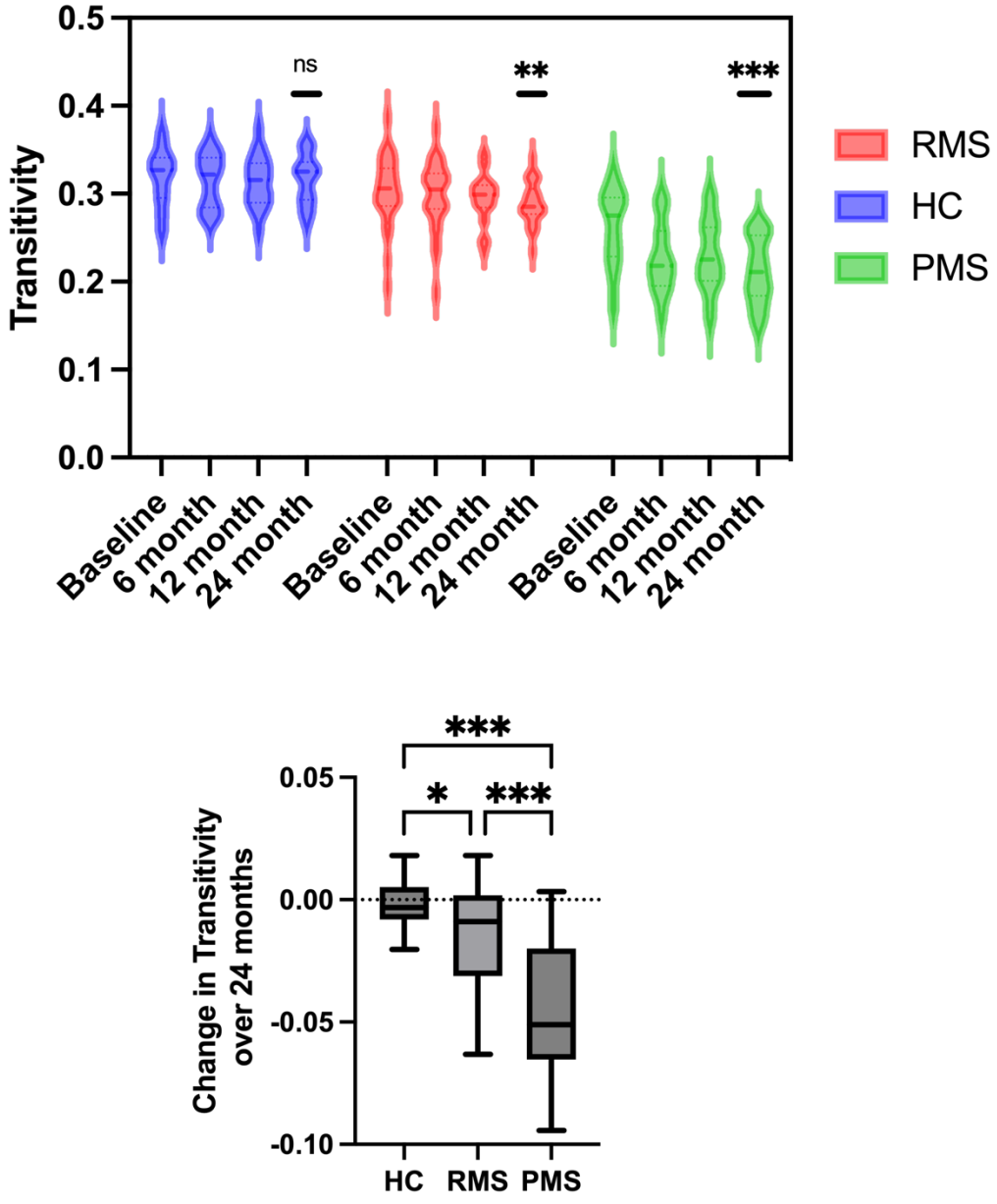

Fig. 4.13.

Partial Pearson's correlations were calculated between the change in community network measures and clinical metrics over 24 months, corrected for disease course, disease duration, age, whole brain T2 lesion volume, and whole brain volume. Change in right inferior frontal – thalamus strength was positively correlated to change in T25FW (z-score) (r=0.392, p=0.041) over 24 months. Investigating the scatter plot showed the major contribution to the correlation was from the RMS cohort (see Fig.14.). Separating the groups the RMS cohort had a partial correlation of r=0.354, p=0.009, whilst the PMS partial correlation was r=0.091, p=0.748.

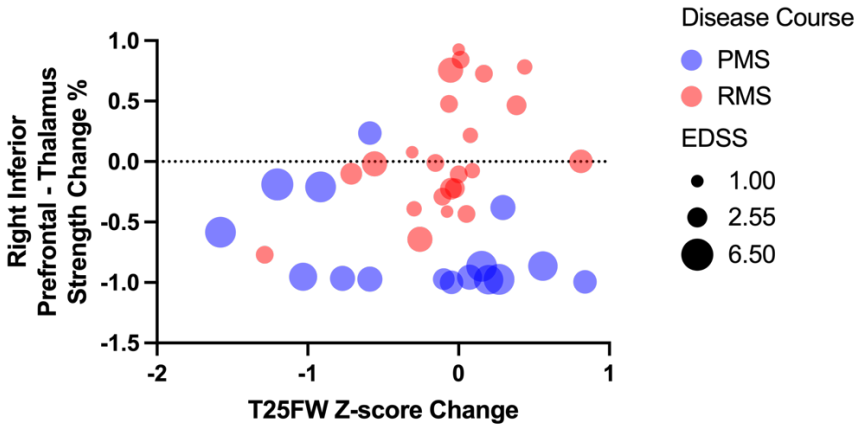

Fig. 4.14.

No other correlations were significant between the change in community network measures and clinical metrics over 24 months, including mean modularity and transitivity.

A logistic regression model was developed to examine the predictive value of network metrics in disability progression. A model including baseline EDSS, whole brain T2 lesion volume, combined thalamic strength and combined thalamic clustering coefficient (Table 4.3) outperformed a model of baseline EDSS, disease duration, disease course and non-network MRI metrics (whole brain T2 lesion volume, whole brain atrophy) in predicting progression in MSFC at 24 months. Notably transitivity and mean modularity did not improve the model.

Predictor	Coefficient (b)	aOR (95% CI)	*p*
Constant	1.032	2.807 (0.06368 to 107.0)	0.58
Baseline EDSS	0.4793	1.615 (1.134 to 2.465)	0.01
T2 lesion volume	0.0001033	1.0001 (1.0 to 1.0002)	0.02
Thalamic clustering coefficient	-0.1899	0.827 (0.6841 to 0.9763)	0.05
Thalamic strength	-0.04957	0.949 (0.885 to 0.992)	0.05

Table 4.3. Logistic regression table for predicting progression of MSFC at 24 months

The overall model had a sensitivity of 89.3% and specificity of 71.4% at a cutoff of 0.49 (see Figure 4.15.). The area under the ROC curve was 0.8316 (95% CI 0.7075 to 0.9557) The log-likelihood ratio versus the intercept-only model was 16.95 (p value = 0.002) showing significance.

This model outperformed the model of factors including disease course (RMS vs PMS), disease duration, baseline EDSS, T2 lesion volume, normalised whole brain volume with an Akaike information criterion (AICc) difference of-4.275.

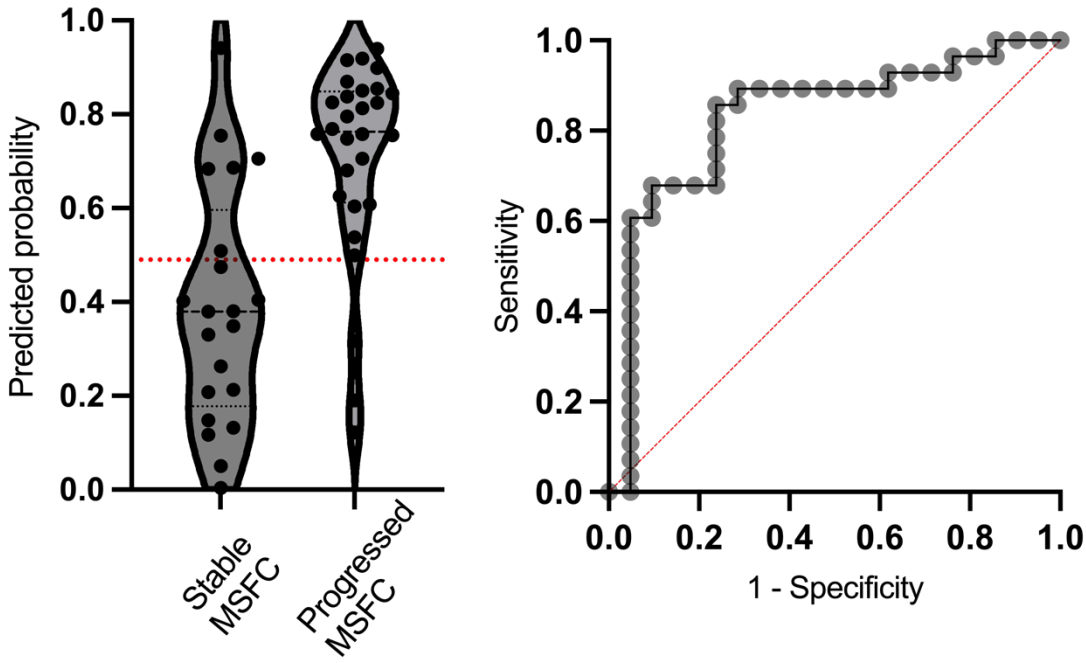

Fig. 4.15. Logistic regression model predicting MSFC progression at 24 months. Left – distribution of predicted probabilities of stable MSFC and progressed MSFC groups, cutoff value of 0.49 (red dotted line); Right – ROC curve area = 0.8316

4.3.4 Discussion

In this study we investigated the utility of community network topology as a longitudinal biomarker in MS, using a tractography pipeline adapted for the presence focal white matter damage due to MS lesions. In summary, several graph theory measures of community structure showed specific decline in RMS and PMS compared to HC, which correlated with physical and cognitive disability and contributed to the prediction of progression in disability, as measured by the MSFC, over 24 months.

Global network metrics of transitivity and mean modularity describe a unique aspect of community network structure, as they explain the topology of the brain network in terms of regional modules. These graph metrics have unique potential within connectome analysis in neuroscience and neuropathology, as they describe aspects of cerebral structure not easily appreciated with other methods. In this study, transitivity was reduced in RMS in comparison to HC, and reduced further in PMS, whilst mean modularity was reduced in PMS. This is consistent with previous studies that have shown reduced module structure in MS with increasing lesion volume (Ravano et al., 2021) and reduced transitivity in PMS compared to RMS (Pagani et al., 2019). The reduction in modularity and clustering suggests a dismantling of specialised structures in the brain of pwMS. In keeping with this we saw a correlation of transitivity to upper limb function and information processing speed, and in turn the MSFC at baseline. This effect was present across both RMS and PMS with moderate correlation (r ~0.3), even after controlling for confounders that are known to contribute to disability in MS, such as age, brain atrophy and T2 lesion volume. Over the 24-month study, transitivity reduced in RMS and PMS cohorts but not HC, showing a gradual decline in community order. Furthermore the effect size over 24 months was significantly greater for PMS compared to RMS (see Fig. 4.13.), highlighting a potential specific degenerative component of MS. Despite this link to neurodegenerative phenotypes, transitivity is unlikely to be confounded by atrophy. Whole brain atrophy, with attendant widespread reductions in nodal strength and streamline density, would not reduce transitivity as per graph theory measurement; nor would the loss of a regional node effect transitivity to any great extent, as it could impact a feature such as betweenness centrality (Sporns, 2018). Rather, transitivity is a measure of the local

arrangement of nodes within the graph and change in transitivity over time suggests a restructuring of the topology as opposed to generalised or local strength reduction.

Regional community structure in the form of clustering around the thalamus was not found to be significantly different in pwMS compared to HC. However, regional efficiency, in the form of thalamic local efficiency, was positively correlated with SDMT. This was evident for both left and right thalami as well as an average between the two, with a moderate correlation (r=0.385) after controlling for confounders. As previously discussed in section 3.4.4.1, information processing speed is likely a function of widespread cortical disconnection with significant mediators being highly connected regions such as the thalamus (Marzi et al., 2023; Sandroff et al., 2022). Efficiency is the capacity of a graph to pass information via short paths and tends to increase with increasing clustering coefficients (Sporns, 2018). Reduction in local efficiency of a centralised hub such as the thalamus impairs the ability of information to be passed economically through its widespread network, explaining a potential mechanism for slower information processing in MS.

Overall strength of the thalami, i.e. the sum of weighted streamlines connected to the thalami, was reduced in PMS compared to RMS for both left and right thalami, although not in PMS compared to HC (0.05 and 0.07 respectively). More notable was the distinct reduction in strength between the inferior-prefrontal cortex and thalamus on both sides in PMS. The disconnection of this edge was found previously (see section 3.4.4.1) to mediate T25FW and EDSS in MS. Assessing longitudinal change in connectivity, right interior-prefrontal cortex-thalamus disconnection positively correlated with slower walking speed, although this was only evident in the RMS cohort (see Fig. 4.14.). This is an interesting result given that this connection lost strength in most of the PMS cohort over the 24 months, but did not correlate with change in T25FW, as it did with RMS. This may be explained by the lower baseline T25FW in the PMS cohort, or the prevalence of spinal cord disease in patients with PMS patients (Cawley et al., 2017; Tsagkas et al., 2018), which presumably obscures effect of cerebral network change. The replication of this connection as a mediator of T25FW deserves further attention and specifically, the impact of executive functioning and cognition on physical disease parameters. Notably, right interior-prefrontal cortex- thalamus disconnection was evident at lower EDSS levels and in RMS, and was independent of age and disease duration, suggesting that walking

change can be affected by damage to this connection in early disease. Walking disability, both measured objectively and reported by patients, has been described as an early feature of MS, even present in CIS (Thrue et al., 2021). Indeed, rates of walking disability in early MS increase further when more subtle testing is employed, such as step-step variability (Flegel et al., 2012; Kalron et al., 2011). Furthermore, specific challenges in patients with MS are seen with gait-cognitive dual tasking (Kalron et al., 2010), which may be clinically analogous to the disconnection described here.

Community structure graph metrics and thalamic strength were explored in a logistic regression model to predict progression of MSFC over 24 months. When combining thalamic clustering coefficient and thalamic strength with baseline EDSS and T2 lesion volume, the model outperformed a model incorporating more classic prognostic markers such as disease course (RMS vs PMS), disease duration and normalised whole brain volume. The sensitivity and specificity (89.3%, 71.4% respectively) reveal a good predictive performance. Improvement in predictive power with the inclusion of thalamic strength and clustering points to the importance of network disconnection in disability in MS. Interestingly, disease course and disease duration did not improve the model, highlighting the importance of network damage to all phenotypes and all stages of the disease. Despite the importance of network metrics, the model still benefited from the input of T2 lesion volume, which can be explained by several factors. In addition to brain function being mediated by networks, it is clear that focal damage can directly mediate disability as is seen in the CST (Hardy et al., 2016) and spinal cord (Sechi et al., 2020), which is potentially captured by T2 lesion volume. In addition, the network metrics used in this model were focused on the thalamus, and would not capture network damage, or focal lesion damage, in separate parts of the network. Global network metrics such as transitivity and mean modularity did not contribute to the predictive power of the model; T2 lesion volume was therefore the only metric capable of capturing widespread damage in the brain.

A potential inaccuracy in this study relates to the measurement of nodal strength, in particular thalamic strength, as a network marker of interest. Raw streamline counts have been shown to be unreliable in a number of circumstances of structural connectome construction (Hagmann et al., 2008). In this study, the use of FOD normalisation (Dhollander et al., 2021), SIFT weighting

and dynamic seeding based on the SIFT model (R. E. Smith et al., 2015a) improves the distribution of reconstructed streamline density and weights the streamlines based on underlying fibre density, which allows for inter-subject comparison. Furthermore, in the presence of pathological thalamic atrophy in MS, it is uncertain how the variability in thalamic size influences streamline tracking. Notably, Schiavi et al. found no association between atrophy measures and network metrics in so-called “raw” or unweighted structural connectomes, but observed a significant correlation with T2 lesion volume. The authors concluded that topological difference observed in MS from unweighted structural connectomes was due to connectome density, which in turn was influenced by T2 lesion volume rather than atrophy (Schiavi et al., 2020b). Along with the SIFT approach, this suggests that accurate connectome reconstruction can be maintained in the presence of atrophy.

A limitation of this study includes the lack of spinal cord assessment, especially in terms of atrophy which has been shown to mediate and predict disability, particularly in PMS (Zeydan et al., 2018). It would be interesting to include spinal cord atrophy in the predictive model of progression, and to tease out the relative contribution of network disconnection and spinal cord pathology. It is likely, as previously considered, that spinal cord lesions and atrophy mask the effect of network disconnection on gait and lower limb function, but are less likely to affect upper limb function and unlikely to affect cognitive performance.

4.3.5 Conclusion

This study provides evidence for the independent influence of reduced clustering and transitivity topology on disability in MS. In addition, thalamic disconnection and efficiency loss mediates cognitive change in MS; and contributes independently to progression of disability over 24 months. These findings suggest that these metrics hold promise as potential biomarkers of disease progression in research settings, enabling more accurate monitoring and assessment of MS patients' outcomes.

4.4 Chapter Summary

This chapter provides a comprehensive exploration of diffusion-based structural network analysis in the context of MS. It begins by introducing the concept of constructing white matter bundles and connectomes in MRI subject space, highlighting the advantages this approach offers. The chapter also acknowledges the complexities and challenges that arise when applying tractography to MS and other CNS pathologies characterised by axonal truncation.

To address these challenges, the chapter investigates the application of a custom FOD amplitude threshold in the tractography algorithm. This threshold value was carefully chosen to improve the characterisation of streamline tract density within MS lesions, but to still maintain the ability to resolve multiple fibre orientations within each voxel. Through empirical investigation, the study shows that modestly increasing the threshold value enhances the accuracy of delineating the tract density within lesions as measured against a marker of axonal loss within MS lesions, namely T1 hypointensity. Importantly, this adjustment does not compromise the construction of the broader connectome in healthy controls, with maintenance of global and regional network community structures. This ensures that while the adjustment increases the specificity of tractography for MS pathology, it maintains the validity and reliability to measure the broader connectome and thus an accurate "disconnectome" specific to MS.

In addition to exploring the technical advancements in tractography, the chapter also delves into the clinical implications of network analysis in MS. A longitudinal study spanning 24 months was conducted on a cohort of patients with RRMS and PMS. The study aimed to investigate the relationship between network community characteristics and MS disability, as well as to identify potential markers of disease progression. The analysis yielded compelling results.

The results showed that transitivity was reduced in RMS compared to HC, and further reduced in PMS consistent with previous studies showing reduced module structure and transitivity in MS. Additionally, the study found a correlation between transitivity and upper limb function and information processing speed, indicating its relevance to MS-related disability. Over the 24-month period, transitivity decreased in both RMS and PMS cohorts, but not in HC,

highlighting a potential degenerative component specific to MS. Importantly, transitivity is not likely to be affected by brain atrophy, and its change over time indicates a restructuring of the brain network topology rather than a general reduction in strength. The longitudinal reduction in transitivity provides valuable insights into the temporal evolution of network structure in MS, suggesting a dismantling of specialised brain structures.

It was also shown that thalamic clustering coefficient and thalamic strength contributed significantly to predicting disability progression with high sensitivity and specificity. This emphasises the role of network disconnection in MS-related disability, regardless of disease course or duration.

Overall, this chapter highlights the need for tailored structural tractography techniques that effectively incorporate the unique aspects of MS pathology. The findings underscore the importance of refining tractography methods specific to MS to overcome the challenges associated with axonal truncation. Furthermore, the chapter emphasises the significance of community structure in network dysfunction, offering promising possibilities as a potential biomarker for tracking disease progression in MS. The implications of these advancements extend beyond research and have the potential to influence clinical management.

Chapter 5

Conclusion

MRI has been the most widely employed biomarker in MS, with indispensable utility in MS diagnosis, ongoing clinical assessment, clinical trials and research (Filippi et al., 2016; Giorgio & De Stefano, 2018; Mahajan & Ontaneda, 2017). However there is still a need for further development of non-invasive biomarkers that can be used for individual assessment as opposed to group level markers (Rocca et al., 2021; Steenwijk et al., 2016). This need is particularly important for PMS, where markers of neurodegeneration such as atrophy have not easily been translated into the clinic (Beadnall et al., 2019; C. Wang et al., 2016), but are commonly used as clinical trial endpoints (Arnold, Piani-Meier, et al., 2022). With the forthcoming increase in therapeutic trials for PMS, including those targeting remyelination (Cadavid et al., 2017), inflammatory and non-inflammatory neurodegenerative mechanisms (Tourbah et al., 2016), reliable biomarkers assessing these mechanisms will be necessary to improve clinical trial design and efficiency (Moccia et al., 2017; Ontaneda et al., 2015).

This thesis explored extending the utility of dMRI to capture axonal degeneration and network dysfunction in MS, including the assessment of potential predictive or longitudinal biomarkers. Each chapter focused on a different aspect of dMRI analysis and introduced novel methodologies to investigate and characterise processes specific to MS. The findings presented in these chapters have significant implications for understanding disease progression and identifying potential biomarkers.

In Chapter 2, a novel method of tractometry was developed to measure the impact of MS lesions on white matter tracts and identify markers of neurodegeneration associated with focal lesions. The chapter highlighted a method for accurately controlling focal microstructural diffusion metrics by using control data from a healthy control atlas. The results revealed an increase in RD distal to lesions which was deemed to be the most sensitive marker indicating Wallerian degeneration in lesional fibres. Additionally, a specific biomarker of Wallerian degeneration, characterised by a reduction in AD, was identified in progressive MS patients. These results support previous evidence that suggests that focal lesions mediate long range neurodegeneration and atrophy in MS (C. Wang et al., 2019). Average patient-wise measurement of AD close to lesions was found to contribute to disability in MS, further signifying the biomarker as suitable for exploration in clinical and trial applications.

Chapter 3 focused on atlas-based network analysis in MS, refining the existing approach of previous studies by incorporating disease-specific mechanisms. The chapter demonstrated the importance of accurate MRI registration in MS, given the heterogeneity of MS pathology topology, involving both deep white matter and juxta cortical lesions. A multimodal registration technique incorporating T1, FA, and MD tissue contrast sequences improved registration accuracy compared to unimodal techniques. Furthermore, a novel concept of modelling cumulative damage along streamlines was introduced, proving its utility with better correlation with functional measurements. This method, which used a logistic transform of summative damage along tractography streamlines, outperformed purely binary lesion damage and the weakest link hypothesis. This result adds significantly to our understanding of white matter tract damage and disconnection in MS and warrants further exploration and use in other models of CNS disease.

Chapter 3 applied this refined atlas-based tractography approach to a longitudinal cohort of MS patients, revealing subnetworks in the basal ganglia and posterior fossa that mediate disability and contribute to progressive MS. Reduced modularity was identified as a predictor of future disability, highlighting its potential as a biomarker. These findings advanced the field of atlas-based network analysis, offering insights into MS pathophysiology and providing potential biomarkers for disability prediction and monitoring.

In Chapter 4, diffusion-based structural network analysis in MS was explored. The chapter introduced the concept of constructing white matter bundles and connectomes in MRI subject space, addressing the challenges associated with tractography in MS and axonal truncation. The study showed that adjusting the FOD amplitude threshold improved the correlation of constructed tract density to internal MS lesion microstructure, without compromising the broader connectome construction in healthy controls. These findings emphasise the importance of tailored tractography techniques for individual disease processes such as MS.

Chapter 4 also presented a longitudinal study utilising this refined tractography technique and demonstrated reduced transitivity in MS overall, with further reduction in progressive MS, highlighting the relevance of community network disruption in MS. The study also identified the role of thalamic clustering coefficient and strength in predicting disability progression. Such

results underscore the significance of community structure in network dysfunction, providing potential biomarkers for tracking disease progression.

A concept that runs through this thesis is developing MRI analysis pipelines that capture specific disease mechanisms. This idea is crucial to accurately analysing concepts such as network disruption, as diverse CNS diseases affect axonal structure differently. Although each results chapter analysed PMS with different approaches each sought to validate the methods used, informed by disease mechanisms specific to neurodegeneration in MS. In addition, the focus of structural diffusion analysis of each chapter expanded from individual tracts (Chapter 2) to subnetworks (Chapter 3) and finally to whole brain networks (Chapter 4), drawing on the idea that accurate whole brain network disruption should be built on valid assumptions at the smaller scales. In this case, evidence of the impact of focal destructive MS lesions on connected white matter tracts informs the assumptions inherent to measuring the effect of focal white matter lesions in network analysis. Similarly evidence of the validity of subnetwork disconnection analysis in MS justifies measuring the whole brain network structure. It is likely that the gains described in this thesis will be built upon by further developing this approach.

The research presented in these chapters opens several avenues for future investigation in MS. One important aspect would be the validation and replication of the biomarkers of axonal degeneration and network dysfunction identified. While the findings in this thesis provide promising insights and are consistent with recent literature, it is crucial to validate them in larger MS cohorts. Replication studies will help establish the robustness of the identified biomarkers, and exploration of utility in clinical decision-making and as surrogate endpoints in clinical trials will establish their generalisability. Furthermore, exploring the dynamic changes in axonal degeneration and network dysfunction over time is crucial for understanding disease progression in MS, and will broaden the results found in this thesis and elsewhere. Longitudinal studies with extended follow-up periods could provide insights into the temporal evolution of these processes and help identify critical time points or windows of opportunity for therapeutic interventions.

Immediate improvements can be made by utilising advanced microstructural markers such as fixel based analysis, apparent fibre density, neurite orientation dispersion and density imaging

(NODDI) into lesional fibre tractometry analysis. These improvements have the possibility of overcoming some of the drawbacks of tensor-based metrics for analysing crossing fibres and dispersion of fibres near the cortex and may help resolve the issues of assessing for retrograde degeneration found in Chapter 2. Similar approaches could also be incorporated into the structural tractography pipelines.

This thesis found credible evidence of focal destructive lesions mediating neurodegeneration and disconnection in MS. Further advancements in measuring cumulative focal damage in white matter structures were described. However, this approach is still likely to be simplistic. As described in Chapter 1, the pathophysiology of neurodegeneration in MS is multifaceted with inflammation and non-inflammatory mechanisms evident, multifocal with damage in the cortical and deep grey matter in addition to white matter structures, and diffuse with widepread demyelination, axonal damage and microglial activation. The inclusion of cortical and deep grey matter lesions into tractometry and tractography studies, as well as the inclusion of diffuse pathological changes found in NAWM, will further bolster this type of analysis. For instance, possible future applications of the method developed in Chapter 3 with atlas-based network analysis, would be to incorporate a measure of grey matter damage (atrophy or lesions) to the nodes of the graphs themselves. Weighting the grey matter regions by focal damage (or weighting the edges that connect to these regions) may further improve predictions of disability and prognosis, and is a plausible hypothesis to follow given the underlying pathophysiology of MS. Additionally, comparing a disconnectome measured with focal white matter lesion with a disconnectome measured with diffuse metrics such as atrophy may give further insight into the relative contributions played by focal or diffuse processes to network dysfunction in MS.

In conclusion, the research presented in this thesis signals future directions in MS research. Continued advancements in these areas will contribute to understanding mechanisms of progression in MS and improving disease monitoring.

References

Abdelnour, F., Kuceyeski, A., Raj, A., Iturria-Medina, Y., & Deslauriers-Gauthier, S. (2022). Editorial: Advances in brain functional and structural networks modeling via graph theory. *Frontiers in Neuroscience*, *16*, 1031280. https://doi.org/10.3389/fnins.2022.1031280

Absinta, M., Maric, D., Gharagozloo, M., Garton, T., Smith, M. D., Jin, J., Fitzgerald, K. C., Song, A., Liu, P., Lin, J.-P., Wu, T., Johnson, K. R., McGavern, D. B., Schafer, D. P., Calabresi, P. A., & Reich, D. S. (2021). A lymphocyte-microglia-astrocyte axis in chronic active multiple sclerosis. *Nature*. https://doi.org/10.1038/s41586-021-03892-7

Absinta, M., Sati, P., Masuzzo, F., Nair, G., Sethi, V., Kolb, H., Ohayon, J., Wu, T., Cortese, I. C. M., & Reich, D. S. (2019). Association of Chronic Active Multiple Sclerosis Lesions With Disability In Vivo. *JAMA Neurology*. https://doi.org/10.1001/jamaneurol.2019.2399

Abulaban, A. (2020). The lateralization of clinical findings might not affect the clinical outcome in multiple sclerosis. *Neurosciences*, *25*(5), 423–424. https://doi.org/10.17712/nsj.2020.5.20200078

Achard, S., & Bullmore, E. (2007). Efficiency and Cost of Economical Brain Functional Networks. *PLOS Computational Biology*, *3*(2), e17. https://doi.org/10.1371/journal.pcbi.0030017

Administration (TGA), T. G. (2022, May 26). *Mayzent* [Text]. Therapeutic Goods Administration (TGA); Therapeutic Goods Administration (TGA). https://www.tga.gov.au/resources/auspmd/mayzent

Aerts, H., Schirner, M., Dhollander, T., Jeurissen, B., Achten, E., Van Roost, D., Ritter, P., & Marinazzo, D. (2020). Modeling brain dynamics after tumor resection using The Virtual Brain. *NeuroImage*, *213*, 116738. https://doi.org/10.1016/j.neuroimage.2020.116738

Amato, M. P., Portaccio, E., Goretti, B., Zipoli, V., Battaglini, M., Bartolozzi, M. L., Stromillo, M. L., Guidi, L., Siracusa, G., Sorbi, S., Federico, A., & De Stefano, N. (2007). Association of neocortical volume changes with cognitive deterioration in relapsing-remitting multiple sclerosis. *Archives of Neurology*, *64*(8), 1157–1161. https://doi.org/10.1001/archneur.64.8.1157

Amezcua, L. (2022). Progressive Multiple Sclerosis. *CONTINUUM: Lifelong Learning in Neurology*, *28*(4), 1083–1103. https://doi.org/10.1212/CON.0000000000001157

Andelova, M., Vodehnalova, K., Krasensky, J., Hardubejova, E., Hrnciarova, T., Srpova, B., Uher, T., Menkyova, I., Stastna, D., Friedova, L., Motyl, J., Lizrova Preiningerova, J., Kubala Havrdova, E., Maréchal, B., Fartaria, M. J., Kober, T., Horakova, D., & Vaneckova, M. (2022). Brainstem lesions are associated with diffuse spinal cord involvement in early multiple sclerosis. *BMC Neurology*, *22*(1), 270. https://doi.org/10.1186/s12883-022-02778-z

Andersson, J. L. R., Skare, S., & Ashburner, J. (2003). How to correct susceptibility distortions in spin-echo echo-planar images: Application to diffusion tensor imaging. *NeuroImage*, *20*(2), 870–888. https://doi.org/10.1016/S1053-8119(03)00336-7

Archer, D. B., Vaillancourt, D. E., & Coombes, S. A. (2018). A Template and Probabilistic Atlas of the Human Sensorimotor Tracts using Diffusion MRI. *Cerebral Cortex*, *28*(5), 1685–1699. https://doi.org/10.1093/cercor/bhx066

Ardekani, B. A., & Bachman, A. H. (2009). Model-based automatic detection of the anterior and posterior commissures on MRI scans. *NeuroImage*, *46*(3), 677–682. https://doi.org/10.1016/j.neuroimage.2009.02.030

Arnemann, K. L., Chen, A. J.-W., Novakovic-Agopian, T., Gratton, C., Nomura, E. M., & D'Esposito, M. (2015). Functional brain network modularity predicts response to cognitive training after brain injury. *Neurology*, *84*(15), 1568–1574. https://doi.org/10.1212/WNL.0000000000001476

Arnold, D. L., Piani-Meier, D., Bar-Or, A., Benedict, R. H., Cree, B. A., Giovannoni, G., Gold, R., Vermersch, P., Arnould, S., Dahlke, F., Hach, T., Ritter, S., Karlsson, G., Kappos, L., Fox, R. J., & for the EXPAND Clinical Investigators. (2022). Effect of siponimod on magnetic resonance imaging measures of neurodegeneration and myelination in secondary progressive multiple sclerosis: Gray matter atrophy and magnetization transfer ratio analyses from the EXPAND phase 3 trial. *Multiple Sclerosis Journal*, 135245852210767. https://doi.org/10.1177/13524585221076717

Arnold, D. L., Sprenger, T., Bar-Or, A., Wolinsky, J. S., Kappos, L., Kolind, S., Bonati, U., Magon, S., van Beek, J., Koendgen, H., Bortolami, O., Bernasconi, C., Gaetano, L., & Traboulsee, A. (2022). Ocrelizumab reduces thalamic volume loss in patients with RMS and PPMS. *Multiple Sclerosis (Houndmills, Basingstoke, England)*, *28*(12), 1927–1936. https://doi.org/10.1177/13524585221097561

Ascherio, A., & Munger, K. L. (2015). EBV and Autoimmunity. *Current Topics in Microbiology and Immunology*, *390*(Pt 1), 365–385. https://doi.org/10.1007/978-3-319-22822-8_15

Ashton, K., Fuchs, T. A., Oship, D., Zivadinov, R., Jakimovski, D., Bergsland, N., Ramasamy, D. P., Vaughn, C., Weinstock-Guttman, B., Benedict, R. H. B., & Dwyer, M. G. (2021). Diagnosis of depression in multiple sclerosis is predicted by frontal-parietal white matter tract disruption. *Journal of Neurology*, *268*(1), 169–177. https://doi.org/10.1007/s00415-020-10110-3

Avants, B. B., Tustison, N., & Johnson, H. (n.d.). *Advanced Normalization Tools (ANTS)*. 41.

Avants, B., Duda, J. T., Zhang, H., & Gee, J. C. (2007). Multivariate Normalization with Symmetric Diffeomorphisms for Multivariate Studies. In N. Ayache, S. Ourselin, & A. Maeder (Eds.), *Medical Image Computing and Computer-Assisted Intervention – MICCAI 2007* (Vol. 4791, pp. 359–366). Springer Berlin Heidelberg. https://doi.org/10.1007/978-3-540-75757-3_44

Avants, B., Epstein, C., Grossman, M., & Gee, J. (2008). Symmetric diffeomorphic image registration with cross-correlation: Evaluating automated labeling of elderly and neurodegenerative brain. *Medical Image Analysis*, *12*(1), 26–41. https://doi.org/10.1016/j.media.2007.06.004

Aymerich, F. X., Auger, C., Alonso, J., Alberich, M., Sastre-Garriga, J., Tintoré, M., Montalban, X., & Rovira, A. (2017). Cervical Cord Atrophy and Long-Term Disease Progression in Patients with Primary-Progressive Multiple Sclerosis. *American Journal of Neuroradiology*. https://doi.org/10.3174/ajnr.A5495

Azevedo, C. J., Cen, S. Y., Khadka, S., Liu, S., Kornak, J., Shi, Y., Zheng, L., Hauser, S. L., & Pelletier, D. (2018). Thalamic Atrophy in MS: An MRI Marker of Neurodegeneration Throughout Disease. *Annals of Neurology*. https://doi.org/10.1002/ana.25150

Babak, A., S, G., A, B., Mj, H., M, W., & J, N. (2005). Quantitative comparison of algorithms for inter-subject registration of 3D volumetric brain MRI scans. *Journal of Neuroscience Methods*, *142*(1). https://doi.org/10.1016/j.jneumeth.2004.07.014

Bagnato, F. (2003). Evolution of T1 black holes in patients with multiple sclerosis imaged monthly for 4 years. *Brain*, *126*(8), 1782–1789. https://doi.org/10.1093/brain/awg182

Baniqued, P. L., Gallen, C. L., Voss, M. W., Burzynska, A. Z., Wong, C. N., Cooke, G. E., Duffy, K., Fanning, J., Ehlers, D. K., Salerno, E. A., Aguiñaga, S., McAuley, E., Kramer, A. F., & D'Esposito, M. (2018). Brain Network Modularity Predicts Exercise-Related Executive Function Gains in Older Adults. *Frontiers in Aging Neuroscience*, *9*, 426. https://doi.org/10.3389/fnagi.2017.00426

Barkhof, F. (2002). The clinico-radiological paradox in multiple sclerosis revisited. *Current Opinion in Neurology*, *15*(3), 239.

Barkhof, F., Calabresi, P. A., Miller, D. H., & Reingold, S. C. (2009). Imaging outcomes for neuroprotection and repair in multiple sclerosis trials. *Nature Reviews Neurology*, *5*(5), 256–266. https://doi.org/10.1038/nrneurol.2009.41

Barnett, Y., Garber, J. Y., & Barnett, M. H. (2020). MRI biomarkers of disease progression in multiple sclerosis: Old dog, new tricks? *Quantitative Imaging in Medicine and Surgery*, *10*(2), 527–532. https://doi.org/10.21037/qims.2020.01.04

Bartnik, A., Fuchs, T. A., Ashton, K., Kuceyeski, A., Li, X., Mallory, M., Oship, D., Bergsland, N., Ramasamy, D., Jakimovski, D., Benedict, R. H. B., Weinstock-Guttman, B., Zivadinov, R., & Dwyer, M. G. (2022). Functional alteration due to structural damage is network dependent: Insight from multiple sclerosis. *Cerebral Cortex*, bhac486. https://doi.org/10.1093/cercor/bhac486

Basser, P. (1998). Fiber-Tractography via Diffusion Tensor MRI (DT-MRI). *Proceedings of the International Society for Magnetic Resonance in Medicine*.

Bassett, D. S., & Bullmore, E. T. (2017). Small-World Brain Networks Revisited. *The Neuroscientist*, *23*(5), 499–516. https://doi.org/10.1177/1073858416667720

Bauer, C., Dyrby, T. B., Sellebjerg, F., Madsen, K. S., Svolgaard, O., Blinkenberg, M., Siebner, H. R., & Andersen, K. W. (2020). Motor fatigue is associated with asymmetric connectivity properties of the corticospinal tract in multiple sclerosis. *NeuroImage. Clinical*, *28*, 102393. https://doi.org/10.1016/j.nicl.2020.102393

Beadnall, H. N., Wang, C., Van Hecke, W., Ribbens, A., Billiet, T., & Barnett, M. H. (2019). Comparing longitudinal brain atrophy measurement techniques in a real-world multiple sclerosis clinical practice cohort: Towards clinical integration? *Therapeutic Advances in Neurological Disorders*, *12*, 175628641882346. https://doi.org/10.1177/1756286418823462

Beaudoin, A.-M., Rheault, F., Theaud, G., Laberge, F., Whittingstall, K., Lamontagne, A., & Descoteaux, M. (2021). Modern Technology in Multi-Shell Diffusion MRI Reveals Diffuse White Matter Changes in Young Adults With Relapsing-Remitting Multiple Sclerosis. *Frontiers in Neuroscience*, *15*, 665017. https://doi.org/10.3389/fnins.2021.665017

Belbasis, L., Bellou, V., Evangelou, E., Ioannidis, J. P. A., & Tzoulaki, I. (2015). Environmental risk factors and multiple sclerosis: An umbrella review of systematic reviews and meta-analyses. *The Lancet Neurology*, *14*(3), 263–273. https://doi.org/10.1016/S1474-4422(14)70267-4

Benedict, R. H. B., Cookfair, D., Gavett, R., Gunther, M., Munschauer, F., Garg, N., & Weinstock-Guttman, B. (2006). Validity of the minimal assessment of cognitive function in multiple

sclerosis (MACFIMS). *Journal of the International Neuropsychological Society: JINS*, *12*(4), 549–558. https://doi.org/10.1017/s1355617706060723

Benedict, R. H., DeLuca, J., Phillips, G., LaRocca, N., Hudson, L. D., Rudick, R., & Multiple Sclerosis Outcome Assessments Consortium. (2017). Validity of the Symbol Digit Modalities Test as a cognition performance outcome measure for multiple sclerosis. *Multiple Sclerosis Journal*, *23*(5), 721–733. https://doi.org/10.1177/1352458517690821

Benedict, R. H., & Walton, M. K. (2012). Evaluating cognitive outcome measures for MS clinical trials: What is a clinically meaningful change? *Multiple Sclerosis Journal*, *18*(12), 1673–1679. https://doi.org/10.1177/1352458512454774

Bergsland, N., Dwyer, M. G., Jakimovski, D., Weinstock-Guttman, B., & Zivadinov, R. (2021). Diffusion tensor imaging reveals greater microstructure damage in lesional tissue that shrinks into cerebrospinal fluid in multiple sclerosis. *Journal of Neuroimaging*, jon.12891. https://doi.org/10.1111/jon.12891

Bergsland, N., Tavazzi, E., Laganà, M. M., Baglio, F., Cecconi, P., Viotti, S., Zivadinov, R., Baselli, G., & Rovaris, M. (2017). White Matter Tract Injury is Associated with Deep Gray Matter Iron Deposition in Multiple Sclerosis: WM Injury and Iron Deposition in MS. *Journal of Neuroimaging*, *27*(1), 107–113. https://doi.org/10.1111/jon.12364

Bergsland, N., Tavazzi, E., Schweser, F., Jakimovski, D., Hagemeier, J., Dwyer, M. G., & Zivadinov, R. (2019). Targeting Iron Dyshomeostasis for Treatment of Neurodegenerative Disorders. *CNS Drugs*. https://doi.org/10.1007/s40263-019-00668-6

Bernabéu-Sanz, Á., Morales, S., Naranjo, V., & Sempere, Á. P. (2021). Contribution of Gray Matter Atrophy and White Matter Damage to Cognitive Impairment in Mildly Disabled Relapsing-Remitting Multiple Sclerosis Patients. *Diagnostics*, *11*(3), 578. https://doi.org/10.3390/diagnostics11030578

Bernstein, M. A., King, K. F., & Zhou, Z. J. (2004). *Handbook of MRI pulse sequences*. Academic Press.

Bisecco, A., Rocca, M. A., Pagani, E., Mancini, L., Enzinger, C., Gallo, A., Vrenken, H., Stromillo, M. L., Copetti, M., Thomas, D. L., Fazekas, F., Tedeschi, G., Barkhof, F., Stefano, N. D., Filippi, M., & MAGNIMS Network. (2015). Connectivity-based parcellation of the thalamus in multiple sclerosis and its implications for cognitive impairment: A multicenter study. *Human Brain Mapping*, *36*(7), 2809–2825. https://doi.org/10.1002/hbm.22809

Bitsch, A., Kuhlmann, T., Stadelmann, C., Lassmann, H., Lucchinetti, C., & Brück, W. (2001). A longitudinal MRI study of histopathologically defined hypointense multiple sclerosis lesions. *Annals of Neurology*, *49*(6), 793–796. https://doi.org/10.1002/ana.1053

Bittner, S., & Zipp, F. (2021). A lymphocyte-glia connection sets the pace for smoldering inflammation. *Cell*, *184*(23), 5696–5698. https://doi.org/10.1016/j.cell.2021.10.018

Bjornevik, K., Cortese, M., Healy, B. C., Kuhle, J., Mina, M. J., Leng, Y., Elledge, S. J., Niebuhr, D. W., Scher, A. I., Munger, K. L., & Ascherio, A. (2022). Longitudinal analysis reveals high prevalence of Epstein-Barr virus associated with multiple sclerosis. *Science*, *375*(6578), 296–301. https://doi.org/10.1126/science.abj8222

Bonkhoff, A. K., Rehme, A. K., Hensel, L., Tscherpel, C., Volz, L. J., Espinoza, F. A., Gazula, H., Vergara, V. M., Fink, G. R., Calhoun, V. D., Rost, N. S., & Grefkes, C. (2021). Dynamic connectivity predicts

acute motor impairment and recovery post-stroke. *Brain Communications*, *3*(4), fcab227. https://doi.org/10.1093/braincomms/fcab227

Boonstra, F. M., Clough, M., Strik, M., van der Walt, A., Butzkueven, H., White, O. B., Law, M., Fielding, J., & Kolbe, S. C. (2022). Longitudinal tracking of axonal loss using diffusion magnetic resonance imaging in multiple sclerosis. *Brain Communications*, *4*(2), fcac065. https://doi.org/10.1093/braincomms/fcac065

Boscheron, J., Ruet, A., Deloire, M., Charré-Morin, J., Saubusse, A., Brochet, B., Tourdias, T., & Koubiyr, I. (2021). Insights on the Relationship Between Hippocampal Connectivity and Memory Performances at the Early Stage of Multiple Sclerosis. *Frontiers in Neurology*, *12*, 667531. https://doi.org/10.3389/fneur.2021.667531

Bosticardo, S., Schiavi, S., Schaedelin, S., Lu, P.-J., Barakovic, M., Weigel, M., Kappos, L., Kuhle, J., Daducci, A., & Granziera, C. (2021). Microstructure-weighted connectomics in multiple sclerosis. *Brain Connectivity*, brain.2021.0047. https://doi.org/10.1089/brain.2021.0047

Bozzali, M., Spanò, B., Parker, G., Giulietti, G., Castelli, M., Basile, B., Rossi, S., Serra, L., Magnani, G., Nocentini, U., Caltagirone, C., Centonze, D., & Cercignani, M. (2013). Anatomical brain connectivity can assess cognitive dysfunction in multiple sclerosis. *Multiple Sclerosis Journal*, *19*(9), 1161–1168. https://doi.org/10.1177/1352458512474088

Brown, A. (1992). Survey of Image Registration Techniques, Department of Computer Science, Columbia University. *ACM Computing Surveys*, *24*(4).

Browne, P., Chandraratna, D., Angood, C., Tremlett, H., Baker, C., Taylor, B. V., & Thompson, A. J. (2014). Atlas of Multiple Sclerosis 2013: A growing global problem with widespread inequity. *Neurology*, *83*(11), 1022–1024. https://doi.org/10.1212/WNL.0000000000000768

Brück, W., Bitsch, A., Kolenda, H., Brück, Y., Stiefel, M., & Lassmann, H. (1997). Inflammatory central nervous system demyelination: Correlation of magnetic resonance imaging findings with lesion pathology. *Annals of Neurology*, *42*(5), 783–793. https://doi.org/10.1002/ana.410420515

Budde, M. D., Xie, M., Cross, A. H., & Song, S.-K. (2009). Axial Diffusivity Is the Primary Correlate of Axonal Injury in the Experimental Autoimmune Encephalomyelitis Spinal Cord: A Quantitative Pixelwise Analysis. *Journal of Neuroscience*, *29*(9), 2805–2813. https://doi.org/10.1523/JNEUROSCI.4605-08.2009

Bullmore, E., & Sporns, O. (2009). Complex brain networks: Graph theoretical analysis of structural and functional systems. *Nature Reviews Neuroscience*, *10*(3), 186–198. https://doi.org/10.1038/nrn2575

Burgetova, A., Dusek, P., Uher, T., Vaneckova, M., Vejrazka, M., Burgetova, R., Horakova, D., Srpova, B., Krasensky, J., & Lambert, L. (2022). Oxidative Stress Markers in Cerebrospinal Fluid of Newly Diagnosed Multiple Sclerosis Patients and Their Link to Iron Deposition and Atrophy. *Diagnostics (Basel, Switzerland)*, *12*(6), 1365. https://doi.org/10.3390/diagnostics12061365

Buss, A., & Schwab, M. E. (2003). Sequential loss of myelin proteins during Wallerian degeneration in the rat spinal cord. *Glia*, *42*(4), 424–432. https://doi.org/10.1002/glia.10220

Cabezas, M., Luo, Y., Kyle, K., Ly, L., Wang, C., & Barnett, M. (2021). Estimating lesion activity through feature similarity: A dual path Unet approach for the MSSEG2 MICCAI challenge. *MICCAI 2021 - Poster*.

Cadavid, D., Balcer, L., Galetta, S., Aktas, O., Ziemssen, T., Vanopdenbosch, L., Frederiksen, J., Skeen, M., Jaffe, G. J., Butzkueven, H., Ziemssen, F., Massacesi, L., Chai, Y., Xu, L., & Freeman, S. (2017). Safety and efficacy of opicinumab in acute optic neuritis (RENEW): A randomised, placebo-controlled, phase 2 trial. *The Lancet Neurology*, *16*(3), 189–199. https://doi.org/10.1016/S1474-4422(16)30377-5

Calabrese, M., Atzori, M., Bernardi, V., Morra, A., Romualdi, C., Rinaldi, L., McAuliffe, M. J. M., Barachino, L., Perini, P., Fischl, B., Battistin, L., & Gallo, P. (2007). Cortical atrophy is relevant in multiple sclerosis at clinical onset. *Journal of Neurology*, *254*(9), 1212–1220. https://doi.org/10.1007/s00415-006-0503-6

Calamante, F., Tournier, J.-D., Jackson, G. D., & Connelly, A. (2010). Track-density imaging (TDI): Super-resolution white matter imaging using whole-brain track-density mapping. *NeuroImage*, *53*(4), 1233–1243. https://doi.org/10.1016/j.neuroimage.2010.07.024

Calamante, F., Tournier, J.-D., Smith, R. E., & Connelly, A. (2012). A generalised framework for super-resolution track-weighted imaging. *NeuroImage*, *59*(3), 2494–2503. https://doi.org/10.1016/j.neuroimage.2011.08.099

Calvi, A., Carrasco, F. P., Tur, C., Chard, D. T., Stutters, J., De Angelis, F., John, N., Williams, T., Doshi, A., Samson, R. S., MacManus, D., Gandini Wheeler-Kingshott, C. A., Ciccarelli, O., Chataway, J., Barkhof, F., & MSSMART Investigators. (2022). Association of Slowly Expanding Lesions on MRI With Disability in People With Secondary Progressive Multiple Sclerosis. *Neurology*, 10.1212/WNL.0000000000200144. https://doi.org/10.1212/WNL.0000000000200144

Calvi, A., Tur, C., Chard, D., Stutters, J., Ciccarelli, O., Cortese, R., Battaglini, M., Pietroboni, A., De Riz, M., Galimberti, D., Scarpini, E., De Stefano, N., Prados, F., & Barkhof, F. (2022). Slowly expanding lesions relate to persisting black-holes and clinical outcomes in relapse-onset multiple sclerosis. *NeuroImage. Clinical*, *35*, 103048. https://doi.org/10.1016/j.nicl.2022.103048

Campbell, G. R., Worrall, J. T., & Mahad, D. J. (2014). The central role of mitochondria in axonal degeneration in multiple sclerosis. *Multiple Sclerosis Journal*, *20*(14), 1806–1813. https://doi.org/10.1177/1352458514544537

Cao, Y., Diao, W., Tian, F., Zhang, F., He, L., Long, X., Zhou, F., & Jia, Z. (2021). Gray Matter Atrophy in the Cortico-Striatal-Thalamic Network and Sensorimotor Network in Relapsing-Remitting and Primary Progressive Multiple Sclerosis. *Neuropsychology Review*. https://doi.org/10.1007/s11065-021-09479-3

Cawley, N., Tur, C., Prados, F., Plantone, D., Kearney, H., Abdel-Aziz, K., Ourselin, S., Wheeler-Kingshott, C. A. G., Miller, D. H., Thompson, A. J., & Ciccarelli, O. (2017). Spinal cord atrophy as a primary outcome measure in phase II trials of progressive multiple sclerosis. *Multiple Sclerosis Journal*, 135245851770995. https://doi.org/10.1177/1352458517709954

Cercignani, M., & Gandini Wheeler-Kingshott, C. (2018). From micro- to macro-structures in multiple sclerosis: What is the added value of diffusion imaging. *NMR in Biomedicine*, e3888. https://doi.org/10.1002/nbm.3888

Chan, M. Y., Park, D. C., Savalia, N. K., Petersen, S. E., & Wig, G. S. (2014). Decreased segregation of brain systems across the healthy adult lifespan. *Proceedings of the National Academy of Sciences*, *111*(46). https://doi.org/10.1073/pnas.1415122111

Charalambous, T., Clayden, J. D., Powell, E., Prados, F., Tur, C., Kanber, B., Chard, D., Ourselin, S., Wheeler-Kingshott, C. A. M. G., Thompson, A. J., & Toosy, A. T. (2020). Disrupted principal network organisation in multiple sclerosis relates to disability. *Scientific Reports*, *10*(1), 3620. https://doi.org/10.1038/s41598-020-60611-4

Charalambous, T., Tur, C., Prados, F., Kanber, B., Chard, D. T., Ourselin, S., Clayden, J. D., A M Gandini Wheeler-Kingshott, C., Thompson, A. J., & Toosy, A. T. (2019). Structural network disruption markers explain disability in multiple sclerosis. *Journal of Neurology, Neurosurgery & Psychiatry*, *90*(2), 219–226. https://doi.org/10.1136/jnnp-2018-318440

Chard, D. T., Alahmadi, A. A. S., Audoin, B., Charalambous, T., Enzinger, C., Hulst, H. E., Rocca, M. A., Rovira, À., Sastre-Garriga, J., Schoonheim, M. M., Tijms, B., Tur, C., Gandini Wheeler-Kingshott, C. A. M., Wink, A. M., Ciccarelli, O., & Barkhof, F. (2021). Mind the gap: From neurons to networks to outcomes in multiple sclerosis. *Nature Reviews Neurology*. https://doi.org/10.1038/s41582-020-00439-8

Chard, D. T., Griffin, C. M., Parker, G. J. M., Kapoor, R., Thompson, A. J., & Miller, D. H. (2002). Brain atrophy in clinically early relapsing–remitting multiple sclerosis. *Brain*, *125*(2), 327–337. https://doi.org/10.1093/brain/awf025

Chen, X., Diaz-Pinto, A., Ravikumar, N., & Frangi, A. F. (2021). Deep learning in medical image registration. *Progress in Biomedical Engineering*, *3*(1), 012003. https://doi.org/10.1088/2516-1091/abd37c

Chen, X., Peng, Y., Zheng, Q., Luo, D., Han, Y., Luo, Q., Zhu, Q., Luo, T., & Li, Y. (2022). The different damage patterns of short-, middle- and long-range connections between patients with relapse-remitting multiple sclerosis and neuromyelitis optica spectrum disorder. *Frontiers in Immunology*, *13*, 1007335. https://doi.org/10.3389/fimmu.2022.1007335

Cho, E. B., Kim, D., Jeong, B., Shin, J. H., Chung, Y. H., Kim, S. T., Kim, B. J., Han, C. E., & Min, J.-H. (2022). Disrupted structural network of inferomedial temporal regions in relapsing-remitting multiple sclerosis compared with neuromyelitis optica spectrum disorder. *Scientific Reports*, *12*(1), 5152. https://doi.org/10.1038/s41598-022-09065-4

Choi, S. R., Howell, O. W., Carassiti, D., Magliozzi, R., Gveric, D., Muraro, P. A., Nicholas, R., Roncaroli, F., & Reynolds, R. (2012). Meningeal inflammation plays a role in the pathology of primary progressive multiple sclerosis. *Brain*, *135*(10), 2925–2937. https://doi.org/10.1093/brain/aws189

Ciccarelli, O., Catani, M., Johansen-Berg, H., Clark, C., & Thompson, A. (2008). Diffusion-based tractography in neurological disorders: Concepts, applications, and future developments. *The Lancet. Neurology*, *7*(8), 715–727. https://doi.org/10.1016/S1474-4422(08)70163-7

Ciccarelli, O., Werring, D. J., Barker, G. J., Griffin, C. M., Wheeler-Kingshott, C. A. M., Miller, D. H., & Thompson, A. J. (2003). A study of the mechanisms of normal-appearing white matter damage in multiple sclerosis using diffusion tensor imaging—Evidence of Wallerian degeneration. *Journal of Neurology*, *250*(3), 287–292. https://doi.org/10.1007/s00415-003-0992-5

Clarke, M. A., Archer, D., Yoon, K., Oguz, I., Smith, S. A., Xu, J., Cutter, G., & Bagnato, F. (2022). White matter tracts that overlap with the thalamus and the putamen are protected against multiple sclerosis pathology. *Multiple Sclerosis and Related Disorders*, *57*, 103430. https://doi.org/10.1016/j.msard.2021.103430

Comi, G., Bar-Or, A., Lassmann, H., Uccelli, A., Hartung, H., Montalban, X., Sørensen, P. S., Hohlfeld, R., Hauser, S. L., & Expert Panel of the 27th Annual Meeting of the European Charcot Foundation. (2020). Role of B Cells in Multiple Sclerosis and Related Disorders. *Annals of Neurology*, ana.25927. https://doi.org/10.1002/ana.25927

Confavreux, C. (2003). Early clinical predictors and progression of irreversible disability in multiple sclerosis: An amnesic process. *Brain*, *126*(4), 770–782. https://doi.org/10.1093/brain/awg081

Conforti, L., Adalbert, R., & Coleman, M. P. (2007). Neuronal death: Where does the end begin? *Trends in Neurosciences*, *30*(4), 159–166. https://doi.org/10.1016/j.tins.2007.02.004

Correale, J. (2014). The role of microglial activation in disease progression. *Multiple Sclerosis Journal*, *20*(10), 1288–1295. https://doi.org/10.1177/1352458514533230

Correale, J., Gaitán, M. I., Ysrraelit, M. C., & Fiol, M. P. (2016). Progressive multiple sclerosis: From pathogenic mechanisms to treatment. *Brain*, aww258. https://doi.org/10.1093/brain/aww258

Cree, B. A. C. (2014). Genetics of primary progressive multiple sclerosis. *Handbook of Clinical Neurology*, *122*, 211–230. https://doi.org/10.1016/B978-0-444-52001-2.00042-X

Cree, B. A. C., Arnold, D. L., Chataway, J., Chitnis, T., Fox, R. J., Pozo Ramajo, A., Murphy, N., & Lassmann, H. (2021). Secondary Progressive Multiple Sclerosis: New Insights. *Neurology*, *97*(8), 378–388. https://doi.org/10.1212/WNL.0000000000012323

Cree, B. A. C., Hollenbach, J. A., Bove, R., Kirkish, G., Sacco, S., Caverzasi, E., Bischof, A., Gundel, T., Zhu, A. H., Papinutto, N., Stern, W. A., Bevan, C., Romeo, A., Goodin, D. S., Gelfand, J. M., Graves, J., Green, A. J., Wilson, M. R., Zamvil, S. S., … Hauser, S. L. (2019). Silent progression in disease activity–free relapsing multiple sclerosis. *Annals of Neurology*, *85*(5), 653–666. https://doi.org/10.1002/ana.25463

Daducci, A., Dal Palu, A., Lemkaddem, A., & Thiran, J.-P. (2015). COMMIT: Convex Optimization Modeling for Microstructure Informed Tractography. *IEEE Transactions on Medical Imaging*, *34*(1), 246–257. https://doi.org/10.1109/TMI.2014.2352414

Dale, A., Fischl, B., & Sereno, M. I. (1999). Cortical Surface-Based Analysis: I. Segmentation and Surface Reconstruction. *NeuroImage*, *9*(2), 179–194.

Davies, S. J. A., Fitch, M. T., Memberg, S. P., Hall, A. K., Raisman, G., & Silver, J. (1997). Regeneration of adult axons in white matter tracts of the central nervous system. *Nature*, *390*(6661), Article 6661. https://doi.org/10.1038/37776

de Haan, W., van der Flier, W. M., Koene, T., Smits, L. L., Scheltens, P., & Stam, C. J. (2012). Disrupted modular brain dynamics reflect cognitive dysfunction in Alzheimer's disease. *NeuroImage*, *59*(4), 3085–3093. https://doi.org/10.1016/j.neuroimage.2011.11.055

De Stefano, N., Airas, L., Grigoriadis, N., Mattle, H. P., O'Riordan, J., Oreja-Guevara, C., Sellebjerg, F., Stankoff, B., Walczak, A., Wiendl, H., & Kieseier, B. C. (2014). Clinical Relevance of Brain

Volume Measures in Multiple Sclerosis. *CNS Drugs*, *28*(2), 147–156. https://doi.org/10.1007/s40263-014-0140-z

De Stefano, N., Giorgio, A., Battaglini, M., Rovaris, M., Sormani, M. P., Barkhof, F., Korteweg, T., Enzinger, C., Fazekas, F., Calabrese, M., Dinacci, D., Tedeschi, G., Gass, A., Montalban, X., Rovira, A., Thompson, A., Comi, G., Miller, D. H., & Filippi, M. (2010). Assessing brain atrophy rates in a large population of untreated multiple sclerosis subtypes. *Neurology*, *74*(23), 1868–1876. https://doi.org/10.1212/WNL.0b013e3181e24136

De Stefano, N., Stromillo, M. L., Giorgio, A., Bartolozzi, M. L., Battaglini, M., Baldini, M., Portaccio, E., Amato, M. P., & Sormani, M. P. (2015). Establishing pathological cut-offs of brain atrophy rates in multiple sclerosis. *Journal of Neurology, Neurosurgery & Psychiatry*, jnnp-2014-309903. https://doi.org/10.1136/jnnp-2014-309903

Dendrou, C. A., Fugger, L., & Friese, M. A. (2015). Immunopathology of multiple sclerosis. *Nature Reviews Immunology*, *15*(9), 545–558. https://doi.org/10.1038/nri3871

Desikan, R. S., Ségonne, F., Fischl, B., Quinn, B. T., Dickerson, B. C., Blacker, D., Buckner, R. L., Dale, A. M., Maguire, R. P., Hyman, B. T., Albert, M. S., & Killiany, R. J. (2006). An automated labeling system for subdividing the human cerebral cortex on MRI scans into gyral based regions of interest. *NeuroImage*, *31*(3), 968–980. https://doi.org/DOI: 10.1016/j.neuroimage.2006.01.021

Dhollander, T., Raffelt, D., & Connelly, A. (2018). *Accuracy of response function estimation algorithms for 3-tissue spherical deconvolution of diverse quality diffusion MRI data*.

Dhollander, T., Tabbara, R., Rosnarho-Tornstrand, J., Tournier, J.-D., Raffelt, D., & Connelly, A. (2021). Multi-tissue log-domain intensity and inhomogeneity normalisation for quantitative apparent fibre density. *Proc. ISMRM*, *29*, 2472.

Diem, R., Demmer, I., Boretius, S., Merkler, D., Schmelting, B., Williams, S. K., Sättler, M. B., Bähr, M., Michaelis, T., Frahm, J., Brück, W., & Fuchs, E. (2008). Autoimmune optic neuritis in the common marmoset monkey: Comparison of visual evoked potentials with MRI and histopathology. *Investigative Ophthalmology & Visual Science*, *49*(8), 3707–3714. https://doi.org/10.1167/iovs.08-1896

Drake, A., Weinstock-Guttman, B., Morrow, S., Hojnacki, D., Munschauer, F., & Benedict, R. (2010). Psychometrics and normative data for the Multiple Sclerosis Functional Composite: Replacing the PASAT with the Symbol Digit Modalities Test. *Multiple Sclerosis Journal*, *16*(2), 228–237. https://doi.org/10.1177/1352458509354552

Dubitzky, W., Wolkenhauer, O., Cho, K.-H., & Yokota, H. (Eds.). (2013). *Encyclopedia of Systems Biology*. Springer New York. https://doi.org/10.1007/978-1-4419-9863-7

Dwyer, M. G., Bergsland, N., Ramasamy, D. P., Jakimovski, D., Weinstock-Guttman, B., & Zivadinov, R. (2018). Atrophied Brain Lesion Volume: A New Imaging Biomarker in Multiple Sclerosis: Atrophied Lesions in MS. *Journal of Neuroimaging*, *28*(5), 490–495. https://doi.org/10.1111/jon.12527

ECTRIMS 2022 – ePoster. (2022). *Multiple Sclerosis Journal*, *28*(3_suppl), 692–945. https://doi.org/10.1177/13524585221123682

Elliott, C., Belachew, S., Wolinsky, J. S., Hauser, S. L., Kappos, L., Barkhof, F., Bernasconi, C., Fecker, J., Model, F., Wei, W., & Arnold, D. L. (2019). Chronic white matter lesion activity predicts clinical progression in primary progressive multiple sclerosis. *Brain*, *142*(9), 2787–2799. https://doi.org/10.1093/brain/awz212

Elliott, C., Wolinsky, J. S., Hauser, S. L., Kappos, L., Barkhof, F., Bernasconi, C., Wei, W., Belachew, S., & Arnold, D. L. (2019). Slowly expanding/evolving lesions as a magnetic resonance imaging marker of chronic active multiple sclerosis lesions. *Multiple Sclerosis Journal*, *25*(14), 1915–1925. https://doi.org/10.1177/1352458518814117

EMA. (2019, November 12). *Mayzent* [Text]. European Medicines Agency. https://www.ema.europa.eu/en/medicines/human/EPAR/mayzent

Engl, C., Tiemann, L., Grahl, S., Bussas, M., Schmidt, P., Pongratz, V., Berthele, A., Beer, A., Gaser, C., Kirschke, J. S., Zimmer, C., Hemmer, B., & Mühlau, M. (2020). Cognitive impairment in early MS: Contribution of white matter lesions, deep grey matter atrophy, and cortical atrophy. *Journal of Neurology*, *267*(8), 2307–2318. https://doi.org/10.1007/s00415-020-09841-0

Estrada, E., & Hatano, N. (2008). Communicability in complex networks. *Physical Review. E, Statistical, Nonlinear, and Soft Matter Physics*, *77*(3 Pt 2), 036111. https://doi.org/10.1103/PhysRevE.77.036111

Etemadifar, M., Ashourizadeh, H., Nouri, H., Kargaran, P. K., Salari, M., Rayani, M., Aghababaee, A., & Abhari, A. P. (2021). MRI signs of CNS demyelinating diseases. *Multiple Sclerosis and Related Disorders*, *47*, 102665. https://doi.org/10.1016/j.msard.2020.102665

Farquharson, S., Tournier, J.-D., Calamante, F., Fabinyi, G., Schneider-Kolsky, M., Jackson, G. D., & Connelly, A. (2013). White matter fiber tractography: Why we need to move beyond DTI. *Journal of Neurosurgery*, 1367–1377. https://doi.org/10.3171/2013.2.JNS121294

Farrell, P. J. (2019). Epstein-Barr Virus and Cancer. *Annual Review of Pathology*, *14*, 29–53. https://doi.org/10.1146/annurev-pathmechdis-012418-013023

FDA. (2020, January 27). *Drug Trials Snapshots: MAYZENT*. FDA; FDA. https://www.fda.gov/drugs/drug-approvals-and-databases/drug-trials-snapshots-mayzent

Feys, P., Lamers, I., Francis, G., Benedict, R., Phillips, G., LaRocca, N., Hudson, L. D., & Rudick, R. (2017). The Nine-Hole Peg Test as a manual dexterity performance measure for multiple sclerosis. *Multiple Sclerosis (Houndmills, Basingstoke, England)*, *23*(5), 711–720. https://doi.org/10.1177/1352458517690824

Filippi, M., Cercignani, M., Inglese, M., Horsfield, M. A., & Comi, G. (2001). Diffusion tensor magnetic resonance imaging in multiple sclerosis. *Neurology*, *56*(3), 304–311. https://doi.org/10.1212/WNL.56.3.304

Filippi, M., & Rocca, M. A. (2005). MRI evidence for multiple sclerosis as a diffuse disease of the central nervous system. *Journal of Neurology*, *252*(S5), v16–v24. https://doi.org/10.1007/s00415-005-5004-5

Filippi, M., Rocca, M. A., Barkhof, F., Brück, W., Chen, J. T., Comi, G., DeLuca, G., De Stefano, N., Erickson, B. J., & Evangelou, N. (2012). Association between pathological and MRI findings in multiple sclerosis. *The Lancet Neurology*, *11*(4), 349–360.

Filippi, M., Rocca, M. A., Ciccarelli, O., De Stefano, N., Evangelou, N., Kappos, L., Rovira, A., Sastre-Garriga, J., Tintorè, M., Frederiksen, J. L., Gasperini, C., Palace, J., Reich, D. S., Banwell, B., Montalban, X., & Barkhof, F. (2016). MRI criteria for the diagnosis of multiple sclerosis: MAGNIMS consensus guidelines. *The Lancet Neurology*, *15*(3), 292–303. https://doi.org/10.1016/S1474-4422(15)00393-2

Fink, J. N., Selim, M. H., Kumar, S., Silver, B., Linfante, I., Caplan, L. R., & Schlaug, G. (2002). Is the Association of National Institutes of Health Stroke Scale Scores and Acute Magnetic Resonance Imaging Stroke Volume Equal for Patients With Right- and Left-Hemisphere Ischemic Stroke? *Stroke*, *33*(4), 954–958. https://doi.org/10.1161/01.STR.0000013069.24300.1D

Fischer, J. S., Rudick, R. A., Cutter, G. R., & Reingold, S. C. (1999). The Multiple Sclerosis Functional Composite Measure (MSFC): An integrated approach to MS clinical outcome assessment. National MS Society Clinical Outcomes Assessment Task Force. *Multiple Sclerosis (Houndmills, Basingstoke, England)*, *5*(4), 244–250. https://doi.org/10.1177/135245859900500409

Fischl, B. (2012). FreeSurfer. *NeuroImage*, *62*(2), 774–781. https://doi.org/10.1016/j.neuroimage.2012.01.021

Flegel, M., Knox, K., & Nickel, D. (2012). Step-Length Variability in Minimally Disabled Women with Multiple Sclerosis or Clinically Isolated Syndrome. *International Journal of MS Care*, *14*(1), 26–30. https://doi.org/10.7224/1537-2073-14.1.26

Fleischer, V., Gröger, A., Koirala, N., Droby, A., Muthuraman, M., Kolber, P., Reuter, E., Meuth, S. G., Zipp, F., & Groppa, S. (2017). Increased structural white and grey matter network connectivity compensates for functional decline in early multiple sclerosis. *Multiple Sclerosis (Houndmills, Basingstoke, England)*, *23*(3), 432–441. https://doi.org/10.1177/1352458516651503

Fling, B. W., Martini, D. N., Zeeboer, E., Hildebrand, A., & Cameron, M. (2019). Neuroplasticity of the sensorimotor neural network associated with walking aid training in people with multiple sclerosis. *Multiple Sclerosis and Related Disorders*, *31*, 1–4. https://doi.org/10.1016/j.msard.2019.03.004

Fornito, A., & Bullmore, E. T. (2015). Connectomics: A new paradigm for understanding brain disease. *European Neuropsychopharmacology*, *25*(5), 733–748. https://doi.org/10.1016/j.euroneuro.2014.02.011

Fornito, A., Zalesky, A., & Breakspear, M. (2015). The connectomics of brain disorders. *Nature Reviews Neuroscience*, *16*(3), Article 3. https://doi.org/10.1038/nrn3901

Fox, J., Kraemer, M., Schormann, T., Dabringhaus, A., Hirsch, J., Eisele, P., Szabo, K., Weiss, C., Amann, M., Weier, K., Naegelin, Y., Kappos, L., & Gass, A. (2016). Individual Assessment of Brain Tissue Changes in MS and the Effect of Focal Lesions on Short-Term Focal Atrophy Development in MS: A Voxel-Guided Morphometry Study. *International Journal of Molecular Sciences*, *17*(4), 489. https://doi.org/10.3390/ijms17040489

Fraussen, J., de Bock, L., & Somers, V. (2016). B cells and antibodies in progressive multiple sclerosis: Contribution to neurodegeneration and progression. *Autoimmunity Reviews*, *15*(9), 896–899. https://doi.org/10.1016/j.autrev.2016.07.008

Friese, M. A., Schattling, B., & Fugger, L. (2014). Mechanisms of neurodegeneration and axonal dysfunction in multiple sclerosis. *Nature Reviews Neurology*, *10*(4), 225–238. https://doi.org/10.1038/nrneurol.2014.37

Friston, K. (2002). Beyond Phrenology: What Can Neuroimaging Tell Us About Distributed Circuitry? *Annual Review of Neuroscience*, *25*(1), 221–250. https://doi.org/10.1146/annurev.neuro.25.112701.142846

Fuchs, T. A., Carolus, K., Benedict, R. H. B., Bergsland, N., Ramasamy, D., Jakimovski, D., Weinstock-Guttman, B., Kuceyeski, A., Zivadinov, R., & Dwyer, M. G. (2018). Impact of Focal White Matter Damage on Localized Subcortical Gray Matter Atrophy in Multiple Sclerosis: A 5-Year Study. *American Journal of Neuroradiology*, ajnr;ajnr.A5720v1. https://doi.org/10.3174/ajnr.A5720

Fuchs, T. A., Dwyer, M. G., Kuceyeski, A., Choudhery, S., Carolus, K., Li, X., Mallory, M., Weinstock-Guttman, B., Jakimovski, D., Ramasamy, D., Zivadinov, R., & Benedict, R. H. B. (2018). White matter tract network disruption explains reduced conscientiousness in multiple sclerosis. *Human Brain Mapping*, *39*(9), 3682–3690. https://doi.org/10.1002/hbm.24203

Fuchs, T. A., Ziccardi, S., Benedict, R. H. B., Bartnik, A., Kuceyeski, A., Charvet, L. E., Oship, D., Weinstock-Guttman, B., Wojcik, C., Hojnacki, D., Kolb, C., Escobar, J., Campbell, R., Tran, H. D., Bergsland, N., Jakimovski, D., Zivadinov, R., & Dwyer, M. G. (2020). Functional Connectivity and Structural Disruption in the Default-Mode Network Predicts Cognitive Rehabilitation Outcomes in Multiple Sclerosis. *Journal of Neuroimaging*, *30*(4), 523–530. https://doi.org/10.1111/jon.12723

Fünfschilling, U., Supplie, L. M., Mahad, D., Boretius, S., Saab, A. S., Edgar, J., Brinkmann, B. G., Kassmann, C. M., Tzvetanova, I. D., Möbius, W., Diaz, F., Meijer, D., Suter, U., Hamprecht, B., Sereda, M. W., Moraes, C. T., Frahm, J., Goebbels, S., & Nave, K.-A. (2012). Glycolytic oligodendrocytes maintain myelin and long-term axonal integrity. *Nature*, *485*(7399), 517–521. https://doi.org/10.1038/nature11007

Gallen, C. L., Baniqued, P. L., Chapman, S. B., Aslan, S., Keebler, M., Didehbani, N., & D'Esposito, M. (2016). Modular Brain Network Organization Predicts Response to Cognitive Training in Older Adults. *PLOS ONE*, *11*(12), e0169015. https://doi.org/10.1371/journal.pone.0169015

Gamboa, O. L., Tagliazucchi, E., von Wegner, F., Jurcoane, A., Wahl, M., Laufs, H., & Ziemann, U. (2014). Working memory performance of early MS patients correlates inversely with modularity increases in resting state functional connectivity networks. *NeuroImage*, *94*, 385–395. https://doi.org/10.1016/j.neuroimage.2013.12.008

Ge, Y., Grossman, R. I., Udupa, J. K., Wei, L., Mannon, L. J., Polansky, M., & Kolson, D. L. (2000). Brain Atrophy in Relapsing-Remitting Multiple Sclerosis and Secondary Progressive Multiple Sclerosis: Longitudinal Quantitative Analysis. *Radiology*, *214*(3), 665–670. https://doi.org/10.1148/radiology.214.3.r00mr30665

Geng, X., Ross, T. J., Gu, H., Shin, W., Zhan, W., Chao, Y.-P., Lin, C.-P., Schuff, N., & Yang, Y. (2011). Diffeomorphic Image Registration of Diffusion MRI Using Spherical Harmonics. *IEEE Transactions on Medical Imaging*, *30*(3), 10.1109/TMI.2010.2095027. https://doi.org/10.1109/TMI.2010.2095027

Genovese, A. V., Hagemeier, J., Bergsland, N., Jakimovski, D., Dwyer, M. G., Ramasamy, D. P., Lizarraga, A. A., Hojnacki, D., Kolb, C., Weinstock-Guttman, B., & Zivadinov, R. (2019). Atrophied Brain T2

Lesion Volume at MRI Is Associated with Disability Progression and Conversion to Secondary Progressive Multiple Sclerosis. *Radiology*, 190306. https://doi.org/10.1148/radiol.2019190306

George, R., & Griffin, J. W. (1994). Delayed Macrophage Responses and Myelin Clearance during Wallerian Degeneration in the Central Nervous System: The Dorsal Radiculotomy Model. *Experimental Neurology*, *129*(2), 225–236. https://doi.org/10.1006/exnr.1994.1164

Gill, A. J., Schorr, E. M., Gadani, S. P., & Calabresi, P. A. (2023). Emerging imaging and liquid biomarkers in multiple sclerosis. *European Journal of Immunology*, e2250228. https://doi.org/10.1002/eji.202250228

Giorgio, A., & De Stefano, N. (2018). Effective Utilization of MRI in the Diagnosis and Management of Multiple Sclerosis. *Neurologic Clinics*, *36*(1), 27–34. https://doi.org/10.1016/j.ncl.2017.08.013

Goldman-Rakic, P. S. (1987). Motor control function of the prefrontal cortex. *Ciba Foundation Symposium*, *132*, 187–200. https://doi.org/10.1002/9780470513545.ch12

Guerrero, B. L., & Sicotte, N. L. (2020). Microglia in Multiple Sclerosis: Friend or Foe? *Frontiers in Immunology*, *11*, 374. https://doi.org/10.3389/fimmu.2020.00374

Hagemeier, J., Ramanathan, M., Schweser, F., Dwyer, M. G., Lin, F., Bergsland, N., Weinstock-Guttman, B., & Zivadinov, R. (2017). Iron-related gene variants and brain iron in multiple sclerosis and healthy individuals. *NeuroImage : Clinical*, *17*, 530–540. https://doi.org/10.1016/j.nicl.2017.11.003

Hagmann, P., Cammoun, L., Gigandet, X., Meuli, R., Honey, C. J., Wedeen, V. J., & Sporns, O. (2008). Mapping the structural core of human cerebral cortex. *PLoS Biology*, *6*(7), e159. https://doi.org/10.1371/journal.pbio.0060159

Haider, L., Zrzavy, T., Hametner, S., Höftberger, R., Bagnato, F., Grabner, G., Trattnig, S., Pfeifenbring, S., Brück, W., & Lassmann, H. (2016). The topograpy of demyelination and neurodegeneration in the multiple sclerosis brain. *Brain*, *139*(3), 807–815. https://doi.org/10.1093/brain/awv398

Hametner, S., Wimmer, I., Haider, L., Pfeifenbring, S., Brück, W., & Lassmann, H. (2013). Iron and neurodegeneration in the multiple sclerosis brain: Iron in the MS Brain. *Annals of Neurology*, *74*(6), 848–861. https://doi.org/10.1002/ana.23974

Hardy, T. A., Wang, C., Beadnall, H. N., Lagopoulos, J., Barnett, Y., Klistorner, A., & Barnett, M. H. (2016). Wallerian Degeneration in the Corticospinal Tract Following Tumefactive Demyelination: Conventional and Advanced Magnetic Resonance Imaging. *Canadian Journal of Neurological Sciences / Journal Canadien Des Sciences Neurologiques*, *43*(05), 726–727. https://doi.org/10.1017/cjn.2016.253

Hart, P. H., Gorman, S., & Finlay-Jones, J. J. (2011). Modulation of the immune system by UV radiation: More than just the effects of vitamin D? *Nature Reviews. Immunology*, *11*(9), 584–596. https://doi.org/10.1038/nri3045

Has Silemek, A. C., Fischer, L., Pöttgen, J., Penner, I.-K., Engel, A. K., Heesen, C., Gold, S. M., & Stellmann, J.-P. (2020). Functional and structural connectivity substrates of cognitive performance in relapsing remitting multiple sclerosis with mild disability. *NeuroImage: Clinical*, *25*, 102177. https://doi.org/10.1016/j.nicl.2020.102177

Hawkes, C. H. (2007). Smoking is a risk factor for multiple sclerosis: A metanalysis. *Multiple Sclerosis Journal*, *13*(5), 610–615. https://doi.org/10.1177/1352458506073501

Hedström, A. K., Brenner, N., Butt, J., Hillert, J., Waterboer, T., Olsson, T., & Alfredsson, L. (2021). Overweight/obesity in young adulthood interacts with aspects of EBV infection in MS etiology. *Neurology - Neuroimmunology Neuroinflammation*, *8*(1), e912. https://doi.org/10.1212/NXI.0000000000000912

Hedström, A., Olsson, T., & Alfredsson, L. (2016). Smoking is a major preventable risk factor for multiple sclerosis. *Multiple Sclerosis Journal*, *22*(8), 1021–1026. https://doi.org/10.1177/1352458515609794

Heidari, M., Radcliff, A. B., McLellan, G. J., Ver Hoeve, J. N., Chan, K., Kiland, J. A., Keuler, N. S., August, B. K., Sebo, D., Field, A. S., & Duncan, I. D. (2019). Evoked potentials as a biomarker of remyelination. *Proceedings of the National Academy of Sciences of the United States of America*, *116*(52), 27074–27083. https://doi.org/10.1073/pnas.1906358116

Hemmer, B., Archelos, J. J., & Hartung, H.-P. (2002). New concepts in the immunopathogenesis of multiple sclerosis. *Nature Reviews Neuroscience*, *3*(4), 291–301. https://doi.org/10.1038/nrn784

Heuvel, M. P. van den, & Sporns, O. (2013). Network hubs in the human brain. *Trends in Cognitive Sciences*, *17*(12), 683–696. https://doi.org/10.1016/j.tics.2013.09.012

Horbruegger, M., Loewe, K., Kaufmann, J., Wagner, M., Schippling, S., Pawlitzki, M., & Schoenfeld, M. A. (2019). Anatomically constrained tractography facilitates biologically plausible fiber reconstruction of the optic radiation in multiple sclerosis. *NeuroImage: Clinical*, *22*, 101740. https://doi.org/10.1016/j.nicl.2019.101740

Hubbard, E. A., Wetter, N. C., Sutton, B. P., Pilutti, L. A., & Motl, R. W. (2016). Diffusion tensor imaging of the corticospinal tract and walking performance in multiple sclerosis. *Journal of the Neurological Sciences*, *363*, 225–231. https://doi.org/10.1016/j.jns.2016.02.044

Ibrahim, M. A., Hazhirkarzar, B., & Dublin, A. B. (2023). Gadolinium Magnetic Resonance Imaging. In *StatPearls*. StatPearls Publishing. http://www.ncbi.nlm.nih.gov/books/NBK482487/

Inglese, M., & Bester, M. (2010). Diffusion imaging in multiple sclerosis: Research and clinical implications. *NMR in Biomedicine*, *23*(7), 865–872. https://doi.org/10.1002/nbm.1515

Jandric, D., Parker, G. J. M., Haroon, H., Tomassini, V., Muhlert, N., & Lipp, I. (2022). A tractometry principal component analysis of white matter tract network structure and relationships with cognitive function in relapsing-remitting multiple sclerosis. *NeuroImage. Clinical*, *34*, 102995. https://doi.org/10.1016/j.nicl.2022.102995

Jenkinson, M., Bannister, P., Brady, M., & Smith, S. (2002). Improved optimization for the robust and accurate linear registration and motion correction of brain images. *NeuroImage*, *17*(2), 825–841.

Jeurissen, B., Descoteaux, M., Mori, S., & Leemans, A. (2019). Diffusion MRI fiber tractography of the brain. *NMR in Biomedicine*, *32*(4), e3785. https://doi.org/10.1002/nbm.3785

Jeurissen, B., Leemans, A., Tournier, J.-D., Jones, D. K., & Sijbers, J. (2013). Investigating the prevalence of complex fiber configurations in white matter tissue with diffusion magnetic resonance imaging. *Human Brain Mapping*, *34*(11), 2747–2766. https://doi.org/10.1002/hbm.22099

Jeurissen, B., Tournier, J.-D., Dhollander, T., Connelly, A., & Sijbers, J. (2014). Multi-tissue constrained spherical deconvolution for improved analysis of multi-shell diffusion MRI data. *NeuroImage*, *103*, 411–426. https://doi.org/10.1016/j.neuroimage.2014.07.061

Jones, S. J., & Brusa, A. (2003). Neurophysiological evidence for long-term repair of MS lesions: Implications for axon protection. *Journal of the Neurological Sciences*, *206*(2), 193–198. https://doi.org/10.1016/s0022-510x(02)00428-8

Jörgens, D., Descoteaux, M., & Moreno, R. (2021). Challenges for Tractogram Filtering. In E. Özarslan, T. Schultz, E. Zhang, & A. Fuster (Eds.), *Anisotropy Across Fields and Scales* (pp. 149–168). Springer International Publishing. https://doi.org/10.1007/978-3-030-56215-1_7

Kalkers, N. F., de Groot, V., Lazeron, R. H., Killestein, J., Adèr, H. J., Barkhof, F., Lankhorst, G. J., & Polman, C. H. (2000). MS functional composite: Relation to disease phenotype and disability strata. *Neurology*, *54*(6), 1233–1239. https://doi.org/10.1212/wnl.54.6.1233

Kalron, A., Achiron, A., & Dvir, Z. (2011). Muscular and Gait Abnormalities in Persons With Early Onset Multiple Sclerosis. *Journal of Neurologic Physical Therapy*, *35*(4), 164. https://doi.org/10.1097/NPT.0b013e31823801f4

Kalron, A., Dvir, Z., & Achiron, A. (2010). Walking while talking—Difficulties incurred during the initial stages of multiple sclerosis disease process. *Gait & Posture*, *32*(3), 332–335. https://doi.org/10.1016/j.gaitpost.2010.06.002

Kamagata, K., Zalesky, A., Yokoyama, K., Andica, C., Hagiwara, A., Shimoji, K., Kumamaru, K. K., Takemura, M. Y., Hoshino, Y., Kamiya, K., Hori, M., Pantelis, C., Hattori, N., & Aoki, S. (2019). MR g-ratio-weighted connectome analysis in patients with multiple sclerosis. *Scientific Reports*, *9*(1), 13522. https://doi.org/10.1038/s41598-019-50025-2

Kanakaraj, P., Cai, L. Y., Rheault, F., Yehe, F.-C., Rogers, B. P., Schilling, K. G., & Landman, B. A. (2023). Mapping the impact of nonlinear gradient fields with noise on diffusion MRI. *Magnetic Resonance Imaging*, *98*, 124–131. https://doi.org/10.1016/j.mri.2023.01.004

Kappos, L., Bar-Or, A., Cree, B. A. C., Fox, R. J., Giovannoni, G., Gold, R., Vermersch, P., Arnold, D. L., Arnould, S., Scherz, T., Wolf, C., Wallström, E., Dahlke, F., Achiron, A., Achtnichts, L., Agan, K., Akman-Demir, G., Allen, A. B., Antel, J. P., … Ziemssen, T. (2018). Siponimod versus placebo in secondary progressive multiple sclerosis (EXPAND): A double-blind, randomised, phase 3 study. *The Lancet*, *391*(10127), 1263–1273. https://doi.org/10.1016/S0140-6736(18)30475-6

Kappos, L., Wolinsky, J. S., Giovannoni, G., Arnold, D. L., Wang, Q., Bernasconi, C., Model, F., Koendgen, H., Manfrini, M., Belachew, S., & Hauser, S. L. (2020). Contribution of Relapse-Independent Progression vs Relapse-Associated Worsening to Overall Confirmed Disability Accumulation in Typical Relapsing Multiple Sclerosis in a Pooled Analysis of 2 Randomized Clinical Trials. *JAMA Neurology*, *77*(9), 1132–1140. https://doi.org/10.1001/jamaneurol.2020.1568

Kappus, N., Weinstock-Guttman, B., Hagemeier, J., Kennedy, C., Melia, R., Carl, E., Ramasamy, D. P., Cherneva, M., Durfee, J., Bergsland, N., Dwyer, M. G., Kolb, C., Hojnacki, D., Ramanathan, M., & Zivadinov, R. (2016). Cardiovascular risk factors are associated with increased lesion burden

and brain atrophy in multiple sclerosis. *Journal of Neurology, Neurosurgery & Psychiatry*, *87*(2), 181–187. https://doi.org/10.1136/jnnp-2014-310051

Karavasilis, E., Christidi, F., Velonakis, G., Tzanetakos, D., Zalonis, I., Potagas, C., Andreadou, E., Efstathopoulos, E., Kilidireas, C., Kelekis, N., & Evdokimidis, I. (2019). Hippocampal structural and functional integrity in multiple sclerosis patients with or without memory impairment: A multimodal neuroimaging study. *Brain Imaging and Behavior*, *13*(4), 1049–1059. https://doi.org/10.1007/s11682-018-9924-y

Kato, S., Hagiwara, A., Yokoyama, K., Andica, C., Tomizawa, Y., Hoshino, Y., Uchida, W., Nishimura, Y., Fujita, S., Kamagata, K., Hori, M., Hattori, N., Abe, O., & Aoki, S. (2022). Microstructural white matter abnormalities in multiple sclerosis and neuromyelitis optica spectrum disorders: Evaluation by advanced diffusion imaging. *Journal of the Neurological Sciences*, 120205. https://doi.org/10.1016/j.jns.2022.120205

Katz Sand, I., Krieger, S., Farrell, C., & Miller, A. E. (2014). Diagnostic uncertainty during the transition to secondary progressive multiple sclerosis. *Multiple Sclerosis (Houndmills, Basingstoke, England)*, *20*(12), 1654–1657. https://doi.org/10.1177/1352458514521517

Keegan, B. M., Kaufmann, T. J., Weinshenker, B. G., Kantarci, O. H., Schmalstieg, W. F., Soldan, M. M. P., & Flanagan, E. P. (2018). Progressive motor impairment from a critically located lesion in highly restricted CNS-demyelinating disease. *Multiple Sclerosis Journal*, 8.

Kerbrat, A., Gros, C., Badji, A., Bannier, E., Galassi, F., Combès, B., Chouteau, R., Labauge, P., Ayrignac, X., Carra-Dalliere, C., Maranzano, J., Granberg, T., Ouellette, R., Stawiarz, L., Hillert, J., Talbott, J., Tachibana, Y., Hori, M., Kamiya, K., … Cohen-Adad, J. (2020). Multiple sclerosis lesions in motor tracts from brain to cervical cord: Spatial distribution and correlation with disability. *Brain*, *143*(7), 2089–2105. https://doi.org/10.1093/brain/awaa162

Kezele, I., Arnold, D., & Collins, D. (2008). Atrophy in white matter fiber tracts in multiple sclerosis is not dependent on tract length or local white matter lesions. *Multiple Sclerosis Journal*, *14*(6), 779–785. https://doi.org/10.1177/1352458507088106

Kipp, M., Wagenknecht, N., Beyer, C., Samer, S., Wuerfel, J., & Nikoubashman, O. (2015). Thalamus pathology in multiple sclerosis: From biology to clinical application. *Cellular and Molecular Life Sciences*, *72*(6), 1127–1147. https://doi.org/10.1007/s00018-014-1787-9

Kiselev, I., Bashinskaya, V., Baulina, N., Kozin, M., Popova, E., Boyko, A., Favorova, O., & Kulakova, O. (2019). Genetic differences between primary progressive and relapsing-remitting multiple sclerosis: The impact of immune-related genes variability. *Multiple Sclerosis and Related Disorders*, *29*, 130–136. https://doi.org/10.1016/j.msard.2019.01.033

Klein, A., Andersson, J., Ardekani, B. A., Ashburner, J., Avants, B., Chiang, M.-C., Christensen, G. E., Collins, D. L., Gee, J., Hellier, P., Song, J. H., Jenkinson, M., Lepage, C., Rueckert, D., Thompson, P., Vercauteren, T., Woods, R. P., Mann, J. J., & Parsey, R. V. (2009). Evaluation of 14 nonlinear deformation algorithms applied to human brain MRI registration. *NeuroImage*, *46*(3), 786–802. https://doi.org/10.1016/j.neuroimage.2008.12.037

Klistorner, A., Chai, Y., Leocani, L., Albrecht, P., Aktas, O., Butzkueven, H., Ziemssen, T., Ziemssen, F., Frederiksen, J., Xu, L., Cadavid, D., & RENEW MF-VEP Investigators. (2018). Assessment of Opicinumab in Acute Optic Neuritis Using Multifocal Visual Evoked Potential. *CNS Drugs*, *32*(12), 1159–1171. https://doi.org/10.1007/s40263-018-0575-8

Klistorner, A., Graham, E. C., Yiannikas, C., Barnett, M., Parratt, J., Garrick, R., Wang, C., You, Y., & Graham, S. L. (2017). Progression of retinal ganglion cell loss in multiple sclerosis is associated with new lesions in the optic radiations. *European Journal of Neurology*, *24*(11), 1392–1398. https://doi.org/10.1111/ene.13404

Klistorner, A., & Graham, S. L. (2021). Role of Multifocal Visually Evoked Potential as a Biomarker of Demyelination, Spontaneous Remyelination, and Myelin Repair in Multiple Sclerosis. *Frontiers in Neuroscience*, *15*, 725187. https://doi.org/10.3389/fnins.2021.725187

Klistorner, A., Vootakuru, N., Wang, C., Yiannikas, C., Graham, S. L., Parratt, J., Garrick, R., Levin, N., Masters, L., Lagopoulos, J., & Barnett, M. H. (2015). Decoding Diffusivity in Multiple Sclerosis: Analysis of Optic Radiation Lesional and Non-Lesional White Matter. *PLOS ONE*, *10*(3), e0122114. https://doi.org/10.1371/journal.pone.0122114

Klistorner, A., Wang, C., Fofanova, V., Barnett, M. H., Yiannikas, C., Parratt, J., You, Y., & Graham, S. L. (2016). Diffusivity in multiple sclerosis lesions: At the cutting edge? *NeuroImage: Clinical*, *12*, 219–226. https://doi.org/10.1016/j.nicl.2016.07.003

Klistorner, A., Wang, C., Yiannikas, C., Parratt, J., Dwyer, M., Barton, J., Graham, S. L., You, Y., Liu, S., & Barnett, M. H. (2018). Evidence of progressive tissue loss in the core of chronic MS lesions: A longitudinal DTI study. *NeuroImage: Clinical*, *17*, 1028–1035. https://doi.org/10.1016/j.nicl.2017.12.010

Kocsis, K., Szabó, N., Tóth, E., Király, A., Faragó, P., Kincses, B., Veréb, D., Bozsik, B., Boross, K., Katona, M., Bodnár, P., László, N. G., Vécsei, L., Klivényi, P., Bencsik, K., & Kincses, Z. T. (2021). Two Classes of T1 Hypointense Lesions in Multiple Sclerosis With Different Clinical Relevance. *Frontiers in Neurology*, *12*, 619135. https://doi.org/10.3389/fneur.2021.619135

Krieger, S. C., Cook, K., De Nino, S., & Fletcher, M. (2016). The topographical model of multiple sclerosis: A dynamic visualization of disease course. *Neurology - Neuroimmunology Neuroinflammation*, *3*(5), e279. https://doi.org/10.1212/NXI.0000000000000279

Krieger, S. C., & Sumowski, J. (2018). New Insights into Multiple Sclerosis Clinical Course from the Topographical Model and Functional Reserve. *Neurologic Clinics*, *36*(1), 13–25. https://doi.org/10.1016/j.ncl.2017.08.003

Kuceyeski, A., Maruta, J., Niogi, S. N., Ghajar, J., & Raj, A. (2011). The generation and validation of white matter connectivity importance maps. *NeuroImage*, *58*(1), 109–121. https://doi.org/10.1016/j.neuroimage.2011.05.087

Kuceyeski, A., Maruta, J., Relkin, N., & Raj, A. (2013). The Network Modification (NeMo) Tool: Elucidating the Effect of White Matter Integrity Changes on Cortical and Subcortical Structural Connectivity. *Brain Connectivity*, *3*(5), 451–463. https://doi.org/10.1089/brain.2013.0147

Kuceyeski, A., Monohan, E., Morris, E., Fujimoto, K., Vargas, W., & Gauthier, S. A. (2018). Baseline biomarkers of connectome disruption and atrophy predict future processing speed in early multiple sclerosis. *NeuroImage: Clinical*, *19*, 417–424. https://doi.org/10.1016/j.nicl.2018.05.003

Kumar, D. R., Aslinia, F., Yale, S. H., & Mazza, J. J. (2011). Jean-Martin Charcot: The Father of Neurology. *Clinical Medicine & Research*, *9*(1), 46–49. https://doi.org/10.3121/cmr.2009.883

Kurtzke, J. F. (1983). Rating neurologic impairment in multiple sclerosis: An expanded disability status scale (EDSS). *Neurology*, *33*(11), 1444–1444. https://doi.org/10.1212/WNL.33.11.1444

Lahti, K., Parkkola, R., Jääsaari, P., Haataja, L., Saunavaara, V., & PIPARI Study Group. (2021). The impact of susceptibility correction on diffusion metrics in adolescents. *Pediatric Radiology*, *51*(8), 1471–1480. https://doi.org/10.1007/s00247-021-05000-3

Lapucci, C., Romano, N., Schiavi, S., Saitta, L., Uccelli, A., Boffa, G., Pardini, M., Signori, A., Castellan, L., Inglese, M., & Roccatagliata, L. (2020). Degree of microstructural changes within T1-SE versus T1-GE hypointense lesions in multiple sclerosis: Relevance for the definition of "black holes". *European Radiology*. https://doi.org/10.1007/s00330-020-06761-5

Lapucci, C., Schiavi, S., Signori, A., Sbragia, E., Bommarito, G., Cellerino, M., Uccelli, A., Inglese, M., Roccatagliata, L., & Pardini, M. (2022). The role of disconnection in explaining disability in multiple sclerosis. *European Radiology Experimental*, *6*(1), 23. https://doi.org/10.1186/s41747-022-00277-x

Lashkari, A., Davoodi-Bojd, E., Fahmy, L., Li, L., Nejad-Davarani, S. P., Chopp, M., Jiang, Q., & Cerghet, M. (2021). Impairments of white matter tracts and connectivity alterations in five cognitive networks of patients with multiple sclerosis. *Clinical Neurology and Neurosurgery*, *201*, 106424. https://doi.org/10.1016/j.clineuro.2020.106424

Lassmann, H., Brück, W., & Lucchinetti, C. F. (2007). The Immunopathology of Multiple Sclerosis: An Overview. *Brain Pathology*, *17*(2), 210–218. https://doi.org/10.1111/j.1750-3639.2007.00064.x

Lassmann, H., van Horssen, J., & Mahad, D. (2012). Progressive multiple sclerosis: Pathology and pathogenesis. *Nature Reviews Neurology*, *8*(11), 647–656. https://doi.org/10.1038/nrneurol.2012.168

Le Bihan, D., & Johansen-Berg, H. (2012). Diffusion MRI at 25: Exploring brain tissue structure and function. *NeuroImage*, *61*(2), 324–341. https://doi.org/10.1016/j.neuroimage.2011.11.006

Le Bihan, D., Poupon, C., Amadon, A., & Lethimonnier, F. (2006). Artifacts and pitfalls in diffusion MRI. *Journal of Magnetic Resonance Imaging*, *24*(3), 478–488. https://doi.org/10.1002/jmri.20683

Lee, Y., Morrison, B. M., Li, Y., Lengacher, S., Farah, M. H., Hoffman, P. N., Liu, Y., Tsingalia, A., Jin, L., Zhang, P.-W., Pellerin, L., Magistretti, P. J., & Rothstein, J. D. (2012). Oligodendroglia metabolically support axons and contribute to neurodegeneration. *Nature*, *487*(7408), 443–448. https://doi.org/10.1038/nature11314

Levy, S., Sandry, J., Beck, E. S., Brandstadter, R., Katz Sand, I., & Sumowski, J. F. (2022). Pattern of thalamic nuclei atrophy in early relapse-onset multiple sclerosis. *Multiple Sclerosis and Related Disorders*, *67*, 104083. https://doi.org/10.1016/j.msard.2022.104083

Li, D. K. B., Held, U., Petkau, J., Daumer, M., Barkhof, F., Fazekas, F., Frank, J. A., Kappos, L., Miller, D. H., Simon, J. H., Wolinsky, J. S., Filippi, M., & Sylvia Lawry Centre for MS Research. (2006). MRI T2 lesion burden in multiple sclerosis: A plateauing relationship with clinical disability. *Neurology*, *66*(9), 1384–1389. https://doi.org/10.1212/01.wnl.0000210506.00078.5c

Li, Y., Wang, J., Yang, T., Zhang, P., Ai, K., Li, M., Wang, R., Ren, X., Xiong, D., Liu, G., Han, N., Gan, T., & Zhang, J. (2022). Alterations of Thalamic Nuclei Volumes and the Intrinsic Thalamic Structural

Network in Patients with Multiple Sclerosis-Related Fatigue. *Brain Sciences*, *12*(11), 1538. https://doi.org/10.3390/brainsci12111538

Lin, X., Tench, C. R., Morgan, P. S., & Constantinescu, C. S. (2008). Use of combined conventional and quantitative MRI to quantify pathology related to cognitive impairment in multiple sclerosis. *Journal of Neurology, Neurosurgery & Psychiatry*, *79*(4), 437–441. https://doi.org/10.1136/jnnp.2006.112177

Lipp, I., Parker, G. D., Tallantyre, E. C., Goodall, A., Grama, S., Patitucci, E., Heveron, P., Tomassini, V., & Jones, D. K. (2020). Tractography in the presence of multiple sclerosis lesions. *NeuroImage*, *209*, 116471. https://doi.org/10.1016/j.neuroimage.2019.116471

Liu, Y., Duan, Y., Dong, H., Barkhof, F., Li, K., & Shu, N. (2018). Disrupted Module Efficiency of Structural and Functional Brain Connectomes in Clinically Isolated Syndrome and Multiple Sclerosis. *Frontiers in Human Neuroscience*, *12*, 138. https://doi.org/10.3389/fnhum.2018.00138

Llufriu, S., Martinez-Heras, E., Solana, E., Sola-Valls, N., Sepulveda, M., Blanco, Y., Martinez-Lapiscina, E. H., Andorra, M., Villoslada, P., Prats-Galino, A., & Saiz, A. (2017). Structural networks involved in attention and executive functions in multiple sclerosis. *NeuroImage: Clinical*, *13*, 288–296. https://doi.org/10.1016/j.nicl.2016.11.026

Llufriu, S., Rocca, M. A., Pagani, E., Riccitelli, G. C., Solana, E., Colombo, B., Rodegher, M., Falini, A., Comi, G., & Filippi, M. (2019). Hippocampal-related memory network in multiple sclerosis: A structural connectivity analysis. *Multiple Sclerosis Journal*, *25*(6), 801–810. https://doi.org/10.1177/1352458518771838

Lope-Piedrafita, S. (2018). Diffusion Tensor Imaging (DTI). *Methods in Molecular Biology (Clifton, N.J.)*, *1718*, 103–116. https://doi.org/10.1007/978-1-4939-7531-0_7

Lopez-Soley, E., Solana, E., Martínez-Heras, E., Andorra, M., Radua, J., Prats-Uribe, A., Montejo, C., Sola-Valls, N., Sepulveda, M., Pulido-Valdeolivas, I., Blanco, Y., Martinez-Lapiscina, E. H., Saiz, A., & Llufriu, S. (2020). Impact of Cognitive Reserve and Structural Connectivity on Cognitive Performance in Multiple Sclerosis. *Frontiers in Neurology*, *11*, 581700. https://doi.org/10.3389/fneur.2020.581700

Lorscheider, J., Buzzard, K., Jokubaitis, V., Spelman, T., Havrdova, E., Horakova, D., Trojano, M., Izquierdo, G., Girard, M., Duquette, P., Prat, A., Lugaresi, A., Grand'Maison, F., Grammond, P., Hupperts, R., Alroughani, R., Sola, P., Boz, C., Pucci, E., … on behalf of the MSBase Study Group. (2016). Defining secondary progressive multiple sclerosis. *Brain*, *139*(9), 2395–2405. https://doi.org/10.1093/brain/aww173

Lovato, L., Willis, S. N., Rodig, S. J., Caron, T., Almendinger, S. E., Howell, O. W., Reynolds, R., O'Connor, K. C., & Hafler, D. A. (2011). Related B cell clones populate the meninges and parenchyma of patients with multiple sclerosis. *Brain*, *134*(2), 534–541. https://doi.org/10.1093/brain/awq350

Lublin, F. D., Reingold, S. C., Cohen, J. A., Cutter, G. R., Sorensen, P. S., Thompson, A. J., Wolinsky, J. S., Balcer, L. J., Banwell, B., Barkhof, F., Bebo, B., Calabresi, P. A., Clanet, M., Comi, G., Fox, R. J., Freedman, M. S., Goodman, A. D., Inglese, M., Kappos, L., … Polman, C. H. (2014). Defining the clinical course of multiple sclerosis: The 2013 revisions. *Neurology*, *83*(3), 278–286. https://doi.org/10.1212/WNL.0000000000000560

Lv, J., Zeng, R., Ho, M. P., D'Souza, A., & Calamante, F. (2022). Building a tissue-unbiased brain template of fiber orientation distribution and tractography with multimodal registration. *Magnetic Resonance in Medicine*, mrm.29496. https://doi.org/10.1002/mrm.29496

Ma, Y., Zhang, C., Cabezas, M., Song, Y., Tang, Z., Liu, D., Cai, W., Barnett, M., & Wang, C. (2022). Multiple Sclerosis Lesion Analysis in Brain Magnetic Resonance Images: Techniques and Clinical Applications. *IEEE Journal of Biomedical and Health Informatics*, *26*(6), 2680–2692. https://doi.org/10.1109/JBHI.2022.3151741

Magliozzi, R., Fadda, G., Brown, R. A., Bar-Or, A., Howell, O. W., Hametner, S., Marastoni, D., Poli, A., Nicholas, R., Calabrese, M., Monaco, S., & Reynolds, R. (2022). 'Ependymal-in' Gradient of Thalamic Damage in Progressive Multiple Sclerosis. *Annals of Neurology*, *92*(4), 670–685. https://doi.org/10.1002/ana.26448

Magliozzi, R., Howell, O. W., Reeves, C., Roncaroli, F., Nicholas, R., Serafini, B., Aloisi, F., & Reynolds, R. (2010). A Gradient of neuronal loss and meningeal inflammation in multiple sclerosis. *Annals of Neurology*, *68*(4), 477–493. https://doi.org/10.1002/ana.22230

Mahajan, K. R., & Ontaneda, D. (2017). The Role of Advanced Magnetic Resonance Imaging Techniques in Multiple Sclerosis Clinical Trials. *Neurotherapeutics*, *14*(4), 905–923. https://doi.org/10.1007/s13311-017-0561-8

Martinelli, V., Dalla Costa, G., Colombo, B., Dalla Libera, D., Rubinacci, A., Filippi, M., Furlan, R., & Comi, G. (2014). Vitamin D levels and risk of multiple sclerosis in patients with clinically isolated syndromes. *Multiple Sclerosis Journal*, *20*(2), 147–155. https://doi.org/10.1177/1352458513494959

Martínez-Heras, E., E, S., F, P., M, A., A, S., E, L.-S., C, M., I, P.-V., S, A.-A., N, S.-V., M, S., Y, B., A, S., J, R., & S, L. (2020). Characterization of multiple sclerosis lesions with distinct clinical correlates through quantitative diffusion MRI. *NeuroImage. Clinical*, *28*. https://doi.org/10.1016/j.nicl.2020.102411

Marzi, C., d'Ambrosio, A., Diciotti, S., Bisecco, A., Altieri, M., Filippi, M., Rocca, M. A., Storelli, L., Pantano, P., Tommasin, S., Cortese, R., De Stefano, N., Tedeschi, G., Gallo, A., & INNI Network. (2023). Prediction of the information processing speed performance in multiple sclerosis using a machine learning approach in a large multicenter magnetic resonance imaging data set. *Human Brain Mapping*, *44*(1), 186–202. https://doi.org/10.1002/hbm.26106

Marzullo, A., Kocevar, G., Stamile, C., Durand-Dubief, F., Terracina, G., Calimeri, F., & Sappey-Marinier, D. (2019). Classification of Multiple Sclerosis Clinical Profiles via Graph Convolutional Neural Networks. *Frontiers in Neuroscience*, *13*, 594. https://doi.org/10.3389/fnins.2019.00594

Mattos, D. J. S., Rutlin, J., Hong, X., Zinn, K., Shimony, J. S., & Carter, A. R. (2023). The Role of Extra-motor Networks in Upper Limb Motor Performance Post-stroke. *Neuroscience*, *514*, 1–13. https://doi.org/10.1016/j.neuroscience.2023.01.033

McDonald, W. I., Compston, A., Edan, G., Goodkin, D., Hartung, H. P., Lublin, F. D., McFarland, H. F., Paty, D. W., Polman, C. H., Reingold, S. C., Sandberg-Wollheim, M., Sibley, W., Thompson, A., van den Noort, S., Weinshenker, B. Y., & Wolinsky, J. S. (2001). Recommended diagnostic criteria for multiple sclerosis: Guidelines from the International Panel on the diagnosis of multiple sclerosis. *Annals of Neurology*, *50*(1), 121–127. https://doi.org/10.1002/ana.1032

Meijer, K. A., Steenwijk, M. D., Douw, L., Schoonheim, M. M., & Geurts, J. J. G. (2020). Long-range connections are more severely damaged and relevant for cognition in multiple sclerosis. *Brain*, *143*(1), 150–160. https://doi.org/10.1093/brain/awz355

Meyer-Moock, S., Feng, Y.-S., Maeurer, M., Dippel, F.-W., & Kohlmann, T. (2014). Systematic literature review and validity evaluation of the Expanded Disability Status Scale (EDSS) and the Multiple Sclerosis Functional Composite (MSFC) in patients with multiple sclerosis. *BMC Neurology*, *14*, 58. https://doi.org/10.1186/1471-2377-14-58

Miclea, A., Bagnoud, M., Chan, A., & Hoepner, R. (2020). A Brief Review of the Effects of Vitamin D on Multiple Sclerosis. *Frontiers in Immunology*, *11*, 781. https://doi.org/10.3389/fimmu.2020.00781

Mistri, D., Cacciaguerra, L., Storelli, L., Meani, A., Cordani, C., Rocca, M. A., & Filippi, M. (2022). The association between cognition and motor performance is beyond structural damage in relapsing-remitting multiple sclerosis. *Journal of Neurology*, *269*(8), 4213–4221. https://doi.org/10.1007/s00415-022-11044-8

Moccia, M., de Stefano, N., & Barkhof, F. (2017). Imaging outcome measures for progressive multiple sclerosis trials. *Multiple Sclerosis Journal*, *23*(12), 1614–1626.

Montalban, X., Hauser, S. L., Kappos, L., Arnold, D. L., Bar-Or, A., Comi, G., de Seze, J., Giovannoni, G., Hartung, H.-P., Hemmer, B., Lublin, F., Rammohan, K. W., Selmaj, K., Traboulsee, A., Sauter, A., Masterman, D., Fontoura, P., Belachew, S., Garren, H., … Wolinsky, J. S. (2017). Ocrelizumab versus Placebo in Primary Progressive Multiple Sclerosis. *New England Journal of Medicine*, *376*(3), 209–220. https://doi.org/10.1056/NEJMoa1606468

Mori, S., Crain, B. J., & Zijl, P. C. M. V. (1998). 3D brain fiber reconstruction from diffusion MRI. *NeuroImage*, *7*(4 PART II). https://doi.org/10.1016/s1053-8119(18)31543-x

Motl, R. W., Cohen, J. A., Benedict, R., Phillips, G., LaRocca, N., Hudson, L. D., Rudick, R., & Multiple Sclerosis Outcome Assessments Consortium. (2017). Validity of the timed 25-foot walk as an ambulatory performance outcome measure for multiple sclerosis. *Multiple Sclerosis (Houndmills, Basingstoke, England)*, *23*(5), 704–710. https://doi.org/10.1177/1352458517690823

MSVirtual 2020 – Poster Abstracts. (2020). *Multiple Sclerosis Journal*, *26*(3_suppl), 118–659. https://doi.org/10.1177/1352458520974937

Naghavi, S., Ashtari, F., Adibi, I., Shaygannejad, V., Ramezani, N., Pourmohammadi, A., Davanian, F., Karimi, Z., Khaligh-Razavi, S.-M., & Sanayei, M. (2023). Effect of deep gray matter atrophy on information processing speed in early relapsing-remitting multiple sclerosis. *Multiple Sclerosis and Related Disorders*, *71*, 104560. https://doi.org/10.1016/j.msard.2023.104560

Newman, M. E. J., & Girvan, M. (2004). Finding and evaluating community structure in networks. *Physical Review E*, *69*(2), 026113. https://doi.org/10.1103/PhysRevE.69.026113

Nigro, S., Passamonti, L., Riccelli, R., Toschi, N., Rocca, F., Valentino, P., Nisticò, R., Fera, F., & Quattrone, A. (2015). Structural 'connectomic' alterations in the limbic system of multiple sclerosis patients with major depression. *Multiple Sclerosis (Houndmills, Basingstoke, England)*, *21*(8), 1003–1012. https://doi.org/10.1177/1352458514558474

Nourbakhsh, B., Azevedo, C., Maghzi, A.-H., Spain, R., Pelletier, D., & Waubant, E. (2016). Subcortical grey matter volumes predict subsequent walking function in early multiple sclerosis. *Journal of the Neurological Sciences*, *366*, 229–233. https://doi.org/10.1016/j.jns.2016.04.054

Ochoa-Repáraz, J., Kirby, T. O., & Kasper, L. H. (2018). The Gut Microbiome and Multiple Sclerosis. *Cold Spring Harbor Perspectives in Medicine*, *8*(6), a029017. https://doi.org/10.1101/cshperspect.a029017

Onoda, K., & Yamaguchi, S. (2013). Small-worldness and modularity of the resting-state functional brain network decrease with aging. *Neuroscience Letters*, *556*, 104–108. https://doi.org/10.1016/j.neulet.2013.10.023

Ontaneda, D., Fox, R. J., & Chataway, J. (2015). Clinical trials in progressive multiple sclerosis: Lessons learned and future perspectives. *The Lancet. Neurology*, *14*(2), 208–223. https://doi.org/10.1016/S1474-4422(14)70264-9

Öztürk, G., Cengiz, N., Erdoğan, E., Him, A., Oğuz, E. K., Yenidünya, E., & Ayşit, N. (2013). Two distinct types of dying back axonal degeneration *in vitro*: Dying back degeneration. *Neuropathology and Applied Neurobiology*, *39*(4), 362–376. https://doi.org/10.1111/j.1365-2990.2012.01295.x

Pagani, E., Rocca, M. A., De Meo, E., Horsfield, M. A., Colombo, B., Rodegher, M., Comi, G., & Filippi, M. (2019). Structural connectivity in multiple sclerosis and modeling of disconnection. *Multiple Sclerosis Journal*, 135245851882075. https://doi.org/10.1177/1352458518820759

Pardini, M., Cutter, G., & Sormani, M. P. (2019). Multiple sclerosis: Clinical trial design 2019. *Current Opinion in Neurology*, *32*(3), 358–364. https://doi.org/10.1097/WCO.0000000000000697

Pardini, M., Yaldizli, Ö., Sethi, V., Muhlert, N., Liu, Z., Samson, R. S., Altmann, D. R., Ron, M. A., Wheeler-Kingshott, C. A. M., Miller, D. H., & Chard, D. T. (2015). Motor network efficiency and disability in multiple sclerosis. *Neurology*, *85*(13), 1115–1122. https://doi.org/10.1212/WNL.0000000000001970

Parmar, K., Fonov, V. S., Naegelin, Y., Amann, M., Wuerfel, J., Collins, D. L., Gaetano, L., Magon, S., Sprenger, T., Kappos, L., Granziera, C., & Tsagkas, C. (2022). Regional Cerebellar Volume Loss Predicts Future Disability in Multiple Sclerosis Patients. *Cerebellum (London, England)*, *21*(4), 632–646. https://doi.org/10.1007/s12311-021-01312-0

Passingham, R. E., Stephan, K. E., & Kötter, R. (2002). The anatomical basis of functional localization in the cortex. *Nature Reviews Neuroscience*, *3*(8), 606–616. https://doi.org/10.1038/nrn893

Patenaude, B., Smith, S. M., Kennedy, D. N., & Jenkinson, M. (2011). A Bayesian model of shape and appearance for subcortical brain segmentation. *NeuroImage*, *56*(3), 907–922. https://doi.org/10.1016/j.neuroimage.2011.02.046

Patsopoulos, N. A., Barcellos, L. F., Hintzen, R. Q., Schaefer, C., Van Duijn, C. M., Noble, J. A., Raj, T., IMSGC, ANZgene, Gourraud, P.-A., Stranger, B. E., Oksenberg, J., Olsson, T., Taylor, B. V., Sawcer, S., Hafler, D. A., Carrington, M., De Jager, P. L., & De Bakker, P. I. W. (2013). Fine-Mapping the Genetic Association of the Major Histocompatibility Complex in Multiple Sclerosis: HLA and Non-HLA Effects. *PLoS Genetics*, *9*(11), e1003926. https://doi.org/10.1371/journal.pgen.1003926

Paz Soldán, M. M., Novotna, M., Abou Zeid, N., Kale, N., Tutuncu, M., Crusan, D. J., Atkinson, E. J., Siva, A., Keegan, B. M., Pirko, I., Pittock, S. J., Lucchinetti, C. F., Weinshenker, B. G., Rodriguez, M., & Kantarci, O. H. (2015). Relapses and disability accumulation in progressive multiple sclerosis. *Neurology*, *84*(1), 81–88. https://doi.org/10.1212/WNL.0000000000001094

Peng, H., Orlichenko, A., Dawe, R. J., Agam, G., Zhang, S., & Arfanakis, K. (2009). Development of a Human Brain Diffusion Tensor Template. *NeuroImage*, *46*(4), 967. https://doi.org/10.1016/j.neuroimage.2009.03.046

Peterson, J. W., Bö, L., Mörk, S., Chang, A., & Trapp, B. D. (2001). Transected neurites, apoptotic neurons, and reduced inflammation in cortical multiple sclerosis lesions: Cortical Lesions in MS. *Annals of Neurology*, *50*(3), 389–400. https://doi.org/10.1002/ana.1123

Petzold, A., de Boer, J. F., Schippling, S., Vermersch, P., Kardon, R., Green, A., Calabresi, P. A., & Polman, C. (2010). Optical coherence tomography in multiple sclerosis: A systematic review and meta-analysis. *The Lancet Neurology*, *9*(9), 921–932. https://doi.org/10.1016/S1474-4422(10)70168-X

Pike, A. R., James, G. A., Drew, P. D., & Archer, R. L. (2022). Neuroimaging predictors of longitudinal disability and cognition outcomes in multiple sclerosis patients: A systematic review and meta-analysis. *Multiple Sclerosis and Related Disorders*, *57*, 103452. https://doi.org/10.1016/j.msard.2021.103452

Polman, C. H., Reingold, S. C., Banwell, B., Clanet, M., Cohen, J. A., Filippi, M., Fujihara, K., Havrdova, E., Hutchinson, M., Kappos, L., Lublin, F. D., Montalban, X., O'Connor, P., Sandberg-Wollheim, M., Thompson, A. J., Waubant, E., Weinshenker, B., & Wolinsky, J. S. (2011). Diagnostic criteria for multiple sclerosis: 2010 Revisions to the McDonald criteria. *Annals of Neurology*, *69*(2), 292–302. https://doi.org/10.1002/ana.22366

Pontillo, G., Petracca, M., Monti, S., Quarantelli, M., Criscuolo, C., Lanzillo, R., Tedeschi, E., Elefante, A., Brescia Morra, V., Brunetti, A., Cocozza, S., & Palma, G. (2021). Unraveling Deep Gray Matter Atrophy and Iron and Myelin Changes in Multiple Sclerosis. *AJNR. American Journal of Neuroradiology*, *42*(7), 1223–1230. https://doi.org/10.3174/ajnr.A7093

Portaccio, E., Fonderico, M., Iaffaldano, P., Pastò, L., Razzolini, L., Bellinvia, A., De Luca, G., Ragonese, P., Patti, F., Brescia Morra, V., Cocco, E., Sola, P., Inglese, M., Lus, G., Pozzilli, C., Maimone, D., Lugaresi, A., Gazzola, P., Comi, G., … Italian Multiple Sclerosis Register Centers Group. (2022). Disease-Modifying Treatments and Time to Loss of Ambulatory Function in Patients With Primary Progressive Multiple Sclerosis. *JAMA Neurology*, *79*(9), 869–878. https://doi.org/10.1001/jamaneurol.2022.1929

Poser, C. M., Paty, D. W., Scheinberg, L., McDonald, W. I., Davis, F. A., Ebers, G. C., Johnson, K. P., Sibley, W. A., Silberberg, D. H., & Tourtellotte, W. W. (1983). New diagnostic criteria for multiple sclerosis: Guidelines for research protocols. *Annals of Neurology*, *13*(3), 227–231. https://doi.org/10.1002/ana.410130302

Powell, F., Tosun, D., Raj, A., & Alzheimer's Disease Neuroimaging Initiative. (2021). Network-constrained technique to characterize pathology progression rate in Alzheimer's disease. *Brain Communications*, *3*(3), fcab144. https://doi.org/10.1093/braincomms/fcab144

Power, J. D., Schlaggar, B. L., Lessov-Schlaggar, C. N., & Petersen, S. E. (2013). Evidence for Hubs in Human Functional Brain Networks. *Neuron*, *79*(4), 798–813. https://doi.org/10.1016/j.neuron.2013.07.035

Preziosa, P., Pagani, E., Meani, A., Moiola, L., Rodegher, M., Filippi, M., & Rocca, M. A. (2022). Slowly Expanding Lesions Predict 9-Year Multiple Sclerosis Disease Progression. *Neurology(R) Neuroimmunology & Neuroinflammation*, *9*(2), e1139. https://doi.org/10.1212/NXI.0000000000001139

Preziosa, P., Rocca, M. A., & Filippi, M. (2021). Central vein sign and iron rim in multiple sclerosis: Ready for clinical use? *Current Opinion in Neurology*, *34*(4), 505–513. https://doi.org/10.1097/WCO.0000000000000946

Prineas, J. W., Kwon, E. E., Cho, E. S., Sharer, L. R., Barnett, M. H., Oleszak, E. L., Hoffman, B., & Morgan, B. P. (2001). Immunopathology of secondary-progressive multiple sclerosis. *Annals of Neurology*, *50*(5), 646–657. https://doi.org/10.1002/ana.1255

Puthenparampil, M., Federle, L., Poggiali, D., Miante, S., Signori, A., Pilotto, E., Rinaldi, F., Perini, P., Sormani, M. P., Midena, E., & Gallo, P. (2017). Trans-synaptic degeneration in the optic pathway. A study in clinically isolated syndrome and early relapsing-remitting multiple sclerosis with or without optic neuritis. *PLOS ONE*, *12*(8), e0183957. https://doi.org/10.1371/journal.pone.0183957

Qin, W., Zhang, M., Piao, Y., Guo, D., Zhu, Z., Tian, X., Li, K., & Yu, C. (2012). Wallerian Degeneration in Central Nervous System: Dynamic Associations between Diffusion Indices and Their Underlying Pathology. *PLoS ONE*, *7*(7), e41441. https://doi.org/10.1371/journal.pone.0041441

Radetz, A., Koirala, N., Krämer, J., Johnen, A., Fleischer, V., Gonzalez-Escamilla, G., Cerina, M., Muthuraman, M., Meuth, S. G., & Groppa, S. (2020). Gray matter integrity predicts white matter network reorganization in multiple sclerosis. *Human Brain Mapping*, *41*(4), 917–927. https://doi.org/10.1002/hbm.24849

Radü, E. W., Bendfeldt, K., Mueller-Lenke, N., Magon, S., & Sprenger, T. (2013). Brain atrophy: An in-vivo measure of disease activity in multiple sclerosis. *Swiss Medical Weekly*, *143*, w13887. https://doi.org/10.4414/smw.2013.13887

Raffelt, D. A., Tournier, J.-D., Smith, R. E., Vaughan, D. N., Jackson, G., Ridgway, G. R., & Connelly, A. (2017). Investigating white matter fibre density and morphology using fixel-based analysis. *NeuroImage*, *144*, 58–73. https://doi.org/10.1016/j.neuroimage.2016.09.029

Raffelt, D., Dhollander, T., Tournier, J.-D., Tabbara, R., Smith, R. E., Pierre, E., & Connelly, A. (2017). Bias Field Correction and Intensity Normalisation for Quantitative Analysis of Apparent Fibre Density. *Proc. ISMRM*.

Raffelt, D., Tournier, J.-D., Fripp, J., Crozier, S., Connelly, A., & Salvado, O. (2011). Symmetric diffeomorphic registration of fibre orientation distributions. *NeuroImage*, *56*(3), 1171–1180. https://doi.org/10.1016/j.neuroimage.2011.02.014

Raffelt, D., Tournier, J.-D., Rose, S., Ridgway, G. R., Henderson, R., Crozier, S., Salvado, O., & Connelly, A. (2012). Apparent Fibre Density: A novel measure for the analysis of diffusion-weighted magnetic resonance images. *NeuroImage*, *59*(4), 3976–3994. https://doi.org/10.1016/j.neuroimage.2011.10.045

Rahmanzadeh, R., Galbusera, R., Lu, P., Bahn, E., Weigel, M., Barakovic, M., Franz, J., Nguyen, T. D., Spincemaille, P., Schiavi, S., Daducci, A., La Rosa, F., Absinta, M., Sati, P., Cuadra, M. B., Radue, E., Leppert, D., Kuhle, J., Kappos, L., … Granziera, C. (2022). A new advanced MRI biomarker

for remyelinated lesions in Multiple Sclerosis. *Annals of Neurology*, ana.26441. https://doi.org/10.1002/ana.26441

Rao, S. M., Losinski, G., Mourany, L., Schindler, D., Mamone, B., Reece, C., Kemeny, D., Narayanan, S., Miller, D. M., Bethoux, F., Bermel, R. A., Rudick, R., & Alberts, J. (2017). Processing speed test: Validation of a self-administered, iPad®-based tool for screening cognitive dysfunction in a clinic setting. *Multiple Sclerosis (Houndmills, Basingstoke, England)*, *23*(14), 1929–1937. https://doi.org/10.1177/1352458516688955

Ravano, V., Andelova, M., Fartaria, M. J., Mahdi, M. F. A.-W., Maréchal, B., Meuli, R., Uher, T., Krasensky, J., Vaneckova, M., Horakova, D., Kober, T., & Richiardi, J. (2021). Validating atlas-based lesion disconnectomics in multiple sclerosis: A retrospective multi-centric study. *NeuroImage: Clinical*, *32*, 102817. https://doi.org/10.1016/j.nicl.2021.102817

Reich, D. S., Lucchinetti, C. F., & Calabresi, P. A. (2018). Multiple Sclerosis. *New England Journal of Medicine*, *378*(2), 169–180. https://doi.org/10.1056/NEJMra1401483

Ribbons, K. A., McElduff, P., Boz, C., Trojano, M., Izquierdo, G., Duquette, P., Girard, M., Grand'Maison, F., Hupperts, R., Grammond, P., Oreja-Guevara, C., Petersen, T., Bergamaschi, R., Giuliani, G., Barnett, M., Pesch, V. van, Amato, M.-P., Iuliano, G., Fiol, M., … Lechner-Scott, J. (2015). Male Sex Is Independently Associated with Faster Disability Accumulation in Relapse-Onset MS but Not in Primary Progressive MS. *PLOS ONE*, *10*(6), e0122686. https://doi.org/10.1371/journal.pone.0122686

Rimkus, C. M., Schoonheim, M. M., Steenwijk, M. D., Vrenken, H., Eijlers, A. J., Killestein, J., Wattjes, M. P., Leite, C. C., Barkhof, F., & Tijms, B. M. (2018). Gray matter networks and cognitive impairment in multiple sclerosis. *Multiple Sclerosis Journal*, 1352458517751650.

Rise, H. H., Brune, S., Chien, C., Berge, T., Bos, S. D., Andorrà, M., Valdeolivas, I. P., Beyer, M. K., Sowa, P., Scheel, M., Brandt, A. U., Asseyer, S., Blennow, K., Pedersen, M. L., Zetterberg, H., de Schotten, M. T., Cellerino, M., Uccelli, A., Paul, F., … Høgestøl, E. A. (2022). Brain disconnectome mapping derived from white matter lesions and serum neurofilament light levels in multiple sclerosis: A longitudinal multicenter study. *NeuroImage: Clinical*, *35*, 103099. https://doi.org/10.1016/j.nicl.2022.103099

Roca, M., Torralva, T., Meli, F., Fiol, M., Calcagno, M., Carpintiero, S., De Pino, G., Ventrice, F., Martín, M., Vita, L., Manes, F., & Correale, J. (2008). Cognitive deficits in multiple sclerosis correlate with changes in fronto-subcortical tracts. *Multiple Sclerosis Journal*, *14*(3), 364–369. https://doi.org/10.1177/1352458507084270

Rocca, M. A., Mesaros, S., Preziosa, P., Pagani, E., Stosic-Opincal, T., Dujmovic-Basuroski, I., Drulovic, J., & Filippi, M. (2013). Wallerian and trans-synaptic degeneration contribute to optic radiation damage in multiple sclerosis: A diffusion tensor MRI study. *Multiple Sclerosis Journal*, *19*(12), 1610–1617. https://doi.org/10.1177/1352458513485146

Rocca, M. A., Valsasina, P., Meani, A., Gobbi, C., Zecca, C., Rovira, A., Sastre-Garriga, J., Kearney, H., Ciccarelli, O., Matthews, L., Palace, J., Gallo, A., Bisecco, A., Lukas, C., Bellenberg, B., Barkhof, F., Vrenken, H., Preziosa, P., Filippi, M., & on Behalf of the MAGNIMS Study Group. (2021). Association of Gray Matter Atrophy Patterns With Clinical Phenotype and Progression in Multiple Sclerosis. *Neurology*, *96*(11), e1561–e1573. https://doi.org/10.1212/WNL.0000000000011494

Rojas, J. I., Murphy, G., Sanchez, F., Patrucco, L., Fernandez, M. C., Miguez, J., Funes, J., Golimstok, A., & Cristiano, E. (2018). Thalamus volume change and cognitive impairment in early relapsing–remitting multiple sclerosis patients. *The Neuroradiology Journal*, *31*(4), 350–355. https://doi.org/10.1177/1971400918781977

Rolls, E. T. (2004). The functions of the orbitofrontal cortex. *Brain and Cognition*, *55*(1), 11–29. https://doi.org/10.1016/S0278-2626(03)00277-X

Rovaris, M., Gallo, A., Valsasina, P., Benedetti, B., Caputo, D., Ghezzi, A., Montanari, E., Sormani, M. P., Bertolotto, A., Mancardi, G., Bergamaschi, R., Martinelli, V., Comi, G., & Filippi, M. (2005). Short-term accrual of gray matter pathology in patients with progressive multiple sclerosis: An in vivo study using diffusion tensor MRI. *NeuroImage*, *24*(4), 1139–1146. https://doi.org/10.1016/j.neuroimage.2004.10.006

Rubinov, M., & Sporns, O. (2010). Complex network measures of brain connectivity: Uses and interpretations. *NeuroImage*, *52*(3), 1059–1069. https://doi.org/10.1016/j.neuroimage.2009.10.003

Sahraian, M. A., & Eshaghi, A. (2010). Role of MRI in diagnosis and treatment of multiple sclerosis. *Clinical Neurology and Neurosurgery*, *112*(7), 609–615. https://doi.org/10.1016/j.clineuro.2010.03.022

Salvalaggio, A., De Filippo De Grazia, M., Zorzi, M., Thiebaut de Schotten, M., & Corbetta, M. (2020). Post-stroke deficit prediction from lesion and indirect structural and functional disconnection. *Brain: A Journal of Neurology*, *143*(7), 2173–2188. https://doi.org/10.1093/brain/awaa156

Sandroff, B. M., Motl, R. W., Román, C. A. F., Wylie, G. R., DeLuca, J., Cutter, G. R., Benedict, R. H. B., Dwyer, M. G., & Zivadinov, R. (2022). Thalamic atrophy moderates associations among aerobic fitness, cognitive processing speed, and walking endurance in persons with multiple sclerosis. *Journal of Neurology*, *269*(10), 5531–5540. https://doi.org/10.1007/s00415-022-11205-9

Sarwar, T., Ramamohanarao, K., & Zalesky, A. (2019). Mapping connectomes with diffusion MRI: Deterministic or probabilistic tractography? *Magnetic Resonance in Medicine*, *81*(2), 1368–1384. https://doi.org/10.1002/mrm.27471

Savini, G., Pardini, M., Castellazzi, G., Lascialfari, A., Chard, D., D'Angelo, E., & Gandini Wheeler-Kingshott, C. A. M. (2019). Default Mode Network Structural Integrity and Cerebellar Connectivity Predict Information Processing Speed Deficit in Multiple Sclerosis. *Frontiers in Cellular Neuroscience*, *13*, 21. https://doi.org/10.3389/fncel.2019.00021

Sawcer, S., Franklin, R. J. M., & Ban, M. (2014). Multiple sclerosis genetics. *The Lancet Neurology*, *13*(7), 700–709. https://doi.org/10.1016/S1474-4422(14)70041-9

Sbardella, E., Tona, F., Petsas, N., & Pantano, P. (2013). DTI Measurements in Multiple Sclerosis: Evaluation of Brain Damage and Clinical Implications. *Multiple Sclerosis International*, *2013*, 1–11. https://doi.org/10.1155/2013/671730

Schiavi, S., Azzari, A., Mensi, A., Graziano, N., Daducci, A., Bicego, M., Inglese, M., & Petracca, M. (2022). Classification of multiple sclerosis patients based on structural disconnection: A robust feature selection approach. *Journal of Neuroimaging: Official Journal of the American Society of Neuroimaging*, *32*(4), 647–655. https://doi.org/10.1111/jon.12991

Schiavi, S., Petracca, M., Battocchio, M., El Mendili, M. M., Paduri, S., Fleysher, L., Inglese, M., & Daducci, A. (2020a). Sensory-motor network topology in multiple sclerosis: Structural connectivity analysis accounting for intrinsic density discrepancy. *Human Brain Mapping*, hbm.24989. https://doi.org/10.1002/hbm.24989

Schiavi, S., Petracca, M., Battocchio, M., El Mendili, M. M., Paduri, S., Fleysher, L., Inglese, M., & Daducci, A. (2020b). Sensory-motor network topology in multiple sclerosis: Structural connectivity analysis accounting for intrinsic density discrepancy. *Human Brain Mapping*, *41*(11), 2951–2963. https://doi.org/10.1002/hbm.24989

Schmidt, H., Williamson, D., & Ashley-Koch, A. (2007). HLA-DR15 Haplotype and Multiple Sclerosis: A HuGE Review. *American Journal of Epidemiology*, *165*(10), 1097–1109. https://doi.org/10.1093/aje/kwk118

Schoonheim, M. M., Broeders, T. A. A., & Geurts, J. J. G. (2022). The network collapse in multiple sclerosis: An overview of novel concepts to address disease dynamics. *NeuroImage: Clinical*, *35*, 103108. https://doi.org/10.1016/j.nicl.2022.103108

Schoonheim, M. M., Douw, L., Broeders, T. A., Eijlers, A. J., Meijer, K. A., & Geurts, J. J. (2021). The cerebellum and its network: Disrupted static and dynamic functional connectivity patterns and cognitive impairment in multiple sclerosis. *Multiple Sclerosis Journal*, 135245852199927. https://doi.org/10.1177/1352458521999274

Schoonheim, M. M., Pinter, D., Prouskas, S. E., Broeders, T. A., Pirpamer, L., Khalil, M., Ropele, S., Uitdehaag, B. M., Barkhof, F., Enzinger, C., & Geurts, J. J. (2021). Disability in multiple sclerosis is related to thalamic connectivity and cortical network atrophy. *Multiple Sclerosis (Houndmills, Basingstoke, England)*, 13524585211008744. https://doi.org/10.1177/13524585211008743

Schulz, R., Runge, C. G., Bönstrup, M., Cheng, B., Gerloff, C., Thomalla, G., & Hummel, F. C. (2019). Prefrontal-Premotor Pathways and Motor Output in Well-Recovered Stroke Patients. *Frontiers in Neurology*, *10*. https://www.frontiersin.org/articles/10.3389/fneur.2019.00105

Sechi, E., Keegan, B. M., Kaufmann, T. J., Kantarci, O. H., Weinshenker, B. G., & Flanagan, E. P. (2019). Unilateral motor progression in MS: Association with a critical corticospinal tract lesion. *Neurology*, *93*(7), e628–e634. https://doi.org/10.1212/WNL.0000000000007944

Sechi, E., Messina, S., Keegan, B. M., Buciuc, M., Pittock, S. J., Kantarci, O. H., Weinshenker, B. G., & Flanagan, E. P. (2020). Critical spinal cord lesions associate with secondary progressive motor impairment in long-standing MS: A population-based case-control study. *Multiple Sclerosis Journal*, 135245852092919. https://doi.org/10.1177/1352458520929192

Sedel, F., Bernard, D., Mock, D. M., & Tourbah, A. (2016). Targeting demyelination and virtual hypoxia with high-dose biotin as a treatment for progressive multiple sclerosis. *Neuropharmacology*, *110*, 644–653. https://doi.org/10.1016/j.neuropharm.2015.08.028

Sepulcre, J., Sastre-Garriga, J., Cercignani, M., Ingle, G. T., Miller, D. H., & Thompson, A. J. (2006). Regional Gray Matter Atrophy in Early Primary Progressive Multiple Sclerosis: A Voxel-Based Morphometry Study. *Archives of Neurology*, *63*(8), 1175. https://doi.org/10.1001/archneur.63.8.1175

Shi, Z., Pan, Y., Yan, Z., Ding, S., Hu, H., Wei, Y., Luo, D., Xu, Y., Zhu, Q., & Li, Y. (2023). Microstructural alterations in different types of lesions and their perilesional white matter in relapsing-

remitting multiple sclerosis based on diffusion kurtosis imaging. *Multiple Sclerosis and Related Disorders*, *71*, 104572. https://doi.org/10.1016/j.msard.2023.104572

Shu, N., Duan, Y., Huang, J., Ren, Z., Liu, Z., Dong, H., Barkhof, F., Li, K., & Liu, Y. (2018). Progressive brain rich-club network disruption from clinically isolated syndrome towards multiple sclerosis. *NeuroImage: Clinical*, *19*, 232–239. https://doi.org/10.1016/j.nicl.2018.03.034

Shu, N., Duan, Y., Xia, M., Schoonheim, M. M., Huang, J., Ren, Z., Sun, Z., Ye, J., Dong, H., Shi, F.-D., Barkhof, F., Li, K., & Liu, Y. (2016). Disrupted topological organization of structural and functional brain connectomes in clinically isolated syndrome and multiple sclerosis. *Scientific Reports*, *6*(1), Article 1. https://doi.org/10.1038/srep29383

Shu, N., Liu, Y., Li, K., Duan, Y., Wang, J., Yu, C., Dong, H., Ye, J., & He, Y. (2011). Diffusion Tensor Tractography Reveals Disrupted Topological Efficiency in White Matter Structural Networks in Multiple Sclerosis. *Cerebral Cortex*, *21*(11), 2565–2577. https://doi.org/10.1093/cercor/bhr039

Simpson, S., Taylor, B., Blizzard, L., Ponsonby, A.-L., Pittas, F., Tremlett, H., Dwyer, T., Gies, P., & Van Der Mei, I. (2010). Higher 25-hydroxyvitamin D is associated with lower relapse risk in MS. *Annals of Neurology*, n/a-n/a. https://doi.org/10.1002/ana.22043

Simpson, S., Wang, W., Otahal, P., Blizzard, L., van der Mei, I. A. F., & Taylor, B. V. (2019). Latitude continues to be significantly associated with the prevalence of multiple sclerosis: An updated meta-analysis. *Journal of Neurology, Neurosurgery, and Psychiatry*, *90*(11), 1193–1200. https://doi.org/10.1136/jnnp-2018-320189

Sled, J. G., Zijdenbos, A. P., & Evans, A. C. (1998). A nonparametric method for automatic correction of intensity nonuniformity in MRI data. *IEEE Transactions on Medical Imaging*, *17*(1), 87–97. https://doi.org/10.1109/42.668698

Smith, R. E., Calamante, F., & Connelly, A. (2020a). Mapping connectomes with diffusion MRI: Deterministic or probabilistic tractography? *Magnetic Resonance in Medicine*, *83*(3), 787–790. https://doi.org/10.1002/mrm.27916

Smith, R. E., Calamante, F., & Connelly, A. (2020b). Notes on 'A cautionary note on the use of SIFT in pathological connectomes'. *Magnetic Resonance in Medicine*, *84*(5), 2303–2307. https://doi.org/10.1002/mrm.28266

Smith, R. E., Calamante, F., Gajamange, S., Kolbe, S., & Connelly, A. (2020). *Modulation of white matter bundle connectivity in the presence of axonal truncation pathologies* [Preprint]. Neuroscience. https://doi.org/10.1101/2020.01.14.903559

Smith, R. E., Tournier, J.-D., Calamante, F., & Connelly, A. (2012). Anatomically-constrained tractography: Improved diffusion MRI streamlines tractography through effective use of anatomical information. *NeuroImage*, *62*(3), 1924–1938. https://doi.org/10.1016/j.neuroimage.2012.06.005

Smith, R. E., Tournier, J.-D., Calamante, F., & Connelly, A. (2013). SIFT: Spherical-deconvolution informed filtering of tractograms. *NeuroImage*, *67*, 298–312. https://doi.org/10.1016/j.neuroimage.2012.11.049

Smith, R. E., Tournier, J.-D., Calamante, F., & Connelly, A. (2015a). SIFT2: Enabling dense quantitative assessment of brain white matter connectivity using streamlines tractography. *NeuroImage*, *119*, 338–351. https://doi.org/10.1016/j.neuroimage.2015.06.092

Smith, R. E., Tournier, J.-D., Calamante, F., & Connelly, A. (2015b). The effects of SIFT on the reproducibility and biological accuracy of the structural connectome. *NeuroImage*, *104*, 253–265. https://doi.org/10.1016/j.neuroimage.2014.10.004

Smith, R., Skoch, A., Bajada, C. J., Caspers, S., & Connelly, A. (2020). *Hybrid surface-volume segmentation for improved anatomically-constrained tractography*.

Smith, S. M., Jenkinson, M., Woolrich, M. W., Beckmann, C. F., Behrens, T. E. J., Johansen-Berg, H., Bannister, P. R., De Luca, M., Drobnjak, I., Flitney, D. E., Niazy, R. K., Saunders, J., Vickers, J., Zhang, Y., De Stefano, N., Brady, J. M., & Matthews, P. M. (2004). Advances in functional and structural MR image analysis and implementation as FSL. *NeuroImage*, *23*, S208–S219. https://doi.org/10.1016/j.neuroimage.2004.07.051

Solana, E., Martinez-Heras, E., Casas-Roma, J., Calvet, L., Lopez-Soley, E., Sepulveda, M., Sola-Valls, N., Montejo, C., Blanco, Y., Pulido-Valdeolivas, I., Andorra, M., Saiz, A., Prados, F., & Llufriu, S. (2019). Modified connectivity of vulnerable brain nodes in multiple sclerosis, their impact on cognition and their discriminative value. *Scientific Reports*, *9*(1), 20172. https://doi.org/10.1038/s41598-019-56806-z

Solana, E., Martinez-Heras, E., Martinez-Lapiscina, E. H., Sepulveda, M., Sola-Valls, N., Bargalló, N., Berenguer, J., Blanco, Y., Andorra, M., Pulido-Valdeolivas, I., Zubizarreta, I., Saiz, A., & Llufriu, S. (2018). Magnetic resonance markers of tissue damage related to connectivity disruption in multiple sclerosis. *NeuroImage: Clinical*, *20*, 161–168. https://doi.org/10.1016/j.nicl.2018.07.012

Solaro, C., Grange, E., Di Giovanni, R., Cattaneo, D., Bertoni, R., Prosperini, L., Messmer Uccelli, M., & Marengo, D. (2020). Nine Hole Peg Test asymmetry in refining upper limb assessment in multiple sclerosis. *Multiple Sclerosis and Related Disorders*, *45*, 102422. https://doi.org/10.1016/j.msard.2020.102422

Soldan, S. S., & Lieberman, P. M. (2023). Epstein-Barr virus and multiple sclerosis. *Nature Reviews. Microbiology*, *21*(1), 51–64. https://doi.org/10.1038/s41579-022-00770-5

Sollid, L. M. (2022). Epstein-Barr virus as a driver of multiple sclerosis. *Science Immunology*, *7*(70), eabo7799. https://doi.org/10.1126/sciimmunol.abo7799

Song, S.-K., Sun, S.-W., Ramsbottom, M. J., Chang, C., Russell, J., & Cross, A. H. (2002). Dysmyelination Revealed through MRI as Increased Radial (but Unchanged Axial) Diffusion of Water. *NeuroImage*, *17*(3), 1429–1436. https://doi.org/10.1006/nimg.2002.1267

Spampinato, M. V., Kocher, M. R., Jensen, J. H., Helpern, J. A., Collins, H. R., & Hatch, N. U. (2017). Diffusional Kurtosis Imaging of the Corticospinal Tract in Multiple Sclerosis: Association with Neurologic Disability. *American Journal of Neuroradiology*, *38*(8), 1494–1500. https://doi.org/10.3174/ajnr.A5225

Sperber, C., Griffis, J., & Kasties, V. (2022). Indirect structural disconnection-symptom mapping. *Brain Structure & Function*, *227*(9), 3129–3144. https://doi.org/10.1007/s00429-022-02559-x

Sporns, O. (2018). Graph theory methods: Applications in brain networks. *Translational Research*, *20*(2), 11.

Sporns, O., & Kötter, R. (2004). Motifs in Brain Networks. *PLOS Biology*, *2*(11), e369. https://doi.org/10.1371/journal.pbio.0020369

Steenwijk, M. D., Geurts, J. J. G., Daams, M., Tijms, B. M., Wink, A. M., Balk, L. J., Tewarie, P. K., Uitdehaag, B. M. J., Barkhof, F., Vrenken, H., & Pouwels, P. J. W. (2016). Cortical atrophy patterns in multiple sclerosis are non-random and clinically relevant. *Brain*, *139*(1), 115–126. https://doi.org/10.1093/brain/awv337

Stellmann, J.-P., Hodecker, S., Cheng, B., Wanke, N., Young, K. L., Hilgetag, C., Gerloff, C., Heesen, C., Thomalla, G., & Siemonsen, S. (2017). Reduced rich-club connectivity is related to disability in primary progressive MS. *Neurology - Neuroimmunology Neuroinflammation*, *4*(5), e375. https://doi.org/10.1212/NXI.0000000000000375

Storelli, L., Pagani, E., Meani, A., Preziosa, P., Filippi, M., & Rocca, M. A. (2022). Advanced diffusion-weighted imaging models better characterize white matter neurodegeneration and clinical outcomes in multiple sclerosis. *Journal of Neurology*, *269*(9), 4729–4741. https://doi.org/10.1007/s00415-022-11104-z

Sumowski, J. F., Benedict, R., Enzinger, C., Filippi, M., Geurts, J. J., Hamalainen, P., Hulst, H., Inglese, M., Leavitt, V. M., Rocca, M. A., Rosti-Otajarvi, E. M., & Rao, S. (2018). Cognition in multiple sclerosis: State of the field and priorities for the future. *Neurology*, *90*(6), 278–288. https://doi.org/10.1212/WNL.0000000000004977

Teuwen, J., Gouw, Z. A. R., & Sonke, J.-J. (2022). Artificial Intelligence for Image Registration in Radiation Oncology. *Seminars in Radiation Oncology*, *32*(4), 330–342. https://doi.org/10.1016/j.semradonc.2022.06.003

Thiebaut de Schotten, M., Dell'Acqua, F., Ratiu, P., Leslie, A., Howells, H., Cabanis, E., Iba-Zizen, M. T., Plaisant, O., Simmons, A., Dronkers, N. F., Corkin, S., & Catani, M. (2015). From Phineas Gage and Monsieur Leborgne to H.M.: Revisiting Disconnection Syndromes. *Cerebral Cortex (New York, N.Y.: 1991)*, *25*(12), 4812–4827. https://doi.org/10.1093/cercor/bhv173

Thompson, A. J., Banwell, B. L., Barkhof, F., Carroll, W. M., Coetzee, T., Comi, G., Correale, J., Fazekas, F., Filippi, M., Freedman, M. S., Fujihara, K., Galetta, S. L., Hartung, H. P., Kappos, L., Lublin, F. D., Marrie, R. A., Miller, A. E., Miller, D. H., Montalban, X., … Cohen, J. A. (2017). Diagnosis of multiple sclerosis: 2017 revisions of the McDonald criteria. *The Lancet Neurology*. https://doi.org/10.1016/S1474-4422(17)30470-2

Thrue, C., Riemenschneider, M., Hvid, L., Stenager, E., & Dalgas, U. (2021). Time matters: Early-phase multiple sclerosis is accompanied by considerable impairments across multiple domains. *Multiple Sclerosis Journal*, *27*(10), 1477–1485. https://doi.org/10.1177/1352458520936231

Tiftikcioglu, B. I. (2018). Multiple Sclerosis Functional Composite: Scoring Instructions. *Archives of Neuropsychiatry*. https://doi.org/10.29399/npa.23330

Toschi, N., De Santis, S., Granberg, T., Ouellette, R., Treaba, C. A., Herranz, E., & Mainero, C. (2019). Evidence for Progressive Microstructural Damage in Early Multiple Sclerosis by Multi-Shell Diffusion MRI. *Neuroscience*. https://doi.org/10.1016/j.neuroscience.2019.01.022

Tourbah, A., Lebrun-Frenay, C., Edan, G., Clanet, M., Papeix, C., Vukusic, S., De Sèze, J., Debouverie, M., Gout, O., & Clavelou, P. (2016). MD1003 (high-dose biotin) for the treatment of progressive multiple sclerosis: A randomised, double-blind, placebo-controlled study. *Multiple Sclerosis Journal*, *22*(13), 1719–1731.

Tournier, J.-D., Calamante, F., & Connelly, A. (2007). Robust determination of the fibre orientation distribution in diffusion MRI: Non-negativity constrained super-resolved spherical deconvolution. *NeuroImage*, *35*(4), 1459–1472. https://doi.org/10.1016/j.neuroimage.2007.02.016

Tournier, J.-D., Calamante, F., & Connelly, A. (2010). *Improved probabilistic streamlines tractography by 2nd order integration over fibre orientation distributions*.

Tournier, J.-D., Calamante, F., Gadian, D. G., & Connelly, A. (2004). Direct estimation of the fiber orientation density function from diffusion-weighted MRI data using spherical deconvolution. *NeuroImage*, *23*(3), 1176–1185. https://doi.org/10.1016/j.neuroimage.2004.07.037

Tournier, J.-D., Smith, R., Raffelt, D., Tabbara, R., Dhollander, T., Pietsch, M., Christiaens, D., Jeurissen, B., Yeh, C.-H., & Connelly, A. (2019). MRtrix3: A fast, flexible and open software framework for medical image processing and visualisation. *NeuroImage*, *202*, 116137. https://doi.org/10.1016/j.neuroimage.2019.116137

Tovar-Moll, F., Evangelou, I. E., Chiu, A. W., Auh, S., Chen, C., Ehrmantraut, M., Ohayon, J. M., Richert, N., & Bagnato, F. (2015). Diffuse and Focal Corticospinal Tract Disease and Its Impact on Patient Disability in Multiple Sclerosis: Corticospinal Disease in Multiple Sclerosis. *Journal of Neuroimaging*, *25*(2), 200–206. https://doi.org/10.1111/jon.12171

Tozlu, C., Jamison, K., Gu, Z., Gauthier, S. A., & Kuceyeski, A. (2021). Estimated connectivity networks outperform observed connectivity networks when classifying people with multiple sclerosis into disability groups. *NeuroImage. Clinical*, *32*, 102827. https://doi.org/10.1016/j.nicl.2021.102827

Tozlu, C., Jamison, K., Nguyen, T., Zinger, N., Kaunzner, U., Pandya, S., Wang, Y., Gauthier, S., & Kuceyeski, A. (2021). Structural disconnectivity from paramagnetic rim lesions is related to disability in multiple sclerosis. *Brain and Behavior*, *11*(10), e2353. https://doi.org/10.1002/brb3.2353

Tsagkas, C., Chakravarty, M. M., Gaetano, L., Naegelin, Y., Amann, M., Parmar, K., Papadopoulou, A., Wuerfel, J., Kappos, L., Sprenger, T., & Magon, S. (2020). Longitudinal patterns of cortical thinning in multiple sclerosis. *Human Brain Mapping*, hbm.24940. https://doi.org/10.1002/hbm.24940

Tsagkas, C., Huck-Horvath, A., Cagol, A., Haas, T., Barakovic, M., Amann, M., Ruberte, E., Melie-Garcia, L., Weigel, M., Pezold, S., Schlaeger, R., Kuhle, J., Sprenger, T., Kappos, L., Bieri, O., Cattin, P., Granziera, C., & Parmar, K. (2022). Anterior horn atrophy in the cervical spinal cord: A new biomarker in progressive multiple sclerosis. *Multiple Sclerosis (Houndmills, Basingstoke, England)*, 13524585221139152. https://doi.org/10.1177/13524585221139152

Tsagkas, C., Magon, S., Gaetano, L., Pezold, S., Naegelin, Y., Amann, M., Stippich, C., Cattin, P., Wuerfel, J., Bieri, O., Sprenger, T., Kappos, L., & Parmar, K. (2018). Spinal cord volume loss: A marker of disease progression in multiple sclerosis. *Neurology*, *91*(4), e349–e358. https://doi.org/10.1212/WNL.0000000000005853

Tsagkas, C., Magon, S., Gaetano, L., Pezold, S., Naegelin, Y., Amann, M., Stippich, C., Cattin, P., Wuerfel, J., Bieri, O., Sprenger, T., Kappos, L., & Parmar, K. (2019). Preferential spinal cord volume loss in primary progressive multiple sclerosis. *Multiple Sclerosis Journal*, *25*(7), 947–957. https://doi.org/10.1177/1352458518775006

Tsagkas, C., Naegelin, Y., Amann, M., Papadopoulou, A., Barro, C., Chakravarty, M. M., Gaetano, L., Wuerfel, J., Kappos, L., Kuhle, J., Granziera, C., Sprenger, T., Magon, S., & Parmar, K. (2021). Central nervous system atrophy predicts future dynamics of disability progression in a real-world multiple sclerosis cohort. *European Journal of Neurology*, *28*(12), 4153–4166. https://doi.org/10.1111/ene.15098

Tur, C., Eshaghi, A., Altmann, D. R., Jenkins, T. M., Prados, F., Grussu, F., Charalambous, T., Schmidt, A., Ourselin, S., Clayden, J. D., Wheeler-Kingshott, C. A. M. G., Thompson, A. J., Ciccarelli, O., & Toosy, A. T. (2018). Structural cortical network reorganization associated with early conversion to multiple sclerosis. *Scientific Reports*, *8*(1), 10715. https://doi.org/10.1038/s41598-018-29017-1

Tur, C., Grussu, F., Prados, F., Charalambous, T., Collorone, S., Kanber, B., Cawley, N., Altmann, D. R., Ourselin, S., Barkhof, F., Clayden, J. D., Toosy, A. T., Wheeler-Kingshott, C. A. G., & Ciccarelli, O. (2019). A multi-shell multi-tissue diffusion study of brain connectivity in early multiple sclerosis. *Multiple Sclerosis Journal*, 135245851984510. https://doi.org/10.1177/1352458519845105

Tur, C., Kanber, B., Eshaghi, A., Altmann, D. R., Khaleeli, Z., Prados, F., Ourselin, S., Thompson, A. J., Wheeler-Kingshott, C. A. G., Toosy, A. T., & Ciccarelli, O. (2019). Clinical relevance of cortical network dynamics in early primary progressive MS. *Multiple Sclerosis Journal*, 15.

Tur, C., Moccia, M., Barkhof, F., Chataway, J., Sastre-Garriga, J., Thompson, A. J., & Ciccarelli, O. (2018). Assessing treatment outcomes in multiple sclerosis trials and in the clinical setting. *Nature Reviews Neurology*, *14*(2), 75–93. https://doi.org/10.1038/nrneurol.2017.171

Upton, A. R., & McComas, A. J. (1973). The double crush in nerve entrapment syndromes. *Lancet (London, England)*, *2*(7825), 359–362. https://doi.org/10.1016/s0140-6736(73)93196-6

van der Walt, A., Kolbe, S., Mitchell, P., Wang, Y., Butzkueven, H., Egan, G., Yiannikas, C., Graham, S., Kilpatrick, T., & Klistorner, A. (2015). Parallel Changes in Structural and Functional Measures of Optic Nerve Myelination after Optic Neuritis. *PLOS ONE*, *10*(5), e0121084. https://doi.org/10.1371/journal.pone.0121084

Van Essen, D. C., Smith, S. M., Barch, D. M., Behrens, T. E. J., Yacoub, E., & Ugurbil, K. (2013). The WU-Minn Human Connectome Project: An Overview. *NeuroImage*, *80*, 62–79. https://doi.org/10.1016/j.neuroimage.2013.05.041

van Waesberghe, J. H., Kamphorst, W., De Groot, C. J., van Walderveen, M. A., Castelijns, J. A., Ravid, R., Lycklama à Nijeholt, G. J., van der Valk, P., Polman, C. H., Thompson, A. J., & Barkhof, F. (1999). Axonal loss in multiple sclerosis lesions: Magnetic resonance imaging insights into substrates of disability. *Annals of Neurology*, *46*(5), 747–754. https://doi.org/10.1002/1531-8249(199911)46:5<747::aid-ana10>3.3.co;2-w

van Walderveen, M. A. A., Kamphorst, W., Scheltens, P., van Waesberghe, J. H. T. M., Ravid, R., Valk, J., Polman, C. H., & Barkhof, F. (1998). Histopathologic correlate of hypointense lesions on T1-weighted spin-echo MRI in multiple sclerosis. *Neurology*, *50*(5), 1282–1288. https://doi.org/10.1212/WNL.50.5.1282

Vaneckova, M., Piredda, G. F., Andelova, M., Krasensky, J., Uher, T., Srpova, B., Havrdova, E. K., Vodehnalova, K., Horakova, D., Hilbert, T., Maréchal, B., Fartaria, M. J., Ravano, V., & Kober, T. (2022). Periventricular gradient of T1 tissue alterations in multiple sclerosis. *NeuroImage. Clinical*, *34*, 103009. https://doi.org/10.1016/j.nicl.2022.103009

Varentsova, A., Zhang, S., & Arfanakis, K. (2014). Development of a High Angular Resolution Diffusion Imaging Human Brain Template. *NeuroImage*, *91*, 177. https://doi.org/10.1016/j.neuroimage.2014.01.009

Vargas, M. E., & Barres, B. A. (2007). Why Is Wallerian Degeneration in the CNS So Slow? *Annual Review of Neuroscience*, *30*(1), 153–179. https://doi.org/10.1146/annurev.neuro.30.051606.094354

Wagenknecht, N., Becker, B., Scheld, M., Beyer, C., Clarner, T., Hochstrasser, T., & Kipp, M. (2016). Thalamus Degeneration and Inflammation in Two Distinct Multiple Sclerosis Animal Models. *Journal of Molecular Neuroscience*, *60*(1), 102–114. https://doi.org/10.1007/s12031-016-0790-z

Walton, C., King, R., Rechtman, L., Kaye, W., Leray, E., Marrie, R. A., Robertson, N., La Rocca, N., Uitdehaag, B., Van Der Mei, I., Wallin, M., Helme, A., Angood Napier, C., Rijke, N., & Baneke, P. (2020). Rising prevalence of multiple sclerosis worldwide: Insights from the Atlas of MS, third edition. *Multiple Sclerosis Journal*, *26*(14), 1816–1821. https://doi.org/10.1177/1352458520970841

Wang, C., Barnett, M. H., Yiannikas, C., Barton, J., Parratt, J., You, Y., Graham, S. L., & Klistorner, A. (2019). Lesion activity and chronic demyelination are the major determinants of brain atrophy in MS. *Neurology - Neuroimmunology Neuroinflammation*, *6*(5), e593. https://doi.org/10.1212/NXI.0000000000000593

Wang, C., Beadnall, H. N., Hatton, S. N., Bader, G., Tomic, D., Silva, D. G., & Barnett, M. H. (2016). Automated brain volumetrics in multiple sclerosis: A step closer to clinical application. *Journal of Neurology, Neurosurgery & Psychiatry*, *87*(7), 754–757. https://doi.org/10.1136/jnnp-2015-312304

Wang, C., Klistorner, A., Ly, L., & Barnett, M. H. (2018). White matter tract-specific quantitative analysis in multiple sclerosis: Comparison of optic radiation reconstruction techniques. *PLOS ONE*, *13*(1), e0191131. https://doi.org/10.1371/journal.pone.0191131

Wang, Y., Sun, P., Wang, Q., Trinkaus, K., Schmidt, R. E., Naismith, R. T., Cross, A. H., & Song, S.-K. (2015). Differentiation and quantification of inflammation, demyelination and axon injury or loss in multiple sclerosis. *Brain*, *138*(5), 1223–1238. https://doi.org/10.1093/brain/awv046

Ward, M., & Goldman, M. D. (2022). Epidemiology and Pathophysiology of Multiple Sclerosis. *CONTINUUM: Lifelong Learning in Neurology*, *28*(4), 988–1005. https://doi.org/10.1212/CON.0000000000001136

Wasserthal, J., Neher, P., & Maier-Hein, K. H. (2018). TractSeg—Fast and accurate white matter tract segmentation. *NeuroImage*, *183*, 239–253. https://doi.org/10.1016/j.neuroimage.2018.07.070

Wattjes, M. P., Ciccarelli, O., Reich, D. S., Banwell, B., Stefano, N. de, Enzinger, C., Fazekas, F., Filippi, M., Frederiksen, J., Gasperini, C., Hacohen, Y., Kappos, L., Li, D. K. B., Mankad, K., Montalban, X., Newsome, S. D., Oh, J., Palace, J., Rocca, M. A., … Oh, J. (2021). 2021 MAGNIMS–CMSC–

NAIMS consensus recommendations on the use of MRI in patients with multiple sclerosis. *The Lancet Neurology*, *20*(8), 653–670. https://doi.org/10.1016/S1474-4422(21)00095-8

Waubant, E., Lucas, R., Mowry, E., Graves, J., Olsson, T., Alfredsson, L., & Langer-Gould, A. (2019). Environmental and genetic risk factors for MS: An integrated review. *Annals of Clinical and Translational Neurology*, *6*(9), 1905–1922. https://doi.org/10.1002/acn3.50862

Weeda, M. M., Pruis, I. J., Westerveld, A. S. R., Brouwer, I., Bellenberg, B., Barkhof, F., Vrenken, H., Lukas, C., Schneider, R., & Pouwels, P. J. W. (2020). Damage in the Thalamocortical Tracts is Associated With Subsequent Thalamus Atrophy in Early Multiple Sclerosis. *Frontiers in Neurology*, *11*, 575611. https://doi.org/10.3389/fneur.2020.575611

Welton, T., Constantinescu, C. S., Auer, D. P., & Dineen, R. A. (2020). Graph Theoretic Analysis of Brain Connectomics in Multiple Sclerosis: Reliability and Relationship with Cognition. *Brain Connectivity*, *10*(2), 95–104. https://doi.org/10.1089/brain.2019.0717

Xiao, H., Teng, X., Liu, C., Li, T., Ren, G., Yang, R., Shen, D., & Cai, J. (2021). A review of deep learning-based three-dimensional medical image registration methods. *Quantitative Imaging in Medicine and Surgery*, *11*(12), 4895–4916. https://doi.org/10.21037/qims-21-175

Yeatman, J. D., Dougherty, R. F., Myall, N. J., Wandell, B. A., & Feldman, H. M. (2012). Tract Profiles of White Matter Properties: Automating Fiber-Tract Quantification. *PLoS ONE*, *7*(11), e49790. https://doi.org/10.1371/journal.pone.0049790

Yeh, C.-H., Jones, D. K., Liang, X., Descoteaux, M., & Connelly, A. (2021). Mapping Structural Connectivity Using Diffusion MRI: Challenges and Opportunities. *Journal of Magnetic Resonance Imaging: JMRI*, *53*(6), 1666–1682. https://doi.org/10.1002/jmri.27188

Yeh, W. Z., Gresle, M., Jokubaitis, V., Stankovich, J., Walt, A., & Butzkueven, H. (2020). Immunoregulatory effects and therapeutic potential of vitamin D in multiple sclerosis. *British Journal of Pharmacology*, *177*(18), 4113–4133. https://doi.org/10.1111/bph.15201

Yoon, K., Archer, D. B., Clarke, M. A., Smith, S. A., Oguz, I., Cutter, G., Xu, J., & Bagnato, F. (2022). Transcallosal and Corticospinal White Matter Disease and Its Association With Motor Impairment in Multiple Sclerosis. *Frontiers in Neurology*, *13*, 811315. https://doi.org/10.3389/fneur.2022.811315

You, Y., Joseph, C., Wang, C., Gupta, V., Liu, S., Yiannikas, C., Chua, B. E., Chitranshi, N., Shen, T., Dheer, Y., Invernizzi, A., Borotkanics, R., Barnett, M., Graham, S. L., & Klistorner, A. (2019). Demyelination precedes axonal loss in the transneuronal spread of human neurodegenerative disease. *Brain*, *142*(2), 426–442. https://doi.org/10.1093/brain/awy338

Yourganov, G., Fridriksson, J., Rorden, C., Gleichgerrcht, E., & Bonilha, L. (2016). Multivariate Connectome-Based Symptom Mapping in Post-Stroke Patients: Networks Supporting Language and Speech. *The Journal of Neuroscience: The Official Journal of the Society for Neuroscience*, *36*(25), 6668–6679. https://doi.org/10.1523/JNEUROSCI.4396-15.2016

Yu, C., Zhu, C., Zhang, Y., Chen, H., Qin, W., Wang, M., & Li, K. (2009). A longitudinal diffusion tensor imaging study on Wallerian degeneration of corticospinal tract after motor pathway stroke. *NeuroImage*, *47*(2), 451–458. https://doi.org/10.1016/j.neuroimage.2009.04.066

Zalesky, A., Fornito, A., & Bullmore, E. T. (2010). Network-based statistic: Identifying differences in brain networks. *NeuroImage*, *53*(4), 1197–1207. https://doi.org/10.1016/j.neuroimage.2010.06.041

Zalesky, A., Sarwar, T., & Kotagiri, R. (2020). SIFT in pathological connectomes: Follow-up response to Smith and colleagues. *Magnetic Resonance in Medicine*, *84*(5), 2308–2311. https://doi.org/10.1002/mrm.28412

Zalesky, A., Sarwar, T., & Ramamohanarao, K. (2020). A cautionary note on the use of SIFT in pathological connectomes. *Magnetic Resonance in Medicine*, *83*(3), 791–794. https://doi.org/10.1002/mrm.28037

Zeydan, B., Gu, X., Atkinson, E. J., Keegan, B. M., Weinshenker, B. G., Tillema, J.-M., Pelletier, D., Azevedo, C. J., Lebrun-Frenay, C., Siva, A., Okuda, D. T., Kantarci, K., & Kantarci, O. H. (2018). Cervical spinal cord atrophy: An early marker of progressive MS onset. *Neurology - Neuroimmunology Neuroinflammation*, *5*(2), e435. https://doi.org/10.1212/NXI.0000000000000435

Zhong, J., Nantes, J. C., Holmes, S. A., Gallant, S., Narayanan, S., & Koski, L. (2016). Abnormal functional connectivity and cortical integrity influence dominant hand motor disability in multiple sclerosis: A multimodal analysis: FC, Structural and Behavioural Changes in MS. *Human Brain Mapping*, *37*(12), 4262–4275. https://doi.org/10.1002/hbm.23307

Zimmerman, M., Gottsäter, A., & Dahlin, L. B. (2022). Carpal Tunnel Syndrome and Diabetes-A Comprehensive Review. *Journal of Clinical Medicine*, *11*(6), 1674. https://doi.org/10.3390/jcm11061674

Zivadinov, R., Bergsland, N., Dolezal, O., Hussein, S., Seidl, Z., Dwyer, M. G., Vaneckova, M., Krasensky, J., Potts, J. A., Kalincik, T., Havrdová, E., & Horáková, D. (2013). Evolution of Cortical and Thalamus Atrophy and Disability Progression in Early Relapsing-Remitting MS during 5 Years. *American Journal of Neuroradiology*, *34*(10), 1931–1939. https://doi.org/10.3174/ajnr.A3503

Zivadinov, R., Brown, M. H.-, Schirda, C. V., Poloni, G. U., Bergsland, N., Magnano, C. R., Durfee, J., Kennedy, C., Carl, E., Hagemeier, J., Benedict, R. H. B., Weinstock-Guttman, B., & Dwyer, M. G. (2012). Abnormal subcortical deep-gray matter susceptibility-weighted imaging filtered phase measurements in patients with multiple sclerosis. *NeuroImage*, *59*(1), 331–339. https://doi.org/10.1016/j.neuroimage.2011.07.045

Zivadinov, R., & Leist, T. P. (2005). Clinical-Magnetic Resonance Imaging Correlations in Multiple Sclerosis. *Journal of Neuroimaging*, *15*, 10S-21S. https://doi.org/10.1177/1051228405283291

Zivadinov, R., Uher, T., Hagemeier, J., Vaneckova, M., Ramasamy, D. P., Tyblova, M., Bergsland, N., Seidl, Z., Dwyer, M. G., Krasensky, J., Havrdova, E., & Horakova, D. (2016). A serial 10-year follow-up study of brain atrophy and disability progression in RRMS patients. *Multiple Sclerosis Journal*, *22*(13), 1709–1718. https://doi.org/10.1177/1352458516629769

Zrzavy, T., Hametner, S., Wimmer, I., Butovsky, O., Weiner, H. L., & Lassmann, H. (2017). Loss of 'homeostatic' microglia and patterns of their activation in active multiple sclerosis. *Brain*, *140*(7), 1900–1913. https://doi.org/10.1093/brain/awx113